ISSN 0031 - 9465

PHYTOPATHOLOGIA MEDITERRANEA

Plant health and food safety

Volume 59 • No. 2 • August 2020

The international journal of the
Mediterranean Phytopathological Union

FIRENZE UNIVERSITY PRESS

PHYTOPATHOLOGIA MEDITERRANEA

The international journal of the Mediterranean Phytopathological Union

Volume 59, August, 2020

Firenze University Press

***Phytopathologia Mediterranea*. The international journal of the Mediterranean Phytopathological Union**

Published by
Firenze University Press – University of Florence, Italy
Via Cittadella, 7 - 50144 Florence - Italy
http://www.fupress.com/pm

Direttore Responsabile: **Giuseppe Surico**, University of Florence, Italy

Phytopathologia Mediterranea
The international journal of the
Mediterranean Phytopathological Union

Firenze University Press
www.fupress.com/pm

Research Papers

Heterosporicola beijingense sp. nov. (*Leptosphaeriaceae, Pleosporales*) associated with *Chenopodium quinoa* leaf spots

Rashika S. BRAHMANAGE[1,2,3,#], Mei LIU[1,#], Dhanushka N. WANASINGHE[4], Monika C. DAYARATHNE[2,7], Li MEI[5], Rajesh JEEWON[6], Xinghong LI[1,*], Kevin D. HYDE[2,4,8,*]

[1] *Institute of Plant and Environment Protection, Beijing Academy of Agriculture and Forestry Sciences, Beijing 100097, People's Republic of China*
[2] *Center of Excellence in Fungal Research, Mae Fah Luang University, Chiang Rai, 57100, Thailand*
[3] *School of Science, Mae Fah Luang University, Chiang Rai, 57100, Thailand*
[4] *CAS key Laboratory for Plant Biodiversity and Biogeography of East Asia (KLPB), Kunming Institute of Botany, Chinese Academy of Science, Kunming 650201, Yunnan, China*
[5] *Beijing Agricultural technology extension station, Beijing 100029, China*
[6] *Department of Health Sciences, Faculty of Science, University of Mauritius, Reduit, Mauritius*
[7] *Department of Plant Pathology, Agriculture College, Guizhou University, Guiyang, Guizhou Province, 550025, China*
[8] *Innovative Institute of Plant Health, Zhongkai University of Agriculture and Engineering, Haizhu District, Guangzhou 510225, P.R. China*
*Corresponding authors: lixinghong1962@163.com, kdhyde3@gmail.com
# Both authors contributed equally

Summary. A coelomycetous fungus with hyaline, aseptate, oblong to ellipsoidal conidia was isolated from living *Chenopodium quinoa* leaves with leaf spots, in Beijing, China. Maximum likelihood and Bayesian analyses of a combined LSU, SSU, ITS and TEF sequence dataset confirmed its placement in *Heterosporicola* in *Leptosphaeriaceae*. The new taxon resembles other *Heterosporicola* species, but is phylogenetically distinct, and is introduced as a new species. *Heterosporicola beijingense* sp. nov. is compared with other *Heterosporicola* species, and comprehensive descriptions and micrographs are provided.

Key words. DNA analyses, morpho-molecular taxonomy, pathogens.

OPEN ACCESS

Citation: R.S. Brahmanage, M. Liu, D.N. Wanasinghe, M.C. Dayarathne, L. Mei, R. Jeewon, X. Li, K.D. Hyde (2020) *Heterosporicola beijingense* sp. nov. (*Leptosphaeriaceae*, *Pleosporales*) associated with *Chenopodium quinoa* leaf spots. *Phytopathologia Mediterranea* 59(2): 219-227. DOI: 10.14601/Phyto-11113

Accepted: April 17, 2020

Published: August 31, 2020

Data Availability Statement: All relevant data are within the paper and its Supporting Information files.

Competing Interests: The Author(s) declare(s) no conflict of interest.

Editor: Vladimiro Guarnaccia, DiSAFA - University of Torino, Italy.

INTRODUCTION

Quinoa (*Chenopodium quinoa*) is a dicotyledonous pseudocereal (Vega-Galvez *et al.,* 2010) which maintains high productivity in low fertility soils and under conditions of water shortage and high salinity (Tapia *et al.,* 1997). Quinoa seeds are rich in nutrients, with high protein content including all

nine essential amino acids with high concentrations of histidine, lysine and methionine. The seeds also lack gluten and contain high amounts of several minerals (including calcium, magnesium and iron), and health-promoting compounds such as flavonoids (Dini *et al.,* 1992; Wright *et al.,* 2002). Quinoa was first introduced to Shanxi Province (China) in 2011 and transferred rapidly to other provinces, including Gansu, Jilin, Sichuan and Qinghai (Li *et al.,* 2017). With the increase in quinoa crops, the number of pests and diseases of quinoa have also increased (Li *et al.,* 2017). Among them, fungal diseases are responsible for significant production losses (Lee *et al.,* 2019). Brown stalk rot, downy mildew, gray mould, leaf spot and root rot are the major fungal diseases that affect quinoa production in China and worldwide (Valencia-Chamorro, 2003; Testen *et al.,* 2013; Li *et al.,* 2017).

Vilca (1972) described *Ascochyta hyalospora* from leaf spots of quinoa (Boerema *et al.,* 1977). The first symptoms are light spots of indefinite area on the quinoa leaves (Boerema *et al.,* 1977; Alandia *et al.,* 1979; Li *et al.,* 2017), and with time pycnidia can be observed, and the leaves become dry and fall (Li *et al.,* 2017). Leaf spots have become a rapidly increasing fungal disease in the cultivation of quinoa in China (Wang *et al.,* 2014).

Heterosporicola (as *Heterospora*) was initially considered as a section of *Phoma* by Boerema (1977). De Gruyter *et al*. (2013) raised *Heterospora* to generic rank to accommodate two species (*H. chenopodii* and *H. dimorphospora*) of *Phoma* sect. *Heterospora* that clustered in *Leptosphaeriaceae*. The current name *Heterosporicola* was proposed to accommodate *Heterospora* by Wijayawardene *et al*. (2018) as the remaining species of *Phoma* sect. *Heterospora* clustered in the family *Didymellaceae* (Aveskamp *et al.,* 2010). The sexual morph of *Heterospora* is presently undetermined (De Gruyter *et al.,* 2013 Ariyawansa *et al.,* 2015; Wijayawardene *et al.,* 2017; Hyde *et al.,* 2018).

The present study introduces a novel potential plant pathogenic *Heterosporicola* species, associated with quinoa leaf spots occurring in Mentougou and Yanging districts (Beijing) in China. A multigene-based phylogram is also presented to infer phylogenetic relationships of this species.

MATERIALS AND METHODS

Sample collections, examination and isolation

Symptomatic quinoa leaves were collected from six fields in Beijing Mentougou and Yanging districts in August and July 2018. Leaf samples placed in Zip-lock plastic bags were brought to the laboratory and incubated at room temperature (25°C). An attempt was made to obtain axenic cultures following the single spore isolation method (Chomnunti *et al*., 2014) onto potato dextrose agar (PDA) and malt extract agar (MEA). A tissue isolation method was also used in attempts to isolate fungi from diseased leaves. Small leaf pieces (0.5 × 0.5 cm) were surface sterilized (Schulz *et al*., 1993) to eliminate epiphytic fungi, and were then incubated on PDA or MEA. Three replicates from each sample were maintained.

Digital images of fruiting structures were captured with a Canon 450D digital camera fitted to a Nikon ECLIPSE 80i compound microscope. Squash mount preparations were made from conidiomata near symptomatic leaf areas. Measurements of fungus structures were made using the Tarosoft (R) Image Frame Work program, and the images used for figures were processed with Adobe Photoshop CS3 Extended v. 10.0 (Adobe®). Herbarium specimens of the new species were deposited in the Mae Fah Luang University Herbarium (MFLU) and the Beijing Academy of Agricultural and Forestry Sciences (JZB), China. Faces of fungi and Index Fungorum numbers were registered according to Jayasiri *et al*. (2015) and Index Fungorum (2020). The new species was established following the guidelines of Jeewon and Hyde (2016).

DNA extraction, PCR amplifications and sequencing

A DNA extraction kit (E.Z.N.A.® Forensic DNA kit, D3591-01, Omega Bio-Tek) was used to extract DNA from fresh fruiting bodies from fungal isolates, following the manufacturer's instructions (as conidia did not germinate on any of the media used). Extracted DNA was used for PCR reactions with the following ingredients: each amplification reaction contained 0.125 µL of 5 units μL^{-1} Ex-Taq DNA polymerase (TaKaRa), 2.5 µL of 10 × PCR buffer, 2 µL of 2 mM $MgCl_2$, 2.5 µL of 2 mM dNTPs, 1 µL of 0.2–1.0 µM primer, <500 ng DNA template, and was adjusted with double-distilled water to a total volume of 25 µL. PCR amplification and sequencing was performed of the ITS gene region using the primer pair ITS5 and ITS4 (Carbone and Kohn, 1999). The LSU, SSU and TEF gene regions were amplified and sequenced, respectively, using the primer pairs LR0R/LR5 (Vilgalys and Hester, 1990), NS1/NS4 (White *et al.,* 1990) and EF1-983F/EF1-2218R (Rehner and Buckley, 2005). The amplification profiles for all four gene regions were as follows: an initial denaturing step for 2 min at 94°C, followed by 35 amplification cycles of denaturation at 94°C for 60 s, annealing at 55°C for 60 s and exten-

sion at 72°C for 90 s, and a final extension step of 72°C for 10 min (Brahmanage *et al.,* 2019). Purification and sequencing of PCR products were carried out using the above-mentioned PCR primers at Bio-med Biotech Company (Beijing, China). Sequences were checked for ambiguity, assembled and deposited in GenBank.

Phylogenetic analysis

Sequence data were compared by BLAST searches in the GenBank database at the National Centre for Biotechnology Information (NCBI) (https://www.ncbi.nlm.nih.gov/nucleotide/). Initial BLAST similarity indices showed that the isolates were very similar to *Heterosporicola*. *Heterosporicola* strains were compared with other related sequences of *Leptosphaeriaceae*, following procedures of Dayarathne *et al*. (2015) and Tennakoon *et al*. (2017) (Table 1). Sequences were aligned with MAFFT v. 7.0 (Kuraku *et al.,* 2013), combined using Bioedit 7 (Hall, 1999) and refined manually. Phylogenetic trees were generated using maximum likelihood (ML) and Bayesian inference (BI). The ML trees were generated with RAxML-HPC2 on XSEDE (v. 8.2.8) (Stamatakis, 2014) in the CIPRES Science Gateway platform (Miller *et al.,* 2010), using the GTR+I+G model of evolution. Bayesian analyses were performed for both individual and combined datasets using MrBayes v. 3.0b4 (Ronquist and Huelsenbeck, 2003). Nucleotide substitution models were determined with MrModeltest v. 2.2 (Nylander, 2004). A dirichlet state frequency was predicted for all four data partitions and GTR+I+G was the best model. The heating parameter was set to 0.2 and trees were saved every 1,000 generations (Ronquist *et al.,* 2012). Posterior probabilities (PP) (Rannala *et al.,* 1998; Zhaxybayeva and Gogarten, 2002) were defined by the Bayesian Markov Chain Monte Carlo (BMCMC) sampling method in MrBayes v. 3.0b4 (Huelsenbeck and Ronquist, 2001). The resulting trees were viewed with FigTree v.1.4.0 (Rambaut, 2009) and the final layout was done using Microsoft PowerPoint (2016).

RESULTS AND DISCUSSION

Symptoms

Numerous yellowish brown to reddish brown circular spots with lighter surrounding tissues were observed on affected quinoa leaves at the initial stage of disease development. Whirls of black conidiomata and shot holes on the leaves also were observed at later stages (Figure 1).

Phylogenetic analysis

The combined LSU, SSU, ITS, and TEF sequence dataset belonging to *Leptosphaeriaceae*, with *Phoma herbarum* (CBS 615.75) as the outgroup taxon, comprised 36 taxa with 2,436 nucleotide characters. RAxML analysis of the combined dataset yielded a best tree (Figure 2) with a final ML optimization likelihood value of -8815.833844. The matrix had 438 distinct alignment patterns, with 20.53% undetermined characters or gaps. Estimated base frequencies were; A = 0.244796, C = 0.219925, G = 0.271915, T = 0.263364. Substitution rates were AC = 1.726279, AG = 2.859320, AT = 2.066497, CG = 0.464869, CT = 6.764103, and GT = 1.000000. The gamma distribution shape parameter α = 0.171569. Phylogenetic trees obtained from ML and BI were similar in topology. Phylogenetic results indicated that isolates of *Heterosporicola beijingense* clustered together in a subclade with strong support (100% ML, 1.00 PP), and closely related to *H. chenopodii* and *H. dimorphospora* (Figure 2).

Taxonomy

Heterosporicola beijingense Brahmanage & K.D. Hyde, ***sp. nov.*** **Figure 2**

Index Fungorum: IF 557214, *Facesoffungi number*: FoF 07325

Etymology: Name refers to the geographical region Beijing, China, where the species was first found.

Holotype: JZB3400001

Saprobic or *pathogenic* on leaves of quinoa (*Chenopodium quinoa*). *Leaf spots* on quinoa leaves irregular, necrotic, with conidiomata arranged in several whorls. Sexual morph: undetermined. Asexual morph: Coelomycetous. *Conidiomata* 200–600 µm wide, pycnidia immersed to semi-immersed, globose to subglobose, black and each with an inconspicuous ostiole. *Conidiomatal wall* 15–60 µm wide, composed of 3–5 layers of cells of *textura angularis*, pale yellowish brown. *Conidiogenous cells* 4–8 × 4–6 µm ($\bar{x}$ = 6 × 5 µm, n = 20), phialidic, subglobose to short conical. *Microconidia* 3.8–4.4 × 1.4–2.1 µm ($\bar{x}$ = 4.2 × 1.8 µm, n = 30) hyaline, aseptate, oblong to ellipsoidal with two to many guttules. *Macroconidia* not observed.

Material examined: CHINA, Beijing, Mentougou, on living leaves of *Chenopodium quinoa* (*Amaranthaceae*), July 2018, Rashika S. Brahmanage, LC41 (JZB3400001, holotype), *ibid*., LC43 (JZB3400002), *ibid*., Yanging district, on living leaves of *Chenopodium quinoa* (*Amaranthaceae*), July 2018, Rashika S. Brahmanage, LC44

Table 1. Taxa used in this study and their GenBank accession numbers for SSU, LSU, ITS and TEF DNA sequence data. Type strains are indicated with ^{T} and newly generated sequences are in bold.

Taxa	Strain number	GenBank accessions			
		ITS	SSU	LSU	TEF
Alloleptosphaeria italica^{T}	MFLUCC 14-0934	KT454722[a]	-	KT454714	-
Alternariaster bidentis^{T}	CBS 134021	NR159551	-	KC609341	-
Alternariaster helianthi^{T}	CBS 327.69	KC609335	KC584627	KC584369	-
Alternariaster centaureae-diffusae^{T}	MFLUCC 14-0992	KT454724	KT454731	KT454716	-
Alternariaster trigonosporus^{T}	MFLU 15-2237	NR159558	-	KY674858	-
Heterosporicola chenopodii^{T}	CBS 448.68	FJ427023	EU754088	EU754187	-
Heterosporicola chenopodii	CBS 115.96	JF740227	-	EU754188	GU349077
Heterosporicola dimorphospora	CBS 345.78	JF740203	-	GU238069	-
Heterosporicola dimorphospora	CBS 165.78	JF740204	JF740098	JF740281	-
Heterosporicola beijingense	**JZB3400001**	**MN733734**	**MN733738**	**MN737597**	**MN786372**
Heterosporicola beijingense	**JZB3400002**	**MN733735**	**MN733739**	**MN737598**	**MN786373**
Heterosporicola beijingense	**JZB3400003**	**MN733736**	**MN733740**	**MN737599**	**MN786374**
Heterosporicola beijingense	**JZB3400004**	**MN733737**	**MN733741**	**MN737600**	**MN786375**
Leptosphaeria slovacica	CBS 389.80	JF740247	JF740101	JF740315	-
Leptosphaeria doliolum^{T}	CBS 505.75	JF740205	NG062778	GU301827	GU349069
Leptosphaeria doliolum	MFLUCC 15-1875	KT454727	-	KT454734	-
Leptosphaeria ebuli^{T}	MFLUCC 14-0828	NR155323	KP753954	KP744488	-
Leptosphaeria conoidea	CBS 616.75	MH860957	JF740099	MH872726	-
Neoleptosphaeria rubefaciens^{T}	CBS 223.77	JF740243	-	JF740312	-
Neoleptosphaeria jonesii^{T}	MFLUCC 16-1442	NR152375	NG063625	KY211870	KY211872
Paraleptosphaeria macrospora	CBS 114198	JF740238	-	JF740305	-
Paraleptosphaeria nitschkei^{T}	CBS 306.51	JF740239	-	JF740308	-
Paraleptosphaeria rubi^{T}	MFLUCC 14-0211	KT454726	KT454733	KT454718	-
Paraphoma radicina	CBS 111.79	NR156556	EU754092	EU754191	KF253130
Plenodomus pimpinellae	CBS 101637	JF740240	-	JF740309	-
Plenodomus guttulatus	MFLUCC 151876	KT454721	KT454729	KT454713	-
Plenodomus salviae	MFLUCC 130219	KT454725	KT454732	KT454717	-
Pseudoleptosphaeria etheridgei^{T}	CBS 125980	NR111620	-	MH875320	-
Sphaerellopsis macroconidiale	CBS 658.78	KP170659	-	KP170727	KP170684
Sphaerellopsis hakeae	CPC 29566	NR155859	-	KY173555	-
Sphaerellopsis paraphysata	CPC 21841	NR137956	-	-	-
Subplenodomus valerianae	CBS 630.68	JF740251	KY554199	GU238150	-
Subplenodomus violicola^{T}	CBS 306.68	FJ427083	GU238231	GU238156	-
Subplenodomus galicola^{T}	MFLU 15-1863	NR154454	-	KY554199	-

CBS: Centraalbureau voor Schimmelcultures, Westerdijk Fungal Biodiversity Institute, Utrecht, The Netherlands; JZB: Beijing Academy of Agricultural and Forestry Sciences; MFLU: Mae Fah Luang University Herbarium; MFLUCC: Mae Fah Luang University Culture Collection
[a] Sequence data from Dayarathne *et al.* (2015) and Tennakoon *et al.* (2017).

(JZB3400003), *ibid.*, LC45 (JZB3400004). Living cultures are not available.

Notes: *Heterosporicola beijingense* isolated from *Chenopodium quinoa* resembles *H. chenopodii* and *H. dimorphospora* (Van der Aa and van Kesteren, 1979, de Gruyter *et al.*, 2013). To support establishment of the new taxon as per the guidelines of Jeewon and Hyde (2016), we examined the nucleotide differences within the ITS and TEF regions. ITS base pair differences between *H. beijingense* and *H. chenopodii* were 6.5% (36 out of 550bp), and 6.9% (38 out of 550 bp) between *H. beijinense* and *H. dimorphospora*. The TEF base pair difference between *H. beijingense* and *H. chenopodii* was 2.3% (23 out of 895bp), but there were no TEF data generated from *H. dimorphospora* for comparison.

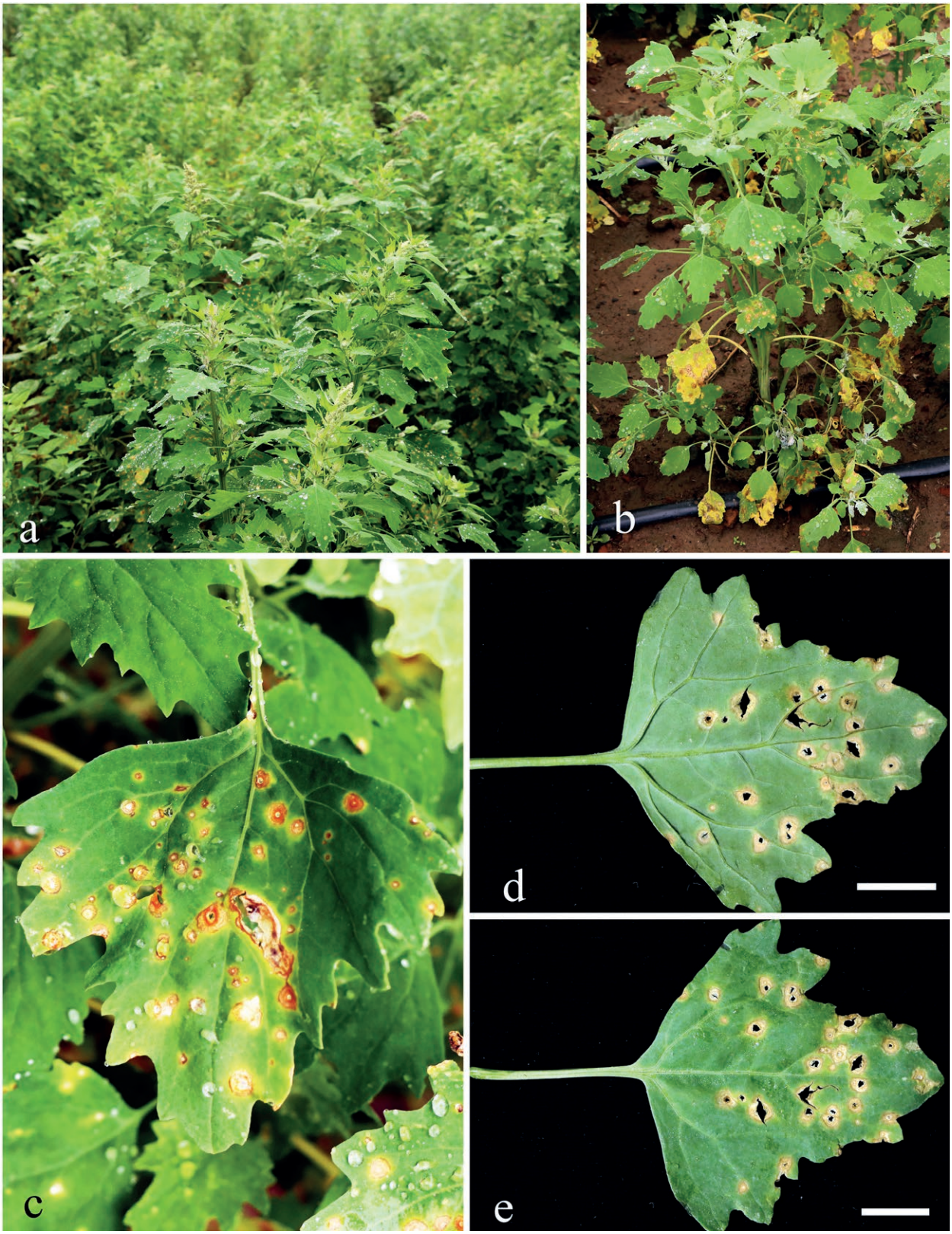

Figure 1. *Chenopodium quinoa* leaf spots. a–b, Diseased plants in the field. c, Closeup of a diseased plant. d–e, Closeup of a diseased leaf (e, upper surface, d, lower surface). Scale bars: = 1 cm.

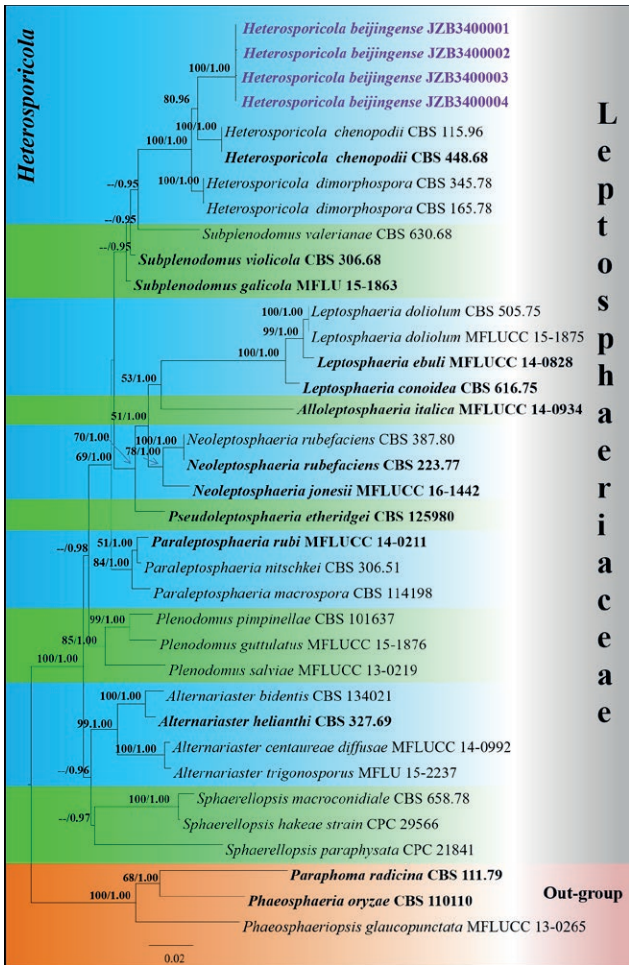

Figure 2. Maximum Likelihood tree generated by RAxML based on combined LSU, SSU, ITS and TEF sequence data from taxa of *Leptosphaeriaceae*. Bootstrap support values for ML ≥65% and Bayesian posterior probabilities >0.95 are given above each branch. Newly generated strains are in blue bold and ex-type sequences are in bold black.

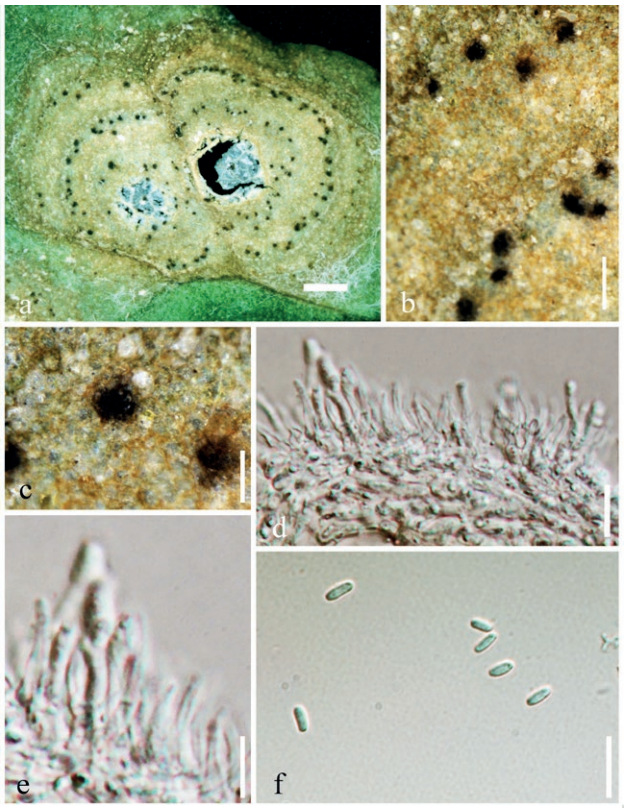

Figure 3. *Heterosporicola beijingense* on Quinoa leaves (JZB3400001 holotype). a–c, Pycnidia on leaf surface. d–e, Conidial contacts. f, Conidia. Scale bars: a = 100 µm, b = 500 µm, c = 200 µm, d-f = 10 µm.

DISCUSSION

Heterosporicola species have been reported as pathogens on *Chenopodium* species (Boerema, 1997; De Gruyter *et al.*, 2013 Alves *et al.*, 2013). Among two previously reported *Heterosporicola* species, *H. dimorphospora* is a parasite on species of *Chenopodium* in North- and South-America (van der Aa and van Kesteren, 1979). In some parts of South America, this fungus causes eye-shaped stem lesions on *Chenopodium quinoa* (van der Aa and van Kesteren, 1979). *Heterosporicola chenopodii* (= *Phoma variospora*) is a very common pathogen on species of *Chenopodium* in Europe. On account of the septate macroconidia *in vivo, H. chenopodii* is sometimes confused with *Ascochyta caulina*. *Heterosporicola* is closely related to *Subplenodomus*. No sexual morph is known for *Heterosporicola* (De Gruyter *et al.*, 2013).

The new species reported here, *H. beijingense*, produces "bird eye"-like yellowish brown to reddish brown spots in characteristic circular arrangements on living *Chenopodium quinoa* leaves. However, *Heterosporicola chenopodii* produces pale yellowish brown or whitish leaf spots with narrow purplish-brown borders mostly on *C. album*, while *H. dimorphospora* formed pale brown leaf spots or eye-shaped lesions on stems especially on *C. quinoa* (Boerema *et al.*, 1997).

Morphological differences between *H. beijingense*, *H. chenopodii* and *H. dimorphospora* are described in Table 2, and it is clear that these three species differ from one another in conidiomata, conidiogenous cell and conidium dimensions. The other two *Heterosporicola* species produce two types of conidia (macro- and micro-conidia). However, we did not observe macroconidia in *H. beijingense*.

We could not obtain axenic cultures for this species on PDA and MEA or oatmeal agar (OA), either by single spore isolation or tissue isolation methods. However, *H. chenopodii* and *H. dimorphospora* are known from cul-

Table 2. Morphological comparison of *Heterosporicola* species.

Species name	Size (μm)				References
	Conidiomata width	Conidiomatal wall	Conidiogenous cells	Conidia	
H. chenopodii	100–550 wide	6–14	4–10	Macroconidia 15–20(–27) × (3–)3.5–4.5, Microconidia 3–6 × 1.2–1.7	van der Aa and van Kesteren (1979)
H. dimorphospora	80–200 seldom up to 300 wide	10–25	3–8	Macroconidia 16.2–22.5(25) × 3.8– 4.5(7) Microconidia 4.2–5.0 × 2–2.5	van der Aa and van Kesteren (1979)
H. beijingense	200–600 wide	15–60	4–8 × 4–6	Macroconidia not observed Microconidia 3.8–4.4 × 1.4–2.1	This study

tures on different media including PDA and OA (Boerema *et al.*, 1997). *Heterosporicola beijingense* may have specific growth requirements for macroconidium production.

This study focused on identifying fungal species associated with leaf spots on quinoa, and confirmation of their identity. Data were not collected to estimate disease severity, incidence and pathogenicity of *Heterosporicola beijingense*. Pathogenicity experiments, disease severity and incidence evaluations with appropriate field trials are recommended to confirm the pathogenicity of this species.

ACKNOWLEDGEMENTS

This study was funded by grants from the Thailand Research Fund (project No. TRG5880152) and the Mushroom Research Foundation. Rashika Brahmanage thanks Prof. Alan Phillips, Dr Kasun Thambugala, Dr Ruvishika Jayawardena and Ms Pranami Abeywickrama for their helpful comments and advice. Mei Liu thanks the Beijing Agriculture Innovation Consortium (BAIC07-2020) and the project of Improvement and Demonstration of Simplified and High-efficiency Cultivation Techniques of quinoa (Item Number: 20180311). D.N. Wanasinghe thanks the CAS President's International Fellowship Initiative (PIFI) for funding his postdoctoral research (number 2019PC0008), the National Science Foundation of China and the Chinese Academy of Sciences gave financial support (Grant numbers 41761144055, 41771063 and Y4ZK111B01). Rajesh Jeewon thanks the University of Mauritius for support.

LITERATURE CITED

Ariyawansa H.A., Phukhamsakda C., Thambugala K.M., Bulgakov T.S., Wanasinghe D.N., … Bahkali A.H., 2015. Revision and phylogeny of Leptosphaeriaceae. *Fungal Diversity* 74: 19–51.

Alandia S, Otazu´ V, Salas B., 1979. Enfermedades. In: Tapia M, ed. Quinua Y Kañiwa Cultivos Andinos. Bogota´, Colombia: Instituto Interamericano de Ciencias Agrı´colas, Turrialba, Costa Rica, 137–48.

Aveskamp M.M., De Gruyter J., Woudenberg J.H.C., Verkley G.J.M., Crous P.W., 2010. Highlights of the Didymellaceae: a polyphasic approach to characterize *Phoma* and related pleosporalean genera. *Studies in Mycology* 65: 1–60.

Alves J.L., Woudenberg J.H.C., Durate L.L., Crousand P.W., Barreto R.W., 2013. Reappraisal of the genus *Alternariaster* (Dothideomycetes). *Persoonia* 31: 77–85.

Boerema G.H., Mathur S.B., Neergaard P., 1977. *Ascochyta hyalospora* (Cooke &Ell.) comb. nov. in seeds of *Chenopodium quinoa*. *Netherlands Journal of Plant Pathology* 83: 153–159.

Boerema G.H., 1997. Contributions toward a monograph of *Phoma* (coelomycetes) V. Subdivision of the genus in sections. *Mycotaxon* 64: 321–333.

Brahmanage R.S., Wanasinghe D.N., Dayarathne M.C., Jeewon R., Yan J., … Li X., 2019. Morphology and phylogeny reveal *Stemphylium dianthi* sp. nov. and new host records for the sexual morphs of *S. beticola*, *S. gracilariae*, *S. simmonsii* and *S. vesicarium* from Italy and Russia. *Phytotaxa* 411: 243–263.

Carbone I., Kohn L.M., 1999. A method for designing primer sets for speciation studies in filamentous ascomycetes. *Mycologia* 91: 553–556.

Chomnunti P., Hongsanan S., Aguirre-Hudson B., Tian Q., Peršoh D., Dhami M.K., … Hyde K.D., 2014. The sooty moulds. *Fungal Diversity* 66: 1–36.

Dayarathne M.C., Phookamsak R., Ariyawansa H.A., Jones E.B.G., Camporesi E., Hyde K.D., 2015. Phylogenetic and morphological appraisal of *Leptosphaeria italica* sp. nov. (*Leptosphaeriaceae*, Pleosporales) from Italy. *Mycosphere* 6: 634–642.

De Gruyter J., Woudenberg J.H.C., Aveskamp M.M., Verkley G.J.M., Groenewald J.Z., Crous P.W., 2013. Redisposition of Phoma-like anamorphs in Pleosporales. *Studies in Mycology* 75: 1–36.

Dini A., Rastrelli L., Saturnino P., Schettino O., 1992. A compositional study of *Chenopodium quinoa* seeds. *Nahrung* 36: 400–404.

Hall T.A., 1999. BioEdit: a user-friendly biological sequence alignment editor and analysis program for Windows 95/98/NT. In: *Nucleic Acids Symposium series* 41: 95–98.

Huelsenbeck J.P., Ronquist F., 2001. MRBAYES: Bayesian inference of phylogenetic trees. *Bioinformatics* 17: 754–755. https://www.ncbi.nlm.nih.gov/nucleotide (accessed: January 2020).

Hyde K.D., Chaiwan N., Norphanphoun C., Boonmee S., Camporesi E., … Zhao Q., 2018. Mycosphere notes 169–224. *Mycosphere* 9: 271–430.

Index Fungorum, 2020. http://www.indexfungorum.org/Names/Names.asp. (accessed: January 2020).

Jayasiri S.C., Hyde K.D., Ariyawansa H.A., Bhat J., Buyck B., … Promputtha I., 2015. The Faces of Fungi database: fungal names linked with morphology, phylogeny and human impacts. *Fungal Diversity* 74 3–18.

Jeewon R. Hyde K.D., 2016. Establishing species boundaries and new taxa among fungi: recommendations to resolve taxonomic ambiguities. *Mycosphere* 7: 1669–1677.

Kuraku S., Zmasek C.M., Nishimura O. Katoh K., 2013. A Leaves facilitates on-demand exploration of metazoan gene family trees on MAFFT sequence alignment server with enhanced interactivity. *Nucleic Acids Research* 41(W1): W22–W28.

Lee M.S., Yang Y.L., Wu C.Y., Chen Y.L., Lee C.K., … Lee T.H., 2019. Efficient identification of fungal antimicrobial principles by tandem MS and NMR database. *Journal of Food and Drug Analysis* 27: 860–868.

Li J., Zhou X., Huang H., Li G., 2017. Diseases characteristic and control measurements for *Chenopodium quinoa* Willd. In 2017 6th International Conference on Energy and Environmental Protection (ICEEP 2017). Atlantis Press, Paris, France, 305–308.

Miller M.A., Pfeiffer W., Schwartz T., 2010. Creating the CIPRES science gateway for inference of large phylogenetic trees. *Proceedings of the Gateway Computing Environments Workshop (GCE)*, New Orleans, LA, 2010, 1–8, DOI: 10.1109/GCE.2010.5676129.

Nylander J.A.A., 2004. MrModeltest 2.2: Program distributed by the author. Evolutionary Biology Centre, Uppsala University, Sweden.

Rambaut A., 2009. FigTree, v. 1.4. 0: 2006–2012.

Rannala B., Huelsenbeck J., Yang Z., R. Nielsen R., 1998. Taxon Sampling and the Accuracy of Large Phylogenies. *Systematic Biology* 47: 702–710.

Rehner S.A., Buckley E.P., 2005. A *Beauveria* phylogeny inferred from nuclear ITS and EF1-alpha sequences: evidence for cryptic diversification and links to *Cordyceps* teleomorphs. *Mycologia* 97: 84–98.

Ronquist F., Huelsenbeck J.P., 2003. MrBayes 3: Bayesian phylogenetic inference under mixed models. *Bioinformatics* 19: 1572–1574.

Ronquist F.M., Teslenko P., Van Der Mark, Ayres D.L., Darling A., … Huelsenbeck J.P., 2012. MrBayes 3.2: efficient Bayesian phylogenetic inference and model choice across a large model space. *Systematic Biology* 61: 539–542.

Schulz B., Wanke U., Drager S., Aust H.J., 1993. Endophytes from herbaceous plants and shrubs: Effectiveness of surface sterilization methods. *Mycological Research* 97: 1447–1450.

Stamatakis A., 2014. RAxML version 8, a tool for phylogenetic analysis and post–analysis of large phylogenies. *Bioinformatics* 30: 1312–1313.

Tapia M., 1997. Cultivos andinos subexplotados y su aporte a la alimentacio´n. FAO-RLAC, Santiago, Chile: 99–103.

Tennakoon D.S., Phookamsak R., Wanasinghe D.N., Yang J.B., Lumyong S., Hyde K.D., 2017. Morphological and phylogenetic insights resolve *Plenodomus sinensis* (Leptosphaeriaceae) as a new species. *Phytotaxa* 324: 73–82.

Testen A.T., Jiménez-Gasco M.D.M., Ochoa J.B., Backman P.A., 2013. Molecular detection of *Peronospora variabilis* in quinoa seed and phylogeny of the quinoa downy mildew pathogen in South America and the United States. *Plant Disease* 104: 379–386.

Valencia-Chamorro S.A., 2003. Quinoa. in: *Encyclopedia of Food Science and Nutrition*, (Caballero B. ed.), Academic Press, Amsterdam, The Netherlands, 4895–4902.

Van der H.A. Van Kesteren H.A., 1979. Some pycnidial fungi occurring on *Atriplex* and *Chenopodium*. *Persoonia-Molecular Phylogeny and Evolution of Fungi* 10: 267–276.

Vega-Galvez A., Miranda M., Vergara J., Uribe E., Puente L. Martinez E.A.,2010. Nutrition facts and functional potential of quinoa (*Chenopodium quinoa* Willd.), an ancient Andean grain: a review. *Journal of the Science of Food and Agriculture* 90: 2541–2547.

Vilca A., 1972. *Estudio de la Mancha Foliar en Quinua*. PhD Tesis, Ing. Agro, Universidad Nacional Técnica del Altiplano de Puno, Perú.

Vilgalys R., Hester M., 1990. Rapid genetic identification and mapping of enzymatically amplified ribosomal

DNA from several Cryptococcus species. *Journal of Bacteriology* 172: 4238–4246.

Wang C.X., Zhao L.G., Mao Q., 2014. A review of characteristics and utilization of *Chenopodium quinoa*. *Journal of Zhejiang A&F University* 31: 296–301.

White T., Bruns T., Lee S., Taylor J., 1990. Amplification and direct sequencing of fungal ribosomal RNA genes for phylogenetics. PCR Protocols, In: *A Guide to Methods and Applications*, Academic Press, London, UK, 482 pp.

Wijayawardene N.N., Hyde K.D., Lumbsch H.T., Liu J.K., Maharachchikumbura S.S., … Phookamsak R., 2018. Outline of Ascomycota, 2017. *Fungal Diversity* 88: 167–263.

Wijayawardene N.N., Papizadeh M., Phillips A.J.L., Wanasinghe D.N., Bhat D.J., … Huang Y.Q., 2017. Mycosphere Essays 19: Recent advances and future challenges in taxonomy of coelomycetous fungi. *Mycosphere* 8: 934–950.

Wright K.H., Pike O.A., Fairbanks D.J., Huber S.C., 2002. Composition of *Atriplex hortensis*, sweet and bitter *Chenopodium quinoa* seeds. *Food Chemical Toxicology* 67: 1383–1385.

Zhaxybayeva O., Gogarten J.P., 2002. Bootstrap, Bayesian probability and maximum likelihood mapping: exploring new tools for comparative genome analyses. *BMC Genomics* 3: 4.

Phytopathologia Mediterranea
The international journal of the
Mediterranean Phytopathological Union

Firenze University Press
www.fupress.com/pm

Research Papers

Fungal pathogens associated with stem blight and dieback of blueberry in northern Italy

Vladimiro GUARNACCIA[1,2,*], Ilaria MARTINO[2], Giulia TABONE[2], Luca BRONDINO[1,3], M. Lodovica GULLINO[1,2]

[1] *Department of Agricultural, Forest and Food Sciences (DISAFA), University of Torino, Largo Braccini 2, 10095 Grugliasco (TO), Italy*
[2] *Centre for Innovation in the Agro-Environmental Sector, AGROINNOVA, University of Torino, Largo Braccini 2, 10095 Grugliasco (TO), Italy*
[3] *Ortofruit Italia Soc. Agr. Coop. O.P., Via Colombaro dei Rossi 16/bis, 12037 Saluzzo (CN), Italy*
*Corresponding author: vladimiro.guarnaccia@unito.it

Summary. *Vaccinium* spp. are cultivated worldwide due to their important commercial value and fruit health benefits. However, the increasing global trade of berries and plants has resulted in major incidence of the diseases related to this crop. Stem blight and dieback associated with different fungal pathogens are the most common symptoms observed, and represent serious threats to blueberry production. Surveys were conducted in highbush blueberry orchards in Cuneo province, Northern Italy, to assess the fungal species diversity associated with stem blight and dieback. A total of 38 isolates were collected from symptomatic plants of the cultivars 'Last Call', 'Blue Ribbon' and 'Top Shelf'. Four fungal species were identified through multi-locus typing and morphological characters: *Neofusicoccum parvum*, *Diaporthe rudis*, *Cadophora luteo-olivacea* and *Peroneutypa scoparia*. Molecular analyses included three different genomic regions: ITS, *tub2*, and *tef1*. Pathogenicity tests showed that all four species were pathogenic to blueberry plants. *Neofusicoccum parvum* was the most aggressive species. The present study increases understanding of the fungi associated with blueberry stem blight and dieback, providing preliminary knowledge for further studies on disease epidemiology and management strategies. This is the first report worldwide of *P. scoparia* and *C. luteo-olivacea* on *Vaccinium corymbosum*, as well as the first report of *D. rudis* on blueberry in Italy.

Keywords. *Vaccinium corymbosum,* multi-locus typing, *Neofusicoccum*, *Diaporthe*, *Cadophora*, *Peroneutypa*.

OPEN ACCESS

Citation: V. Guarnaccia, I. Martino, G. Tabone, L. Brondino, M.L. Gullino (2020) Fungal pathogens associated with stem blight and dieback of blueberry in northern Italy. *Phytopathologia Mediterranea* 59(2): 229-245. DOI: 10.14601/Phyto-11278

Accepted: May 1, 2020

Published: August 31, 2020

Data Availability Statement: All relevant data are within the paper and its Supporting Information files.

Competing Interests: The Author(s) declare(s) no conflict of interest.

Editor: Armengol Forti J., Polytechnical University of Valencia, Spain.

INTRODUCTION

Cultivated highbush blueberry (*Vaccinium corymbosum* L., *Ericaceae*) is a woody deciduous shrub native to North America. Blueberry is an economically important crop, grown in Argentina, Australia, Canada, Chile, China, Europe, Mexico, Morocco, New Zealand, Peru, and USA (FAOSTAT 2019). In Europe, the first plantation of this crop was reported in The Netherlands,

and this region is currently one of the major producers together with Spain, Portugal, Poland, Germany, UK, France and Italy (Retamales and Hancock, 2018). In Italy, blueberry production has been considerably increased since 2010 to 2018, due to adoption of modern agricultural practices and new cultivars able to adapt to diverse pedoclimatic conditions. Total annual production in Italy is 1,675 tonnes of berries (FAOSTAT 2019). The most important blueberry production areas in this country are Trentino Alto Adige, Veneto and Piedmont (Brazelton, 2011). In total, 1,143 ha are cultivated with blueberry, and more than half of this amount (633 ha) are in Piedmont (FAOSTAT 2019).

The berries are highly considered in the food and pharmaceutical industries due to their content of beneficial nutrients (Nestby *et al*., 2011) and bioactive compounds such as antioxidants (Norberto *et al*., 2013). Thus, this crop has received high attention (Ma *et al*., 2018) leading to intercontinental movement of plant material associated with human activities and global changes, resulting in an increased spread of diseases in new cultivation areas (Polashock *et al*., 2017; Hilário *et al*., 2020a,b).

The most common disease symptoms observed in blueberry plantations consist of stem blight and dieback, associated with the presence of fungal pathogens (Lombard *et al*., 2014; Pérez *et al*., 2014; Xu *et al*., 2015; Cardinaals *et al*., 2018; Tennakoon *et al*., 2018; Scarlett *et al*., 2019; Hilário *et al*., 2020b), which limit the longevity of blueberry plants and reduce their fruit yields (Elfar *et al*., 2013). These blight and dieback symptoms have been associated with several fungal species belonging to *Botryosphaeria, Diaporthe*, *Neofusicoccum, Neopestalotiopsis,* and *Phoma*-like genera (McDonald and Eskalen, 2011; Lombard *et al*., 2014; Pérez *et al*., 2014; Xu *et al*., 2015; Cardinaals *et al*., 2018; Tennakoon *et al*., 2018; Scarlett *et al*., 2019; Hilário *et al*., 2020b).

Blueberry stem blight and dieback can be divided into three groups: Botryosphaeria, Fusicoccum and Phomopsis cankers. Botryosphaeria stem canker is mainly related to *Botryosphaeria corticis*, while *B. dothidea* is commonly known as the causal agent of Botryosphaeria stem blight (Polashock *et al*., 2017). However, among the *Botryosphaeriaceae*, different species have been reported in association with highbush blueberry stem cankers and dieback. These include *Botryosphaeria corticis, B. dothidea*, *Diplodia seriata, Lasiodiplodia theobromae*, *Neofusicoccum arbuti, N .australe, N. luteum, N. nonquaesitum*, *N. parvum,* and *N. ribis* (Phillips *et al*., 2006; Wright and Harmon, 2010; Pérez *et al*., 2014; Xu *et al*., 2015). Fusicoccum canker, also known as Godronia canker, is caused by *Godronia cassandrae* f. sp. *vaccinii* (synonym *Fusicoccum putrefaciens*), which has been reported to cause severe losses in North America and Europe (Strømeng and Stensvand, 2011).

Phomopsis canker is caused by *Phomopsis vaccinii*, known as *Diaporthe vaccinii* after the abolition of the dual nomenclature (Schoch *et a*l., 2012; Lombard *et al*., 2014). In Europe, *D. vaccinii* has been reported in Lithuania, Romania, United Kingdom, Latvia and the Netherlands and is included in the EPPO A2 list (Lombard *et al*., 2014; Cardinaals *et al*., 2018). However, several other *Diaporthe* spp. have been detected on blueberry bushes, causing twig blight, stem cankers and fruit rot. *Diaporthe eres* has been reported in Croatia (Ivić *et al*., 2018), and in the Netherlands with *D. rudis* (Lombard *et al*., 2014), while *D. ambigua*, *D. australafricana*, *D. foeniculina* and *D. passiflorae* have been found in Chile (Latorre *et al*., 2012; Elfar *et al*., 2013). Lombard *et al*. (2014) described *D. asheicola*, *D. baccae*, and *D. sterilis* as new species associated with wood diseases of blueberry plants from Chile and Italy.

Fungal species in *Botryosphaeriaceae* and *Diaporthe* are well known as endophytic, latent and woody pathogens on a wide range of host plants (Xu *et al*., 2015; Marsberg *et al*., 2017; Marin-Felix *et al*., 2017). The endophytic phase could persist until stressful conditions for plant growth arise, after which symptoms can occur (Slippers and Wingfield, 2007). Due to this behaviour, these pathogens are often not detected by quarantine systems (Marsberg *et al*., 2017). Different fungal species could also coexist on the same host, so disease diagnoses based on symptoms or on fungal morphological traits are not reliable (Michalecka *et al*., 2017). A multigene approach to phylogenetic analyses is needed to obtain a high level of confidence in pathogen identifications (Elfar *et al*., 2013; Lombard *et al*., 2014).

During the spring of 2019, stem blight and dieback symptoms were observed in several blueberry orchards in Piedmont, Northern Italy. The present study aimed to: (i) assess the fungal species diversity associated with stem blight and dieback using molecular and phylogenetic tools; (ii) establish morphological analyses of the species identified and determine the average growth rate at different temperatures; and (iii) test the pathogenicity of the species obtained to compare their virulence and to fulfil Koch's postulates.

MATERIALS AND METHODS

Field sampling and fungal isolation

Surveys were carried out from March to September 2019, in four blueberry plantations in Lagnasco (CN),

Piedmont, Northern Italy. Samples from symptomatic plants of 'Last Call', 'Blue Ribbon' and 'Top Shelf' were collected from wilted stems and branches and canker lesions. Disease incidence (DI) was assessed on approx. 60 plants in each of the four orchards in June, and the average percentage of symptomatic and dead plants was determined. Ten symptomatic plants were collected from each orchard. All the investigated plantations were covered by anti-hail nets, and represented high relative humidity levels up to 78%. The wood samples (5–10 mm) were surface sterilised in 70% ethanol for 1 min, rinsed in sterile distilled water (SDW) for 1 min, and then dried on sterile absorbent paper. Small fragments (2–3 mm) were cut from the edges of healthy and necrotic tissues and plated on potato dextrose agar (PDA, Oxoid) amended with 100 μg mL^{-1} of streptomycin sulphate (PDA-S, Sigma-Aldrich). The plates were incubated at 25 ± 1°C under a 12 h photoperiod. Following 48 to 72 h of incubation, mycelium plugs from the margins of resulting colonies were placed on new PDA plates. After 5 d, pure cultures were established from single hyphal tip transfers.

A total of 38 isolates were obtained and used for molecular characterization (Table 1). Stock cultures of these isolates are kept at -80°C in the AGROINNOVA Centre of Competence (University of Torino) culture collection, Torino, Italy.

DNA extraction, polymerase chain reaction (PCR) amplification, and sequencing

For all fungal isolates, total DNA was extracted from 0.1 g of mycelium grown on PDA, using the E.Z.N.A.® Fungal DNA Mini Kit (Omega Bio-Tek), following the manufacturer's instructions. Species identification was achieved through DNA amplification and sequencing of a combined dataset of genes: the nuclear ribosomal internal transcribed spacer (ITS) region, and partial regions of the β-tubulin (*tub2*) and translation elongation factor-1α (*tef1*) genes. ITS region of each isolate was amplified using the universal primers ITS1 and ITS4 (White *et al*., 1990). The primers EF1-728F and EF1-986R (Carbone and Kohn, 1999) were used to amplify part of the *tef1* gene in isolates identified as *Neofusicoccum* spp. (Marin-Felix *et al*., 2017), *Diaporthe* spp., and *Cadophora* spp. (Marin-Felix *et al*., 2019). The primers T1 and Bt2b (Glass and Donaldson, 1995; O'Donnell and Cigelnik, 1997) were used to amplify the partial *tub2* gene in isolates identified as *Neofusicoccum* spp. (Marin-Felix *et al*., 2017), *Diaporthe* spp. (Guarnaccia *et al*., 2018; Marin-Felix *et al*., 2019), and *Peroneutypa* spp. (Carmarán *et al*., 2006). The PCR amplification mixtures and cycling conditions adopted for all three loci were followed as described in each of the cited references (above). An amount of 5 μL of PCR product for each PCR reaction was examined by electrophoresis at 100V on 1% agarose (VWR Life Science AMRESCO® biochemicals) gels stained with GelRedTM. PCR products were sequenced in both directions by Eurofins Genomics Service (Ebersberg). The DNA sequences generated were analysed and consensus sequences were computed using the program Geneious v. 11.1.5 (Auckland, New Zealand).

Phylogenetic analyses

New sequences obtained in this study were blasted against the NCBI's GenBank nucleotide database to determine the closest relatives for a taxonomic framework of the studied isolates. Alignments of different gene regions, including sequences obtained from this study and sequences downloaded from GenBank, were initially performed with the MAFFT v. 7 online server (http://mafft.cbrc.jp/alignment/server/index.html) (Katoh and Standley 2013), and then manually adjusted in MEGA v. 7 (Kumar *et al.,* 2016).

An initial phylogenetic analysis was conducted using 38 ITS sequences of isolates collected in this study and 38 reference strains deposited in GenBank (Table 1), to give an overview of genus identification. The analysis included sequences from 76 isolates spanning the different genera selected on the preliminary results provided by BLAST analysis and one outgroup taxon (*Colletotrichum gloeosporioides* ICMP 17821). To then distinguish the isolates at species level, a subset of representative isolates was selected based on the results of the overview ITS analysis, and was processed through different phylogenetic analyses conducted individually for each locus (data not shown) and as multilocus sequence analyses using the following locus combinations: ITS, *tef1* and *tub2* for members of *Neofusicoccum* and *Diaporthe* (Marin-Felix *et al*., 2017; 2019); ITS and *tub2* for members of *Peroneutypa* and close species of the *Diatrypaceae* (Trouillas *et al*., 2010; 2011); and ITS and *tef1* for isolates related to *Cadophora* (Travadon *et al*., 2015). The ex-type strain of *Diplodia seriata* (CBS 110875; Marin-Felix *et al*., 2017) was used as the outgroup for the analysis of *Neofusicoccum* spp., and *Diaporthella corilina* (CBS 121124; Marin-Felix *et al*., 2019) was used as outgroup for *Diaporthe* spp. *Liberomyces pistaciae* (CBS 144225; Vitale *et al*., 2018), was used as the outgroup for *Diatrypaceae*, and *Neofusicoccum parvum* (CBS 110301; Travadon *et al*., 2015) were used as the outgroup for *Cadophora* spp. The phylogenies were based on Bayesian

Table 1. Collection details and GenBank accession numbers of isolates included in this study.

Species	Isolate code[1]	Country	Host	Genbank accession number[2]		
				ITS	*tub2*	*tef1*
Cadophora fastigiata	CBS 307.49^T	Sweden	-	AY249073	KM497131	KM497087
Cadophora finlandica	CBS 444.86^T	Finland	-	AF486119	KM497130	KM497086
Cadophora luteo-olivacea	CBS 128571	Spain	*Vitis vinifera*	HQ661085	-	HQ661070
	CBS 128576	Spain	*Vitis vinifera*	HQ661092	-	HQ661077
	CBS 141.41^T	Sweden	-	AY249066	KM497133	KM497089
	CVG 650*	Italy	*Vaccinium corymbosum* 'Blue Ribbon'	*MT261874*	-	MT293544
	CVG 651	Italy	*Vaccinium corymbosum* 'Blue Ribbon'	*MT261875*	-	-
	CVG 652	Italy	*Vaccinium corymbosum* 'Blue Ribbon'	*MT261876*	-	*MT293545*
	CVG 653	Italy	*Vaccinium corymbosum* 'Blue Ribbon'	MT261877	-	-
	CVG 654	Italy	*Vaccinium corymbosum* 'Blue Ribbon'	*MT261878*	-	*MT293546*
	CVG 655	Italy	*Vaccinium corymbosum* 'Blue Ribbon'	*MT261879*	-	-
Cadophora malorum	CBS 165.42^T	Netherlands	*Amblystoma mexicanum*	AY249059	KM497134	KM497090
Cadophora novi eboraci	CBS 101359	Italy	*Actinidia chinensis*	DQ404350	KM497135	KM497092
	NYC13	USA	*Vitis vulpina*	KM497036	KM497117	KM497073
Cadophora melini	CBS 268.33^T	Sweden	-	AY249072	KM497132	KM497088
	U11	USA	*Vitis vinifera* 'Sangiovese'	KM497032	KM497113	KM497069
Cadophora orientoamericana	NYC11	USA	*Vitis vinifera* 'Chardonnay'	KM497024	KM497105	KM497061
	NYC3	USA	*Vitis labruscana* 'Concord'	KM497021	KM497102	KM497058
Cadophora spadicis	CBS111743	Italy	*Actinidia chinensis*	DQ404351	KM497136	KM497091
Cryptosphaeria subcutanea	CBS 240.87	Norway	*Salix borealis*	KT425232	KT425167	-
Diaporthella corylina	CBS 121124^T	China	*Corylus*	KC343004	KC343972	KC343730
Diaporthe acaciigena	CBS 129521	Australia	*Acacia retinoges*	KC343005	KC343973	KC343731
Diaporthe ampelina	CBS 114016^T	France	*Vitis vinifera*	AF230751	JX275452	GQ250351
Diaporthe amygdali	CBS 126679^T	Portugal	*Prunu dulcis*	KC343022	KC343990	KC343748
Diaporthe arecae	CBS 535.75	Suriname	*Citrus* sp.	KC343032	KC344000	KC343758
Diaporthe australfricana	CBS 111886	Australia	*Vits vinifera*	KC343038	KC344006	KC343764
Diaporthe baccae	CBS 136972^T	Italy	*Vaccinium corymbosum*	KJ160565	MF418509	KJ160597
Diaporthe carpini	CBS 114437	Sweden	*Carpinus betulus*	KC343044	KC344012	KC343770
Diaporthe citri	CBS 135422	USA	*Citrus* sp.	KC843311	KC843187	KC843071
Diaporthe eres	CBS 116953	New Zeland	*Pyrus pyrifolia*	KC343147	KC344115	KC343873
	CBS 138594	Germany	*Ulmus laevis*	KJ210529	KJ420799	KJ210550
Diaporthe notophagi	BRIP 54801^T	Australia	*Notophagus cunninghamii*	JX862530	KF170922	JX862536
Diaporthe perjuncta	CBS 109745^T	Austria	*Ulmus glabra*	KC343172	KC344140	KC343898
Diaporthe phaseolorum	CBS 127465	New Zeland	*Actinidia chinensis*	KC343174	KC344142	KC343900
Diaporthe rudis	CBS 113201	Portugal	*Vits vinifera*	KC343234	KC344202	KC343960
	CBS 114436	Sweden	*Sambucus* cf. *racemosa*	KC343236	KC344204	KC343962
	CBS 114011	Portugal	*Vitis vinifera*	KC343235	KC344203	KC343961
	CBS 266.85	Netherlands	*Rosa rugosa*	KC343237	KC344205	KC343963
	CVG 658*	Italy	*Vaccinium corymbosum* 'Last Call'	*MT261894*	-	-
	CVG 659	Italy	*Vaccinium corymbosum* 'Last Call'	*MT261895*	*MT293528*	*MT293536*
	CVG 660	Italy	*Vaccinium corymbosum* 'Last Call'	*MT261896*	*MT293529*	*MT293537*
	CVG 661	Italy	*Vaccinium corymbosum* 'Last Call'	*MT261897*	*MT293530*	*MT293538*
	CVG 662	Italy	*Vaccinium corymbosum* 'Last Call'	*MT261898*	*MT293531*	*MT293539*
Diaporthe sterilis	CBS 136969^T	Italy	*Vaccinium corymbosum*	KJ160579	KJ160528	KJ160611
Diaporthe toxica	CBS 594.93^T	Australia	*Lupinus angustifolis*	KC343220	KC344188	KC343946
Diaporthe vaccinii	CBS 160.32^T	USA	*Vaccinium macrocarpon*	AF317578	KC344196	GQ250326

(Continued)

Table 1. (Continued).

Species	Isolate code[1]	Country	Host	Genbank accession number[2]		
				ITS	*tub2*	*tef1*
	CBS 118571	USA	*Vaccinium corymbosum*	KC343223	KC344191	KC343949
	CBS 122114	USA	*Vaccinium corymbosum*	KC343225	KC344193	KC343951
Diatrype stigma	DCASH200	USA	*Quercus* sp.	GQ294003	GQ293947	-
Diatrypella atlantica	HUEFS 194228	Brazil	-	KR363998	KM396615	-
Diatrypella pulvinata	CBS 181.97	Netherlands	*Quercus robur*	-	AJ302443	-
Diplodia seriata	CBS 110875	South Africa	*Vitis vinifera*	AY343456	KX464827	KX464592
Eutypa cremea	CBS 120837	South Africa	*Prunus salicina*	KY752762	KY752791	-
Eutypa lata	ADSC300	Australia	*Schinus molle* var. *areira*	HQ692610	HQ692493	-
	CBS 121430	South Africa	*Prunus armeniaca*	KY752766	KY752794	-
	EP18	New South Wales	*Vitis vinifera*	HQ692611	HQ692501	-
	SACEA01	Australia	*Ceanothus*sp.	HQ692615	HQ692499	-
Eutypa leptoplaca	ADFIC100	Australia	*Ficus macrophylla*	HQ692608	HQ692485	-
Eutypa maura	CBS 219.87	Switzerland	*Acer pseudoplatanus*	AY684224	DQ006967	-
Eutypa tetragona	CBS 284.87	France	*Sarothamnus scoparius*	DQ006923	DQ006960	-
Eutypella cerviculata	CBS 221.87	Switzerland	*Alnus glutinosa*	AJ302468	-	-
Eutypella citricola	STEU 8098	South Africa	*Vitis vinifera*	KY111634	KY111588	-
Eutypella microtheca	STEU 8107	South Africa	*Vitis vinifera*	KY111629	KY111608	-
Eutypella vitis	MSUELM13	USA	*Vitis vinifera*	DQ006943	DQ006999	-
Liberomyces pistaciae	CBS 144225	Italy	*Pistacia vera*	MH797562	MH797697	-
Neofusicoccum algeriense	CBS 137504^T	Mexico	*Rubus idaeus*	KJ657702	-	KJ657715
Neofusicoccum arbuti	CBS 116131^T	USA: Washington	*Arbutus menziesii*	AY819720	KF531793	KF531792
Neofusicoccum australe	CBS 139662^T	Australia	*Acacia* sp.	AY339262	AY339254	AY339270
	CBS 121115	South Africa	*Prunus persica*	EF445355	KX464948	EF445386
Neofusicoccum batangarum	CBS 124924^T	Cameroon	*Terminalia catappa*	FJ900607	FJ900634	FJ900653
Neofusicoccum cryptoaustrale	CBS 122813^T	South Africa	*Eucalyptus* sp.	FJ752742	FJ752756	FJ752713
Neofusicoccum italicum	MFLUCC 15-0900^T	Italy	*Vitis vinifera*	KY856755	-	KY856754
Neofusicoccum kwambonambiense	CBS 102.17^T	USA: Florida	*Carya illinoensis*	KX464169	KX464964	KX464686
Neofusicoccum luteum	CBS 562.92^T	New Zealand	*Actinidia deliciosa*	KX464170	KX464968	KX464690
Neofusicoccum mangiferae	CBS 118532	Australia	*Mangifera indica*	AY615186	AY615173	DQ093220
Neofusicoccum mediterraneum	CBS 121718^T	Greece	*Eucalyptus* sp.	GU251176	-	GU251308
Neofusicoccum parvum	CBS 123650	South Africa	*Syzygium cordatum*	KX464182	KX464994	KX464708
	CMW 9081^T	New Zealand	*Populus nigra*	AY236943	AY236917	AY236888
	CVG 444*	Italy	*Vaccinium corymbosum* 'Top Shelf'	*MT261980*	*MT293532*	*MT293540*
	CVG 445	Italy	*Vaccinium corymbosum* 'Top Shelf'	*MT261981*	-	-
	CVG 446	Italy	*Vaccinium corymbosum* 'Top Shelf'	*MT261982*	-	-
	CVG 642	Italy	*Vaccinium corymbosum* 'Top Shelf'	*MT261983*	*MT293533*	*MT293541*
	CVG 643	Italy	*Vaccinium corymbosum* 'Top Shelf'	*MT261984*	-	-
	CVG 644	Italy	*Vaccinium corymbosum* 'Top Shelf'	*MT261985*	-	-
	CVG 645	Italy	*Vaccinium corymbosum* 'Top Shelf'	*MT261986*	-	-
	CVG 646	Italy	*Vaccinium corymbosum* 'Top Shelf'	*MT261987*	-	-
	CVG 647	Italy	*Vaccinium corymbosum* 'Top Shelf'	*MT261988*	*MT293534*	*MT293542*
	CVG 648	Italy	*Vaccinium corymbosum* 'Top Shelf'	*MT261989*	-	-
	CVG 649	Italy	*Vaccinium corymbosum* 'Top Shelf'	MT261990	-	-

(Continued)

Table 1. (Continued).

Species	Isolate code[1]	Country	Host	Genbank accession number[2]		
				ITS	*tub2*	*tef1*
	CVG 656	Italy	*Vaccinium corymbosum* 'Top Shelf'	*MT261991*	-	-
	CVG 657	Italy	*Vaccinium corymbosum* 'Top Shelf'	*MT261992*	*MT293535*	*MT293543*
Neofusicoccum pistaciarum	CBS 113083^T	USA, California	*Pistacia vera*	KX464186	KX464998	KX464712
Neofusicoccum protearum	CBS 114176	South Africa	*Leucadendron laureolum*	AF452539	KX465006	KX464720
Neofusicoccum stellenboschiana	CBS 110864^T	South Africa	*Vitis vinifera*	AY343407	KX465047	AY343348
	CBS 121116	South Africa	*Prunus armeniaca*	EF445356	KX465049	EF445387
Neofusicoccum terminaliae	CBS 125264	South Africa	*Terminalia sericea*	GQ471804	KX465053	GQ471782
Neofusicoccum vitifusiforme	CBS 110887^T	South Africa	*Vitis vinifera*	AY343383	KX465061	AY343343
Peroneutypa alsophila	CBS 250.87	France	*Arthrocnemum fruticosum*	AJ302467	-	-
Peroneutypa curvispora	HUEFS 136877	Brazil	-	KM396646	-	-
Peroneutypa diminutiasca	MFLUCC 17-2144	Thailand	-	MG873479	MH316765	-
Peroneutypa diminutispora	HUEFS 192196	Brazil	-	KM396647	-	-
Peroneutypa kochiana	F-092, 373	Spain	*Atriplex halimus*	AJ302462	-	-
Peroneutypa longiasca	MFLUCC 17-0371	Thailand	-	MF959502	-	-
Peroneutypa mackenziei	MFLUCC 16-0072	Thailand	-	KY283083	KY706363	-
Peroneutypa rubiformis	MFLUCC 17-2142	Thailand	-	MG873477	MH316763	-
Peroneutypa scoparia	CBS 242.87	France	*Robinia pseudoacacia*	AJ302465	-	-
	DFMAL100	France	*Robinia pseudoacacia*	GQ293962	GQ294029	-
	MFLUCC 17-2143	Thailand	-	MG873478	MH316764	-
	CVG 561*	Italy	*Vaccinium corymbosum* 'Blue Ribbon'	*MT261914*	*MT293522*	-
	CVG 562	Italy	*Vaccinium corymbosum* 'Blue Ribbon'	*MT261915*	*MT293523*	-
	CVG 563	Italy	*Vaccinium corymbosum* 'Blue Ribbon'	*MT261916*	MT293524	-
	CVG 564	Italy	*Vaccinium corymbosum* 'Blue Ribbon'	*MT261917*	-	-
	CVG 565	Italy	*Vaccinium corymbosum* 'Blue Ribbon'	*MT261918*	-	-
	CVG 566	Italy	*Vaccinium corymbosum* 'Blue Ribbon'	MT261919	-	-
	CVG 567	Italy	*Vaccinium corymbosum* 'Blue Ribbon'	*MT261920*	-	-
	CVG 568	Italy	*Vaccinium corymbosum* 'Blue Ribbon'	*MT261921*	-	-
	CVG 569	Italy	*Vaccinium corymbosum* 'Blue Ribbon'	*MT261922*	-	-
	CVG 570	Italy	*Vaccinium corymbosum* 'Blue Ribbon'	*MT261923*	*MT293525*	-
	CVG 571	Italy	*Vaccinium corymbosum* 'Blue Ribbon'	*MT261924*	*MT293526*	-
	CVG 572	Italy	*Vaccinium corymbosum* 'Blue Ribbon'	*MT261925*	*MT293527*	-
	CVG 580	Italy	*Vaccinium corymbosum* 'Blue Ribbon'	*MT261926*	-	-
	CVG 581	Italy	*Vaccinium corymbosum* 'Blue Ribbon'	*MT261927*	-	-

[1] BRIP: Plant Pathology Herbarium, Department of Primary Industries, Dutton Park, Queensland, Australia; CBS: Westerdijk Fungal Biodiversity Institute, Utrecht, the Netherlands; CMW: Tree Pathology Co-operative Program, Forestry and Agricultural Biotechnology Institute, University of Pretoria, South Africa; CVG: AGROINNOVA, Grugliasco, Torino, Italy; HUEFS Herbarium of the State University of Feira de Santana; MFLUCC: Mae Fah Luang University Culture Collection, Chiang Rai, Thailand; STEU: University of Stellenbosch, Stellenbosch, South Africa. The strains named ADSC300, DCASH200, DFMAL100, EP18, MSUELM13, NYCs, SACEA01 and U11 were reported on further studies (Trouillas *et al.*, 2010, 2011; Travadon *et al.*, 2015; Moyo *et al.*, 2018). Ex-type and ex-epitype cultures are indicated with ^{T}.
[2] ITS: internal transcribed spacers 1 and 2 together with 5.8S nrDNA; *tub2*: beta-tubulin gene; *tef1*: translation elongation factor 1-α gene. Sequences generated in this study indicated in *italics*.
* Isolates used for phenotypic characterization and pathogenicity test.

Inference (BI) and Maximum Parsimony (MP) for the multi-locus analyses. For BI, the best evolutionary model for each partition was determined using MrModeltest v. 2.3 (Nylander, 2004) and incorporated into the analyses. MrBayes v. 3.2.5 (Ronquist *et al*., 2012) was used to generate phylogenetic trees under optimal criteria per partition. The Markov Chain Monte Carlo (MCMC) analysis used four chains and started from a random tree topology. The heating parameter was set at 0.2 and trees were sampled every 1,000 generations. Analyses stopped when the average standard deviation of split frequencies was below 0.01. The MP analyses were performed using Phylogenetic Analysis Using Parsimony (PAUP) v. 4.0b10 (Swofford, 2003). Phylogenetic relationships were estimated by heuristic searches with 100 random addition sequences. Tree bisection-reconnection was used, with the branch swapping option set on 'best trees', with all characters weighted equally and alignment gaps treated as fifth state. Tree length (TL), consistency index (CI), retention index (RI) and rescaled consistence index (RC) were calculated for parsimony, and the bootstrap analyses (Hillis and Bull, 1993) were based on 1,000 replications. Sequences generated in this study were deposited in GenBank (Table 1).

Phenotypic characterization

Agar plugs (5 mm diam.) of representative strains (CVG 444 – *N. parvum*, CVG 658 – *D. rudis*, CVG 561 – *P. scoparia*, and CVG 650 – *C. luteo-olivacea*) were taken from the edges of actively growing cultures on PDA-S and transferred onto the centre of 9 cm diam. Petri dishes containing 2% water agar supplemented with sterile pine needles (PNA; Smith *et al*., 1996), PDA, malt extract agar (MEA; Oxoid), or synthetic nutrient-poor agar (SNA, Leslie and Summerell, 2006), then incubated at 20–21°C under a 12 h photoperiod to induce sporulation. Colony characters were observed after 10 d, and culture colours were determined (Rayner, 1970). Cultures were examined periodically for the development of conidiomata. Conidium characteristics were examined by mounting fungal structures in SDW, and the lengths and widths of 30 conidia were measured for each isolate using a light microscope at ×400 magnification. The average and standard deviations of conidium dimensions were calculated. Isolate growth rates were determined on PDA plates incubated in the dark at 25°C. Three plates were used for each isolate. After 5 d, radii of colonies were measured, and mean radii were calculated to determine the growth rates for each isolate.

Pathogenicity tests

Pathogenicity tests with four species (*N. parvum*, *D. rudis*, *C. luteo-olivacea* and *P. scoparia*) were performed to evaluate Koch's postulates. Four representative strains of each species (Table 1) were used to inoculate potted 1-y-old healthy blueberry plants ('Duke'). Three plants were inoculated with one isolate for each species. For each inoculation, a sterile scalpel was used to cut a piece of the bark tissue exposing the cambium. Each plant was wounded at five points. Mycelium plugs (5 mm diam.) were taken from 10-d-old cultures on PDA and placed with the mycelium in contact with the internal plant tissues. Each inoculation point was wrapped with Parafilm®. The same number of plants were treated with sterile PDA discs as inoculation controls.

The plants were placed in a growth chamber at 24°C for 3 weeks. After this period, the lengths of lesions developed on the internal woody tissues were measured after removing the bark. Fifteen d after inoculation, the symptom severity (SS) associated with each inoculated species was evaluated as the length of wood lesions induced. The shoots were cut and the bark peeled off and the lengths of vascular discolouration were measured upward and downward from the inoculation points. Small portions (0.5 cm) of symptomatic tissue from the edge of shoot lesions were placed onto PDA to re-isolate the fungal species, and these were identified based on their colony characteristics and ITS sequencing. This trial was conducted twice and each trial was considered a replicate. Because no normal distribution was observed in the lesion dimension data, the Kruskal-Wallis non-parametric test (at $P = 0.05$) was performed to determine significant differences among the strains. The data analysis was conducted using SPSS software 26 (IBM Corporate).

RESULTS

Field sampling and fungal isolation

Symptoms of stem blight were observed on all the surveyed blueberry plants, and cultivars, and in all the orchards surveyed (Table 2). Plant stems with necrotic internal tissues were observed. Dieback and death of the plants occurred in all the orchards investigated (Figure 1). Symptoms were detected on young and mature plants. DI of symptomatic plants was between 20% and 30% in the four sites. The proportions of dead plants averaged 10%. Based on colony morphology, phylogenetic analyses, and conidium characteristics (see below), *Neofusicoccum parvum* was isolated from 'Top Shelf' plants, *Diaporthe rudis* was isolated from 'Last Call', and

Table 2. Origin of fungal isolates obtained from *Vaccinium corymbosum*.

Species	Code	*Vaccinium corymbosum* cv.	Orchard/Locality
Cadophora luteo-olivacea	CVG 650–655	Blue Ribbon	Orchard 1/ Lagnasco (CN)
Diaporthe rudis	CVG 658–662	Last Call	Orchard 2/ Lagnasco (CN)
Neofusicoccum parvum	CVG 444–446	Top Shelf	Orchard 3/ Lagnasco (CN)
	CVG 642–649	Top Shelf	Orchard 4/ Lagnasco (CN)
	CVG 656, CVG 657	Top Shelf	Orchard 4/ Lagnasco (CN)
Peroneutypa scoparia	CVG 561–572	Blue Ribbon	Orchard 1/ Lagnasco (CN)
	CVG 580, CVG 581	Blue Ribbon	Orchard 1/ Lagnasco (CN)

Cadophora luteo-olivacea and *Peroneutypa scoparia* were isolated from 'Blue Ribbon'.

Phylogenetic analysis

The overview phylogenetic analysis of the 38 isolates obtained from blueberry plants showed that six isolates belonged to *Cadophora*, 13 isolates clustered in a clade with *Neofusicoccum* spp., five formed a distinct, well-supported, lineage with *Diaporthe* spp. The remaining 14 isolates grouped with *Peroneutypa* spp. in the clade with other strains belonging to the *Diatrypaceae* (Figure 2). The combined locus phylogeny of *Neofusicoccum* consisted of 24 sequences, *Diaporthe* consisted of 28 sequences, *Cadophora* of 18, and the *Diatrypaceae* of 32 sequences, including outgroups. A total of 1,139 characters (ITS: 1–521, *tef1*: 528–732 and *tub2*: 739–1136) were included in the *Neofusicoccum* phylogenetic analyses. A total of 1,373 characters (ITS: 1–563, *tef1*: 570–975 and *tub2*: 982–1373) were included in the *Diaporthe* phylogenetic analyses. The analyses for the *Cadophora* group consisted of 819 nucleotides (ITS: 1–499 and *tef1*: 506–819), and the analyses of *Diatrypaceae* were based on a total of 974 characters (ITS: 1–593 and *tub2*: 600–974). A maximum of 1,000 equally most parsimonious trees were saved, and characteristics of the combined gene partitions used for each phylogenetic analysis are reported in Table 3. Bootstrap support values from the parsimony analysis were plotted on the Bayesian phylogenies presented in Figures 2 to 6. For both of the Bayesian analyses, MrModeltest recommended the models reported in Table 4. Unique site patterns for each partition and all the parameters of the Bayesian analyses are reported in Table 3. In the *Neofusicoccum* species analysis, four isolates from symptomatic *Vaccinium* plants clustered with the ex-type and one reference strain of *N. parvum* (Figure 3), while the final tree generated for *Diaporthe* showed that four isolates grouped with four reference strains of *D. rudis* (Figure 4). Three isolates clustered with the ex-type and two reference strains of *C. luteo-olivacea* (Figure 5), and six isolates clustered as *P. scoparia* in the phylogenetic tree from the analyses of the *Diatrypaceae* (Figure 6).

Phenotypic characterization

Morphological observations, supported by phylogenetic inference, were described for four known species.

Neofusicoccum parvum

Ten-d-old colonies on PDA (Figure 7A), and MEA, were cottony with entire margins and dark to pale grey aerial mycelium. On SNA, the colonies were powdery, with dark to pale grey aerial mycelium. Colony reverse sides were black to light grey and whitish on PDA (Figure 7B) and MEA, and greyish to white on SNA. Conidia were hyaline, ellipsoidal with rounded apices and flat bases, with dimensions of 17–19 × 4.2–6.4 μm, mean ± SD = 17.9 ± 0.6 × 5.3 ± 0.6 μm. The mean daily colony growth rate at 25°C was 4.7 mm.

Diaporthe rudis

Ten-d-old colonies on PDA (Figure 7C), MEA and SNA were flat and fluffy with entire margins and aerial, white to pale grey mycelium. Colony reverse sides were light buff with greyish to brown halos on PDA (Figure 7D), honey buff on MEA and white on SNA. Alpha-conidia were hyaline, aseptate, smooth, biguttulate and ellipsoidal, with subtruncate bases, with dimensions of 6.5–8.4 × 2–2.5 μm, mean ± SD = 7.5 ± 0.6 × 2.3 ± 0.2 μm. The mean daily colony growth rate at 25°C was 4.9 mm.

Cadophora luteo-olivacea

Ten-d-old colonies on PDA were flat and velvety with smooth margins, and the mycelium was grey to white

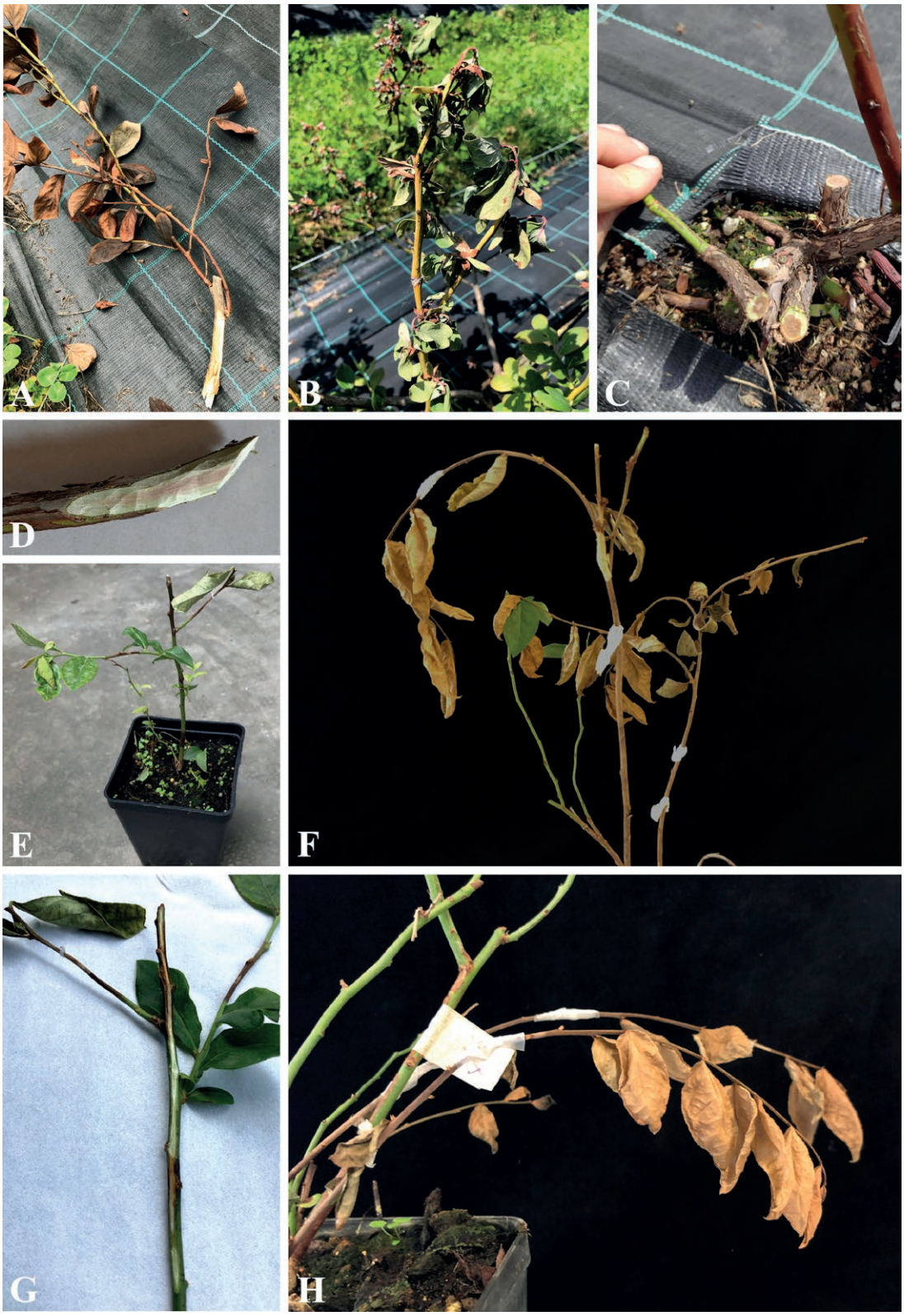

Figure 1. Natural dieback (A) and stem blight (B) of *Vaccinium corymbosum* 'Blue Ribbon' in the field, and a stem showing internal necrosis in the wood of a cultivated plant of 'Top Shelf' (C, D). Wilting and internal discolouration caused by inoculation of *Diaporthe rudis* (E, G), and death of leaves and stems caused by *Neofusicoccum parvum* inoculation (F, H).

Table 3. Parsimony and Bayesian analyses characteristics in this study.

Analysis		Overview tree	*Neofusicoccum*	*Diaporthe*	*Cadophora*	*Peroneutypa*
	Locus(i)	ITS	ITS+*tef1*+*tub2*	ITS+*tef1*+*tub2*	ITS+*tef1*	ITS+*tub2*
Parsimony analysis	Total sites	737	1,124	1,361	847	1,078
	Constant sites	271	854	594	360	425
	Variable sites	76	186	289	204	182
	Parsimony Informative sites	390	84	478	283	471
	Tree length	1,716	368	2,049	779	1,881
	Consistency index	0.579	0.834	0.638	0.883	0.625
	Retention index	0.924	0.850	0.757	0.934	0.809
	Rescaled consistence index	0.535	0.709	0.483	0.825	0.505
Bayesian analysis	Unique site patterns of ITS	474	79	168	137	314
	Unique site patterns of *tef1*	-	79	286	176	-
	Unique site patterns of *tub2*	-	54	184	-	251
	Generation ran	770,000	490,000	1,150,000	1,620,000	390,000
	Generated trees	1542	982	2302	3242	782
	Sampled trees	1158	738	1728	976	588

(Figure 7G). Colonies on MEA were velvety, harbouring fissures, with smooth margins, and grey mycelium. Colonies on SNA were powdery, with light olivaceous mycelium. Colony reverse sides were dark grey to white on PDA (Figure 7H), buff honey on MEA and light olivaceous on SNA. Conidia were hyaline, with up to three guttules, ovoid or oblong ellipsoidal, with dimensions of 4–6.4 × 2–3 µm, mean ± SD = 5.4 ± 0.9 × 2.4 ± 0.4 µm. The mean daily colony growth rate at 25°C was 0.9 mm.

Peroneutypa scoparia

Ten-d-old colonies on PDA (Figure 7E) and MEA were flat and fluffy with entire margins, and white to grey aerial mycelium. Conidiomata were black on PDA and MEA. Colony reverse sides were dark to light grey on PDA (Figure 7F), dark brown to buff honey on MEA, and white on SNA. Conidia were filiform and curved, with dimensions of 10.5–13.8 × 1–1.5 µm, mean ± SD = 12.4 ± 1.3 × 1.2 ± 0.2 µm. The mean daily colony growth rate at 25°C was 1.8 mm.

Pathogenicity

After 30 d, all of the isolates caused lesions on inoculated plants (Figure 8), which were similar to those detected on the field-grown plants, and all the inoculated fungi were re-isolated from plants on which they were inoculated. The frequency of re-isolation was between 90 and 95%. The identities of the respective inoculated and re-isolated species were confirmed using culture and molecular features, fulfilling Koch's postulates. Lesions and internal discolouration were observed in correspondence to the inoculation points (Figure 7). *Neofusicoccum parvum* was the most aggressive pathogen, causing necrotic lesions of average length 5.8 cm. *Diaporthe rudis* caused less severe symptoms on shoots (mean lesions length = 1.5 cm) than *N. parvum*, but with lesion lengths significantly greater than the control plants. *Cadophora luteo-olivacea* and *Peroneutypa scoparia* isolates were the least aggressive with mean lesion lengths, respectively, of 0.9 cm and 0.8 cm. Weak symptoms were observed on control plants (mean lesion length = 0.2 cm), probably due to reaction to wounding. The pairwise comparison obtained from the Kruskal-Wallis test, showed significant differences ($P < 0.05$) between the four isolates and the control. Comparison of the isolates showed significant differences ($P < 0.05$), except for the isolates CVG561 and CVG650 ($P = 0.798$).

DISCUSSION

Blueberry has been cultivated In Italy since the 1970, and is considered as a niche crop (Retamales and Hancock, 2018). Blueberries are included in daily fresh fruit consumption, with annual production of 1,675 tonnes (FAOSTAT 2019). Stem blight and dieback could represent serious threats to this crop. The present study is the first to investigate the species diversity of fungal woody pathogens associated with stem blight and dieback of highbush blueberry in a major production area in Italy. During

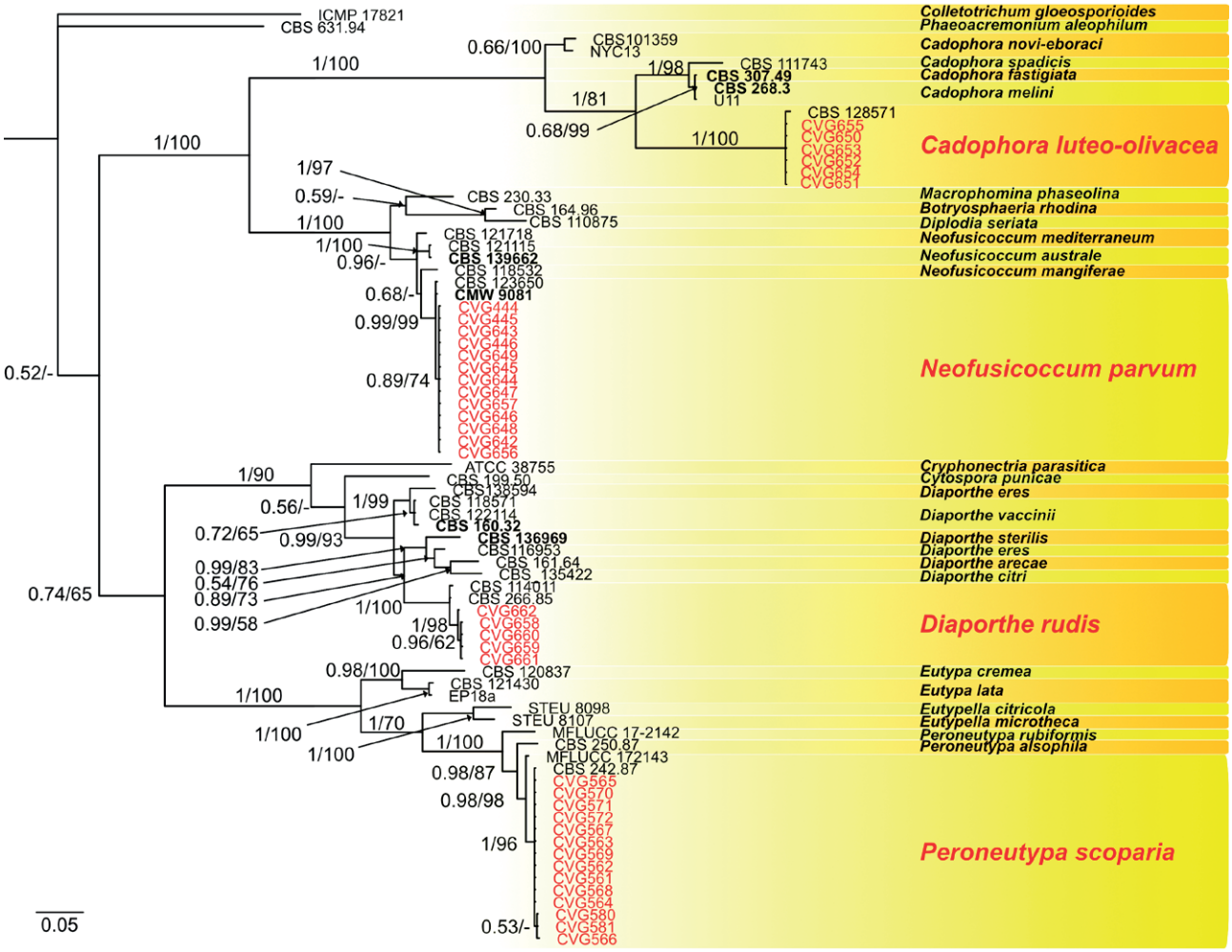

Figure 2. Consensus phylogram of 1,542 trees resulting from a Bayesian analysis of the ITS sequences of 38 fungus isolates collected in this study (in red) and further reference strains. Bayesian posterior probability values and bootstrap support values are indicated at the nodes. The tree was rooted to *Colletotrichum gloeosporioides* (ICMP 17821).

the surveys, the four fungi *Neofusicoccum parvum*, *Diaporthe rudis*, *Cadophora luteo-olivacea* and *Peroneutypa scoparia* were found in association with blueberry stem blight and dieback in four different orchards.

Neofusicoccum parvum has been found in association with blueberry canker and dieback in Asia, Europe, South and North America, (Espinoza *et al.*, 2009; Koike *et al.*, 2014; Xu *et al.*, 2015; Scarlett *et al.*, 2019; Hilário *et al.*, 2020b). In Italy, this fungus has been detected on several fruit plant hosts, as an endophyte and latent pathogen (Carlucci *et al.*, 2013; Guarnaccia *et al.*, 2016; Riccioni *et al.*, 2017; Aiello *et al.*, 2020). In the present study, *N. parvum* was the most aggressive when inoculated on the blueberry 'Duke', which was used for the pathogenicity tests as representative cultivar, because it is the most cultivated worldwide. *Neofusicoccum parvum* produced significant necrotic lesions, progressive discolouration of the internal tissues, and death of inoculated branches This confirms the high level of aggressiveness of this fungus on blueberry, as has been reported previously (Espinoza *et al.*, 2009; Xu *et al.*, 2015; Scarlett *et al.*, 2019; Hilário *et al.*, 2020b).

Diaporthe spp. are well known pathogens occurring as pathogenic or harmless endophytes on blueberry (Latorre *et al.*, 2012; Elfar *et al.*, 2013; Cardinaals *et al.*, 2018; Hilário *et al.*, 2020a), and on other host plants (Guarnaccia *et al.*, 2016; Battilani *et al.*, 2018; Guarnaccia *et al.*, 2018; Guarnaccia and Crous, 2018; Yang *et al.*, 2018). According to Santos *et al.* (2017), molecular tools and multilocus approaches should be used for accurate resolution of species within *Diaporthe*. The present study analysed three sequence

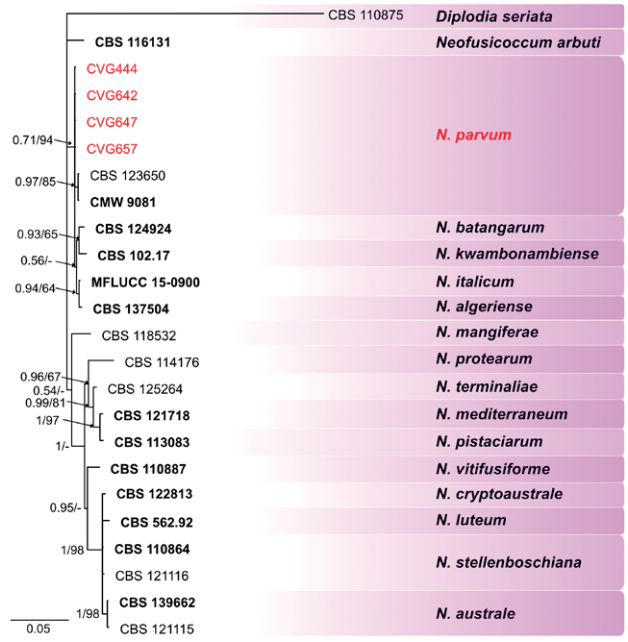

Figure 3. Consensus phylogram of 982 trees resulting from a Bayesian analysis of the combined ITS, *tef1* and *tub2* sequences of *Neofusicoccum* strains. Bayesian posterior probability values and bootstrap support values are indicated at the nodes. The tree was rooted to *Diplodia seriata* (CBS 110875).

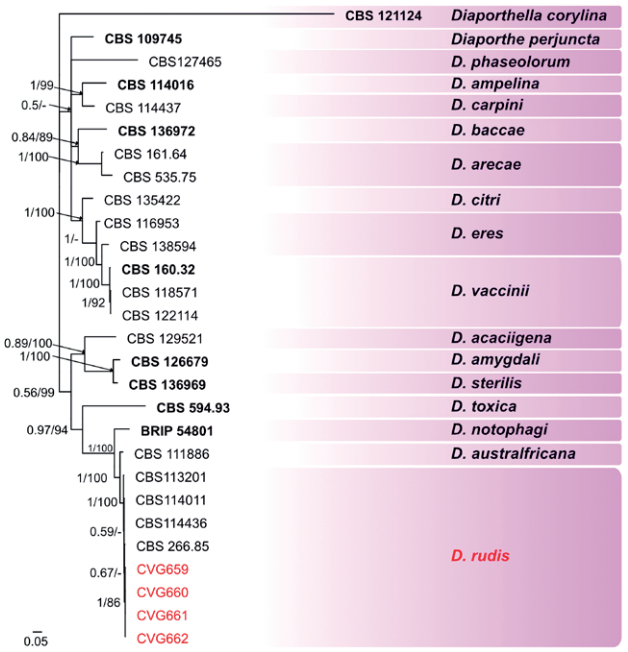

Figure 4. Consensus phylogram of 2,302 trees resulting from a Bayesian analysis of the combined ITS, *tef1* and *tub2* sequences of *Diaporthe* strains. Bayesian posterior probability values and bootstrap support values are indicated at the nodes. The tree was rooted to *Diaporthella corylina* (CBS 121124).

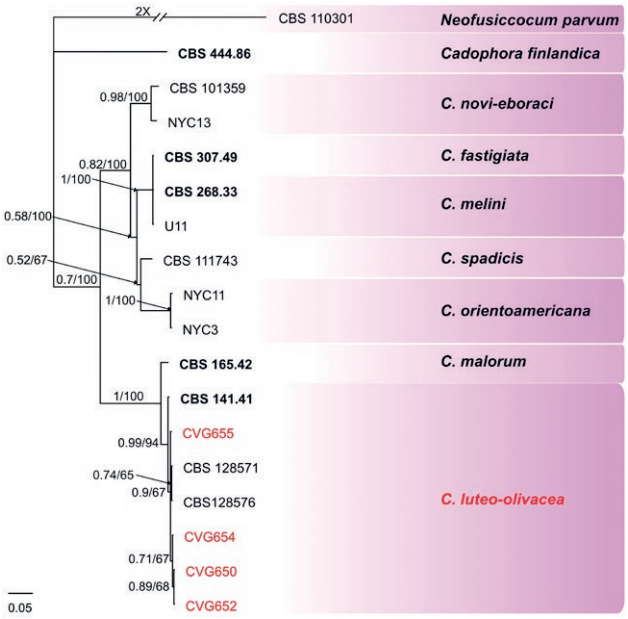

Figure 5. Consensus phylogram of 3,242 trees resulting from a Bayesian analysis of the combined ITS and *tef1* sequences of *Cadophora* strains. Bayesian posterior probability values and bootstrap support values are indicated at the nodes. The tree was rooted to *Neofusicoccum parvum* (CBS 110301).

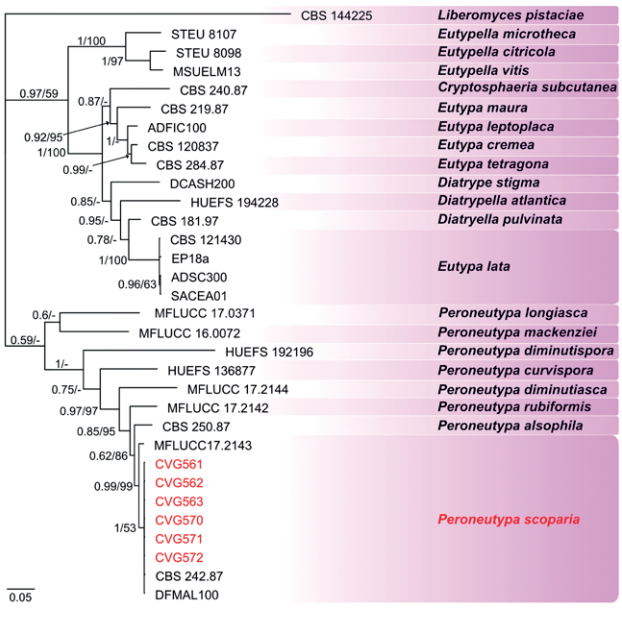

Figure 6. Consensus phylogram of 782 trees resulting from a Bayesian analysis of the combined ITS and *tub2* sequences of *Peroneutypa* and other strains of the Diatrypaceae. Bayesian posterior probability values and bootstrap support values are indicated at the nodes. The tree was rooted to *Liberomyces pistaciae* (CBS 110301).

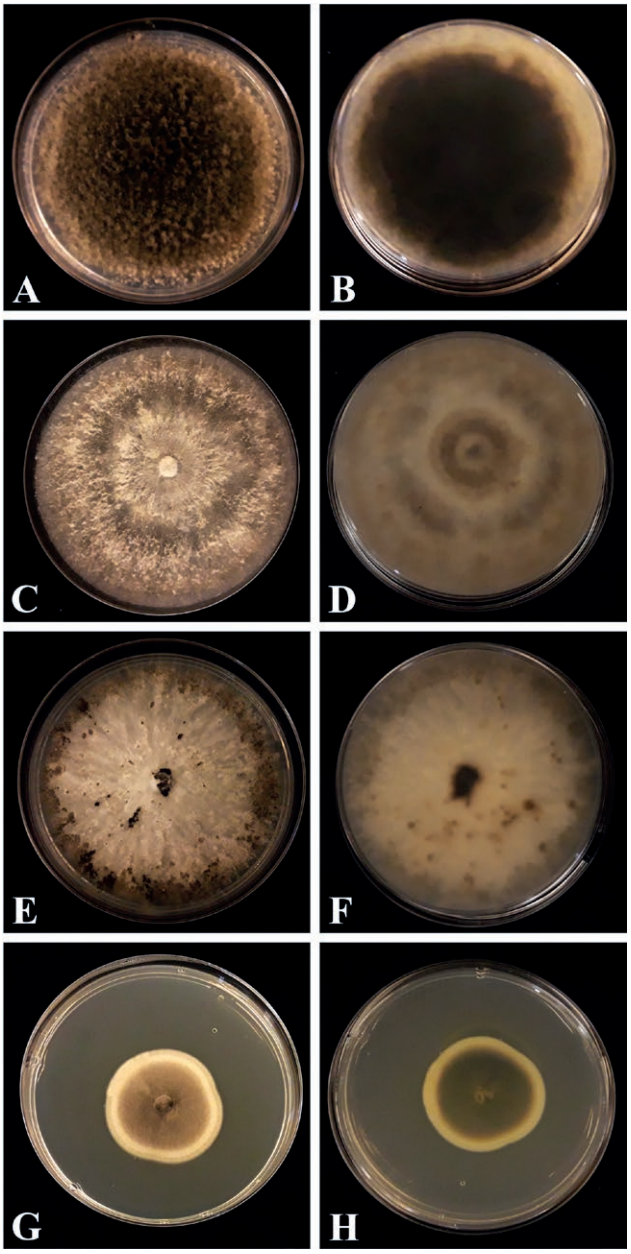

Figure 7. Morphological characteristics of the front and reverse sides of colonies of the different fungal species grown 10 d on PDA. A and B *Neofusicoccum parvum*. C and D *Diaporthe rudis*. E and F. *Peroneutypa scoparia*. G and H *Cadophora luteo-olivacea*.

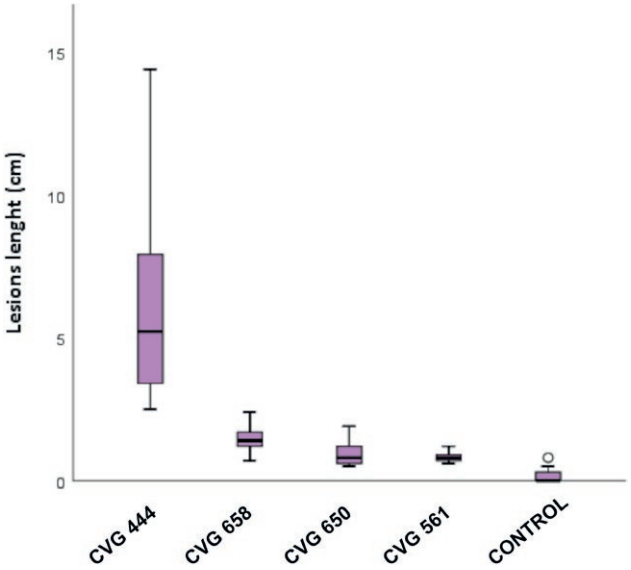

Figure 8. Box plot showing the results of the pathogenicity tests. Boxes represent the interquartile range, while the horizontal line within each box indicates the average value. The Kruskal-Wallis test was carried out to compare the mean lesion lengths (cm) from inoculation with four representative isolates, and significant difference was accepted for $P<0.05$.

Table 4. Evolutionary models as determined by MrModeltest (Nylander 2004).

Genus	Locus	Evolutionary model[1]
Overview tree	ITS	GTR+I+G
Neofusicoccum	ITS	SYM+I+G
	tef1	GTR+I+G
	tub2	HKY+G
Diaporthe	ITS	SYM+I+G
	tef1	GTR+I+G
	tub2	HKY+G
Peroneutypa	ITS	GTR+I+G
	tub2	GTR+G
Cadophora	ITS	SYM+G
	tef1	HKY+G

1 G: Gamma distributed rate variation among sites; GTR: Generalised time-reversible; HKY: Hasegawa-Kishino-Yano; I: Proportion of invariable sites; SYM: Symmetrical model.

datasets (ITS, *tub2*, and *tef1*). *Diaporthe rudis* has been recognized as having a broad host range, and is distributed in Australia, Canada, Chile, Europe, New Zealand and South Africa (Marin-Felix *et al.*, 2019). The present study is the first to report *D. rudis* on *V. corymbosum* in Italy. The pathogenicity tests showed that this species was of intermediate aggressiveness on highbush blueberry plants.

Cadophora luteo-olivacea has been reported in association with grapevine trunk diseases (Gramaje *et al.*, 2011; Travadon *et al.*, 2015; Raimondo *et al.*, 2019), and on several woody hosts (Bien and Damm, 2020; Farr and Rossman, 2020). This fungus also causes postharvest diseases on kiwifruit, pear, and apple (Spadaro *et al.*, 2010; Köhl *et al.*, 2018; Eichmeier *et al.*, 2020). Gramaje *et al.* (2011) reported the high variability in *C. luteo-oli-*

vacea colony pigmentation and the critical role of DNA sequencing to clearly identify this pathogen.

Peroneutypa scoparia belongs to the *Diatrypaceae*, members of which are commonly classified as saprophytes, endophytes, and pathogens on a wide range of woody hosts such as grapevine, pistachio and *Prunus* spp. (Trouillas *et al.*, 2011; Shang *et al.* 2017; Aiello *et al.*, 2019; Mehrabi *et al.*, 2019). Due to the morphological similarities among the *Diatrypaceae*, molecular analyses on ITS and partial β-tubulin regions have been established to resolve and clarify taxonomy within this family (Trouillas *et al.*, 2010, 2011; Shang *et al.* 2017; Mehrabi *et al.*, 2019; Moyo *et al.*, 2019). Carmarán *et al.* (2006) included the *Peroneutypa* within the *Diatrypaceae*, and *P. scoparia* is the currently accepted, with the synonyms *Eutypa scoparia*, *Eutypella scoparia*, *Peroneutypella scoparia*, *Sphaeria scoparia*, and *Valsa scoparia*.

In the present study, *C. luteo-olivacea* and *P. scoparia* were isolated from diseased cv. 'Blue Ribbon' blueberry plants. This is the first report of these species in association with blueberry plants in Italy, as well as worldwide. Furthermore, both these fungi were weakly aggressive on the 'Duke'.

All the fungi pathogens detected during this survey in association with severe losses in blueberry orchards were confirmed as pathogenic. Because pathogenicity was tested only on 'Duke', further pathogenicity tests are planned to assess pathogenicity of these fungi on other blueberry cultivars such as 'Top Shelf', 'Blue Ribbon', 'Last Call' and 'Cargo'. Good agronomic practices such as removing pruning debris, and wound protection after pruning and chilling, could reduce inoculum sources and the disease severity. Healthy propagation material from certified nurseries should be adopted, because these pathogens can survive as endophytes or as latent infections. Favourable climatic conditions and high temperatures during the blueberry production cycle could also play a major role in disease development. Further investigation of climate effects on the fungal pathogen species, and epidemiology of stem blight and dieback diseases of blueberry, should be conducted to develop specific protocols for effective disease management.

ACKNOWLEDGEMENT

This study was supported by the University of Torino in the project "RICERCA LOCALE 2019 - Sviluppo e applicazione di tecniche di diagnostica fitopatologica e di caratterizzazione delle popolazioni di patogeni emergenti collegate alla filiera agroalimentare". The authors thank Prof. A. Garibaldi (AGROINNOVA - University of Torino) for critical reading of the manuscript, Dr. G. Gilardi (AGROINNOVA) for technical support and Prof. C. Peano (DiSAFA - University of Torino) for the support with specimen collection.

LITERATURE CITED

Aiello D., Gusella G., Fiorenza A., Guarnaccia V., Polizzi G., 2020. Identification of *Neofusicoccum parvum* causing canker and twig blight on *Ficus carica* in Italy. *Phytopathologia Mediterranea* 59: 213–218.

Aiello D., Polizzi G., Gusella G., Fiorenza A., Guarnaccia V., 2019. Characterization of *Eutypa lata* and *Cytospora pistaciae* causing dieback and canker of pistachio in Italy. *Phytopathologia Mediterranea* 58: 699–706.

Battilani P., Chiusa G., Arciuolo R., Somenzi M., Fontana M., ... Spigolon N., 2018. *Diaporthe* as the main cause of hazelnut defects in the Caucasus region. *Phytopathologia Mediterranea* 57: 320–333.

Bien S., Damm U., 2020. *Arboricolonus simplex* gen. et sp. nov. and novelties in *Cadophora Minutiella* and *Proliferodiscus* from *Prunus* wood in Germany. *Mycokeys* 63: 119–161.

Brazelton C., 2011. World blueberry acreage and production report. *US Highbush Blueberry Council* 1–51.

Carbone I., Kohn L.M., 1999. A method for designing primer sets for the speciation studies in filamentous ascomycetes. *Mycologia* 91: 553–556.

Cardinaals J., Wenneker M., Voogd J.G.B., van Leeuwen G.C.M., 2018. Pathogenicity of *Diaporthe* spp. on two blueberry cultivars (*Vaccinium corymbosum*). *EPPO Bulletin* 48: 128–134.

Carlucci A., Raimondo M.L., Cibelli F., Phillips A.J.L., Lops F., 2013. *Pleurostomophora richardsiae*, *Neofusicoccum parvum* and *Phaeoacremonium aleophilum* associated with a decline of olives in Southern Italy. *Phytopathologia Mediterranea* 52: 517–527.

Carmarán C.C., Romero A.I., Giussani L.M., 2006. An approach towards a new phylogenetic classification in *Diatrypaceae*. *Fungal Diversity* 23: 67–87.

Eichmeier A., Pecenka J., Spetik M., Necas T., Ondrasek I., … Gramaje D., 2020. Fungal trunk pathogens associated with *Juglans regia* in the Czech Republic. *Plant Disease* 104: 761–771.

Elfar K., Torres R., Díaz G.A., Latorre B.A., 2013. Characterization of *Diaporthe australafricana* and *Diaporthe* spp. associated with stem canker of blueberry in Chile. *Plant Disease* 97: 1042–1050.

Espinoza J.G., Briceño E.X., Chávez E.R., Úrbez-Torres J.R., Latorre B.A., 2009. *Neofusicoccum* spp. associ-

ated with stem canker and dieback of blueberry in Chile *Plant Disease* 93: 1187–1194.

FAOSTAT, 2019. Food and Agriculture Organization of the United Nations. http://www.fao.org/faostat/en/#home. Accessed 26 February 2020.

Farr D.F., Rossman A.Y., 2020. Fungal Databases U.S. National Fungus Collections ARS USDA.

Glass N.L., Donaldson G.C., 1995. Development of primer sets designed for use with the PCR to amplify conserved genes from filamentous ascomycetes. *Applied Environmental Microbiology* 61: 1323–1330.

Gramaje D., Mostert L., Armengol J., 2011. Characterization of *Cadophora luteo-olivacea* and *C. melinii* isolates obtained from grapevines and environmental samples from grapevine nurseries in Spain. *Phytopathologia Mediterranea* 50: S112–S126.

Guarnaccia V., Crous P.W., 2018. Species of *Diaporthe* on *Camellia* and *Citrus* in the Azores Islands. *Phytopathologia Mediterranea* 57: 307–319.

Guarnaccia V., Vitale A., Cirvilleri G., Aiello D., Susca A., … Polizzi G., 2016. Characterisation and pathogenicity of fungal species associated with branch cankers and stem–end rot of avocado in Italy. *European Journal of Plant Pathology* 146: 963–976.

Guarnaccia V., Groenewald J.Z., Woodhall J., Armengol J., Cinelli T., … Crous P.W., 2018. *Diaporthe* diversity and pathogenicity revealed from a broad survey of grapevine diseases in Europe. *Persoonia* 40: 135–153.

Hilário S., Amaral I.A., Gonçalves M.F.M., Lopes A., Santos L., Alves A., 2020a. *Diaporthe* species associated with twig blight and dieback of *Vaccinium corymbosum* in Portugal, with description of four new species. *Mycologia*112: 293–308.

Hilário S., Lopes A., Santos L., Alves A., 2020b. *Botryosphaeriaceae* species associated with blueberry stem blight and dieback in the Centre Region of Portugal. *European Journal of Plant Pathology* 156: 31–44.

Hillis D.M., Bull J.J., 1993. An empirical test of bootstrapping as a method for assessing confidence in phylogenetic analysis. *Systematic Biology* 42: 182–192.

Ivić D., Novak A., Pilipović P., 2018. *Diaporthe eres* Nitschke is the only *Diaporthe* species found on blueberry in Croatia. *Fragmenta Phytomedica* 32: 23–30.

Katoh K., Standley D.M., 2013. MAFFT Multiple sequence alignment software version 7: improvements in performance and usability. *Molecular Biology and Evolution* 30: 772–780.

Köhl J., Wenneker M., Groenenboom-de Haas B.H., Anbergen R., Goossen-van de Geijn H.M., … Kastelein P., 2018. Dynamics of post-harvest pathogens *Neofabraea* spp. and *Cadophora* spp. in plant residues in Dutch apple and pear orchards. *Plant Pathology* 67: 1264–1277.

Koike S.T., Rooney–Latham S., Wright A.F., 2014. First report of stem blight of blueberry in California caused by *Neofusicoccum parvum*. *Plant Disease* 98: 1280.

Kumar S., Stecher G., Tamura K., 2016. MEGA7: Molecular Evolutionary Genetics Analysis version 7.0 for bigger datasets. *Molecular Biology and Evolution* 33: 1870–1874.

Latorre B.A., Elfar K., Espinoza J.G., Torres R., Díaz G.A., 2012. First report of *Diaporthe australafricana* associated with stem canker on blueberry in Chile. *Plant Disease* 96: 768.

Leslie J.F. and Summerell B.A., eds. 2006. The Fusarium Laboratory Manual. Blackwell Publishing Ltd, Oxford, UK.

Lombard L., van Leeuwen G.C.M., Guarnaccia V., Polizzi G., van Rijswick P.C.J., … Crous P., 2014. *Diaporthe* species associated with *Vaccinium* with specific reference to Europe. *Phytopathologia Mediterranea* 53: 287–299.

Ma L., Sun Z., Zeng Y., Luo M., Yang J., 2018. Molecular mechanism and health role of functional ingredients in blueberry for chronic disease in human beings. *International. Journal of Molecular Science* 19: 2785.

Marin–Felix Y., Groenewald J.Z., Cai L., Chen Q., Marincowitz S., … Crous P.W., 2017. Genera of phytopathogenic fungi: GOPHY 1. *Studies in Mycology* 86: 99–216.

Marin–Felix Y., Hernández–Restrepo M., Wingfield M.J., Akulov A., Carnegie A.J., … Crous P.W., 2019. Genera of phytopathogenic fungi: GOPHY2. *Studies in Mycology*.92: 47–133.

Marsberg A., Kemler M., Jami F., Nagel J.H., Postma-Smidt A., … Slippers B. 2017. *Botryosphaeria dothidea*: a latent pathogen of global importance to woody plant health. *Molecular Plant Pathology* 18: 477–488.

McDonald V., Eskalen A., 2011. *Botryosphaeriaceae* species associated with avocado branch cankers in California. *Plant Disease* 95: 1465–1473.

Mehrabi M., Asgari B., Hemmati R., 2019. Two new species of *Eutypella* and a new combination in the genus *Peroneutypa* (Diatrypaceae). *Mycological Progress* 18: 1057–1069.

Michalecka M., Bryk H., Seliga P., 2017. Identification and characterization of *Diaporthe vaccinii* Shear causing upright dieback and viscid rot of cranberry in Poland. *European Journal of Plant Pathology* 148: 595–605.

Moyo P., Mostert L., Halleen F., 2019. Diatrypaceae species overlap between vineyards and natural ecosystems in South Africa. *Fungal Ecology* 39: 142–151.

Nestby R., Percival D., Martinussen I., Opstad N., Rohloff J., 2011. The European blueberry (*Vaccinium myrtillus* L.) and the potential for cultivation. A review. *The European Journal of Plant Science and Biotechnology* 5: 5–16.

Norberto S., Silva S., Meireles M., Faria A., Pintado M., Calhau C., 2013. Blueberry anthocyanins in health promotion: a metabolic overview. *Journal of Functional Foods* 5: 1518–1528.

Nylander JAA., 2004. MrModeltest v. 2. Program distributed by the author. Uppsala Evolutionary Biology Centre Uppsala University.

O'Donnell K., Cigelnik E., 1997. Two divergent intragenomic rDNA ITS2 types within a monophyletic lineage of the fungus *Fusarium* are nonorthologous. *Molecular Phylogenetics and Evolution* 7: 103–116.

Pérez S., Meriño-Gergichevich C., Guerrero J., 2014. Detection of *Neofusicoccum nonquaesitum* causing dieback and canker in highbush blueberry from Southern Chile. *Journal of Soil Science and Plant Nutrition* 14: 581–588.

Phillips A.J.L., Oudemans P.V., Correia A., Alves A., 2006. Characterization and epitypification of *Botryosphaeria corticis*, the cause of blueberry cane canker. *Fungal Diversity* 21: 141–155.

Polashock J.J., Caruso F.L., Averill A.L., Schilder A.C. (eds.), 2017. Compendium of blueberry, cranberry, and lingonberry diseases and pests, 2nd edn. St. Paul, MN, USA: APS Press.

Raimondo M.L., Carlucci A., Ciccarone C., Sadallah A., Lops F., 2019. Identification and pathogenicity of lignicolous fungi associated with grapevine trunk diseases in southern Italy. *Phytopathologia Mediterranea* 58: 639–662.

Rayner R.W., 1970. A mycological colour chart. Kew, UK: Commonwealth Mycological Institute.

Retamales J.B., Hancock J.F., 2018. Blueberries, 2nd edition. CABI, Wallingford, UK.

Riccioni L., Valente M.T., Giambattista G. di, 2017. First report *Neofusicoccum parvum* causing shoot blight and plant decay on pomegranate in Tarquinia, Italy. *Journal of Plant Pathology* 99: 294.

Ronquist F., Teslenko M., Van der Mark P., Ayres D.L., Darling A., … Huelsenbeck J.P., 2012. MrBayes 3.2: efficient Bayesian phylogenetic inference and model choice across a large model space. *Systematic Biology* 61: 539–542.

Santos L., Alves A., Alves R., 2017. Evaluating multi–locus phylogenies for species boundaries determination in the genus *Diaporthe*. *PeerJ* 5: e3120.

Scarlett K.A., Shuttleworth L.A., Collins D., Rothwell C.T., Guest D.I., Daniel R., 2019. Botryosphaeriales associated with stem blight and dieback of blueberry (*Vaccinium* spp.) in New South Wales and Western Australia. *Australasian Plant Pathology* 48: 45–57.

Schoch C.L., Seifert K.A., Huhndorf S., Robert V., Spouge J.L., … Fungal Barcoding Consortium, 2012. Nuclear ribosomal internal transcribed spacer (ITS) region as a universal DNA barcode marker for Fungi. *Proceedings of the National Academy of Sciences* 109: 6241–6246.

Shang Q., Hyde K.D., Phookamsak R., Doilom M., Bhat D.J., … Promputtha I., 2017. *Diatrypella tectonae* and *Peroneutypa mackenziei* spp. nov. (Diatrypaceae) from northern Thailand. *Mycological Progress* 16: 463–476.

Slippers B., Wingfield M.J., 2007. Botryosphaeriaceae as endophytes and latent pathogens of woody plants: diversity, ecology and impact. *Fungal Biology Reviews* 21: 90–106.

Smith H., Wingfield M.J., Crous P.W., Coutinho T.A., 1996. *Sphaeropsis sapinea* and *Botryosphaeria dothidea* endophytic in *Pinus* spp. and *Eucalyptus* spp. in South Africa. *South African Journal of Botany* 62: 86–88.

Spadaro D., Galliano A., Pellegrino C., Gilardi G., Garibaldi A., Gullino M.L., 2010. Dry matter mineral composition and commercial storage practices influence the development of skin pitting caused by *Cadophora luteo-olivacea* on kiwifruit 'Hayward'. *Journal of Plant Pathology* 92: 349–56.

Strømeng G.M., Stensvand A., 2011. Godronia canker (*Godronia cassandrae* f. sp. *vaccinii*) in highbush blueberry. *The European Journal of Plant Science and Biotechnology* 5: 35–41.

Swofford D.L., 2003. PAUP*. Phylogenetic analysis using parsimony (*and other methods) v. 4.0b10. Sunderland; MS, USA: Sinauer Associates.

Tennakoon K.M.S., Ridgway H.J., Jaspers M.V., Jones E.E., 2018. Botryosphaeriaceae species associated with blueberry dieback and sources of primary inoculum in propagation nurseries in New Zealand. *European Journal of Plant Pathology* 150: 363–374.

Travadon R., Lawrence D.P., Rooney–Latham S., Gubler W.D., Wilcox W.F., … Baumgartner K., 2015. *Cadophora* species associated with wood–decay of grapevine in North America. *Fungal Biology* 119: 53–66.

Trouillas F.P., Úrbez–Torres J.R., Gubler W.D., 2010. Diversity of diatrypaceous fungi associated with grapevine canker diseases in California. *Mycologia* 102: 319–336.

Trouillas F.P., Pitt W.M., Sosnowski M.R., Huang R., Peduto F., … Gubler W.D., 2011. Taxonomy and

DNA phylogeny of Diatrypaceae associated with *Vitis vinifera* and other woody plants in Australia. *Fungal Diversity* 49: 203–223.

Vitale S., Aiello D., Guarnaccia V., Luongo L., Galli M., … Voglmayr H., 2018. *Liberomyces pistaciae* sp. nov., the causal agent of pistachio cankers and decline in Italy. *MycoKeys* 40: 29–51.

White T.J., Bruns T., Lee S., Taylor J.W., 1990. Amplification and direct sequencing of fungal ribosomal RNA genes for phylogenetics. In *PCR Protocols: a Guide to Methods and aApplications*. (Innis M.A., Gelfand D.H., Sninsky J.J., White T.J., ed.). Academic Press, San Diego, California, 315–322.

Wright A.F., Harmon P.F., 2010. Identification of species in the *Botryosphaeriaceae* family causing stem blight on southern highbush blueberry in Florida. *Plant Disease* 94: 966–971.

Xu C., Zhang H., Zhou Z., Hu T., Wang S., ... Cao K., 2015. Identification and distribution of Botryosphaeriaceae species associated with blueberry stem blight in China. *European Journal of Plant Pathology* 143: 737–752.

Yang Q., Fan X.L., Guarnaccia V., Tian C.M., 2018. High diversity of *Diaporthe* species associated with dieback diseases in China, with twelve new species described. *MycoKeys* 39: 97–149.

Phytopathologia Mediterranea
The international journal of the
Mediterranean Phytopathological Union

Firenze University Press
www.fupress.com/pm

Research Papers

Interactions between lime witches' broom phytoplasma and phytoplasma strains from 16SrI, 16SrII, and 16SrIX groups in periwinkle

Elham SALEHI[1], Keramatollah IZADPANAH[1,*], Seyed Mohsen TAGHAVI[1], Habibollah HAMZEHZARGHANI[1], Alireza AFSHARIFAR[1], Mohammad SALEHI[2]

[1] *Department of Plant Protection, College of Agriculture, Shiraz University, Shiraz, Iran*
[2] *Plant Protection Research Department, Fars Agricultural and Natural Resources Research and Education Center, AREEO, Zarghan, Iran*
*Corresponding author: izadpana@shirazu.ac.ir

Summary. The interactions of lime witches' broom phytoplasma (LWBP, 16SrII-B) with alfalfa witches' broom phytoplasma (AWBP, 16SrII-C), tomato witches' broom phytoplasma (TWBP, 16SrII-D), sesame phyllody phytoplasma (SPhP, 16SrIX-C) and rapeseed phyllody phytoplasma (RPhP, 16SrI-B) were studied in periwinkle plants graft-inoculated either with each phytoplasma alone or with LWBP and a second phytoplasma. The latter was inoculated below or above the site of LWBP inoculation, and was applied either simultaneously or non-simultaneously. In all treatments and all replications, the plants doubly inoculated with LWBP + SPhP or LWBP + AWBP showed milder symptoms and lived longer than those singly inoculated with LWBP, SPhP, or AWBP. In plants with mixed infection by LWBP + RPhP or LWBP + TWBP, characteristic symptoms were present regardless of the grafting order or inoculation site. Analysis of quantitative PCR data showed that the mean concentrations of LWBP in all doubly inoculated plants were less than in plants inoculated with LWBP alone. In the SPhP inoculated plants, a substantial decrease in LWBP concentration was measured, followed in order of decreasing concentration in the AWBP, TWBP, and RPhP inoculated plants. In the mixed infections, greater reduction in LWBP concentration was found in non-simultaneous inoculations and when the second phytoplasma was grafted below the site of LWBP inoculation. Based on symptoms and quantitative PCR results, the interactions of LWBP with SPhP and AWBP resulted in greater cross-protection than interactions of LWBP with RPhP and TWBP.

Keywords. Mixed infections, symptomatology, quantitative PCR.

OPEN ACCESS

Citation: E. Salehi, K. Izadpanah, S.M. Taghavi, H. Hamzehzarghani, A. Afsharifar, M. Salehi (2020) Interactions between lime witches' broom phytoplasma and phytoplasma strains from 16SrI, 16SrII, and 16SrIX groups in periwinkle. *Phytopathologia Mediterranea* 59(2): 247-259. DOI: 10.14601/Phyto-11035

Accepted: May 11, 2020

Published: August 31, 2020

Data Availability Statement: All relevant data are within the paper and its Supporting Information files.

Competing Interests: The Author(s) declare(s) no conflict of interest.

Editor: Assunta Bertaccini, Alma Mater Studiorum, University of Bologna, Italy.

INTRODUCTION

Diseases caused by phytoplasmas are associated with significant yield losses in more than 1,000 plant species from different families, including many important field, vegetable and fruit crops, ornamental plants, timber and shade trees (McCoy *et al.,* 1989; Lee *et al.,* 2000; Bertaccini and Duduk,

2009). Characteristic symptoms include virescence, phyllody, abnormal proliferation of shoots and witches' broom, foliar yellowing, reddening and other discolorations, reduced leaf and fruit size, phloem necrosis, stunting and overall decline (Seemüller *et al.,* 1998; Bertaccini *et al.,* 2014). Phytoplasma diseases are difficult to control, mainly due to the specific plant-insect vector-pathogen relationship. Control recommendations for these diseases include phytosanitary and other preventive measures as well as control of the insect vectors, but none of these strategies have been shown to be satisfactory in field applications.

Cross-protection was reported as a strategy for control of fruit tree phytoplasma diseases when other approaches failed (Marcone *et al.,* 2010). This strategy has been regarded as induced resistance based on moderation of disease symptoms due to prior infection of host plants by closely related pathogen strains, usually with mild pathogenicity (Pennazio and conti, 2001). In plants mixed virus infections are common, and virus-virus interactions have been studied for many years and shown to be either antagonistic or synergistic (Syller, 2012).

Studies of interaction between mild and severe strains of phytoplasmas in insect vectors and plant hosts date back to the mid-20th century when these phytoplasmas were considered to be viruses (Kunkel, 1955; Freitag, 1964; Valenta, 1959). More recently, antagonistic effects of mild strains on severe strains have been reported for a number of phytoplasmas, including those associated with European stone fruit yellows (16SrX), ash yellows (16SrVI) and apple proliferation (16SrX) (Castelain *et al*., 2007; Kiss *et al*., 2013; Schneider *et al*., 2014; Sinclair and Griffiths, 2000). However, there is little information on interactions between different '*Candidatus* Phytoplasma' species or different 16S ribosomal groups.

Mexican lime [*Citrus aurantifolia* (Christsm.) Swingle)] is one of the most economically important horticultural crops in southern Iran, where it is cultivated in about 41,800 ha. with total annual production of about 400,000 tons (Anonymous, 2006). The lime witches' broom disease associated with the presence of '*Candidatus* Phytoplasma aurantifolia' (LWBP), a 16SrII-B strain (Zreik *et al.,* 1995), is the most devastating disease of Mexican lime and other citrus species in the southern Iran (Salehi *et al*., 2002), Oman and United Arab Emirates (Garnier *et al*., 1991). To date, no mild strains of this phytoplasma have been described, and its host range is expanded to other citrus varieties including grapefruit, sweet orange and mandarin (Mannan *et al.,* 2010). Traditional methods used to control these diseases are eradication, quarantine and use of chemicals (Salehi, 2016).

The aim of the present study was to investigate the interaction of lime witches' broom with four phytoplasma strains, including alfalfa witches' broom, tomato witches' broom, sesame phyllody and rapeseed phyllody, in periwinkle plants after graft inoculations.

MATERIALS AND METHODS

Experimental plants

A pink flower variety of periwinkle [*Catharanthus roseus* (L.) G. Don] was propagated from seed and grown in an insect-free greenhouse. Six-month-old plants were graft-inoculated with the phytoplasma strains described below, at greenhouse temperatures of approx. 30°C in the day time and 26°C at night, and with 15 h light / 9 h dark regime.

Phytoplasma strains

The phytoplasma strains used in this study were lime witches' broom phytoplasma (LWBP, 16SrII-B) from Nikshahr (Sistan-Baluchistan province) (Salehi *et al.,* 2002), alfalfa witches' broom phytoplasma (AWBP, 16SrII-C) from Abarkooh (Yazd province) (Esmailzadeh Hosseini *et al.,* 2015), sesame phyllody phytoplasma (SPhP, 16SrIX-C) from Fasa (Fars province) (Salehi *et al.,* 2017), tomato witches' broom phytoplasma (TWBP, 16SrII-D) from Borazjan (Bushehr province) (Salehi *et al*., 2014), and rapeseed phyllody phytoplasma (RPhP, 16SrI-B) from Zarghan (Fars province) (Salehi *et al.,* 2011). These phytoplasmas were transmitted from the original plant hosts to periwinkle via dodder (*Cuscuta campestris* Yank.), and were propagated and maintained in periwinkle by grafting for 2 years.

Graft inoculation

For graft inoculations of each phytoplasma strain, axillary shoots (each 3 cm long) containing two leaves from a symptomatic periwinkle plant were used as scions. These were side grafted on the main stems of healthy periwinkle plants grown from seed. Each graft site was 10 cm above the soil level. In mixed inoculations, the second scion was grafted at 6 cm below the first graft. Grafted areas were wrapped with parafilm, and the plants were covered with plastic bags for a week to maintain humidity. All grafted and non-graft-

ed experimental control plants were maintained in an insect-proof greenhouse.

Experimental treatments

A factorial experiment in a completely randomized design with three factors and four replicates, comprising a total of 84 plants (Table 2), was conducted to study interactions of LWBP with AWBP, TWBP, RPhP and SPhP. Factor A consisted of mixed infection of LWBP with either AWBP, TWBP, RPhP or SPhP; factor B was the grafting site of the second phytoplasma above or below the site of LWBP grafting on the stem; and factor C was the time of grafting of each phytoplasma in mixed infections, either simultaneous or non-simultaneous (2 weeks after the first grafting). Plants with single phytoplasma grafting, served as experimental controls for symptom expression. Comparisons were made by calculation of the area under phytoplasma concentration growth curves (AUCGC) at several times after grafting, using the following equation:

$$AUCGC = \sum_{i=1}^{n-1} \left[\frac{p_i + p_{i+1}}{2}\right][t_{i+1} - t_i]$$

where p_i and p_{i+1} are the phytoplasma concentrations obtained from grafted plants at consecutive times of t_i and t_{i+1}, and n is the number of times in which the concentration was estimated.

The simple and interactive effects of the factors on the total concentration of LWBP (AUCGC) was investigated using the procglm software, SAS 9.3 (Garret *et al.*, 2004). The mean of the treatments was compared using Duncan Multiple Range Test (DMRT) at the 5% significance level. At each inoculation time, four periwinkle plants were singly grafted with each phytoplasma as positive controls, and four healthy non-grafted periwinkle plants were included as negative controls.

Biological and molecular assessments

The evaluations of disease symptoms in the grafted periwinkle plants began 1 week after grafting, and was repeated every 2 weeks for 14 months. Nested PCR was used for detection, sequencing and identification of LWBP, AWBP, TWBP, RPhP and SPhP in plants, at 8 and 40 weeks after the grafting. Quantitative PCR (qPCR) assays were performed at 1 week after the grafting, and then repeated at 8-week intervals for 57 weeks.

Sampling, total nucleic acid extraction, PCR and sequence analysis

The sampling for phytoplasma detection and quantification started at day 7 after the grafting, and was repeated at 8-week intervals for 57 weeks. At each sampling time, 16 leaves from four shoots (four leaves from each shoot) grown above the grafting site, were collected from each grafted plant. The leaf midribs were separated, mixed and used for DNA extractions. Total nucleic acid (TNA) was extracted from 0.2 g of each sample using the small-scale method of Zhang *et al.* (1998), with the minor modifications proposed by Abou-Jawdah *et al.* (2002). Positive control samples consisted of nucleic acid from periwinkle plants singly grafted with each phytoplasma and negative control samples were nucleic acid from healthy periwinkle plants.

Phytoplasmas in grafted plants were detected by nested PCR using the universal primer pair P1/P7 (Deng and Hiruki, 1991; Schneider *et al.*, 1995), followed by specific length primer pairs designed using online primer3 software (Untergasser *et al.*, 2012) (Table 1) in nested and qPCR assays. Each 50 µL PCR reaction mixture contained 100 ng of TNA from diseased or healthy plants, 0.4 µM of each primer, 0.2 mM of each dNTP and 1.25 U of Taq DNA polymerase (Cinagen, Iran) in l0× PCR buffer. The temperature profile for PCR consisted of a first denaturation step of 2 min at 94°C followed by 35 cycles of 1 min at 94°C, 1 min for annealing, and 2 min at 72°C. A final extension was carried out at 72°C for 3 min. The specificity of the primers was improved by changing the annealing temperatures as listed in Table 1. PCR products were electrophoresed through 1% agarose gel in 1× TBE buffer (67 mM Tris-HCl, 22 mM boric acid, 10 mM EDTA, pH 8.0), stained with ethidium bromide and visualized using a UV transilluminator (Sambrook *et al.*, 1989).

Nested PCR products of primer pairs LWB^F/LWB^R (146 bp), AWB^F/AWB^R (90 bp), TWB^F/TWB^R (96 bp), RPh^F/RPh^R (140 bp) and SPh^F/SPh^R (143 bp) were purified using GF-1 PCR Clean-Up Kit (Vivantis, Malaysia) according to the manufacturer's instructions, and were directly sequenced by Macrogen (South Korea) on both strands. The resulting consensus sequences were deposited in the GenBank database and used in BLAST search (http://blast.ncbi.nlm. nih.gov/Blast.cgi).

Quantitative polymerase chain reaction amplification

For qPCR, in addition to the specific length primer pairs for phytoplasmas, internal control primer pairs ($ef\text{-}1\alpha^F/ef\text{-}1\alpha^R$) (Table 1) were designed from the periwin-

Table 1. Primers used in nested PCR and qPCR assays.

Primer pairs	Sequence (5'→3')	Annealing temperature	Expected fragment size (bp)	References
P_1/P_7	AAGAGTTTGATCCTGGCTCAGG ATTCGTCCTTCATCGGCTCTT	55°C	1,800	Deng and Hiruki, 1991; Schneider *et al*., 1995
LWB^F/LWB^R	GTACACACCGCCCGTCAAAC GATCCATCCCCACCTTCCGG	63°C	146	Present study
AWB^F/AWB^R	GTTTGTACACACCGCCCGTC CCTTAGACAGCGCCCTCTCG	61°C	90	Present study
TWB^F/TWB^R	GCCGCGGTAAGACATAAGGG AGCGTTGCCATTACACCACTG	61°C	96	Present study
RPh^F/ RPh^R	GGAGGAGCTTGCGTCACATT ATTCCCTACTGCTGCCTCCC	61°C	140	Present study
SPh^F/ SPh^R	AGGAACACCAGAGGCGTAGG TCAGTACCGAGCCGAAACCC	63°C	143	Present study
ef-$1\alpha^F$/ ef-$1\alpha^R$	CTCTGCTTGCTTTCACCCTTGG GAGACCTCCTTCACAATTTCATC	55°C	115	Present study

kle elongation factor 1-alpha gene, using online primer3 software (Untergasser *et al*., 2012). The qPCR was performed using a MyiQTM Single Color Real time-PCR Detection System (Bioneer, Exicycler™ 96) with qPCR GreenMaster with LowRox (Jena Bioscience) for quantification of the assayed phytoplasmas in periwinkle plants. The PCR reaction mixture contained the following components in a final volume of 20 µL: 10 µL qPCR Green Master with Low Rox, 0.6 µL of each 10 µM forward and reverse primers, 6.8 µL PCR-grade H_2O and 2.0 µL of DNA template. The parameters used for amplification were 2 min at 95°C followed by 40 cycles of a two-step protocol consisting of 15 s at 95°C and 1 min at 63°C, for the LWB^F/LWB^R and SPh^F/SPh^R primer pairs, or 61°C, for the AWB^F/AWB^R, TWB^F/TWB^R and RPh^F/RPh^R primer pairs. For each treatment, 8 qPCR assays were made at 8-week intervals, and changes in the concentrations of LWBP were recorded during the course of the study (57 weeks).

Statistical analyses

A complete randomized block design in the form of a factorial experiment with four replications was used to evaluate the presence of interactions of LWBP with the four other phytoplasmas, based on symptomatology and qPCR values. Repeated measures analysis of variance was used for detecting changes in the mean parameters at 1, 9, 17, 25, 33, 41, 49 and 57 weeks after the first grafting, using SAS 9.3 software for statistical analysis (Garret *et al.,* 2004). Areas under the concentration growth curves (AUCGC) were determined, and used in statistical analyses for the normalization of the concentration data.

RESULTS

Symptomatology in periwinkle

In all grafted plants, the scions remained alive and grew as expected. In periwinkle, LWBP induced more severe symptoms of witches' broom, little leaf, internode shortening and stunting than the AWBP, TWBP, RPhP or SPhP strains. Time to symptom appearance in periwinkle plants, separately grafted with each phytoplasma, was approx. 8 weeks (Table 2). Disease symptoms in periwinkle plants grafted with LWBP were yellowing, incomplete virescence and severe little leaf, shortened internodes, witches' broom and stunting. In plants singly grafted with AWBP, TWBP, RPhP or SPhP the main disease symptoms were flower virescence and phyllody, little leaf, shortened internodes, yellowing and stunting (Figures 1a-f, and Table 2). In periwinkle plants grafted with LWBP + AWBP and LWBP + SPhP, the symptoms were mild little leaf and yellowing regardless of the grafting time (simultaneous or non-simultaneous) or the relative position of scions (Figures 2a and b, and Table 2). At the end of the observations (57 weeks), periwinkle plants graft inoculated with phytoplasma mixtures produced normal flowers (Figure 2b, and Table 2).

All periwinkle plants grafted with LWBP + TWBP showed symptoms of yellowing, small leaves, shortened internodes, stem proliferation, virescence and phyllody after 20 weeks. At the end of the experiment (57 weeks) all LWBP + TWBP plants showed yellowing, shortened internodes, mild little leaf and rosetting without the virescence, phyllody or witches' broom symptoms which

Table 2. Summary of results obtained in the grafted periwinkle plants.

Treatment type	Grafting type	Symptomatology	Time to symptom appearance (weeks post inoculation)	Number of grafted plants
LWBP[a]	Alone	Y[d], IV, SLL, SSI, SWB, SST	8	4
AWBP	Alone	MY, LL, V, Ph, MST	8	4
TWBP	Alone	MY, LL, V, Ph, MST	8	4
SPhP	Alone	MY, LL, V, Ph, MST	8	4
RPhP	Alone	MY, LL, V, Ph, MST	8	4
LWBP+AWBP	S[b]&NS[c]	MLL, Y, NF	40	16
LWBP+SPhP	S & NS	MLL, Y, NF	40	16
LWBP+TWBP	S & NS	Y, SL, SI, SP, V, Ph, Y, MLL, Ro	20 57	16
		W, De	20	2
LWBP+RPhP	S & NS	MY, LL, SI	57	2
		SLL, SSI, SY, SLD	57	12

[a]AWBP, alfalfa witches' broom phytoplasma; LWBP, lime witches' broom phytoplasma; RPhP, rapeseed phyllody phytoplasma; SPhP, sesame phyllody phytoplasma; TWBP, tomato witches' broom phytoplasma.
[b] S, simultaneous.
[c] NS, non-simultaneous.
[d] Symptom abbreviations: De, death; IV, incomplete flower virescence; LL, little leaf; MLL, mild little leaf; MST, mild stunting; MY, mild yellowing; NF, normal flower; Ph, flower phyllody; Ro, rosetting; SI, shortened internodes; SL, small leaves; SLD, severe leaf drop; SLL, severe little leaf; SP, stem proliferation; SSI, severe shortened internodes; SST, severe stunting; SWB, severe witches' broom; SY, severe yellowing; V, flower virescence; W, wilting; Y, yellowing.

were present in the plants singly grafted with LWBP or TWBP (Figure 2c, and Table 2).

In the periwinkle plants infected with LWBP+RPhP, regardless of grafting time and site, the scions remained stunted. Two of the grafted plants wilted and died after 20 weeks (Figure 2d, and Table 2). At the end of observations (57 weeks), two plants showed mild yellowing, little leaf and very shortened internodes (Figure 2e, and Table 2) and the remaining 12 plants showed severe symptoms of little leaf, shortened internodes, yellowing and leaf drop (Figure 2f, and Table 2).

Detection of phytoplasma strains in graft inoculated periwinkle plants

Nested PCR gave specific amplification of expected 146 bp fragments from the plants inoculated with LWBP, 90 bp fragments from AWBP, 96 bp fragments from TWBP, 140 bp fragments from RPhP, or 143 bp fragments from SPhP (Table 1, Figures 3 and 4d). These fragments were sequenced and deposited in GenBank under accession numbers MH411203 (LWBP), MH647740 (AWBP), MH647741 (TWBP), MH647743 (RPhP) and MH647742 (SPhP), and all aligned with phytoplasma sequences. In all doubly grafted plants, fragments of expected lengths corresponding to those obtained from the inoculated phytoplasmas were amplified (Figure 4a-c), regardless of the grafting time and the relative position of the two grafting sites.

Phytoplasma concentration

In all treatments, the graft inoculated phytoplasmas were present in the plants although at different concentrations. The mean of eight determinations showed that in single phytoplasma graft inoculations, the LWBP concentration was greater than that of the other phytoplasma strains (Figure 5). There were also clear reductions of LWBP concentration in doubly grafted plants compared with singly grafted plants. These differences were consistent in all samplings during the course of the study. The analysis of variance (ANOVA) of the AUCGC for LWBP in mixed and singly grafted periwinkle plants is shown in Table 3. Experimental factors such as treatment, grafting time and grafting site, as well as the interactions of the treatment × grafting site and the grafting site × inoculation time were statistically significant, at least at 5%, on the reduction of the AUCGC for LWBP (Table 3). Among the four phytoplasma strain combinations, LWBP + SPhP showed the greatest reduction of mean concentration of LWBP (Figure 6). The ranking order (from greatest to least) of the examined phytoplasmas for reducing the concentration of LWBP was SPhP, AWBP, TWBP and RPhP (Figure 6).

Figure 1. Disease symptoms in periwinkle plants following graft-inoculation with lime witches' broom phytoplasma (LWBP), alfalfa witches' broom phytoplasma (AWBP), tomato witches' broom phytoplasma (TWBP), sesame phyllody phytoplasma (SPhP) and rapeseed phyllody phytoplasma (RPhP). (A) plants grafted with LWBP showing yellowing and severe symptoms of little leaf, shortened internodes, witches' broom and stunting. (B-D) plants with yellowing, shortened internodes, virescence and phyllody due to AWBP (B), TWBP (C) and SPhP (D). (E) yellowing, shortened internodes, little leaf and stem proliferation due to RPhP. (F) healthy periwinkle plant. Arrows in B and D indicate flower phyllody and virescence.

Figure 2. Disease symptoms in periwinkle plants doubly grafted with lime witches' broom phytoplasma (LWBP) and another phytoplasma strain. (A) mild yellowing in a periwinkle plant grafted with LWBP and alfalfa witches' broom phytoplasma (AWBP). (B) mild yellowing and shortened internodes with normal flowers in a periwinkle plant grafted with LWBP and sesame phyllody phytoplasma (SPhP). (C) mild yellowing, internode shortening, little leaf, and rosetting, in a periwinkle plant grafted with LWBP and tomato witches' broom phytoplasma (TWBP). (D) wilting, rosetting. (E) mild yellowing, shortened internodes, little leaf, crown proliferation. (F) severe symptoms of little leaf, yellowing and leaf drop in periwinkle plants grafted with LWBP and rapeseed phyllody phytoplasma (RPhP). In (A), right and left arrows indicate, respectively, scions from LWBP and AWBP.

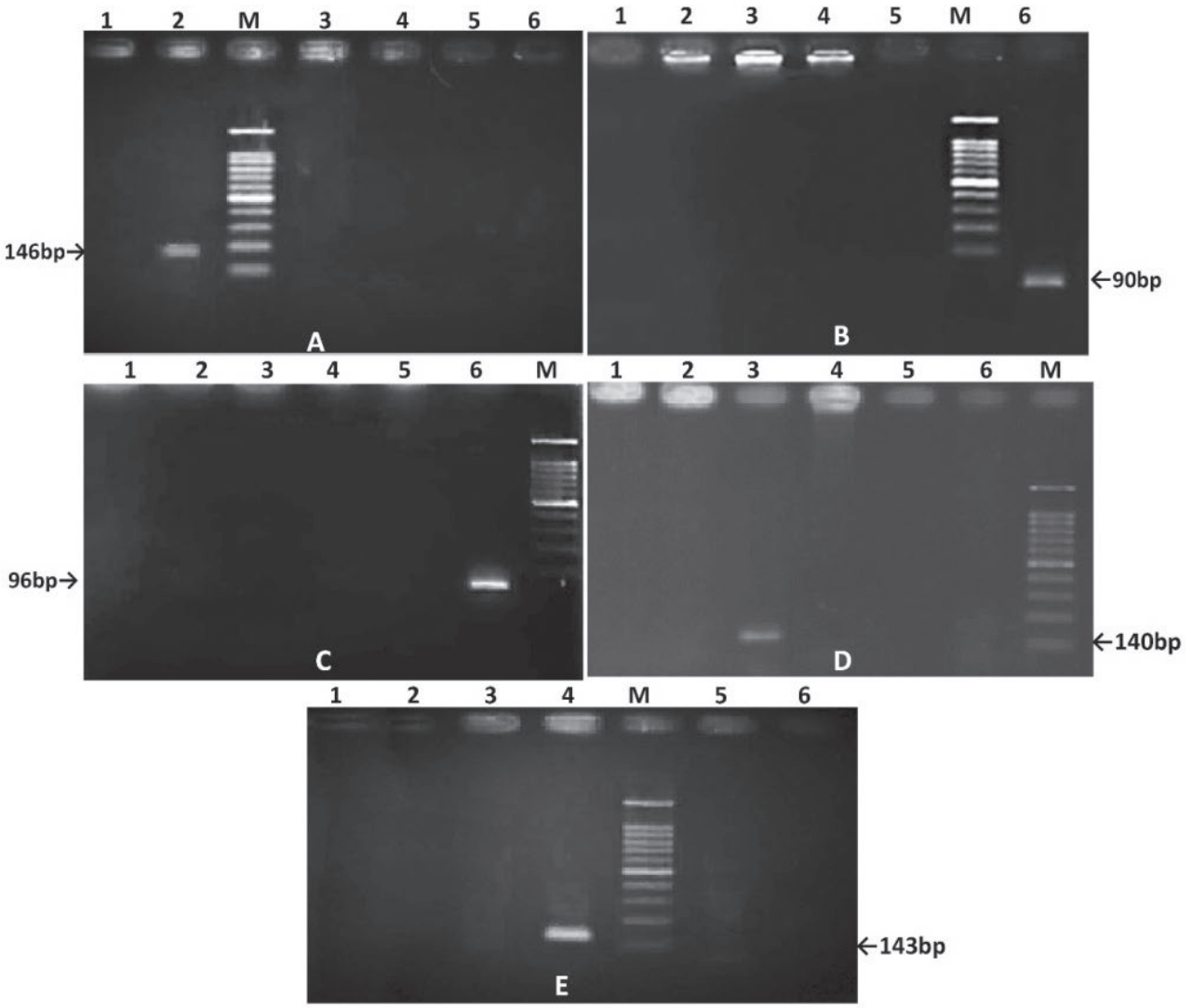

Figure 3. Agarose gel electrophoresis pattern of nested PCR products using P1/P7 primer pair followed by primer pairs LWB^F/LWB^R (146 bp) for detection, in singly graft-inoculated periwinkle plants, of lime witches' broom phytoplasma (LWBP) (A); AWB^F/AWB^R (90 bp), for alfalfa witches' broom phytoplasma (AWBP) (B); TWB^F/TWB^R (96 bp), for tomato witches' broom phytoplasma (TWBP) (C); RPh^F/RPh^R (140 bp), for rapeseed phyllody phytoplasma (RSPh) (D); and SPh^F/SPh^R (143 bp), for sesame phyllody phytoplasma (SPhP) (E). In A, B, D, and E, lanes 1, 2, 3, 4, 5, 6 are from, respectively, healthy periwinkle, LWBP, RPhP, SPhP, TWBP or AWBP graft-inoculated periwinkle plants. In C, lanes 1, 2, 3, 4, 5, 6, are from, respectively, healthy periwinkle, LWBP, RPhP, SPhP, AWBP or TWBP graft-inoculated periwinkle plants. M, 100 bp DNA marker fragments (Fermentas, Vilnius, Lithuania).

Relative grafting site also affected LWBP concentration. All mixed graftings below the position of LWBP infected scions were more effective in decreasing the LWBP concentration than those above the site of LWBP inoculation (Figure 7). A decrease in concentration of LWBP in mixed graft-inoculations was also affected by grafting times: non-simultaneous grafting in mixed infections was more effective in reducing the mean total concentration of LWBP than simultaneous grafting (Figure 8).

DISCUSSION

Previous studies on the interactions between phytoplasmas have been limited to a number of closely related strains (Castelain *et al.,* 2007; Kiss *et al.,* 2013; Schneider *et al.,* 2014; Sinclair and Griffiths, 2000). In the present research, the interaction of LWBP with four phytoplasma strains classified in different 16S ribosomal groups or subgroups (AWBP, SPhP, TWBP and RPhP) was studied.

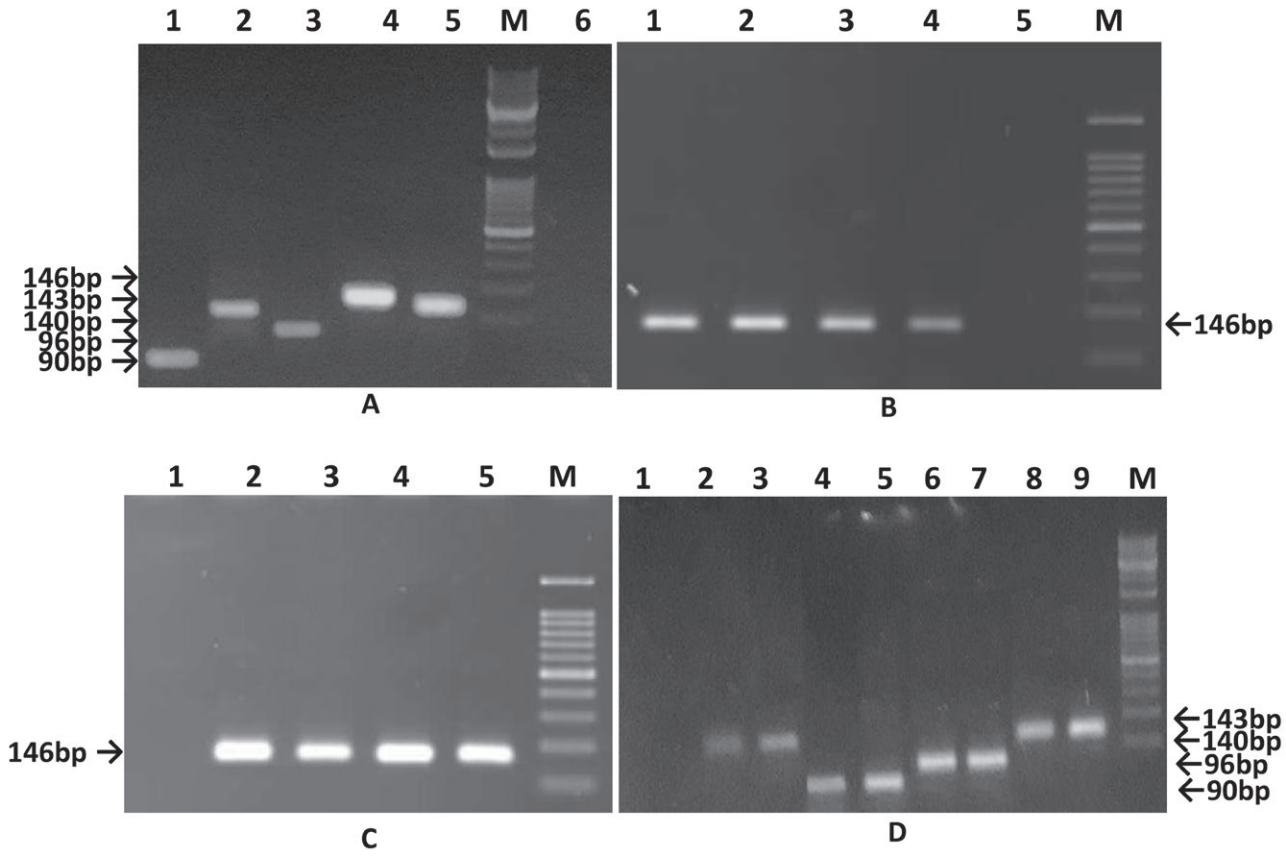

Figure 4. Agarose gel electrophoresis pattern of nested PCR products using P1/P7 primer pair followed by lime witches' broom phytoplasma (LWBP), alfalfa witches' broom phytoplasma (AWBP), tomato witches' broom phytoplasma (TWBP), rapeseed phyllody phytoplasma (RPhP), or sesame phyllody phytoplasma (SPhP) primer pairs amplifying, respectively, 146 bp, 90 bp, 96 bp, 140 bp and 143 bp fragments. (A) lanes 1-5 electrophoresis pattern of nested PCR products from plants singly grafted with, respectively, AWBP, RPhP, TWBP, LWBP or SPhP. (B) lanes 1-4 in simultaneous grafting, and (C) lanes 2-5 in non-simultaneous grafting, 146 bp band of LWBP amplified from periwinkle plants having mixed infection with, respectively, AWBP, TWBP, RPhP or SPhP. (D) pairs of bands from simultaneous (left bands) and non-simultaneous (right bands) grafting of RPhP (lanes 2 and 3), AWBP (lanes 4 and 5), TWBP (lanes 6 and 7) and SPhP (lanes 8 and 9) in mixed infection with LWBP. Lanes 6 in (A), 5 in (B) and 1 in (C) and (D) are from healthy periwinkle plants. M, 100bp DNA marker fragments (Fermentas, Vilnius, Lithuania).

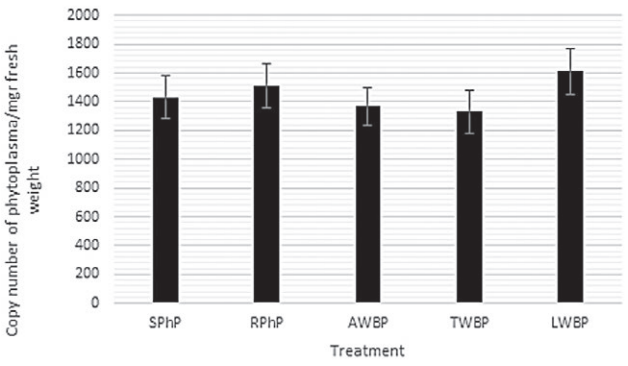

Figure 5. Mean concentrations of lime witches' broom phytoplasma (LWBP), tomato witches' broom phytoplasma (TWBP), alfalfa witches' broom phytoplasma (AWBP), rapeseed phyllody phytoplasma (RPhP) and sesame phyllody phytoplasma (SPhP) in singly grafted periwinkle plants. Bars represent standard deviations.

In all doubly grafted plants, the concentration of LWBP was less than that in the singly grafted plants. A strong antagonistic interaction was observed in mixed infections of LWBP with AWBP or SPhP. The antagonistic relationship was mutual, as the symptoms of both phytoplasmas were greatly reduced. Mixed infections of LWBP + TWBP or LWBP + RPhP resulted in suppression of LWBP concentration, but the symptoms were not suppressed. It is possible that the extent of reduction in concentration of LWBP was not sufficient to affect symptom expression. Another possibility is that there were synergistic effects of these combinations in the host plants for symptom expression, despite the lowered concentrations of the phytoplasmas. Alternatively, other factors besides phytoplasma concentration, such as genes involved

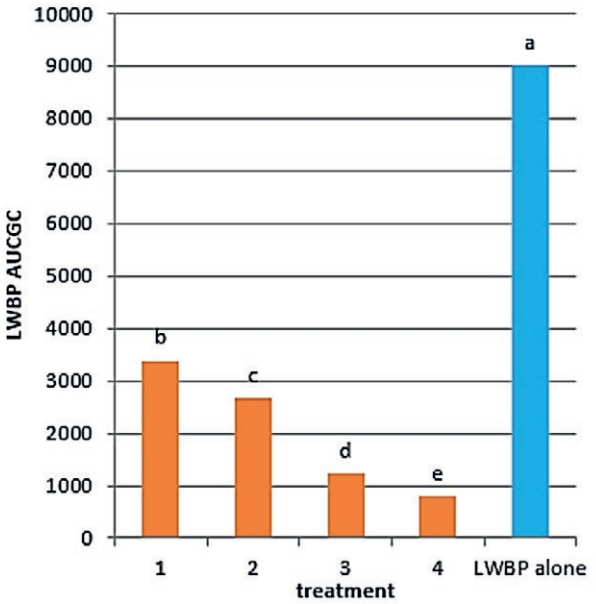

Figure 6. Mean concentrations of lime witches' broom phytoplasma (LWBP) in four mixed infections and a single infection in periwinkle plants, based on areas under concentration growth curves (AUCGC). 1, LWBP (16SrII-B) + rapeseed phyllody phytoplasma (RPhP) (16SrI-B); 2, LWBP + tomato witches' broom phytoplasma (TWBP) (16SrII-D); 3, LWBP + alfalfa witches' broom phytoplasma (AWBP) (16SrII-C); and 4, LWBP + sesame phyllody phytoplasma (SPhP) (16SrIX-C). Means were compared using Duncan Multiple Range Test. Means accompanied by different letters are significantly different ($P \leq 0.05$).

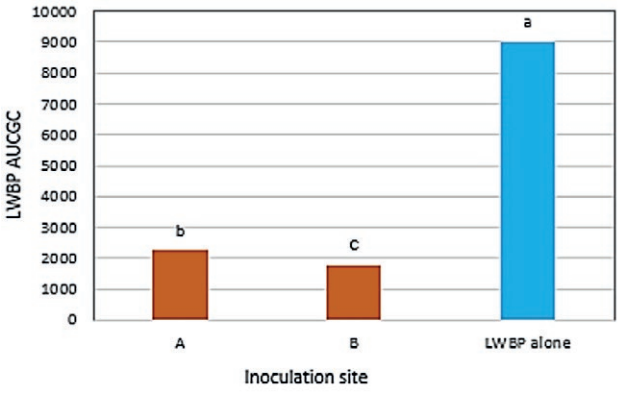

Figure 7. Effect of grafting site on concentration of lime witches' broom phytoplasma (LWBP) (16SrII-B) in mixed grafting and alone: LWBP AUCGC, area under concentration growth curve of LWBP; A, inoculation of the alfalfa witches' broom phytoplasma (AWBP) (16SrII-C), rapeseed phyllody phytoplasma (RPhP) (16SrI-B), sesame phyllody phytoplasma (SPhP) (16SrIX-C) and tomato witches' broom phytoplasmas phytoplasma (TWBP) (16SrII-D) phytoplasmas above the site of the LWBP grafting and B, inoculation of the AWBP, RPhP, SPhP and TWBP below the site of the LWBP grafting. A and B are means of the four mixed inoculations. Means with different letters are significantly different ($P \leq 0.05$).

in pathogenicity and/or virulence, may have affected symptom expression.

The results of these experiments show that effects of possible interactions varies with different phytoplasmas. Previous studies have shown that different strains of the same '*Candidatus* Phytoplasma' species may differ in their effectiveness for conferring cross protection (Schneider *et al*., 2014; Kiss e*t al*., 2013). Kiss *et al*., (2013) found a cross effect between a mild strain of apple proliferation (AP, 16SrX-A) and a related phytoplasma strain, Germany stone fruit yellows phytoplasma (16SrX-B), but not between AP and aster yellows (16SrI-B) phytoplasmas. A mutual antagonistic relationship between LWBP and lettuce phyllody phytoplasma (16SrIX-D, DQ889749) in periwinkle plants inoculated via dodder has been reported previously (Salehi *et al*., 2018).

Cross protection with mild strains has been used to control severe strains of viruses (Pennazio and Conti, 2001). The use of this strategy may be justified for controlling severe phytoplasma epidemics if no alternative disease management strategies are available.

Table 3. Analysis of variance (using SAS 9.3 software) of areas under concentration growth curves of LWBP in mixed and singly grafted periwinkle plants.

Source	DF	Type III SS	Mean Square	F value	Pr>F
Treatment	3	71047487.66	23682495.89	105.63	<.0001**
Grafting site	1	3375487.56	3375487.56	15.06	0.0003**
Grafting time	1	5871171.30	5871171.30	26.19	<.0001**
Treatment × grafting site	3	2271979.20	757326.40	3.38	0.0257*
Treatment × grafting time	3	921103.94	307034.65	1.37	0.2634 ns
Grafting site × grafting time	1	2959690.14	2959690.14	13.20	0.0007**
Treatment × grafting site × grafting time	3	1412122.09	470707.36	2.10	0.1126 ns

ns, non-significant; *, $P \leq 0.05$; **, $P \leq 0.01$.

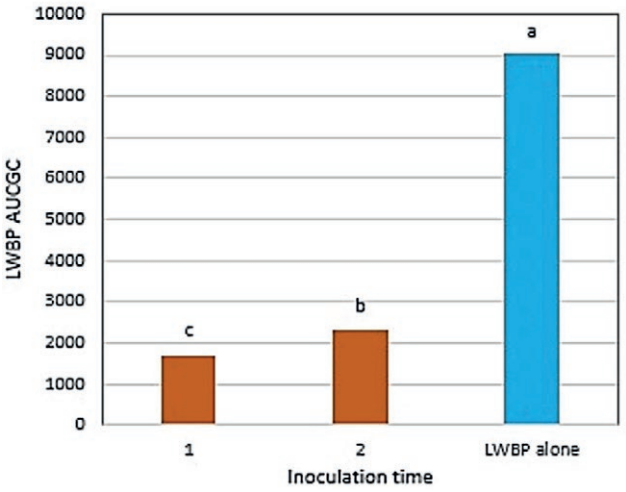

Figure 8. Effect of grafting time (simultaneous and non-simultaneous) on concentration of lime witches' broom phytoplasma (LWBP) in mixed infection with alfalfa witches' broom, rapeseed phyllody, sesame phyllody and tomato witches' broom phytoplasmas as compared with those grafted with LWBP alone: LWBP AUCGC, area under concentration growth curve of LWBP. 1, non-simultaneous and 2, simultaneous grafting. 1 and 2 are means of the four mixed inoculations. Means accompanied by different letters are significantly different ($P \leq 0.05$)

Phytoplasma strains from different 16Sr groups have been reported in citrus plants showing huanglongbing symptoms in *'Candidatus* Liberibacter asiaticus'-free samples or in mixed infection with this pathogen. These phytoplasma strains include 16SrI (Chen *et al.*,2009; Arratia-Castro *et al.*, 2014), 16SrII (Alhudaib *et al.,* 2009; Lou*et al.*, 2013; Saberi *et al.,* 2017), 16SrIII (Wulff *et al.*, 2018), 16SrVI (Das *et al.,* 2016), 16SrIX (Teixeira *et al.,* 2008; Abbasi *et al.*, 2019) and 16SrX-IV (Ghosh *et al.*, 2019). In a survey in some Caribbean countries, phytoplasma strains of 16Sr groups -I, , -III, -IV, -VI, -VII, -XI, and -XII were reported in citrus trees showing "huanglongbing" symptoms, either alone or, more commonly, in mixed infections with '*Ca.* L. asiaticus' (Bertaccini *et al.*, 2019).

The present study has shown that the interactions of LWBP with SPhP or AWBP were more effective in reducing disease symptoms and pathogen titre than those of LWBP with RPhP or TWBP

ACKNOWLEDGEMENTS

This study was part of the first author's PhD research, supported by the Shiraz University Graduate School. The authors declare that they have no conflicts of interest.

LITERATURE CITED

Abbasi A., Hasanzadeh N., Sobh H., Ghayeb Zamharir M., Tohidfar M., 2019. Identification of a group 16SrIX '*Candidatus* Phytoplasma phoenicium' phytoplasma associated with sweet orange exhibiting decline symptoms in Iran. *Australasian Plant Disease Notes* 14: 11.

Abou-Jawdah Y., Karakashina A., Sobh H., Martini M., Lee I-M., 2002. An epidemic of almond witches' broom in Lebanon: classification and phylogenetic relationships of the associated phytoplasma. *Plant Disease* 86: 477–484.

Alhudaib K., Arocha Y., Wilson M., Jones P., 2009. Molecular identification, potential vectors and alternative hosts of the phytoplasma associated with a lime decline disease in Saudi Arabia. *Crop Protection* 28: 13–18.

Anonymous, 2006. Agricultural Statistics of the Year 2006. The Org. of Statistics and information Pub., Tehran, Iran.

Arratia-Castro A. A., Santos-Cervantes M. E., Fernández Herrera E., Chávez-Medina J. A., Flores-Zamora G. L.,…Leyva-López N. E., 2014. Occurrence of '*Candidatus* Phytoplasma asteris' in citrus showing huanglongbing symptoms in Mexico. *Crop Protection* 62:144–151.

Bertaccini A., Duduk B., 2009. Phytoplasma and phytoplasma diseases: a review of recent research. *Phytopathologia Mediterranea* 48: 355–378.

Bertaccini A., Duduk B., Paltrinieri S., Contaldo N., 2014. Phytoplasmas and phytoplasma diseases: a severe threat to agriculture. *American Journal of Plant Sciences* 5:1763–1788.

Bertaccini A., Satta E., Luis-Pantog M., Paredes-Tomás C., Yuneau Y., Myrie W. 2019. '*Candidatus* Phytoplasma' and '*Candidatus* Liberibacter' species detection in citrus. *Phytopathogenic Mollicutes* 9 (1): 186-188.

Castelain C., Jullian J.P., Lemaire J.M., Morvan G., 2007. Lutte biologique contre l'ECA: la prémunition. *Arboriculture* 611: 33–38.

Chen J. Pu. X., Deng X., Liu S., Li H., Civerolo E., 2009. A phytoplasma related to '*Candidatus* phytoplasma asteris' detected in citrus showing "huanglongbing" (yellow shoot disease) symptoms in Guangdong, P.R. China. *Phytopathology* 99: 236–242.

Das A. K., Nerkar S., Thakre N., Kumar A., 2016. First report of '*Candidatus* Phytoplasma trifolii' (16SrVI-group) in Nagpur mandarin (*Citrus reticulata*) showing "huanglongbing" symptoms in central India. *New Disease Reports* 34: 15.

Deng S., Hiruki C., 1991. Amplification of 16S rRNA genes from culturable and nonculturable mollicutes. *Journal of Microbiological Methods* 14: 53–61.

Esmailzadeh-Hosseini S.A., Khodakaramian G., Salehi M., Fani S.R., Bolok Yazdi H.R., Bertaccini A., 2015. Status of alfalfa witches' broom phytoplasma disease in Iran. *Phytopathogenic Mollicutes* 5: S65–S66.

Freitag J.H., 1964. Interaction and mutual suppression among three strains of aster yellows virus. *Virology* 24: 401–413.

Garnier M., Zreik L., Bové J-M., 1991. Witches' broom, a lethal mycoplasmal disease of lime trees in the Sultanate of Oman and the United Arab Emirates. *Plant Disease* 75: 546–555.

Garrett K.A., Madden L.V., Hughes G., Pfender W.F., 2004. New applications of statistical tools in plant pathology. *Phytopathology* 94: 999–1003.

Ghosh D.K., Motghare M., Kokane A., Kokane S., Warghane A., Ladaniya M. S., 2019. First report of a '*Candidatus* Phytoplasma cynodontis'-related strain (group 16SrXIV) associated with Huanglongbing disease on *Citrus grandis*. *Australasian Plant Disease Notes* 14: 9.

Kiss E., Seemuller E., Sule S., 2013. Cross-protection test with *'Candidatus* Phytoplasma mali' 1/93 strain against closely and distantly related phytoplasma strains. *Acta Phytopathologica et Entomologica Hungarica* 48: 207–218.

Kunkel L.O., 1955. Cross protection between strains of aster yellows. *Advances in Virus Research* 3: 251-273.

Lee I-M., Davis R. E., Gundersen-Rindal D. E., 2000. Phytoplasma: Phytopathogenic mollicutes. *Annual Review of Microbiology* 54: 221–255.

Lou B., Bai X., Bai Y., Deng C., Roy Chowdhury M., Song Y., 2013. Detection and molecular characterization of a 16SrII-A* phytoplasma in grapefruit (*Citrus paradise*) with huanglongbing like symptoms in China. *Journal of Phytopathology* 162: 387–395.

Mannan S. H., Ibrahimi M., Chohan S. H. N., Holford P., 2010. Detection of phytoplasma in citrus orchard of Pakistan. *Journal of Phytology* 2: 49-54.

Marcone C., Jarausch B., Jarausch W., 2010. '*Candidatus* Phytoplasma prunorum', the causal agent of European stone fruit yellows: an overview. *Journal of Plant Pathology* 92: 19–34.

McCoy R. E., Caudwell A., Chang C. J., Chen T. A., Chiykowski L. N., Seemüller E., 1989. Plant disease associated with mycoplasma- like organisms. In: *The Mycoplasmas, Vol. V, Spiroplasmas, Acholeplasmas and Mycoplasmas of Plants and Insects* (R.F. Whitcomb, J.G. Tully, ed.), Academic Press, New York, NY, USA, 545–640.

Pennazio R. P., Conti M., 2001. A history of plant virology. Cross protection and application. *Microbiologica* 24: 99–114.

Saberi E., Alavi A. M., Safaie N., Moslemkhany C., Azadvar M., 2017. Bacterial pathogens associated with citrus huanglongbing-like symptoms in southern Iran. *Journal of Crop Protection* 6: 99–113.

Salehi Abarghouei E., Izadpanah K., Taghavi S. M., Hamzezarghani H., Afsharifar A., 2018. Interaction of witches' broom disease of lime phytoplasma and lettuce phyllody phytoplasma in mixed infection of periwinkle plants. *Iranian Journal of Plant Pathology* 54: 131–146.

Salehi E., Salehi M., Taghavi S. M., Izadpanah K., 2014. A 16SrII-D phytoplasma strain associated with tomato witches' broom in Bushehr province. *Journal of Crop Protection* 3: 377–388.

Salehi M., 2016. Control strategies of witches' broom disease of lime in Iran. In: *Proceedings of 22nd Iranian Plant Protection Congress, College of Agriculture and Natural Resources*, *2016,* University of Tehran, Karaj, Iran, 364.

Salehi M., Izadpanah K., Taghizadeh M., 2002. Witches' broom disease of lime in Iran: new distribution areas, experimental herbaceous hosts and transmission trails. In: *Proceedings 15th Conference of International Organization of Citrus Virologists* (IOCV), Riverside, CA, USA, 293–296.

Salehi M., Izadpanah K., Siampour M., 2011. Occurrence, molecular characterization and vector transmission of a phytoplasma associated with rapeseed phyllody in Iran. *Journal of Plant Pathology* 159: 100–105.

Salehi M., Esmailzadeh-Hosseini S. A., Salehi E., Bertaccini A., 2017. Genetic diversity and vector transmission of phytoplasmas associated with sesame phyllody in Iran. *Folia Microbiologica* 62: 99–109.

Sambrook J., Fritsch E. F., Maniatis T., 1989. *Molecular Cloning: A Laboratory Manual. II ed.* Cold Spring Harbour Laboratory Press, Cold Spring Harbour, New York, NY, USA.

Sanches M. M., Wulff N. A., Ferreira E. A., Santos J. F., Angarten M. B. O., …Martins O. A., 2016. Survey for phytoplasmas and '*Candidatus* Liberibacter' sp. from HLB-like symptomatic citrus plants in Brazil. *Citrus Research and Technology* 37: 88–93.

Schneider B., Seemüller E., Smart C. D., Kirkpatrick B. C., 1995. Phylogenetic classification of plant pathogenic mycoplasma like organisms or phytoplasmas. In: *Molecular and Diagnostic Procedures in Mycoplasmology* (S. Razin, J. G. Tully, ed.) Academic Press, San Diego, CA, USA, 369–380.

Schneider B., Sule S., Jelkmann W., Seemüller E., 2014. Suppression of aggressive strains of '*Candidatus* Phytoplasma mali' by mild strains in *Catharanthus roseus* and *Nicotiana occidentalis* and identification

of similar action in apple trees. *Phytopathology* 104: 453–461.

Seemüller E., Marcone C., Lauer U., Ragozzino A., Göschl M., 1998. Current status of molecular classification of the phytoplasmas. *Journal of Plant Pathology* 80: 3–26.

Sinclair W. A., Griffiths H. M., 2000. Variation in aggressiveness of ash yellows phytoplasmas. *Plant Disease* 84: 282–288.

Syller J., 2012. Facilitative and antagonistic interactions between plant viruses in mixed infections. *Molecular Plant Pathology* 13: 204–216.

Teixeira D. C., Wulff N. A., Martins E. C., Kitajima E. W., Bassanezi R., Bové J-M., 2008. A phytoplasma closely related to the pigeon pea witches' broom phytoplasma (16SrIX) is associated with citrus huanglongbing symptoms in the state of Sao Paulo, Brazil. *Phytopathology* 98: 977–984.

Untergasser A., Cutcutache I. K., Koressaar T., Ye. J., Faircloth B. C., Rozen S. G., 2012. Primer3-new capabilities and interfaces. *Nucleic Acids Research* 40: 115.

Valenta V., 1959. Interference studies with yellows-type plant viruses. II. Cross protection tests with European and American viruses. *Acta Virologica* 3: 145–152.

Wulff N. A., Fassini C. G., Marques V. V., Martins E. C., Coletti D. A. B., Bové J-M., 2018. Molecular characterization and detection of 16SrIII group phytoplasma associated with Huanglongbing symptoms. *Phytopathology* 109: 366-374.

Zhang Y., Uyemoto J. K., Kirkpatrick B. C., 1998. A small-scale procedure for extracting nucleic acids from woody plants infected with various phytopathogens for PCR assay. *Journal of Virological Methods* 71: 45–50.

Zreik L., Carle P., Bové J-M., Garnier M., 1995. Characterization of the mycoplasma like organism associated with witches' broom disease of lime and proposition of a candidate taxon for the organism, *'Candidatus* Phytoplasma aurantifolia'. *International Journal of Systematic Bacteriology* 45: 449–453.

Phytopathologia Mediterranea
The international journal of the
Mediterranean Phytopathological Union

Firenze University Press
www.fupress.com/pm

Research Papers

Comparison of conventional and novel molecular diagnostic methods for detection of *Xylella fastidiosa* from insect vectors

Ornella INCERTI[1], Hiba DAKROUB[1], Motasem KHASIB[1], Vincenzo CAVALIERI[2], Toufic ELBEAINO[1,*]

[1] *Istituto Agronomico Mediterraneo di Bari, Via Ceglie 9, 70010 Valenzano (BA), Italy*
[2] *Institute for Sustainable Plant Protection, National Research Council, Via Amendola 122/D, 70126 Bari, Italy*
*Corresponding author: elbeaino@iamb.it

Summary. The efficiency of three diagnostic methods, i.e. PCR, real-time PCR and LAMP, for detection of *Xylella fastidiosa* (*Xf*) genomic DNA from *Philaenus spumarius* (*Ps*) and *Neophilaenus campestris* (*Nc*) insect vectors was evaluated using three total nucleic acids (TNA) extraction methods (EM). In addition, a new real-time LAMP technology, Fluorescence of Loop Primer Upon Self Dequenching-LAMP (FLOS-LAMP), originally developed for human virus diagnoses, was optimized and assessed for detection of Xf in insect vectors. EM1 consisted of entire insects heated in an extraction buffer (EB) containing Tris-EDTA and TRITON-X100. In EM2, TNAs were extracted only from excised heads of insects, and heated again in the EB of EM1. EM3 consisted of grinding entire insects, heads and bodies recuperated from EM2, with a CTAB buffer. The molecular analyses conducted on 100 specimens of Ps and 50 of Nc, collected from a Xf-infected olive orchard (Lecce province, Italy), showed that 29% of specimens (40 Ps and four Nc) were positive to the presence of Xf. The comparison between the three methods revealed that EM3 is the most efficient for extracting Xf-genomic DNA from insect vectors, of which 44 specimens were positive for Xf in each of the diagnostic methods used, including the newly optimized FLOS-LAMP assay. In general, the real-time PCR and LAMP assays were more competent than the conventional PCR for detection of Xf in insect vectors, independently from the EM used. The newly optimized FLOS-LAMP technique had a detection limit of 1 fg μL^{-1} of Xf-genomic DNA, compared to the 10 fg μL^{-1} for conventional LAMP. The high sensitivity of the FLOS-LAMP was evident through the greater number of overall Xf-infected insect vectors detected (60%), compared to those for LAMP (45%,), real-time PCR (28%) and PCR (10%). FLOS-LAMP, being a more sensitive and specific assay, together with EM3, were the most appropriate approaches for an accurate detection of Xf in insect vectors.

Keywords. *Philaenus spumarius*, *Neophilaenus campestris*, PCR, real-time PCR, LAMP, FLOS-LAMP

OPEN ACCESS

Citation: O. Incerti, H. Dakroub, M. Khasib, V. Cavalieri, T. Elbeaino (2020) Comparison of conventional and novel molecular diagnostic methods for detection of *Xylella fastidiosa* from insect vectors. *Phytopathologia Mediterranea* 59(2): 261-267. DOI: 10.14601/Phyto-11222

Accepted: May 26, 2020

Published: August 31, 2020

Data Availability Statement: All relevant data are within the paper and its Supporting Information files.

Competing Interests: The Author(s) declare(s) no conflict of interest.

Editor: Jesus Murillo, Public University of Navarre, Spain.

INTRODUCTION

Xylella fastidiosa (*Xf*) is a xylem-inhabiting, vector-borne, Gram-negative polyphagous plant pathogenic bacteria, which causes important diseases on many crops (Denancé *et al.*, 2019). In Europe, *Xf* has been reported firstly in Italy and subsequently in France, Spain, Portugal and Germany (outbreak eradicated), where three different subspecies of the pathogen have been found (EFSA, 2019). In Italy, *Xf* is associated with the Olive Quick Decline Syndrome (OQDS), causing leaf scorch; extensive dieback and death of plants (Martelli *et al.*, 2016). In nature, the short-distance transmission of *Xf* occurs through xylem-feeding insects, such as sharpshooter leafhoppers (family *Cicadellidae*) and spittlebugs (family *Aphrophoridae*) (Redak *et al.*, 2004). In the Apulia region (south of Italy), the meadow spittlebug *Philaenus spumarius* L. (*Ps*), *P. italosignus* Drosopolous & Remane (*Pi*) and *Neophilaenus campestris* (Fallen) (*Nc*) had been reported as vectors of *Xf*, transmitting the bacterium from infected to uninfected plants (Elbeaino *et al.*, 2014; Bucci ,2018; Cavalieri *et al.*, 2019). Furthermore, *Ps* has been recognized as the major vector involved in the spread of *Xf* infections among olive trees in the Apulia region, being the most abundant and prevalent insect vector species (Cavalieri *et al.*, 2019).

The diagnostic methods used to detect *Xf* in infected plant material and/or insect vectors include serological (DAS-ELISA, DTBIA) and molecular (PCR, real-time PCR and LAMP) techniques; and molecular techniques are recommended exclusively for detection of the pathogen in insect vectors (EPPO PM7\24[4], 2019). Molecular techniques are the most widely used due to their high throughput potential for detecting *Xf*-genomic DNA in plants and\or insect vectors. However, their application is hampered by: (i) low concentrations of bacterial DNA in infected sources, (ii) adequate protocols for extracting pure DNA, (iii) host microbiome-related DNA similar to that of *Xf*, (iv) heavy reliance on indirect detection methods including non-specific dyes, (v) on site application (laboratory, field, inspection points), (vi) techniques with laborious handling, and (vi) high costs.

To cope with these constraints, the present study aimed to compare PCR, real-time PCR and LAMP assays, and to evaluate their efficiency and sensitivity for detection of *Xf* in *Ps* and *Nc*. Application of the recently developed technique, Fluorescence of Loop Primer Upon Self Dequenching-LAMP (FLOS-LAMP) was also evaluated. This technique relies on direct detection, whereby a labeled loop probe quenched in its unbound state, fluoresces only when bound to its target (Gadkar *et al.*, 2018). This new approach of using labeled fluorescent primers in the LAMP assay offers increased sensitivity and specificity in the detection of *Xf*, which could cope with the constraints mentioned above. These evaluation trials were conducted on three different total nucleic acids (TNA) extraction methods (EM) of *Xf*-genomic DNA from insect vectors.

MATERIALS AND METHODS

Collection of infected plant material and insect vectors

In September 2018, 24 samples of scorched leaves were collected from olive trees situated in, and nearby to, the '*De Donno*' *Xf*-affected orchard (Gallipoli, Lecce province, Italy). This orchard was also screened for the presence of *Ps* and *Nc* insect vectors. Insects were manually trapped using a sweeping net, which was passed over the olive canopy and ground vegetation. Individual insects were stored in a solution of 95% ethanol and were brought to the laboratory for species identification. The classification and nomenclature of captured insects were based on key taxonomic factors described in Elbeaino *et al.* (2014). During the identification, only *Ps* and *Nc* specimens were retained and were stored at -20°C for the molecular analyses.

Extraction of total nucleic acids from plants and insect vectors

Bacterium DNA was extracted from leaf tissues of infected olive plants following the CTAB protocol (2% hexadecyl trimethyl-ammonium bromide, 0.1 M Tris-HCl pH 8, 20 mM EDTA and 1.4 M NaCl) (Hendson *et al.*, 2001). Briefly and for each sample, a 0.3 g piece of fresh leaf midrib and petiole was homogenized with 2 mL of CTAB buffer, using an automated hammer. Extracted sap was incubated at 65°C and then chloroform treated. TNA was precipitated with 0.6 volume of cold 2-propanol and resuspended in 120 µL of sterile water. Samples were used in various molecular assays as positive controls. TNAs were extracted from *Ps* and *Nc* insects by three different EM that were performed as the following:

(i) EM1: Insects were each rinsed with sterile water, dried on a tissue paper, and then immersed in 200 µL of extraction buffer (EB) containing 1× TE (10mM Tris-HCl, 1mM EDTA-Na_2, pH 8.0) and 0.5% TRITON-X100. The mixture was then incubated for 5 min at 94°C, followed by chilling on ice. A 25 µL volume of TNA from the EM1 was stored at -20°C for further molecular analysis. The remaining 175 µL containing the TNAs

in suspension, and not the insect, were added to the TNAs obtained from EM2 and all were precipitated in one plastic tube with cold 2-propanol at 10 000 g for 20 min. Through this operation, 87.5% of the TNA (175 µL of 200 µL of EB) obtained from each insect in EM1 was recovered; and by adding it to that extracted in EM2, the total amount of TNA that should normally be extracted in EM2 would not be compromised. Consequently, the comparison of the different diagnostic tests applied on the TNA models of each EM would be valid.

(ii) EM2: The heads of individual adult insect specimens were excised from the bodies, as reported in Elbeaino *et al.* (2014). Each insect body was stored in a plastic tube for further manipulation in EM3. Each excised head was added to 200 µL of EB and heated as described in EM1. A 25 µL volume containing the TNA was also stored separately for subsequent molecular assays. The remaining 175 µL were further precipitated with the TNAs obtained during EM3.

(iii) EM3: the head and body of each insect, recovered from EM1 and EM2, was ground in a mortar and pestle containing 500 µL of CTAB and carborundum particles. The extract was incubated at 65°C for 10 min and subsequently treated with chloroform for further purification. The supernatant was centrifuged at 8,000 g for 5 min, and then precipitated together with the 175 µL TNAs from EM2 with 0.6 volume of cold 2-propanol. The recovered TNAs were resuspended in 30 µL of sterile water. TNA samples from various methods were used in different molecular assays.

PCR, real-time PCR, LAMP and FLOS-LAMP

The TNA samples obtained from each insect using the three methods were subjected to PCR, real-time PCR and LAMP assays for the detection of *Xf*. Conventional PCR has been performed on TNA of olive plants to identify infected samples to be used as *Xf*-positive controls in the different molecular procedures. PCR reactions were performed using primers RST31/33, widely used in the detection of different *Xf* subspecies (Minsavage *et al.*, 1994), in a 1× amplification buffer in a final volume of 25 µL containing 2.5 µL of TNA, 0.2 mM of dNTPs, 0.2 µM of each primer and 1.25 U of DreamTaq™ DNA polymerase (Thermofisher). PCR cycles were as follows: 95°C for 1 min followed by 40 cycles of (95°C for 30 s, 55°C for 30 s, 72°C for 45 s) and a final step of 72°C for 5 min. All reactions were submitted to electrophoresis in 1.2% TAE agarose gels.

Real-time PCR was performed as described by Harper *et al.* (2010, *erratum* 2013), in 20 µL reaction volumes containing 10 µL of the SsoAdvanced ™ Universal Probes Supermix (BioRad), 0.3 µM *Xf*-forward (*XF*-F) and *Xf*-reverse (*XF*-R) primers, 0.1 µM of labeled *XF*-P probe and 2.5 µL of TNA. Thermocycling conditions were as follows: 95°C for 6 min, followed by 40 cycles of 94°C for 10 s and 62°C for 40 s. Reactions were conducted in a CFX96 thermocycler (BioRad,). A cycle threshold (Ct) value below 35 was scored as a positive result.

LAMP assays were carried out using Enbiotech's LAMP system® (Yaseen *et al.*, 2015). Reactions were carried out in 25 µL of final volume using 2.5 µL of TNA and 22.5 µL of LAMP Mix, at 65°C for 30 min in a CFX96 thermocycler.

The FLOS-LAMP approach developed in this study was based on three sets of primers; namely outer, inner and loop, used in LAMP for the detection of *Xf* (Harper *et al.*, 2010 *erratum* 2013). The B3, BIP and LB in, respectively, the outer, inner and loop primers categories, were appropriate to be labeled by substituting the internal thymine (T) residue at the 3' terminus of the primer with the fluorescein (FAM) fluorophore (Table 1). The criteria followed for the exact T residue to which the fluorophore can be attached were those reported in Gad-

Table 1. Six primers of three categories (outer, inner and loop) used in the FLOS-LAMP assay. The internal thymine residues (**T**) at the 3' terminus of primers for each category (B3, BIP, LB) were fluorescein-labeled.

Primer	Sequence (5'-3')	Binding sites on *Xf* genome
Outer		
Xf-F3	CCGTTGGAAAACAGATGGGA	(106,676–106,694)
Lab*Xf*-B3	GAGACTGGCAAGCGTT**T**GA	(106,884–106,865)
Inner		
Xf-FIP	ACCCCGACGAGTATTACTGGGTTTTTCGCTACCGAGAACCACAC	(106,788–106,862)
Lab*Xf*-BIP	GCGCTGCGTGGCACATAGATTTTTGCAACCTTTCCTGGCA**T**CAA	(106,773–106,695)
Loop		
Xf-LF	TGCAAGTACACACCCTTGAAG	(106,824–106,844)
Lab*Xf*-LB	TTCCGTACCACAGA**T**CGCT	(106,753–106,735)

kar *et al.* (2018), *i.e.* (i) presence of cytosine or guanine residue at the terminal 3' end, (ii) T residue at the second or third position from this 3' end, and (iii) one or more G nucleotides flanking the T residue. Different combinations of labelled primers were tested in the FLOS-LAMP assays. PCR reactions were performed in a 25 µL of final volume containing 2.5 µL 10× Isothermal amplification Buffer, 5 µM of $MgSO_4$, 1.4 mM dNTPs mix with 0.06 µM of *XF*-F3/*XF*-B3 outer primers, 0.12 µM pf *XF*-LF/*XF*-LB loop primers, 0.5 µM of *XF*-FIP/*XF*-BIP inner primers, 2,400U of *Bst* 3.0 DNA Polymerase (New England Biolabs) and 2.5 µL of DNA sample. The thermocycler used for FLOS-LAMP was a BioRad CFX96.

Sensitivity of FLOS-LAMP

In order to determine the detection limit of the newly FLOS-LAMP, optimized for the detection of *Xf*, 10-fold serial dilutions of 10 ng μL^{-1} of DNA extracted from a pure culture of *Xf*-ST53 strain were conducted and subjected to FLOS-LAMP assay, following the conditions and cycles described above.

RESULTS

Identification of Ps and Nc

In total, 233 adult specimens of *Ps* and 141 of *Nc* were identified. One hundred *Ps* and 50 *Nc* specimens were randomly selected and used in the molecular analyses. The large number of *Ps* captured from the ground vegetation and canopies of olive trees in the affected orchard reflect the high population density of this species in the Apulian environment, compared to that of *Nc*. This predominance of *Ps* was also recorded in previous epidemiological studies of these two species in the Apulia region (Ben Moussa *et al.*, 2016; Cavalieri *et al.*, 2019).

PCR, real-time PCR, LAMP

PCR assays conducted on olive leaf samples showed that 22 plants (out of 26 tested) were infected with *Xf*. This high proportion of infections was expected, since *Xf* is widespread in the Gallipoli location. PCR assays conducted on TNAs from the three EM detected *Xf* only in aliquots obtained from the EM3, for which 40 specimens of *Ps* and four of *Nc* were positive for presence of *Xf* (Table 2).

The real-time PCR gave negative results when applied to TNA extracts from EM1; whereas those from EM2 and EM3 were more appropriate for amplifying *Xf*-genomic DNA (Figure 1). Twenty-four specimens of *Ps* and three of *Nc* were found with *Xf* in EM2; whereas 40 *Ps* and four of *Nc* positive specimens were detected when TNAs from EM3 were used (Table 2).

LAMP assays showed differential positive reactions when applied on TNAs from EM1, EM2 and EM3 (Figure 1). For *Ps*, this assay detected 16, 34 and 40 *Xf*-infected insects from, respectively, EM1, EM2 and EM3. For *Nc*, only one, two and four *Xf*-infected specimens were detected, respectively, from EM1, EM2 and EM3. The proportions of infections detected with LAMP, using our conditions, were 11% from EM1, 24% from EM2 and 29 % from EM3.

FLOS-LAMP

Among the outer, inner and loop functional categories defined for the six-primer LAMP, the *XF*-LB primer identified only in the loop category in FLOS-LAMP of the *Xf* genomic DNA. Positive fluorescence signals were gener-

Table 2. Comparative analyses between PCR, real-time PCR, LAMP and FLOS-LAMP assays, applied on TNAs extracted by three different methods (EM1, EM2 and EM3) from 100 *Philaenus spumarius* (*Ps*) and 50 *Neophilaenus campestris (Nc*) specimens, for detection of *Xylella fastidiosa* (*Xf*).

Insect species	PCR			Real-time PCR			LAMP			FLOS-LAMP		
	EM1	EM2	EM3	EM1	EM2	EM3	EM1	EM2	EM3	EM1	EM2	EM3
Xf-positive *Ps*	0	0	40	0	24	40	16	34	40	34	36	40
Xf-positive *Nc*	0	0	4	0	3	4	1	2	4	3	3	4
Ps-, *Nc*-*Xf* positive	0	0	44	0	27	44	17	36	44	37	39	44
Infection %	0	0	29.3	0	18	29.3	11.3	24	29.3	24.6	26	29.3
Detection %	0	0	100	0	61.3	100	38.6	81.8	100	84	88.6	100
Mean detection %		9.7			27.7			45			60.3	

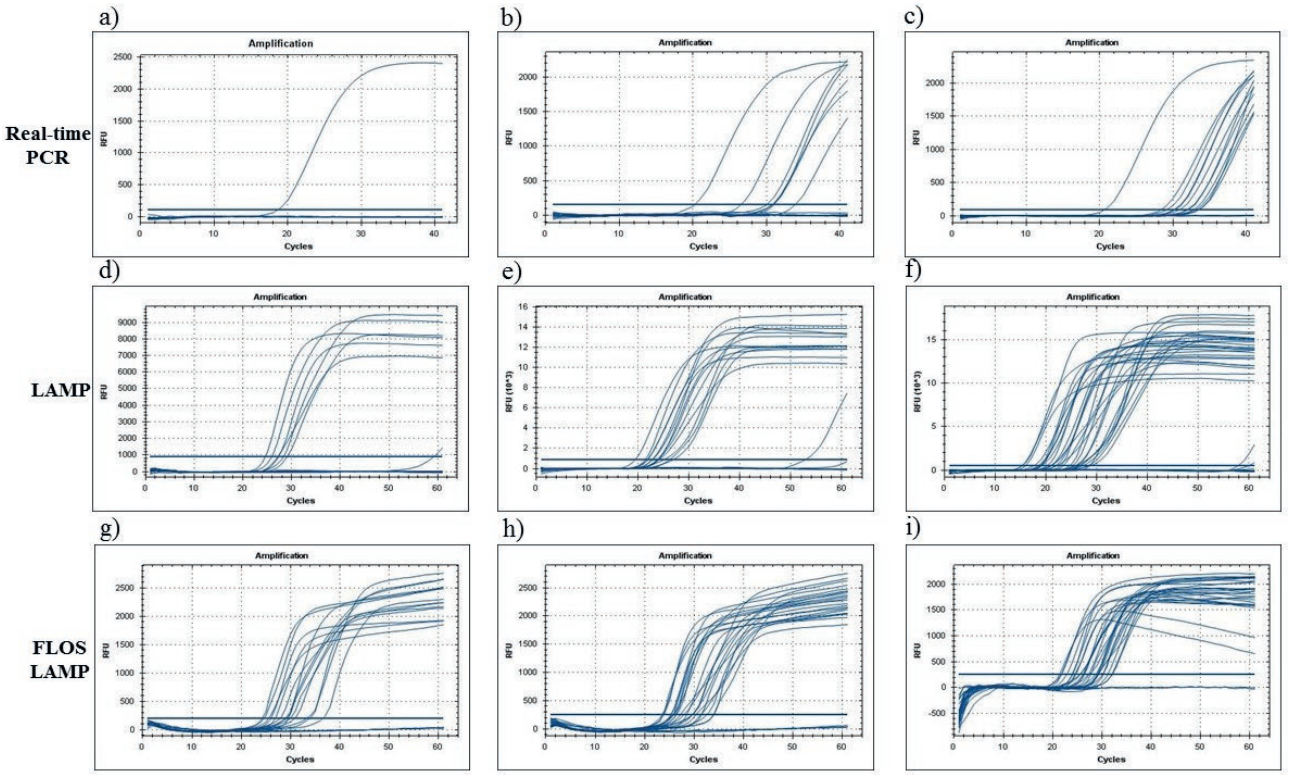

Figure 1. Differential responses of real-time PCR, LAMP and FLOS-LAMP assays to *Xylella fastidiosa* (*Xf*) infections in *Philaenus spumarius* and 50 *Neophilaenus campestris* specimens, using TNA extracted with three different methods (EM1, EM2 and EM3) for the same insects. *Xf*-positive reactions increased when TNA from EM1, EM2 and EM3, and from real-time PCR to FLOS-LAMP were used. A cycle threshold (Ct) values below 35 were scored as positives.

ated when the FAM-labeled LB probe was tested against the templates. No signals were detected from FAM-labeled FIP and B3 primers functioning as probes. This indicated that the *XF*-LB self-quenched FLOS probe bound and fluoresced only in the presence of *Xf*-genomic DNA target. The FLOS-LAMP confirmed the PCR results, successfully amplifying all samples found PCR-positive to *Xf*, without producing non-specific reactions from healthy plants.

Of the 150 insects analyzed, 34 *Xf*-infected *Ps* were identified using EM1, 36 using EM2 and 40 were identified using EM3. Three *Nc* positive specimens were detected using EM1 and EM2, and four positives were detected using EM3 (Figure 1). Based on the FLOS-LAMP approach, the proportions of infection were 256% using EM1, 26% using EM2 and of 29% using EM3 (Table 2). These results reflected the different sensitivity and specificity of the two approaches. Overall, FLOS-LAMP applied to samples from EM1, EM2 and EM3 detected greater numbers of *Xf*-infected insect vectors, thus identifying 60% of the *Xf*-positive samples. The LAMP assay identified 45% of the positive samples, with increments of 13% for EM1 and 2% for EM2.

Detection limit of FLOS-LAMP

FLOS-LAMP gave high levels of sensitivity by amplifying all dilutions greater than 1 fg μL^{-1}. Compared to the sensitivity of the other techniques tested here, FLOS-LAMP was 10 times more sensitive than conventional LAMP. The detection limit of LAMP is reported to be 10 fg μL^{-1} for *Xf*-genomic DNA (Yaseen *et al.*, 2015), and 100 times more than that of real-time PCR (Harper *et al.*, 2010, *erratum* 2013). The sensitivity of FLOS-LAMP was demonstrated by the large number of positive samples detected from EM1 (37 *Xf*-infected *Ps* and *Nc* compared to 17 in LAMP) and EM2 (39 *Xf*-infected *Ps* and *Nc* compared to 36 in LAMP).

DISCUSSION

Detection of *Xf* in infected plant material is conventionally carried out using serological (ELISA) and molecular (PCR, real-time PCR and LAMP) diagnostic techniques. When versatility, precision and sensi-

tivity are required, preferential differences occur with application of these approaches. Serological assays have been widely adopted to detect *Xf* in infected plant material but not for detection in insect vectors. The preferential use of some methods is conditioned by the nature of this pathogen. Localization of the pathogen in host xylem tissues makes extraction difficult. Uneven distribution within plants can miss infected tissues with high bacterium concentrations. Latent infections due to the low bacterium concentrations can be less than minimum detection limits for some techniques. Most importantly, some techniques must be validated for not previously identified insect vectors of *Xf*. Therefore, we aimed to compare, validate and refine conventional and new diagnostic methods for the detection of *Xf* in *Ps* and *Nc* vectors of the pathogen. In our conditions, the EM3, *i.e.* grinding whole insects using the CTAB protocol, was the most suitable for extracting enough *Xf*-genomic DNA to be detectable using conventional and new molecular techniques, including the FLOS-LAMP assay here optimized. This was confirmed by identification of the greatest number of *Xf*-infected insects (44 specimens) in all four diagnostic techniques using TNA extracts from EM3.

Among the three EM tested here, EM1 and EM2 were the simplest to perform and least expensive, as few reagents were needed for their preparations. However, their outcomes remain precarious when used in different diagnostic techniques to detect *Xf* in insect vectors. In contrast, EM3 was the most efficient for bacterial DNA extraction but required greater effort than the other two extractions.

In general, the real-time PCR and LAMP techniques were more efficient than the conventional PCR for detection *Xf* in the insect vectors, independently from the EM used. Furthermore, when applied on TNAs from EM2, real-time PCR was more sensitive (18% infection), identifying 24 *Xf*-infected *Ps* and three infected *Nc*, compared with no detection using PCR. The failure of the real-time PCR to detect *Xf* in TNAs from EM1, and of the PCR when extracts from EM1 and EM2 were used, was probably due to the low concentration of bacterial DNA. The real-time PCR was therefore more sensitive than the PCR, and detected *Xf*-infected samples in extracts from EM2 with greater bacterial DNA concentration. However, and as expected, the LAMP method had high sensitivity, detecting 17 *Xf*-infected specimens in TNAs from EM1, while the other techniques did not detect the pathogen. The FLOS-LAMP technique gave even greater sensitivity than the LAMP assay, particularly when applied on TNAs from EM1, with 37 positive specimens detected compared with 17 from LAMP and none from real-time PCR and conventional PCR. This superiority was tested for detection of 1 fg μL^{-1}l of *Xf*-genomic DNA compared to that reported for conventional LAMP (10 fg μL^{-1}) (Yaseen *et al.*, 2015). Another advantage of the FLOS-LAMP was the reduction of non-specific reactions observed in the conventional LAMP assays after a Ct value >35 (Figure 1). This, often-generated misinterpretation of results, for whether those insect vectors should be considered as negative to the presence of *Xf* or positive with low *Xf*-genomic DNA concentrations, resulting in a greater Ct value. These artifacts of LAMP reactions, probably caused by the use of non-specific dyes, are overcome using self-quenching fluorogenic probes, in a direct detection approach. This increases the specificity of LAMP reactions.

In terms of costs, LAMP and FLOS-LAMP are inexpensive when the various components of the reactions are managed in the laboratory without the need to purchase commercial kits. Under our conditions, the estimated costs for LAMP and FLOS-LAMP were, respectively, approx. 0.2 and 0.25 Euro per sample, compared with an average of 10 Euro per sample required by diagnostic companies. The only disadvantage of the FLOS-LAMP, similarly to LAMP, is high sensitivity, which is a disadvantage when dealing with very small DNA contaminations, leading to false positive reactions that would be irrelevant in other techniques (PCR, ELISA).

This study has demonstrated that EM1 and EM2 are not suitable for extracting enough amounts of *Xf*-genomic DNA for amplification using any of the techniques here tested. The FLOS-LAMP technique was found, in our conditions, to be more sensitive and specific than conventional LAMP. We recommend that FLOS-LAMP be used for testing of *Ps* and *Nc* insect vectors for the presence of *Xf* in infested regions.

ACKNOWLEDGMENT

Part of the research conducted in this study was promoted by "EUPHRESCO" with 'non-competitive funding'.

LITERATURE CITED

Ben Moussa I.E., Mazzoni V., Valentini F., Yaseen T., Lorusso D., … D'Onghia A.M., 2016. Seasonal fluctuations of sap-feeding insect species infected by *Xylella fastidiosa* in Apulian olive groves of southern Italy. *Journal of Economic Entomology* 109: 1512–1518.

Bucci E.M., 2018. *Xylella fastidiosa*, a new plant pathogen that threatens global farming: Ecology, molecular biology, search for remedies. *Biochemical and Biophysical Research Communications* 502: 173–182.

Cavalieri V., Altamura G., Fumarola G., Di Carolo M., Saponari M., … Dongiovanni C., 2019. Transmission of *Xylella fastidiosa* subspecies *pauca* sequence type 53 by different insect species. *Insects* 10, 324.

Denancé N., Briand M., Gaborieau R., Gaillard S., Jacques M.A., 2019. Identification of genetic relationships and subspecies signatures in *Xylella fastidiosa*. *BMC Genomics* 20: 239. DOI: 10.1186/s12864-019-5565-9.

Elbeaino T., Yaseen T., Valentini F., Ben Moussa I.E., Mazzoni V., D'Onghia A.M., 2014. Identification of three potential insect vectors of *Xylella fastidiosa* in southern Italy. *Phytopathologia Mediterranea* 53: 328–332.

EFSA, 2019. Pest survey card on *Xylella fastidiosa*. *EFSA supporting publication*: EN-1667: 51. DOI: 10.2903/sp.efsa.2019.EN-1667

EPPO Bulletin, 2019. Volume 49, Issue 2, PM 7/24 (4) *Xylella fastidiosa* DOI: 10.1111/epp.12575.

Gadkar V.J., Goldfarb D.M., Gantt S., Tilley P.A.G., 2018. Real-time Detection and Monitoring of Loop Mediated Amplification (LAMP) Reaction Using Self-quenching and De-quenching Fluorogenic Probes. *Scientific Reports* 8: 5548. DOI: 10.1038/s41598-018-23930-1.

Harper S., Ward L., Clover G., 2010. Development of LAMP and real-time PCR methods for the rapid detection of *Xylella fastidiosa* for quarantine and field applications. *Phytopathology* 100: 1282–1288.

Hendson M., Purcell A.H., Chen D., Smart C., Guilhabert M., Kirkpatrick B., 2001. Genetic diversity of Pierce's disease strain and other pathotypes of *Xylella fastidiosa*. *Applied Environmental Microbiology* 67: 895–903.

Martelli G.P., Boscia D., Porcelli F., Saponari M., 2016. The olive quick decline syndrome in south-east Italy: a threatening phytosanitary emergency. *European Journal of Plant Pathology* 144: 235–243.

Minsavage G.V., Thompson C.M., Hopkins D.L., Leite M.V.B.C., Stall R.E., 1994. Development of a polymerase chain reaction protocol for detection of *Xylella fastidiosa* in plant tissue. *Phytopathology* 84: 456–461.

Redak R.A., Purcell A.H., Lopes J.R.S., Blua M.J., Mizell R.F., Andersen P.C., 2014. The biology of xylem fluid-feeding insect vectors of *Xylella fastidiosa* and their relation to disease epidemiology. *Annual Review of Entomology* 49: 243–245.

Yaseen T., Drago S., Valentini F., Elbeaino T., Stampone G., … D'Onghia A.M., 2015. On-site detection of *Xylella fastidiosa* in host plants and in "spy insects" using the real-time loop-mediated isothermal amplification method. *Phytopathologia Mediterranea* 54: 488–496.

Phytopathologia Mediterranea
The international journal of the
Mediterranean Phytopathological Union

Firenze University Press
www.fupress.com/pm

Research Papers

New insights into scabby canker of *Opuntia ficus-indica*, caused by *Neofusicoccum batangarum*

Francesco ALOI[1,2,§], Selene GIAMBRA[2,§], Leonardo SCHENA[3], Giuseppe SURICO[4], Antonella PANE[1], Giorgio GUSELLA[2], Claudia STRACQUADANIO[1,3], Santella BURRUANO[2], Santa Olga CACCIOLA[1,*]

[1] *Department of Agriculture, Food and Environment (Di3A), University of Catania, Via Santa Sofia 100, I-95123, Catania, Italy*
[2] *Department of Agricultural, Food and Forestry Sciences, University of Palermo, Viale delle Scienze 4, 90128 Palermo, Italy*
[3] *Department of Agriculture, University Mediterranea of Reggio Calabria, Feo di Vito, I89122, Reggio Calabria, Italy*
[4] *Department of Agrifood production and Environmental Sciences, University of Florence, P.le delle Cascine 18, I-50144, Firenze, Italy*
§ These two authors contributed equally to the study
*Corresponding author: olga.cacciola@unict.it

Summary. This study characterizes a fungal disease of cactus pear (*Opuntia ficus-indica*, *Cactaceae*), reported from the minor islands of Sicily. The disease, originally named 'gummy canker', was first reported in 1973 from Linosa, a small island of the Pelagian archipelago, south of Sicily. The causal agent was identified as *Dothiorella ribis* (currently *Neofusicoccum ribis*, *Botryosphaeriaceae*). In a recent survey the disease has been found to be widespread in minor islands around Sicily, including Lampedusa, Linosa, Favignana and Ustica. The causal agent was identified in *Botryosphaeriaceae* as *Neofusicoccum batangarum* on the basis of the phylogenetic analysis of the DNA sequences from ITS, *tef1* and *tub2* sequences, and the disease was renamed 'scabby canker', which describes the typical symptoms on cactus pear cladodes. In artificial inoculations, *N. batangarum* induced symptoms on cactus pear cladodes identical to those observed in naturally infected plants. The fungus also induced cankers on artificially wound-inoculated stems of several common Mediterranean plants including Aleppo pine (*Pinus halepensis*), almond (*Prunus dulcis*), sweet orange (*Citrus* × *sinensis*), citrange (*Citrus sinensis* × *Poncirus trifoliata*) and holm oak (*Quercus ilex*), indicating that the pathogen has a wide potential host range. Isolates of *N. batangarum* from cactus pear from several small islands around Sicily were genetically uniform, as inferred from microsatellite primed (MSP)-PCR electrophoretic profiles, suggesting the pathogen populations in these islands have a common origin. A preliminary report of the identity of the causal agent of this disease has been published as the first record of *N. batangarum* in Europe and on cactus pear worldwide.

Keywords. *Botryosphaeriaceae*, cactus pear, phylogenetic analysis, marker genes, host range.

OPEN ACCESS

Citation: F. Aloi, S. Giambra, L. Schena, G. Surico, A. Pane, G. Gusella, C. Stracquadanio, S. Burruano, S.O. Cacciola (2020) New insights into scabby canker of *Opuntia ficus-indica*, caused by *Neofusicoccum batangarum*. *Phytopathologia Mediterranea* 59(2): 269-284. DOI: 10.14601/Phyto-11225

Accepted: May 26, 2020

Published: August 31, 2020

Data Availability Statement: All relevant data are within the paper and its Supporting Information files.

Competing Interests: The Author(s) declare(s) no conflict of interest.

Editor: Alan J.L. Phillips, University of Lisbon, Portugal.

INTRODUCTION

Cactus pear [*Opuntia ficus-indica* (L.) Mill.] is probably native to Mexico (Kiesling and Metzing, 2017), and, after the discovery of America, this plant was introduced into the Mediterranean basin where it is naturalized (Ochoa and Barbera, 2017). In Sicily, cactus pear has become an economically important fruit crop and is a characteristic feature of the landscape. It is also cultivated in the Sardinia, Apulia, Calabria, and Basilicata regions of Italy, and this country is the second cactus pear fruit producer, after Mexico. Sicily produces approx. 90% of cactus pear fruit in the European Union. Cactus pear was introduced into the small islands around Sicily, where it is mainly grown as productive living fences. According to Pretto *et al.* (2012), *O. ficus-indica* was introduced into the small Mediterranean islands in the nineteenth century, as fodder or to fence fields.

Somma *et al.* (1973) reported a severe and unusual disease of *O. ficus-indica* on Linosa, a small island of the Pelagian archipelago, south of Sicily. The disease was named 'gummy canker', referring to the typical symptoms on cladodes, and the causal agent was identified as *Dothiorella ribis*, currently *Neofusicoccum ribis* (*Botryosphaeriaceae*). In a subsequent review of cactus pear diseases (Granata *et al*., 2017), the 'gummy canker' described by Somma *et al*. (1973) was equated to a disease named 'cladode and fruit rot', and the causal agent was considered to be the cosmopolitan fungus *Lasiodiplodia theobromae* (Pat.) Giff. & Maubl. This fungus is in the same family as *N. ribis*. Recently, 'gummy canker' was seen to be destroying the cactus pear stands in Lampedusa, the southernmost island of the Pelagian archipelago, and the disease was also present in other minor islands near Sicily, including Favignana of the Aegadian archipelago, and Ustica, a small island around 67 km northwest of Palermo in the Tyrrhenian sea (Schena *et al*., 2018). The name of the disease was changed to 'scabby canker', as this was more appropriate to describe the characteristic symptoms on cladodes. The fungus responsible for the disease was identified as *Neofusicoccum batangarum* Begoude, Jol. Roux & Slippers (Schena *et al*., 2018), not previously reported in Europe (Phillips *et al*., 2013; Dissanayake *et al*., 2016a). This was the first report of *N. batangarum* on cactus pear, but there are records of this fungus in Brazil as a pathogen of cochineal cactus [*Nopalea cochenillifera* (L.) Salm-Dyck, syn. *Opuntia cochenillifera* (L.) Mill.], which is a close relative of cactus pear (Conforto *et al*., 2016; Garcete-Gómez *et al*., 2017).

The disease of cochineal cactus, named 'cladode brown spot', has some traits in common with 'scabby canker' occurring in the minor Sicilian islands. However, other fungi, besides *N. batangarum*, are responsible for 'cladode brown spot' in Brazil (Conforto *et al*., 2019; Feijo *et al*., 2019). *Neofusicoccum batangarum* was first described as an endophyte of Indian almond (*Terminalia catappa* L., *Combretaceae*) in Africa (Begoude *et al*., 2010, 2011). This fungus was also reported in Florida (USA) as a contaminant of seeds of *Schinus terebinthifolius*, the Brazilian pepper tree (Shetty *et al*., 2011), and more recently as an aggressive pathogen causing stem cankers of fruit trees in the tropics (Netto *et al*., 2017; Serrato-Diaz *et al*., 2020). The distribution of *N. batangarum* includes Africa, Brazil, Puerto Rico and the United States of America (Phillips *et al*., 2013; Dissanayake *et al*., 2016a; Conforto *et al*., 2019; Serrato-Diaz *et al*., 2020).

The present study aimed to gain insights into the aetiology and epidemiology of 'scabby canker' that is destroying cactus pear on the minor islands of Sicily, and also poses a serious threat to cactus pear crops in Sicily. Specific objectives included: i) to determine the present distribution of 'scabby canker'; ii) to characterize *N. batangarum* isolates from different minor islands of Sicily; and iii) to investigate if the potential host range of this fungus includes other Mediterranean plants which could act as alternative hosts or inoculum reservoirs for this pathogen.

MATERIALS AND METHODS

Fungus isolates, distribution and incidence of the disease

Samples were collected from 2013 to 2018, from the minor islands of Sicily, and a survey was carried out in the islands of Favignana, Lampedusa, Linosa and Ustica (Figure 1) to determine the distribution and the incidence of the disease. Since the extent of these islands is limited, all prickly pear hedges and plantations in each island were examined systematically. Isolations were made from the margins of active cankers developing on cladodes of the host plants. Pieces (5 mm) of diseased tissue were plated onto potato dextrose agar (PDA, Oxoid Limited) supplemented with 1 mg mL^{-1} of streptomycin, and were incubated at 22°C. Isolates were also obtained as single conidium isolations from conidiomata emerging from cankers of diseased plants, as described by Phillips *et al*. (2013). A total of 26 representative isolates of *N. batangarum* from cactus pear were characterized in this study. Table 1 lists these isolates and their origins. Cultures were routinely grown and maintained on PDA in the collection of the Molecular Plant Pathology laboratory of the Di3A, University of Catania.

Figure 1. Sicily and the minor surrounding islands.

Morphological characteristics and cardinal temperatures for growth of the isolates

The isolates were induced to sporulate by plating them on PDA containing sterilized pine needles (Smith *et al*., 1996), and incubating at room temperature (approx. 20 to 25°C) under diffused day light or near-UV light, until pycnidia developed. For microscopy, pycnidia and conidia were mounted in sterile distilled water or 100% lactic acid and observed microscopically at ×40 and ×100 magnifications, with an Axioskop (Zeiss) microscope. Images were captured with an AxioCam MRc5 camera (Zeiss), and measurements were made with the software AxioVision. For each isolate, 50 conidia were randomly selected and their lengths, widths and shape were recorded. For pycnidium dimensions, 20 measurements were made. Colony characters and pigment production were noted after 4 to 6 d of growth on PDA or malt extract agar (MEA) at 25°C, in the dark. Colony colours (upper and lower surfaces) were rated according to Rayner (1970).

Four isolates, one from each island, were deposited at Westerdijk Fungal Biodiversity Institute, with strain code numbers CBS 143023, CBS 143024, CBS 143025, and CBS 143026 (Schena *et al*., 2018).

Radial growth rate and cardinal temperatures for radial growth were determined by growing the isolates on PDA in Petri dishes (9 cm diam.), and incubating at 5, 10, 15, 20, 25, 30 35°C, in the dark. Means of radial growth at the different temperatures were adjusted to a regression curve using Statgraphics Plus 5.1 software (Manugistics Inc.), and the best polynomial model was chosen based on parameter significance ($P < 0.05$) and coefficient of determination (R^2) to estimate the optimum growth temperature for each isolate. Four replicates of each isolate were evaluated and each experiment was repeated twice.

Amplification and sequencing of target genes

Genomic DNA was isolated from 1-week-old cultures grown on PDA at 25°C in the dark using the procedure of Schena and Cooke (2006). The internal transcribed spacer (ITS) region of the ribosomal DNA was amplified and sequenced with primers ITS5/ITS4 (White *et al.* 1990), part of the translation elongation factor 1 alpha gene (*tef1*) was sequenced and amplified with primers EF1-728F/EF1-986R (Carbone and Kohn, 1999), and the β-tubulin gene (*tub2*) was sequenced and amplified with Bt2a and Bt2b (Glass and Donaldson, 1995).

Amplified products with both forward and reverse primers were sequenced by Macrogen Europe. CHROMASPRO v. 1.5 (http://www.technelysium.com.au/) was used to evaluate reliability of sequences and to create consensus sequences. Unreliable sequences were re-sequenced.

Molecular identification and phylogenetic analyses

The preliminary identification of isolates and their association to *N. batangarum* were carried by BLAST analyses. For the accurate identification, sequences of ITS, *tef1* and *tub2* loci from the isolates obtained in the present study were phylogenetically analyzed along with validated sequences representative of *N. batangarum* and closely related species as defined by comprehensive phylogenetic studies (Slippers *et al*., 2013; Lopes *et al*., 2017; Yang *et al*., 2017). Two additional isolates of *N. batangarum* for which ITS, *tef1* and *tub2* sequences were available in GenBank were included in the analysis. Table 2 lists the analyzed isolates. For all isolates, ITS, *tef1* and *tub2* sequences were trimmed to a common length and concatenated using the Sequence Matrix software (Vaidya *et al*., 2011). Concatenated sequences were aligned with MUSCLE (Edgar, 2004) as implemented in Mega Version 7.0 (Kumar *et al*., 2016), and edited manually for check-

Table 1. Identity of the *Neofusicoccum batangarum* isolates studied, and GenBank accession numbers, for isolates recovered from the small islands of Sicily.

Isolate	Species	Island origin	ITS	β -tubulin	EF1-α
FIF G	*N. batangarum*	Favignana	MF414731	MF414750	MF414769
FIF A	*N. batangarum*	Favignana	MF414732	MF414751	MF414770
FIF D	*N. batangarum*	Favignana	MF414730	MF414749	MF414768
FIF F1	*N. batangarum*	Favignana	MF414733	MF414752	MF414771
FIF E	*N. batangarum*	Favignana	MF414734	MF414753	MF414772
FIF F	*N. batangarum*	Favignana	MF414735	MF414754	MF414773
FIF I	*N. batangarum*	Favignana	MF414736	MF414755	MF414774
FIF H	*N. batangarum*	Favignana	MF414737	MF414756	MF414775
FILI F1	*N. batangarum*	Linosa	MF414747	MF414766	MF414785
OB43	*N. batangarum*	Linosa	MG609040	MG609057	MG609074
OB44	*N. batangarum*	Linosa	MG609041	MG609058	MG609075
OB46	*N. batangarum*	Linosa	MG609043	MG609060	MG609077
FIU 1	*N. batangarum*	Ustica	MF414739	MF414758	MF414777
FIU 1B	*N. batangarum*	Ustica	MF414738	MF414757	MF414776
FIU 2	*N. batangarum*	Ustica	MF414740	MF414759	MF414778
FIU 3	*N. batangarum*	Ustica	MF414741	MF414760	MF414779
FIU 3A	*N. batangarum*	Ustica	MF414742	MF414761	MF414780
FIU 3B	*N. batangarum*	Ustica	MF414743	MF414762	MF414781
FIU 4	*N. batangarum*	Ustica	MF414744	MF414763	MF414782
FIU 5	*N. batangarum*	Ustica	MF414745	MF414764	MF414783
FIU 6	*N. batangarum*	Ustica	MF414746	MF414765	MF414784
FILA 4	*N. batangarum*	Lampedusa	MF414748	MF414767	MF414786
OP5	*N. batangarum*	Lampedusa	MG609050	MG609067	MG609084
OP6	*N. batangarum*	Lampedusa	MG609051	MG609068	MG609085
OP9	*N. batangarum*	Lampedusa	MG609052	MG609069	MG609086
OB47	*N. batangarum*	Lampedusa	MG609053	MG609070	MG609087

ing indels and single nucleotide polymorphisms. Phylogenetic analyses were performed in Mega with the maximum likelihood method using the Tamura–Nei model and 1000 bootstrap replications (Tamura and Nei, 1993; Tamura *et al*., 2013).

Analysis of genetic variability of isolates

Six representative isolates (FIU 1B, OP6, FIF D, FILA 4, OB43, and FILI F1) collected from four different islands were characterized according to their microsatellite-primed PCR (MSP-PCR) profiles using primer M13 (Meyer *et al*., 1993; Santos and Phillips, 2009), (CAG)5 (Freeman and Shabi, 1996), and (GGA)5 (Uddin *et al*., 1997). Each amplification was carried out in a total volume of 25 µL, containing 1 µL (50 ng) of fungal DNA, 1 µM of primer, 2 mM [(primer (CAG)5 and (GGA)5] or 4 mM (primer M13) of $MgCl_2$ and 1U of GoTaq DNA Polymerase (Promega Corporation). Reactions were incubated for 2 min at 95°C, followed by 35 cycles of 30s at 95°C, 30 s at 49°C [primers (GGA5)5 and M13] or 52°C [primer CAG)5] and 1 min at 72°C. All reactions ended with a final extension of 5 min at 72°C. PCR profiles were visualized on 2% agarose electrophoresis gels (Merck) in 1× TBE buffer stained with SYBR Safe DNA Gel Stain (Thermo Fisher Scientific).

Pathogenicity tests

Four *N. batangarum* isolates obtained from cactus pear cankers (isolates FIF D, FIU 1B, OP6 and OB43 from, respectively, Favignana, Ustica, Lampedusa and Linosa) were used in pathogenicity tests on cactus pear plants. These isolates were used to inoculate mature cladodes (cladodes of the previous year) and the stems of field-grown cactus pear plants (three plants per isolate and two cladodes per plant). On each cladode, two holes (5 mm diam.) were made 20 cm apart with a cork-borer, while only one hole was made on the stem. An agar plug from a 5-d-old colony grow-

Table 2. GenBank accession numbers of sequences of the *Neofusicoccum* spp. isolates of different country and host origins used as references in phylogenetic analyses

Species	Isolate	Country	Host	Source	GenBank accession number		
					ITS	tef1	β-tubulin
N. algeriense	CAA322	Portugal	*Malus domestica*	Lopes *et al.*, 2017	KX505906	KX505894	KX505916
N. algeriense	CBS137504	Algeria	*Vitis vinifera*	Lopes *et al.*, 2017	KJ657702	KX505893	KX505915
N. batangarum	CBS124922	Cameroon	*Terminalia catappa*	Yang *et al.*, 2017	FJ900606	FJ900652	FJ900633
N. batangarum	CBS127348	USA: Florida	*Schinus terebinthifolius*	Yang *et al.*, 2017	HM357636	KX464674	KX464952
N. batangarum	CMM4553	Brasil	*Anacardium* sp.	Unpublished	KT728917	KT728921	KT728913
N. batangarum	CBS124924 (ex-type)	Cameroon	*Terminalia catappa*	Lopes *et al.*, 2016	FJ900607	FJ900653	FJ900634
N. batangarum	CBS124923	Cameroon	*Terminalia catappa*	Lopes *et al.*, 2016	FJ900608	FJ900654	FJ900635
N. brasiliense	CMM1285	Brazil	*Mangifera indica*	Lopes *et al.*, 2016	JX513628	JX513608	KC794030
N. brasiliense	CMM1338	Brazil	*Mangifera indica*	Lopes *et al.*, 2016	JX513630	JX513610	KC794031
N. cordaticola	CBS123634	South Africa	*Syzygium cordatum*	Lopes *et al.*, 2016	EU821898	EU821868	EU821838
N. cordaticola	CBS123635	South Africa	*Syzygium cordatum*	Lopes *et al.*, 2016	EU821903	EU821873	EU821843
N. kwambonambiense	CBS123639	South Africa	*Syzygium cordatum*	Lopes *et al.*, 2016	EU821900	EU821870	EU821840
N. kwambonambiense	CBS123641	South Africa	*Syzygium cordatum*	Lopes *et al.*, 2016	EU821919	EU821889	EU821859
N. macroclavatum	CBS118223	Australia	*Eucalyptus globulus*	Lopes *et al.*, 2016	DQ093196	DQ093217	DQ093206
N. macroclavatum	WAC12445	Australia	*Eucalyptus globulus*	Lopes *et al.*, 2016	DQ093197	DQ093218	DQ093208
N. occulatum	CBS128008	Australia	*Eucalyptus grandis hybrid*	Lopes *et al.*, 2016	EU301030	EU339509	EU339472
N. occulatum	MUCC286	Australia	*Eucalyptus pellita*	Lopes *et al.*, 2016	EU736947	EU339511	EU339474
N. parvum	CBS110301	Portugal	*Vitis vinifera*	Lopes *et al.*, 2017	AY259098	AY573221	EU673095
N. parvum	CMW 9081	New Zealand	*Populus nigra*	Lopes *et al.*, 2017	AY236943	AY236888	AY236917
N. ribis	CBS115475	USA	*Ribes* sp.	Lopes *et al.*, 2016	AY236935	AY236877	AY236906
N. umdonicola	CBS123645	South Africa	*Syzygium cordatum*	Lopes *et al.*, 2016	EU821904	EU821874	EU821844
N. umdonicola	CBS123646	South Africa	*Syzygium cordatum*	Lopes *et al.*, 2016	EU821905	EU821875	EU821845
Neofusicoccum sp. 5	CBS157.26	Sri Lanka	*Camellia sinensis*	Yang *et al.*, 2017	KX464214	KX464744	KX465034

ing on PDA was inserted into each hole. Three plants inoculated with sterile agar served as controls. Wounds were sealed with the excised tissues and inspected daily for 20 d after inoculation (a.i.). Lesion diameters was recorded 30 d a.i., and the size of the cankers on cladodes was calculated as the circle area. Inoculations were first performed in June 2014 in an experimental field at the University of Catania (Sicily), and these were repeated each year in June for three consecutive years on different healthy cactus pear plants. Commencing from 20 d a.i., inoculated plants were inspected each month to observe development of symptoms. Trials were also repeated in an experimental field at the University of Palermo (Sicily).

Isolates FIFD and FIU1B were also used to inoculate twigs and stems of 2-year-old trees of sweet orange 'Navelina' (*Citrus* × *sinensis*) grafted on citrange 'Carrizo' (*Citrus sinensis* × *Poncirus trifoliata*) rootstock, grown in a greenhouse maintained at 20 to 26°C. These isolates were also used to inoculate the stems of field-grown trees of woody plants typical of the Mediterranean region, in an experimental field at the University of Catania. These included 3-year-old trees of almond [*Prunus dulcis* (Mill.) D.A. Webb], 5-year-old trees of holm oak (*Quercus ilex* L.) and 6-year old trees of Aleppo pine (*Pinus halepensis* Mill.). Inoculations were performed in June 2016. On sweet orange (two twigs per tree) were inoculated (four trees per isolate). A hole in each twig was made with a 3 mm cork-borer. A 3 mm diam. mycelium plug from 5-d-old PDA culture was placed on the freshly wounded surface, the wound was covered with the excised bark disk and sealed with Parafilm®. The stem of each tree (the 'Carrizo' citrange rootstock) was inoculated 10 cm above soil level (a single hole per stem) using the same method. Four trees inoculated with sterile agar served as controls. The length and breadth of each resulting lesion were recorded 30 d a.i., and the outer surface areas of the bark cankers on twigs and stems were calculated as ellipses. Almond, holm oak and Aleppo pine trees were wound inoculated on the stems using a cork borer (5 mm diam.). Four trees per host species were inoculated (three holes per tree 60 cm apart), and the wounds were each covered with the excised bark disk. Four trees inoculated with sterile agar served as controls. The lengths and breadths of the lesions were recorded at 30 and 70 d a.i.

In all pathogenicity tests, re-isolations were made from lesions, and resulting fungal colonies were confirmed morphologically and by sequencing part of the ITS, *tef1* and *tub2* genes, as described above, to fulfill Koch's postulates.

Statistical analyses of data

Data from pathogenicity tests were analyzed using RStudio v.1.2.5 (R). When comparing the means of multiple groups, a one-way ANOVA followed by Tukey's HSD *post hoc* test was performed. Significant differences between groups ($P < 0.05$) were denoted with different letters. When comparing independent groups, Student's t-test was used. The significance level was reported as follows: * = $P < 0.05$, ** = $P < 0.01$, or *** = $P < 0.001$.

RESULTS

Symptoms, distribution and incidence of the disease

Symptoms were visible on cladodes and included radially expanding, crusty, concentric, silvery, perennial cankers, each with a leathery, brown halo (Figure 2A–C). Pycnidia were erumpent from the host epidermis, visible to the naked eye as minute, black dots, formed on the silver-coloured internal area of each canker (Figure 2C) The cankers had radial and tangential cracks (Figure 2B–C). A milky to buff-coloured abundant and viscous exudate of polysaccharide nature, caking on contact with air, oozed from active cankers and formed strips or cerebriform masses. The exudate, being water soluble, was partially washed away by rain, while masses of exudates that remained on the cankers became black due to the growth of sooty molds, giving the cankers an appearance of carbonaceous crusts. The cankers ceased to expand in the coldest season of each year. An individual canker rarely reached a maximum diameter of more than 25 cm, but cankers often coalesced and formed larger lesions extending to the whole cladode or up to its edge, causing wilting. The cladodes collapsed when the bases were girdled by cankers. Infections on thicker cladodes and stems gave rise to very prominent cankers and eruptions of solid exudates at scattered points far from the lesions. Cladodes and stems of heavily infected plants became senescent and the whole plants collapsed, appearing gray and ghostly. In a systematic survey of prickly pear hedges and plantations, symptoms were observed in all hedges and plantings with 80% of plants symptomatic in the island of Lampedusa (20.2 km^2) and 40% of plants symptomatic plants on Linosa (5.43 km^2). Conversely, on Favignana (19.8 km^2), symptoms were observed at two sites three km apart, with incidences of 40% and 100% of plants with symptoms. On the island of Ustica (8.24 km^2), symptoms were observed only at one site on the northern coast, overlooking the sea (Figure 2A). However, this disease out-

Figure 2. A. Cankers on cladodes incited by *Neofusicoccum batangarum* in a cactus pear hedge on the Island of Ustica, May 2014. B. Coalescing, concentric cankers incited by *Neofusicoccum batangarum* on a cactus pear cladode. C. Concentric expanding canker incited by *Neofusicoccum batangarum* on a cactus pear cladode. Note pycnidia, as small dark spots, and cracking on the silvery, intermediate area of the canker, the dark colour and the sooty appearance of the exudate after rain and the tan colour of the edge, indicating that the canker is still active. D. Mycelium emerging from conidiomata of *Neofusicoccum batangarum* formed on cankers (photograph taken using a stereomicroscope).

break was severe, with approx. 400 m of hedges containing 100% of plants with symptoms.

Morphological and molecular identification of the pathogen

A fungus with white aerial mycelium that turned gray with age was consistently recovered from canker tissues, with 100% of positive isolations. The same fungus was obtained by plating single conidia taken from conidiomata emerging individually or in groups from cankers (Figure 2D). Colonies on MEA formed concentric rings. On PDA mycelium was white and became smoky gray to gray-olivaceous after 5 d (Figure 3A). The mycelium was fast-growing (Table 3) and covered the 9 cm diam. Petri dishes after 5 d incubation at 25° C in the dark. Optimum temperature for radial colony growth was between 25 and 30°C for all the isolates tested. Little growth was observed at 10 or 35°C. Stromatic conidiomata were produced in pine needle cultures within 14 d. The condidiomata were solitary, covered by mycelium, obpyriform to ampulliform, and each had

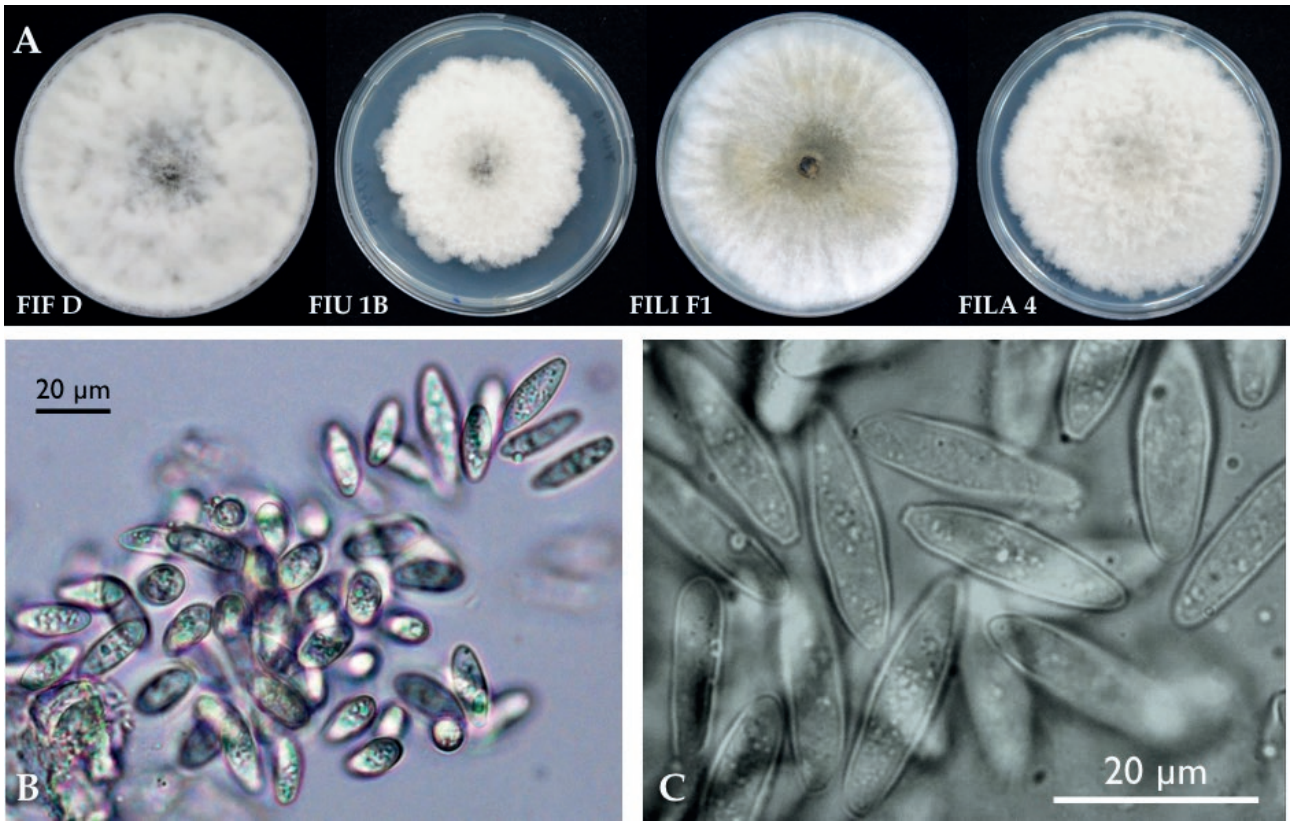

Figure 3. A. Four representative isolates of *Neofusicoccum batangarum* after 5 d of incubation on PDA at 25°C; CBS143023 (FIF D), CBS143024 (FIU 1B), CBS143025 (FILI F1), and CBS143026 (FILA 4). B and C. Unicellular, fusiform, thin-walled hyaline conidia of *Neofusicoccum batangarum*.

Table 3. Mean radial growth rates of colonies of *Neofusicoccum batangarum* isolates on PDA at three different temperatures, as determined after 3 d of incubation.

Isolates of *N. batangarum*	Island origin	15°C (mm d^{-1}) mean ± S.D.[a]	25°C (mm d^{-1}) mean ± S.D.	30°C (mm d^{-1}) mean ± S.D.
FILI-F1	Linosa	3.83 ± 0.35	7.50 ± 0.00	5.90 ± 0.26
FILA 4	Lampedusa	3.97 ± 0.34	7.50 ± 0.00	7.50 ± 0.00
FIU-1B	Ustica	3.00 ± 0.58	6.53 ± 0.63	6.26 ± 0.42
FIF-D	Favignana	3.40 ± 0.41	7.50 ± 0.00	7.50 ± 0.00
OP5	Lampedusa	4.32 ± 0.05	9.77 ± 0.09	9.83 ± 0.06
OP6	Lampedusa	4.20 ± 0.21	12.94 ± 0.23	9.75 ± 0.13
OP9	Lampedusa	4.31 ± 0.09	13.00 ± 0.19	9.33 ± 0.24
OB44	Linosa	3.73 ± 0.81	12.83 ± 0.10	9.69 ± 0.06
OB46	Linosa	3.44 ± 0.44	13.03 ± 0.18	9.23 ± 0.42
OB47	Lampedusa	4.16 ± 0.10	12.94 ± 0.16	9.77 ± 0.11
OB43	Linosa	2.40 ± 0.22	7.82 ± 0.07	6.47 ± 0.06

[a] Mean of four replicate Petri dishes.

a central and circular unilocular ostiole, and measured 250-300 µm in diameter. Conidia were non-septate (bicellular conidia were observed only very occasionally), hyaline, smooth, fusoid to ovoid, thin-walled, and measured 17.1-21.8 × 4.6-8.9 µm, with a mean length to width ratio = 2.9 (Figure 3B–C).

The isolates obtained had identical ITS, *tef1* and *tub2* sequences. Preliminary BLAST analyses of these three genes yielded several identical sequences of *Neofusicoccum* spp., deposited with different taxa names. Consequently, this analysis enabled the identification at the genus level, but did not provide reliable information on the species. The phylogenetic analysis of the combined data set of sequences from ITS, *tef1* and *tub2* sequences (Figure 4) produced trees with a high concordance with those reported by Lopes *et al.* (2017) and Yang *et al.* (2017). According to this analysis, isolates from cactus pear were identified as *N. batangarum*, since they clearly clustered with the ex-type (CBS 124924 from *Terminalia catappa*; Lopes *et al.*, 2016) and other reference isolates of this species, and were differentiated from other *Neofusicoccum* species, including

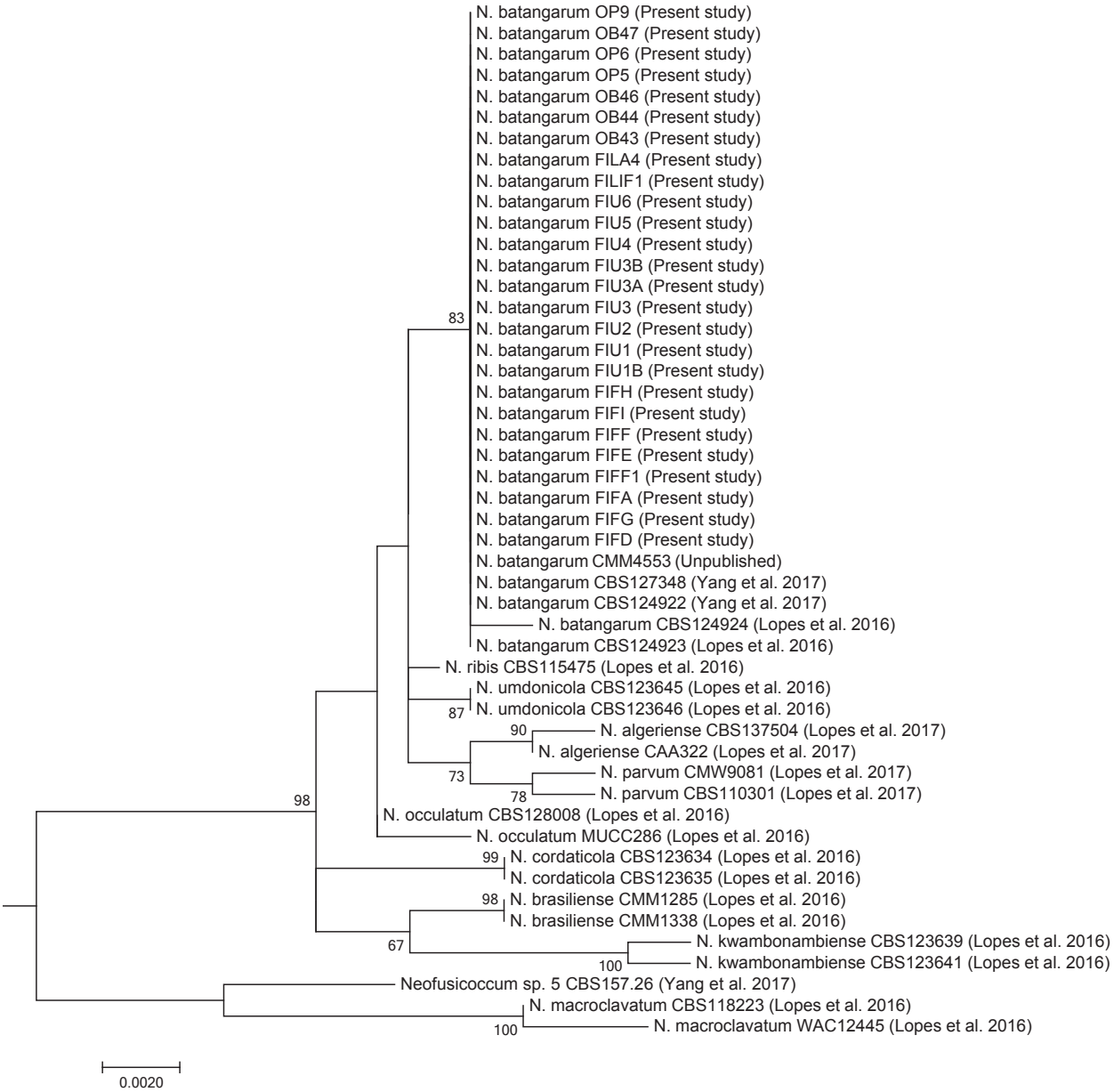

Figure 4. Phylogenetic tree of isolates of *Neofusicoccum* collected in the present study from *Opuntia ficus-indica*, and representative isolates of *Neofusicoccum batangarum* and closely related species as defined by in comprehensive phylogenetic studies (Tables 1 and 2). The tree was built using concatenated sequences of ITS-5.8S-ITS2 region, tef1-α gene and β-tubulin gene. Numbers on nodes indicate the posterior probabilities from the maximum likelihood method.

the closely related species *N. ribis, N. umdonicola,* and *N. occulatum* (Annex 1).

Analysis of the genetic variability of isolates

The MSP-PCR characterization of the six representative isolates of *N. batangarum* revealed high genetic uniformity, since isolates showed identical banding patterns with the three tested primers (Annex 2).

Pathogenicity tests

Four isolates, one from each island, were deposited at Westerdijk Fungal Biodiversity Institute [CBS 143023

Table 4. Mean lesion areas on cladodes of cactus pear (*Opuntia ficus-indica*) 30 d after wound inoculation with representative isolates of *Neofusicoccum batangarum* obtained from cactus pear from four minor islands of Sicily.

Isolate	Island origin	Mean lesion area (cm^2) ± S.D. [a,b]
FIF D	Favignana	4.4 ± 1.2
OP6	Lampedusa	4.4 ± 1.8
OB43	Linosa	4.5 ± 2.3
FIU 1B	Ustica	4.6 ± 0.6

[a] Means of 12 replicate values.
[b] ANOVA, $F_{(3,44)} = 0.372$, $P > 0.05$

Table 5. Mean lesion areas on stems of sweet orange 'Navelina' (*Citrus × sinensis*) trees grafted on 'Carrizo' Citrange (*C. sinensis × Poncirus trifoliata*) rootstock, 30 d after wound inoculation with representative isolates of *Neofusicoccum batangarum* from four minor islands of Sicily

Isolate [f]	Island origin	Mean lesion area (cm^2) ± S.D.[a]	
		rootstock [b,d]	scion[c,e]
FIF D***	Favignana	1.4 ± 0.18	1.8 ± 0.1
FIU 1B**	Ustica	1.4 ± 0.12	1.8 ± 0.2
FILI F1*	Linosa	1.4 ± 0.15	1.7 ± 0.2
FILA 4**	Lampedusa	1.5 ± 0.26	1.9 ± 0.4

[a] Rootstock: means of four replicate values. Scion: means of eight replicate values.
[b] Symptoms included barely noticeable gummy exudate.
[c] Symptoms included abundant gummosis.
[d] ANOVA rootstock, $F_{(3,12)} = 0$, $P > 0.05$.
[e] ANOVA scion, $F_{(3,28)} = 0$, $P > 0.05$.
[f] Comparing rootstock and scion according to Student's t-test.
(* = $P < 0.05$, ** = $P < 0.01$, and *** = $P < 0.001$).

(FIF D), CBS 143024 (FIU 1B), CBS 143025 (FILI F1), and CBS 143026 (FILA 4)], and these were tested for their pathogenicity on cactus pear and other species of plants. Additional isolates from Lampedusa and Linosa were also included in the pathogenicity tests. Since the results of four inoculation series performed, respectively, in 2014, 2015, 2016 and 2017 were very similar, only the results of inoculations performed in 2014 are reported here in detail. All isolates were pathogenic on the inoculated plant species (Tables 4, 5, 6 and 7). The isolates induced cankers in all inoculated plants while no symptoms were observed on the controls.

On cactus pear plants, symptoms appeared after 4 d, as brown circular halos around the inoculation wounds with viscous exudates oozing from the lesions that consolidated in contact with the air to form long strips

Table 6. Mean lesion areas on stems of holm oak (*Quercus ilex*) trees 30 d and 70 d after wound inoculation with representative isolates of *Neofusicoccum batangarum* from two minor islands of Sicily.

Isolate	Island origin	Mean lesion area (cm^2) ± S.D.[a]	
		30 d[b]	70 d[c]
FIF D	Favignana	5.2 ± 1.3	8.2 ± 1.1
FIU 1B	Ustica	5.8 ± 2.4	10.0 ± 3.0

[a] Means of six replicate values.
[b] ANOVA 30 d, $F_{(1,10)} = 0.274$, $P > 0.05$.
[c] ANOVA 70 d, $F_{(1,10)} = 1.517$, $P > 0$ .05.

Table 7. Mean lesion areas on stems of Aleppo pine (*Pinus halepensis*) or almond (*Prunus dulcis*) trees 70 d after wound inoculations with representative isolates of *Neofusicoccum batangarum* from four minor islands of Sicily.

Isolate	Origin	Mean lesion area (cm^2) ± S.D.[a,f]	
		Aleppo pine[b,d]	Almond[c,e]
FIF D	Favignana	7.2 ± 0.6 a	4.9 ± 1.0 a
FIU 1B	Ustica	7.1 ± 0.9 ab	5.1 ± 1.4 a
FILA 4	Lampedusa	7.6 ± 2.8 ab	5.1 ± 1.7 a
FILI F1	Linosa	6.6 ± 0.6 b	5.8 ± 1.7 a

[a] Means of six replicates.
[b] Symptoms included resinous exudates.
[c] Symptoms included abundant gummous exudates.
[d] ANOVA Aleppo pine, $F_{(3,20)} = 6.015$, $P = 0.004$.
[e] ANOVA Almond, $F_{(3,20)} = 2.783$, $P = 0.06$.
[f] Means accompanied by the same letters are not statistically different ($P < 0.05$, Tukey's HSD test).

(Figure 5A–B). Cankers expanded progressively and concentrically (Figure 5D). They were roughly circular, with irregular margins, identical or very similar to those observed on plants with natural infections, and the canker expansion reduced during the coldest months (late December to early February). Some cankers stopped growing permanently and healed, but most cankers resumed growth and the production of exudate when temperatures increased after winter. Table 4 presents the mean lesion areas induced on cactus pear cladodes by the four tested isolates 30 d after wound inoculation. Analysis of variance revealed no statistically significant differences in pathogenicity between the isolates. Five years after the first inoculation, most cankers were still active, and they continued to expand and produce abundant exudates (Figure 5D). In some cases, the cankers expanded more rapidly in one direction and became asymmetrical and irregular (Figure 5D). After rain, the cankers became dark, with a carbonaceous appearance.

Figure 5. A. Brown, circular lesions and waxy exudate oozing from lesions on a cactus pear cladode wound-inoculated with *Neofusicoccum batangarum*, 7 d after inoculation (a.i.) B. Brown lesion and exudate oozing from a lesion on a cactus pear cladode wound-inoculated with *N. batangarum*, 4 d a.i. C. A fusiform dry canker induced by wound-inoculation of *N. batangarum* on the stem of a holm oak tree 70 d a.i. D. A still active canker on a cactus pear cladode artificially inoculated with *Neofusicoccum batangarum* in the field, September 2019, 5 years a.i. E. A resinous canker induced by wound-inoculation with *N. batangarum* on the stem of an Aleppo pine tree, 70 d a.i. F. A gummy canker induced by wound-inoculation with *N. batangarum* on the stem of a young almond tree, 14 d a.i. G. A gummy canker induced by wound-inoculation with *N. batangarum* on the stem of a young 'Navelina' sweet orange tree, 14 d a.i. H. Pycnidia on a canker induced by wound-inoculation with *N. batangarum* on the stem of a young 'Navelina' sweet orange tree, 14 d a.i.

Pycnidia were visible on cankers 14-20 d a.i. From six months to 5 years a.i., small cankers and scattered eruptions of exudate, similar to runny wax, appeared on artificially inoculated cladodes approx. 10-20 cm from the inoculation points.

All four tested *N. batangarum* isolates induced necrotic lesions on the citrange rootstock and the sweet orange scion at 7 d a.i. Symptoms were more severe on the sweet orange scions (Table 5) and included abundant gummosis (Figure 5G), while gummosis was much less abundant on citrange. Pycnidia emerged from the necrotic lesions on sweet orange stems from 10 to 14 d a.i. (Figure 5H). Differences in mean lesion size between the sweet orange scion and the citrange rootstock were significant ($P < 0.05$), according to Student's *t*-test. However, no statistically significant differences in patho-

genicity ($P > 0.05$) were observed among the fungal isolates on both citrus symbionts. No symptoms were observed on the controls.

On holm oak (Table 6), no gummy reaction was observed (Figure 5 C), but cankers expanded progressively along the stems and were still active 3 years after inoculation. No symptoms were observed on the controls. There were no significant differences ($P > 0.05$) among isolates in the pathogenicity test on holm oak at 30 d a.i. or 70 d a.i.

On almond and Aleppo pine (Table 7), *N. batangarum* isolates incited necrotic bark lesions with gummy exudates on almond (Figure 5F) and resinous exudates on Aleppo pine (Figure 5E). No symptoms were observed on the controls. Also on almond and Aleppo pine, cankers were still active 3 years a.i.

In the pathogenicity tests on almond and Aleppo pine there were small but statistically significant differences between the isolates on these two hosts (almond, $P = 0.06$; Aleppo pine, $P = 0.004$). All the *N. batangarum* isolates were re-isolated from inoculated plants, while no fungal pathogens were isolated from control plants, thus fulfilling Koch's postulates for the *N. batangarum* isolates.

DISCUSSION

Identification of the *Botryosphaeriaceae* prior to the application of DNA sequencing and phylogenetic inference should be considered with caution. The classification and nomenclature of these fungi have evolved rapidly and have been substantially revised, as previous classification based on morphological characters was confusing and most species were actually complexes of different taxa (Slippers *et al*., 2004, 2013; Crous *et al*., 2006; Phillips *et al*., 2008, 2013; Crous *et al*., 2017). According to the molecular taxonomy of the *Botryosphaeraceae*, *N. batangarum* is the appropriate name of the fungus responsible for the chronic disease observed on the cladodes of cactus pear in the minor islands of Sicily. *Neofusicoccum batangarum* was confirmed to be the sole causal agent of the 'scabby canker' disease. The fungus was consistently associated with symptomatic cactus pear plants and, when artificially inoculated onto this host, induced the same type of cankers as natural infections. From an etiological and ecological perspective, *N. batangarum* was the only fungus in the family *Botryosphaeriaceae* recovered from infected cactus pear in these small islands belonging to different archipelagos.

Several species of this family frequently occur together on the same host (Jami *et al*., 2017), although not all are able to cause disease (Lawrence *et al*., 2017). In Brazil, *N. batangarum*, alone or in association with other fungi including several species of *Botryosphaeriaceae*, was reported to be responsible for 'brown spot' of cladodes, a severe disease of cochineal cactus that is grown as fodder for livestock in the semi-arid region of the north-east of that country (Conforto *et al*., 2016, 2019). Although the syndromes of 'cladode brown spot' in north-eastern Brazil and 'scabby canker' in minor islands of Sicily have some traits in common, they are distinct. Differences between the symptoms of these diseases include the presence of crusty, silvery, perennial cankers, and exudates oozing from the cankers in the 'scabby canker' disease. However, differences might be due to environmental conditions, host plant and/or cultivation systems. In Brazil, cochineal cactus is pruned repeatedly for the production of fresh forage. The cactus pear fences in the minor islands near Sicily are pruned only occasionally, thus allowing the disease to become chronic on mature cladodes. The cladode brown spot in Brazil is also a complex disease and the causal agent may vary according to the season and the geographical region (Santana *et al*., 2020).

For many years, *Botryosphaeriaceae*, which are widespread in tropical and temperate regions, were considered to be opportunistic pathogens infecting hosts exclusively through wounds or natural openings in their periderms. Since the late 1980s, however, these fungi have been recognized as endophytes that remain latent in woody host plants for long periods. With the onset of abiotic stress conditions (drought, physical damage, water-logging, frost and unsuitable environments for the growth) the latent pathogens cause disease (Slippers and Wingfield, 2007; Pavlic-Zupanc *et al*., 2015; Marsberg *et al*., 2017). The prolonged latent infection or endophytic phase implies that these fungi can easily pass undetected through phytosanitary controls or during the selection of propagation material.

The genus *Neofusicoccum* comprises species with widespread geographical and host distributions, and these fungi are typically endophytes, which in stressful environments can cause symptoms such as dieback, cankers and gummosis (Crous *et al*., 2006; Lopes *et al*., 2017; Zhang *et al*., 2017; Burgess *et al*., 2018). Wounds caused by hailstorms may have been the factor triggering the epidemic outbreak of *N. batangarum* on cactus pear in the small islands of Sicily. The climate of these islands is affected by the proximity to the sea, and this may have favoured the development of the disease and the survival of the inoculum. In *in vitro* tests, *N. batangarum* showed an optimum temperature for growth around 25°C, a minimum of approx. 10°C and a maxi-

mum of approx. 35°C. On artificially inoculated cladodes, the fungus formed pycnidia between 14 and 20 d a.i. In winter, conidia collected from pycnidia formed on cladodes artificially inoculated in the spring or autumn of the previous year were viable.

Most species of *Botryosphaeriaceae* have broad host ranges, and only very few have been described from a limited number of host species or are host specific (Slippers and Wingfield, 2007; Marsberg *et al*., 2017). The ability to infect multiple hosts and to move among unrelated hosts facilitates the establishment and spread of species and genotypes of this family into new areas.

Neofusicoccum batangarum has been reported as an endophyte as well as a pathogen of several host plants in the tropics (Begoude *et al*., 2010, 2011; Shetty *et al*., 2011; Conforto *et al*., 2016; Netto *et al*., 2017). A very recent report has further expanded the known hosts (Serrato-Diaz *et al*., 2020). Pathogenicity tests in the present study showed that this fungus has an even wider potential host range, encompassing woody forest and cultivated plants typical of the Mediterranean macro-region. These hosts include Aleppo pine, almond, citrus and holm oak. Like other *Botryosphaeriaceae*, *N. batangarum* can be regarded as a generalist pathogen, although in natural conditions the host affinity of polyphagous *Botryosphaeriaceae* species is strongly influenced by the environment (Slippers and Wingfield, 2007). On artificially inoculated sweet orange stems, *N. batangarum* induced the typical symptoms of 'gummy cankers' or 'bot gummosis', already known as 'Dothiorella gummosis'. These are minor, but widespread, diseases caused by diverse species of *Botryosphaeriaceae*, and they commonly occur in citrus groves in California and in the Mediterranean basin (Adesemoye *et al*., 2014; Guarnaccia and Crous, 2017). Consistently with the typical symptoms of 'gummy canker' of citrus, in artificially inoculated symbiont citrus plant, symptoms were more severe on the sweet orange scion than on rootstock.

The polyphagy of *N. batangarum* may be related to its ability to produce non-host specific phytotoxins (Masi *et al*., 2020). These toxins may have roles in pathogenicity as virulence factors and may also enhance the ecological fitness of the fungus by inhibiting other microorganisms competing in plant biospheres. Production of diffusible phytotoxins could also explain the systemic spread of symptoms on cactus pear cladodes and their appearance far from inoculation points (Masi *et al*. 2020).

Reports of *Botryosphaeriaceae* associated with various hosts have increased worldwide in recent years. In Italy, this family is common and widespread on a broad range of hosts, and is an increasing concern for agricultural crops and urban and natural forest ecosystems (Burruano *et al*., 2008; Linaldeddu *et al*., 2014, 2016; Dissanayake *et al*., 2016b;). The disease of cactus pear caused by *N. batangarum* was noticed for the first time in Linosa more than 45 years ago (Somma *et al*., 1973), and at that time it was widespread and had been established for many years. Similarly, the chronic nature of symptoms observed recently in Favignana, Lampedusa and Ustica and the widespread occurrence of the disease in Lampedusa, clearly indicate it has not emerged recently. During the last 50 years the disease has probably been favoured by the low frequency of cactus pear pruning as a consequence of the reduced importance of this plant as a crop, and the drastic reduction in the use of cladodes as fodder. Although Sicily is the main cactus pear fruit producer in Italy, with more than 3,500 ha of specialized culture (Ochoa and Barbera, 2017), this disease has not been reported in cactus pear cultivations in Sicily. The present study has shown that *N. batangarum* populations from Favignana, Lampedusa, Linosa and Ustica were genetically uniform, despite their geographical isolation.

It can be assumed that conidia and ascospores of *Botryosphaeriaceae* are dispersed by wind and rain only over short distances. The occurrence of *N. batangarum* only on cactus pear plantations of the minor islands, and the genetic uniformity of the fungus populations, may indicate that these populations have a common origin, and that the widespread distribution of a single genotype of the pathogen has resulted from anthropogenic activity. *Neofusicoccum batangarum*, as an endophytic or latent pathogen, may have been introduced with cactus pear cladodes collected in other geographical areas and used as propagation material. This hypothesis is consistent with cactus pear being introduced on a large scale into small islands of the Mediterranean Sea as fodder for livestock, for field fences or for edible fruit production, at one recent time (Pretto *et al*., 2012). This was when more intensive colonization and exploitation of agriculture in these islands were promoted by the public authorities.

From an ecological perspective, the emergence of this disease in such an aggressive form, which has become a limiting factor for the cultivation of cactus pear in these small islands, may be partly due to the failure of the acclimatization of a non-native plant species. However, the occurrence of a serious disease of a crop of economic and landscaping relevance for Sicily in a restricted geographical area, but very close and frequently connected to the main island by tourist traffic, may have phytosanitary implications. Appropriate actions should be taken to prevent further spread and introduction of *N. batan-*

garum into areas where the non-native cactus pear host is naturalized and intensively cultivated.

LITERATURE CITED

Adesemoye A. O., Mayorquin J. S., Wang D. H., Twizeyimana M., Lynch S. C., Eskalen A. 2014. Identification of species of Botryosphaeriaceae causing bot gummosis in citrus in California. *Plant Dis*ease 98:55–61.

Begoude B.A.D., Slippers B., Wingfield M.J., Roux J. 2010. Botryosphaeriaceae associated with *Terminalia catappa* in Cameroon, South Africa and Madagascar. *Mycological Progress* 9: 101–123.

Begoude B.A.D., Slippers B., Wingfield M.J., Roux J. 2011. The pathogenic potential of endophytic Botryosphaeriaceous fungi on *Terminalia* species in Cameroon. *Forest Pathology* 41: 281–292

Burgess T.I., Tan Y.P., Garnas J., Edwards J., Scarlett K.A., …, Jami F. 2018. Current status of the Botryosphaeriaceae in Australia. *Australasian Plant Pathology* DOI: 10.1007/s13313–018-0577-5

Burruano S., Mondello V., Conigliaro G., Alfonzo A., Spagnolo A., Mugnai L. 2008. Grapevine decline in Italy caused by *Lasiodiplodia theobromae*. *Phytopathologia Mediterranea* 47: 132–136.

Carbone I., Kohn L.M. 1999. A method for designing primer sets for speciation studies in filamentous ascomycetes. *Mycologia* 91: 553–556.

Conforto C., Lima N.B., Garcete-Gómez J.M., Câmara M.P.S., Michereff S.J. 2016. First Report of Cladode Brown Spot in Cactus Prickly Pear Caused by *Neofusicoccum batangarum* in Brazil. *Plant Disease* 100: 1238.

Conforto C., Lima N.B., Silva F.J.A., Câmara M.P.S., Maharachchikumbura S., Michereff S.J. 2019. Characterization of fungal species associated with cladode brown spot on *Nopalea cochenillifera* in Brazil. *European Journal of Plant Pathology* 155: 1179–1194.

Crous P.W., Slippers B., Wingfield M.J., Rheeder J., Marasas W.F.O., …, Groenewald J.Z. 2006. Phylogenetic lineages in the Botryosphaeriaceae. *Studies in Mycology* 55: 235–253.

Crous P.W., Slippers B., Groenewald J.Z., Wingfield M.J. 2017. Botryosphaeriaceae: systematics, pathology, and genetics. *Fungal Biology* 121: 305–306.

Dissanayake A.J., Phillips A.J.L., Li X.H., Hyde K.D. 2016a. *Botryosphaeriaceae*: Current status of genera and species. *Mycosphere* 7: 1001–1073.

Dissanayake A.J., Camporesi E. Hyde K.D., Phillips A.J.L., Fu C.Y., …, Li X.H.2016b. *Dothiorella* species associated with woody hosts in Italy. *Mycosphere* 7: 51–63.

Feijo F.M., Silva M.J.S., Nascimento A.D., Infante N.B., Ramos-Sobrinho R., …, Lima G.S.A. 2019. Botryosphaeriaceae species associated with the prickly pear cactus, *Nopalea cochinellifera*. *Tropical Plant Pathology* 44*:* 452–459.

Freeman S., Shabi, E.E. 1996 Cross-infection of subtropical and temperate fruits by *Colletotrichum* species from various hosts. *Physiological Molecular Plant Pathology* 49:395–404.

Garcete-Gómez J.M., Conforto C., Domínguez-Monge S., Flores-Sánchez J.L.F., Mora-Aguilera G., Michereff S.J. 2017. Sample size for assessment of cladode brown spot in prickly pear cactus. *European Journal of Plant Pathology* 149: 759–763.

Edgar R.C. 2004. Muscle: multiple sequence alignment with high accuracy and high throughput. *Nucleic Acids Research* 32: 1792–1797.

Glass N.L., Donaldson G.C. 1995. Development of primer sets designed for use with the PCR to amplify conserved genes from filamentous ascomycetes. *Applied and Environmental Microbiology* 61: 1323–1330.

Granata G., Faedda R., and Ochoa M.J. 2017. Diseases of cactus pear. In: Crop Ecology, Cultivation and user of Cactus pear (P. Inglese, C. Mondragon, A. Nefzaoui, C. Saenz, eds.), FAO and ICARDA, Rome, Italy, 115–126.

Guarnaccia V., Crous P.W. 2017. Emerging citrus diseases in Europe caused by species of *Diaporthe*. *IMA Fungus* 8: 317–334.

Jami F., Wingfield M.J., Gryenhout M., Slippers B. 2017. Diversity of tree-infecting Botryosphaeriales on native and non-native trees in South Africa and Namibia. *Australasian Plant Pathology* 46: 529–545.

Kiesling R., Metzing D. 2017. Origin and Taxonomy of *Opuntia ficus-indica*. In: Crop Ecology, Cultivation and user of Cactus pear (P. Inglese, C. Mondragon, A. Nefzaoui, C. Saenz eds.), FAO and ICARDA, Rome, Italy, 14–19

Kumar S., Stecher G., Tamura K. 2016. MEGA7: Molecular Evolutionary Genetics Analysis Version 7.0 for Bigger Datasets. *Molecular Biology and Evolution* 33: 1870–1874

Lawrence P.D., Peduto Hand F., Gubler W.D., Trouillas F.T. 2017. *Botryosphaeriaceae* species associated with dieback and canker disease of bay laurel in northern California with the description of *Dothiorella californica* sp. nov. *Fungal Biology* 121: 347–360.

Linaldeddu B.T., Scanu B., Maddau L., Franceschini A. 2014. *Diplodia corticola* and *Phytophthora cinnamomi*: the main pathogens involved in holm oak decline on Caprera island (Italy). *Forest Pathology* 44: 191–200.

Linaldeddu B.T., Alves A., Phillips A.J.L. 2016. *Sardiniella urbana* gen. et sp. nov., a new member of the *Botryosphaeriacea*e isolated from declining *Celtis australis* trees in Sardinian streets capes. *Mycosphere* 7: 893–905.

Lopes A., Barradas C., Phillips A.J.L., Alves A. 2016. Diversity and phylogeny of *Neofusicoccum* species occurring in forest and urban environments in Portugal. *Mycosphere* 7: 906–920.

Lopes A., Phillips A.J.L., Alves A. 2017. Mating type genes in the genus *Neofusicoccum*: Mating strategies and usefulness in species delimitation. *Fungal Biology* 121, 394–404.

Marsberg A., Kemler M., Jami F., Nagel J.H., Postma-Smidt A., …, Slippers B., 2017. *Botryosphaeria dothidea*: a latent pathogen of global importance to woody plant health. *Molecular Plant Pathology* 18: 477–488.

Masi M., Aloi F., Nocera P., Cacciola S.O., Surico G., Evidente A. 2020. Phytotoxic metabolites isolated from *Neofusicoccum batangarum*, the causal agent of the scabby canker of cactus pear (*Opuntia ficus-indica* L.). *Toxins* 12: 126; DOI: 10.3390/toxins12020126

Meyer W., Mitchell T.G., Freedman E.Z., Vilgalys R. 1993. Hybridization probes for conventional DNA fingerprinting used as single primers in the polymerase chain reaction to distinguish strains of *Cryptococcus neoformans*. *Journal of Clinical Microbiology* 31: 2274–2280.

Netto M.S.B., Lima W.G., Correia K.G., Da Silva C.F.B., Thon M., … Camâra M.P.F. 2017. Analysis of phylogeny, distribution and pathogenicity of *Botryosphaeriaceae* species associated with gummosis of *Anacardium* in Brasil, with a new species of *Lasiodiplodia*. *Fungal Biology* 121: 437–451.

Ochoa M.J., Barbera G., 2017. History and economic and agro-ecological importance. In: Crop Ecology, Cultivation and user of Cactus pear (P. Inglese, C. Mondragon, A. Nefzaoui, C. Saenz eds.), FAO and ICARDA, Rome, Italy, 1–12

Pavlic-Zupanc D., Wingfield M.J., Boissin, E., Slippers, B. 2015. The distribution of genetic diversity in the *Neofusicoccum parvum*/*N. ribis* complex suggests structure correlated with level of disturbance. *Fungal Ecology* 13: 93–102.

Phillips A.J.L., Alves A., Pennycook S. R., Johnston P.R., Ramaley A., ..., Crous P.W. 2008. Resolving the phylogenetic and taxonomic status of dark-spored teleomorph genera in the *Botryosphaeriaceae*. *Persoonia* 21: 29–55

Phillips A.J.L., Alves A., Abdollahzadeh J., Slippers B., Wingfield M.J., …, Crous P.W. 2013. The Botryosphaeriaceae: Genera and species known from culture. *Studies in Mycology* 76: 51–167

Pretto F., Celesti-Grapow L., Carli E., Brundu G., Blasi C. 2012. Determinants of non-native plant species richness and composition across small Mediterranean islands. *Biological Invasions* 14: 2559–2572.

Rayner R.W. 1970. *A Mycological Colour Chart*. Commonwealth Mycological Institute, Kew, Surrey, UK.

Santana M.D., de Lima Leite I.C.H., da Silva Santos I.C., Michereff S.J., Freitas-Lopes R.do L., Lopes U.P. 2020. Reduction of cladode brown spot in cactus pear in semiarid growing areas and yield increase using fungicides. *Journal of Plant Pathology* DOI: 10.1007/s42161–019-00462-9

Santos J.M., Phillips A.J.L. 2009. Resolving the complex of *Diaporthe* (*Phomopsis*) species occurring on *Foeniculum vulgare* in Portugal. *Fungal Diversity* 34: 111–125.

Schena L., Cooke D.E.L., 2006. Assessing the potential of regions of the nuclear and mitochondrial genome to develop a "molecular tool box" for the detection and characterization of *Phytophthora* species. *Journal of Microbiological Methods* 67: 70–85.

Schena L., Surico G., Burruano S., Giambra S., Pane A., …, Cacciola S.O. 2018. First report of *Neofusicoccum batangarum* as causal agent of scabby cankers of cactus pear (*Opuntia ficus-indica*) in minor islands of Sicily. *Plant Disease* 102: 445.

Serrato-Diaz L.M., Aviles-Noriega A., Soto-Bauzó A., Rivera-Vargas L.I., Goenaga R., Bayman P. 2020. Botryosphaeriaceae fungi as causal agents of dieback and corky bark in rambutan and longan. *Plant Disease* 104: 105–115.

Shetty K.G., Minnis A.M., Rossman A.Y., Jayachandran K. 2011. The Brazilian peppertree seedborne pathogen, *Neofusicoccum batangarum*, a potential biocontrol agent. *Biological Control* 56: 91–97.

Slippers B., Wingfield M.J. 2007. *Botryosphaeriaceae* as endophytes and latent pathogens of woody plants: diversity, ecology and impact. *Fungal Biology Reviews*21: 90–106.

Slippers B., Crous P.W., Denman S., Coutinho T.A., Wingfield B.D., Wingfield M.J. 2004. Combined multiple gene genealogies and phenotypic characters differentiate several species previously identified as *Botryosphaeria dothidea*. *Mycologia* 96: 83–101.

Slippers B., Boissin E., Phillips A.J.L., Groenewald J.Z., Lombard L., …, Crous P.W. 2013. Phylogenetic lineages in the *Botryosphaeriales*: a systematic and evolutionary framework. *Studies in Mycology* 76: 31–49.

Smith H., Wingfield M.J., Crous P.W., Coutinho T.A., 1996. *Sphaeropsis sapinea* and *Botryosphaeria doth-*

idea endophytic in *Pinus* spp. and *Eucalyptus* spp. in South Africa. *South African Journal of Botany* 62: 86–88.

Somma V., Rosciglione B., Martelli G.P. 1973. Preliminary observations on gummous canker, a new disease of prickly pear. *Tecnica Agricola* 25: 437–443.

Tamura K., Nei M. 1993. Estimation of the number of nucleotide substitutions in the control region of mitochondrial DNA in humans and chimpanzees. *Molecular Biology and Evolution* 10: 512–526.

Tamura K., Stecher G., Peterson D., Filipski A., Kumar S. 2013. MEGA6: Molecular Evolutionary Genetics Analysis Version 6.0. *Molecular Biology and Evolution* 30: 2725–2729.

Uddin W., Stevenson, K.L., Pardo-Schultheiss R.A. 1997. Pathogenicity of a species of *Phomopsis* causing a shoot blight on peach in Georgia and evaluation of possible infection courts. *Plant Disease* 81: 983–998.

Yang T., Groenewald J.Z., Cheewangkoon R., Jami F., Abdollahzadeh J., … , Crous P.W. 2017. Families, genera, and species of *Botryosphaeriales*. *Fungal Biology* 121: 322–346.

Vaidya N.H., Hadjicostis C.N., Dominguez-Garcia A.D. 2011. Distributed algorithms for consensus and coordination in the presence of packet-dropping communication links-part II: Coefficients of ergodicity analysis approach. arXiv preprint arXiv:1109.6392.

White T. J., Bruns T. D., Lee S. B., Taylor J. W. 1990. Amplification and direct sequencing of fungal ribosomal RNA Genes for phylogenetics. In: *PCR - Protocols and Applications - A Laboratory Manual* (M.A. Innis, D.H. Gelfand, J.J. Sninsky, T.J White eds.), Academic Press Inc., New York, USA, 315–322.

Zhang M., Lin S., He W., Zhang Y. 2017. Three species of *Neofusicoccum* (Botryosphaeriaceae, Botryosphaeriales) associated with woody plants from southern China. *Mycosphere* 8: 797–808.

Phytopathologia Mediterranea
The international journal of the
Mediterranean Phytopathological Union

Firenze University Press
www.fupress.com/pm

Research Papers

Unraveling the infection process of garlic by *Fusarium proliferatum*, the causal agent of root rot

Paul L. CHRÉTIEN[1], Sandrine LAURENT[2], Isabelle BORNARD[1], Claire TROULET[1], Mohamed EL MAÂTAOUI[2], Christel LEYRONAS[1,*]

[1] *INRAE, Pathologie Végétale, 84140 Montfavet, France*
[2] *Avignon Université, Qualisud UMR95, 84000 Avignon, France*
*Corresponding author: christel.leyronas@inrae.fr

Summary. Since the mid-2000s, and despite demanding production rules, *Fusarium proliferatum* (Matsushima) Niremberg has been found on garlic heads during storage inducing root and bulbs rots. Brown spots on the surface of garlic cloves and water-soaking of heads were noted. Histological observations of the fungus during early stages of infection were made from clove to the cellular levels. *Fusarium proliferatum* germinates, colonizes roots and degrades the outer root and parechchyma cell layers 72 h post inoculation. Conidium germination and host colonization are facilitated by the emergence of garlic roots, creating cellular debris and natural wounds. Hyphae of the pathogen did not penetrate healthy host cells and appeared to degrade them before penetration. These results provide understanding of when and how quickly *F. proliferatum* penetrates garlic bulbs. This is a primary step towards elucidating the life cycle of this pathogen during the garlic drying process, and development of an efficient and sustainable bulb rot management strategy.

Keywords. Histology, electron microscopy, garlic rot, host-parasite interaction.

OPEN ACCESS

Citation: P.L. Chrétien, S. Laurent, I. Bornard, C. Troulet, M. El Maâtaoui, C. Leyronas (2020) Unraveling the infection process of garlic by *Fusarium proliferatum*, the causal agent of root rot. *Phytopathologia Mediterranea* 59(2): 285-293. DOI: 10.14601/Phyto-11103

Accepted: June 1, 2020

Published: August 31, 2020

Data Availability Statement: All relevant data are within the paper and its Supporting Information files.

Competing Interests: The Author(s) declare(s) no conflict of interest.

Editor: Antonio Moretti, National Research Council, (CNR), Bari, Italy.

Author's contributions: PLC, IB, SL, CT & MEM performed experiments and analysed the results.
IB & PLC performed the electron microscopy experiments and realized the figures.
PLC, SL, MEM and CL participated to the redaction of the manuscript.
CL led the research project and supervised the redaction of the manuscript.

INTRODUCTION

From Hippocratic medicine (Totelin 2015) to modern and sophisticated molecular cuisine (This 2006), garlic has been used throughout history and has a special place in human civilization. World garlic production reached a peak of more than 26 million tons produced in 2016, rising from 11 million in 2000 (FAOSTAT, 2018). Global average price is $US 2.35 kg^{-1} and continues to increase (Tridge, 2019). China produces and exports the most of the world's garlic (80% of world production and 25 millions of tons per year).

France ranks 6th among European producers of garlic, with 21,000 tons produced each year in two main areas of cultivation: the South-East and the South-West of the country. Quality is an important objective for French producers in that French garlic benefits from high quality standards and certification, which ensure control of production such as the restricted geographic areas of production (one AOP – Appellation d'Origine Protégée – and four IGP – Indication Géographique Protégée – labels) (INAO, 2019). For the seed

certification, garlic production in each field must be separated by 5 years, in order to reduce propagation of the nematode *Ditylenchus dipsaci* (Robert and Matthews 1995) and white rot caused by *Sclerotium cepivorum* (Basallote-Ureba and Melero-Vara 1993). All certified varieties are free from *Onion yellow dwarf virus* (OYDV) and *Leek yellow stripe virus* (LYSV), and have been obtained by meristem culture. In the field, all plants that show differences compared to the source material are destroyed. During all production steps before and after storage, damaged garlic heads are destroyed. Despite these control and certification standards for seed and plants, *Fusarium* rot of garlic emerged in France in approx. 2006 (Ricard 2017). During storage, browning of cloves commences from the basal plates and extends to the tops of the heads. Tissues become soft and water-soaked before complete rotting. Losses are variable: less than 1% in 2006 year, increasing to 25% on average in 2015. Some plots have been more affected than the others (from 1 to 80%), and high losses drastically reduce the volumes sold and therefore the income for producers. In extreme cases, farmers have ceased producing several varieties that were highly susceptible to root rot.

Eight *Fusarium* species have been found on symptomatic garlic, with the majority being *F. proliferatum* followed by *F. oxysporum* and then *F. solani* (Koleva 2004; Stankovic *et al*., 2007; Ochoa-Fuentes *et al.,* 2012; Moharam *et al.,* 2013; Delgado-Ortiz *et al.,* 2016; Ignjatov *et al.,* 2017). The disease caused by *F. proliferatum* on garlic is common wherever the crop is grown, and was first reported in 2002 in Germany (Seefelder *et al.,* 2002) and in 2003 in North America (Dugan *et al.,* 2003). The number of countries affected by *F. proliferatum* on garlic has increased to include Serbia in 2007 (Stankovic *et al.,* 2007), India in 2012 (Sankar and Babu 2012) and Egypt in 2013 (Moharam *et al.,* 2013). In France, the pathogen was recently identified as *F. proliferatum* (Matsushima) Niremberg in 2018 (Leyronas *et al.,* 2018). *Fusarium proliferatum* is within the *F. fujikuroi* species complex native to Asia (O'Donnell *et al.,* 2013), and is responsible for bulb, root or fruit diseases on many crop plants, including onion (Toit *et al.,* 2003), soybean (Diaz Arias *et al.,* 2011), chive (Yamazaki *et al.,* 2013), lily (Lebiush-Mordechai *et al.,* 2014), welsh onion (Alberti *et al*., 2017), peach (Xie *et al.,* 2018) and strawberry (Borrero *et al*., 2019).

There is no officially accepted prophylactic or chemical control method for *Fusarium* spp. on garlic in France. One of the hurdles to developing control methods is the lack of knowledge of the pathogen infection processes into garlic bulbs. Mycelium starts to develop around the basal plates of bulbs where the roots emerge (Stankovic *et al.,* 2007; Tonti *et al.,* 2012). Fungal growth also occurs on the bulb apices, where the skin cracks as leaves emerge. Then tissues become brown, and wilt from the bottom to the top at a regular rate. Wilting also starts from wounds on the bulb surfaces. Microscope observations have been made of infection of sorghum plants, showing that hyphae of *F. proliferatum* quickly penetrate (about 2 weeks after sowing) the endodermal and xylem parenchyma layers of roots, colonize complete root cortices (Ndambi *et al.,* 2012).

The objectives of the present study were to investigate the infection processes of garlic by *F. proliferatum*, and in particular to determine when and where the pathogen conidia enter host tissues. Observations were focused on the basal parts of the garlic heads, including the roots and tissues around the heads and the basal plates. Using light and electron microscopy, interactions were observed at different scales, from overall aspects to histological levels.

MATERIALS AND METHODS

Preparation of biological material

Biological material

A *F. proliferatum* strain (FA3-E01) isolated from pink garlic cloves cultivated in France during the summer 2017 was used in this study. This strain was previously purified and added to a laboratory fungal collection, and this strain has been shown to be aggressive on garlic bulbs (Leyronas *et al.,* 2018).

All garlic cloves used in this study were from a single lot of pink garlic from the south of France harvested in late June 2018. The cloves were all asymptomatic at the time of inoculation.

Preparation of conidium suspensions

Inoculum was produced on potato dextrose agar medium (Difco Laboratories) at 21°C under cool white light (12 h photoperiod, 23.8 µmol m^{-2} s^{-1}). Mycelium plugs were taken from 1-week old cultures and were added on 250 mL capacity Erlenmeyer flasks containing 150 mL of potato dextrose broth (Difco Laboratories, Detroit). The flasks were placed on a rotary shaker at 100 rpm at 21°C under cool white light (12 h photoperiod, 23.8 µmol m^{-2} s^{-1}). After 7 d, the medium was filtered through etamine filters (25–35 µm pores) to remove mycelium fragments and retain microconidia. The concentration was evaluated with a haemocytometer, and

adjusted to 1.0×10^6 conidia mL^{-1} using sterile deionized water. This concentration was known to recreate symptoms on cloves.

Inoculation of garlic cloves

Healthy peeled cloves of pink garlic (n = 6) were surface-disinfected with 1% NaOCl for 1 min and rinsed in 3 successive baths of sterile water. Disinfected cloves were soaked in 200 mL of conidial suspension (or sterile water for negative control) inside a beaker placed on a rotary shaker at 100 rpm for 24 h at 21°C. The cloves were then placed inside a sterile plastic box at 23°C with saturated humidity and constant obscurity. Samples were collected after 6, 12, 24, 48 and 72 h for microscopic analyses.

Observations of samples at different scales

Sample preparation for light microscopy

All samples were first observed with an illuminated binocular magnifier. General structures of cloves, basal plates and tissues were described.

Control (uninoculated) and inoculated garlic cloves were longitudinally sliced and fixed in FAA (1/1/8, V/V/V, 37% formalin/glacial acetic acid/90% ethanol). To promote penetration of the fixative products, samples were subjected to vacuum for 20 min. After 48 h of fixation, the specimens were rinsed in distilled water and stored in 70% ethanol at 4°C until required. They were then dissected to collect 5 x 5 mm basal fragments that were processed for cytohistology. Briefly, the samples were dehydrated in a graded ethanol series (80-100 %) and infiltrated in methacrylate resin (Kit Technovit 7100, Heraeus-Kulzer GmbH), according to the manufacturer instructions). Sections (3 µm thick) were serially cut using a retraction microtome (Supercut 2065, Reichert-Young), and collected on microscope slides. For routine observations, sections were stained by toluidine blue, a metachromatic dye (Clark, 1981). For each treatment, sections were stained to visualize major cell components using periodic acid-Schiff's reagent (PAS) for polysaccharides (starch and cellulose) (pink) and naphthol blue-black (NBB) for protein (blue) (El Maâtaoui and Pichot 1999). All microscope analyses were performed using a Leica DMR photomicroscope equipped for bright field, dark field, phase contrast and UV illuminations. Images were captured using a Leica DFC 300 FX digital camera and processed using Leica LAS software. For each treatment, approx. 60 serial sections from five different garlic cloves were analyzed, and representative images were selected to illustrate the major histological traits. Attention was paid to initiation of infection, mycelium progression in clove tissues, and cyto-pathological effects.

Sample preparation for scanning electron microscopy

Garlic tissue samples were fixed in 2.5% (v/w) glutaraldehyde for 1 h and then washed three times with 0.2M sodium cacodylate buffer (pH 7.2). The samples were then dehydrated with a series of ethanol baths of increasing concentration (30% to 100%). The ethanol was replaced by HMDS until it completely invaded the samples and evaporated. After drying, the samples were mounted on aluminium stubs, sputter-coated with a layer of gold, and then observed with an FEI/Philips XL30 scanning electron microscope at 10 kV.

RESULTS

Structure of healthy garlic tissues

Each peeled garlic clove usually had bulbil-like morphostructure, with a basal plate supporting a fleshy external leaf or scale (Figure 1A) attached to a short stem (not shown) that bore numerous root primordia (Figure 1B). After clove germination, root emergence took place between the external scale and the abscission zone of the basal plate, thus enlarging the space at the junction between the external scale and the abscission zone. Microscope analyses of sections from the abscission zone showed that this area was composed of thick-walled, dead cells (Figure 1C). Condensation and retraction of cytoplasm and degradation of chromatin inside nuclei indicated that the cells were dying. Inside cloves, roots embedded in leaf parenchyma (Figure 1D) created each an aperture and many dead collapsed cells while emerging (Figure 1E).

Progression of Fusarium proliferatum *in cloves*

After 72 hpi, hyphae adhered and colonized the junctions between roots and parenchyma of external scale edges (Figure 2A). Inoculated conidia germinated on the surface of epidermis cells (Figure 2B). Mycelium then invaded the entire area composed of the parenchyma of the external scale and suberized tissue (Figure 2C). Abscission zones (AZ) were covered with white mycelium (not shown). Microscope analyses of these areas

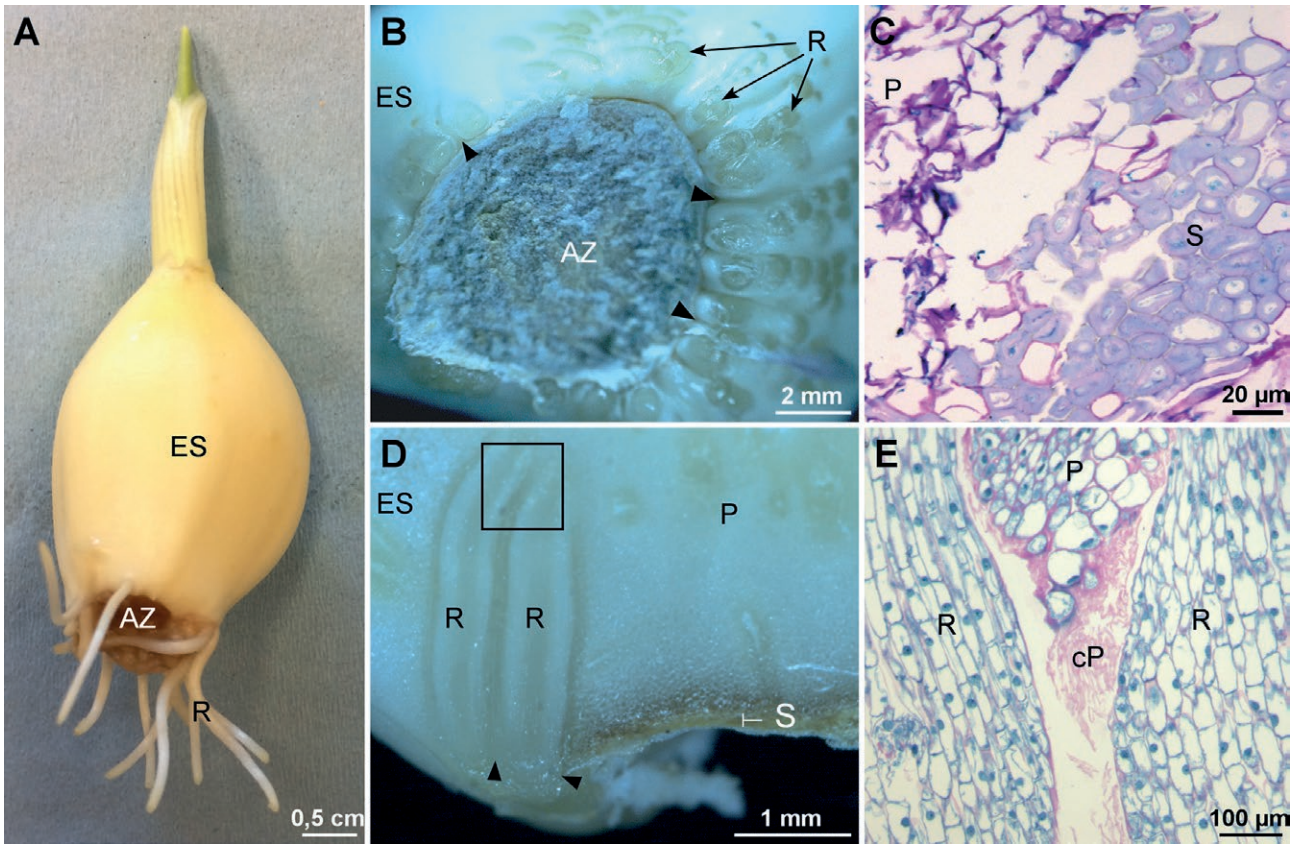

Figure. 1. Morphology and structure of healthy garlic cloves. A, Peeled clove after 3 d in sterile distilled water. B, Abscission zone. C, Section of the abscission zone. D, Longitudinal section of the basal part of an ungerminated clove. E, Section from the area indicated by a square in D. ES: external scale, AZ: abscission zone, R: roots, P: parenchyma, S: thick-walled cells, cP: collapsed parenchymatous cells. Black arrowheads indicate junctions between roots and between AZ boundaries and root primordia. A, B and D, Stereomicrographs. C and E, Light micrographs of PAS/NBB stained samples.

showed dense mycelium growth in the cellular debris close to suberized tissue (Figure 2D). On each clove, a coat of white hyphae appeared all around the roots from the base to the top and at the edge of the external scale (Figure 2E). Specific infection structure were not observed. *Fusarium proliferatum* proliferated as mycelium in a saprophyte-like manner.

Browning of cloves progressed from the base to the top at 72 hpi. The boundary between healthy and diseased tissues was easily discernible, and mycelium entirely covered roots (Figure 3A). At 48 hpi, germinated conidia and mycelium were observed against destructured suberised regions (Fig. 3B). The pathogen was also observed to be growing inside collapsed dead cells from the external clove scales resulting from the root emergence (Figure 3C). At 72 hpi and beneath the mycelium coat, root tissues were degraded and hyphae penetrated only inside the first layers of dead cells (Figure 3D).

De-structuring of clove cell layers

In tissues infected by *F. proliferatum*, the cells died and shrank particularly within the parenchyma of external scales and in the superficial layers of the roots (Figure 4A and B). Three levels of degraded tissue could be discerned; entirely degraded tissue, collapsed cells filled with secondary metabolites (deep blue) and dead matrices of cells filled with fungal mycelium (III), a border between dead and healthy cells (II) and healthy parenchyma cells (I) (Figure 4B). The dead cells accumulated proteins, as indicated by the azure colour of their contents.

DISCUSSION

This study has clarified the pathway by which *F. proliferatum* enters garlic gloves. *Fusarium* species (e.g. *F. oxysporum*, *F. solani* and *F. verticillioides*) are well

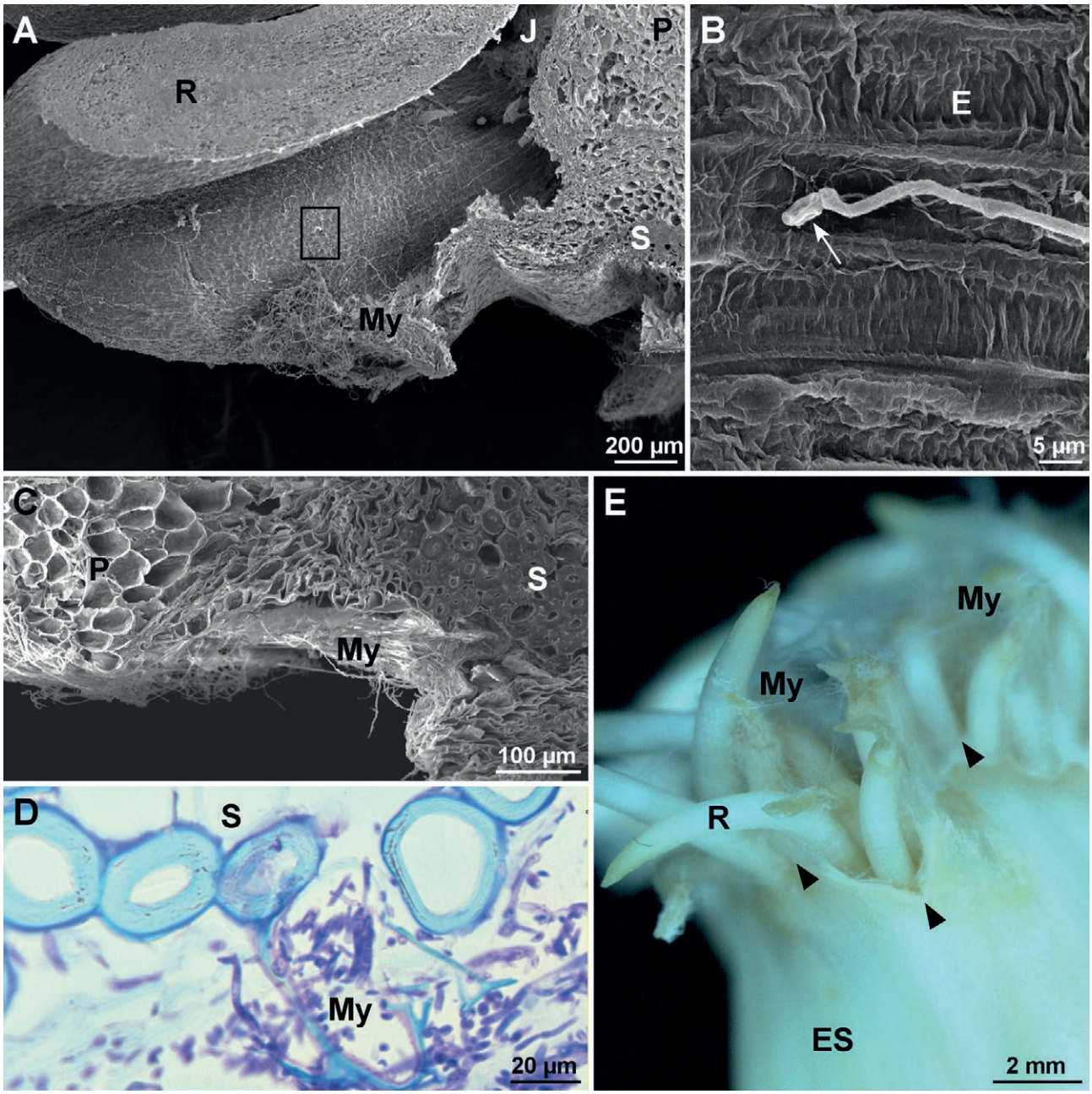

Figure 2. Mycelium development of *Fusarium proliferatum.* A, SEM micrograph of a germinating garlic root. B, High magnification of the area indicated by the square in A. C, Section of the basal part of an infected clove. D, Detail of suberized tissue. E, Basal part of a clove 72 h post inoculation. R: roots, J: junction, P: parenchyma, My: mycelium, E: epidermis, S: thick-walled cells, ES: external scale. White arrow in B indicates a germinated conidium. Black arrowheads in E indicate junctions between roots and between the abscission zone boundary and root primordia. A and B, Scanning electron micrographs. D, Light micrograph after TB staining. E, Stereomicrograph.

known for their capacity to infect vascular and root tissues causing wilt on plants (Agrios, 2005). In the present study, rapid degradation of garlic root cells was observed after inoculation with *F. proliferatum*, but the pathogen did not invade host conductive tissues. *Fusarium proliferatum* progressed from the points of infection in all directions. Proliferation of the fungus in garlic tissue was reduced in the presence of thick-walled cells, and was directed toward the parenchyma. Although this pathogen possesses the enzymes required to degrade

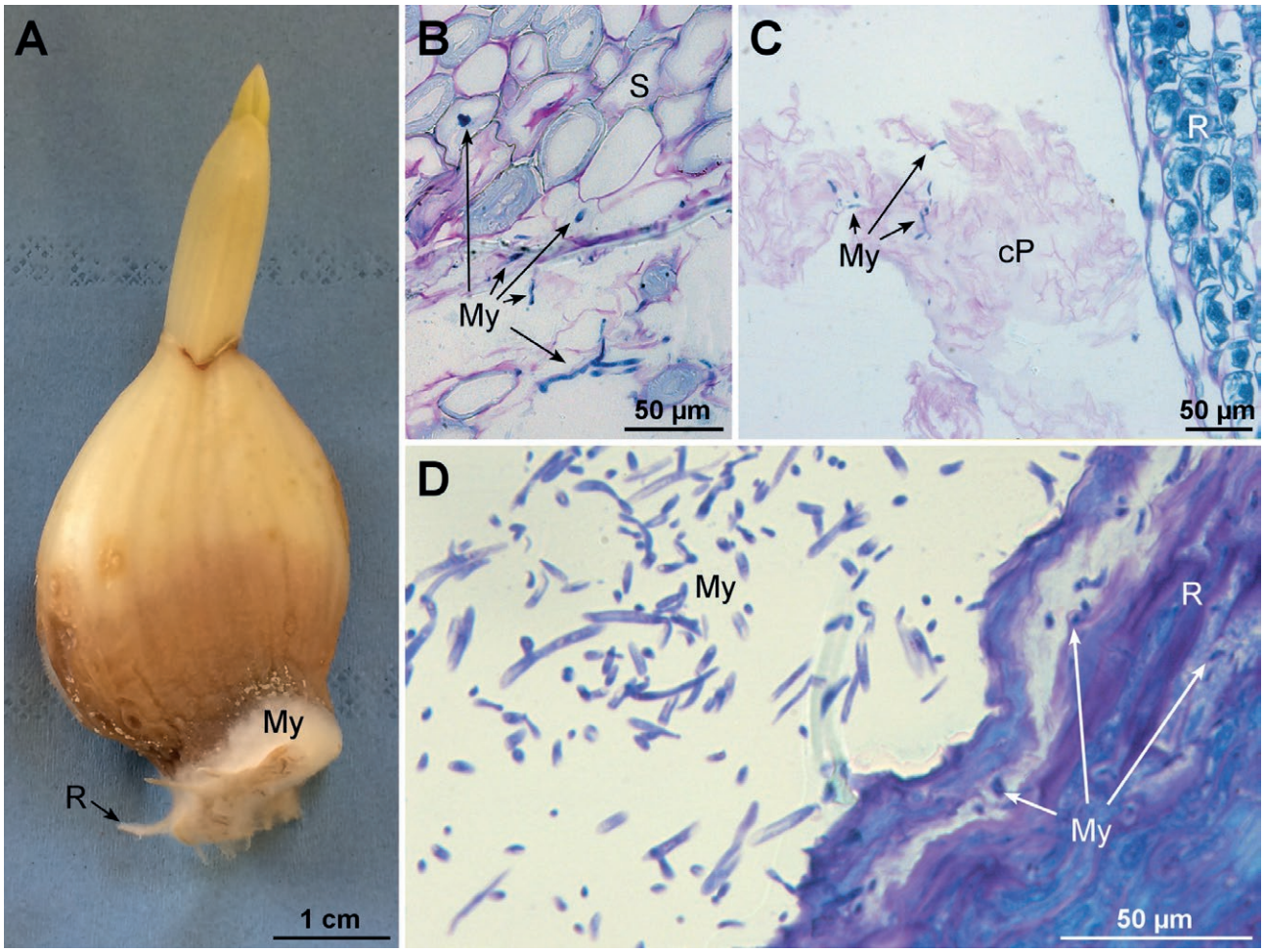

Figure 3. Morphology and cytohistological aspects of *Fusarium proliferatum* infected garlic cloves 48–72 h post inoculation. A, Image of an infected clove. B and C, Micrographs illustrating the progression of clove infection 48 h post inoculation. D, Detail of the decayed root tissue. R: roots, My: mycelium, S: thick-walled cells, cP: collapsed parenchyma cells. A, Stereomicrograph. B and C, Light micrographs after PAS/NBB staining. D, Light micrograph with TB staining.

suberized cells, such as laccases (Regalado *et al.,* 1999; Hernández Fernaud *et al*., 2006), chitinases, glucosidases and galactosidases (Keshri and Magan 2000), *F. proliferatum* probably takes the path of least host resistance.

Fusarium proliferatum rapidly infected garlic root tissues before infecting clove tissues. Germination of roots may have triple positive indirect effects on the development of the root rot. First, while emerging, roots degrade parenchyma cells and release cellular debris that may be utilized for growth of the fungus. Second, the physical barrier of the host epidermis breaks and allows penetration of the pathogen into host tissues. In some preliminary experiments, we have observed that *F. proliferatum* was unable to enter through intact garlic epidermis surfaces. Third, the presence of host and non-host roots in the soil are known to induce germination of fungal conidia and attract hyphae of *F. oxysporum* (Nelson 1981). Further studies could assess if this is also the case for *F. proliferatum* and garlic roots.

In the present study, *F. proliferatum* was observed to colonize decayed host tissues, but not to penetrate healthy cells. Tissues destroyed beyond the margins where fungal growth occurred were seen, indicating that the fungus deployed strategies, such as enzymes and toxin production, to destroy host tissues prior to colonization. The limits between dead and living cells were clearly visible. This could indicate activity of the many organosulfur compounds produced and stored inside garlic cells. These molecules are responsible for the characteristic fragrance of garlic. These compounds, such as allicin, have been widely studied as potential biocontrol agents against fungi, bacteria and

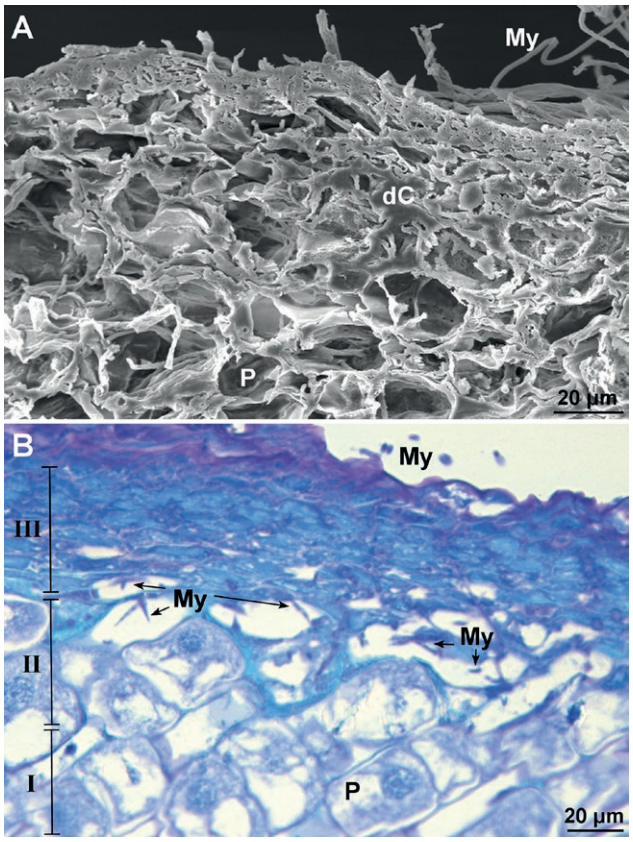

Figure 4. Histopathological effects of *Fusarium proliferatum* on infected clove tissues. A and B, Detail of the first root cells layers 72 h post inoculation. My: mycelium, dC: dead cells, P: parenchyma. A, Scanning electron micrograph. B, Light micrograph after TB staining.

other pests (Curtis *et al.,* 2004). Allicin is synthetized from a precursor molecule (alliin) through the action of alliinase activated when cells are damaged. The fact that *F. proliferatum* is able to grow, colonize and develop on a matrix containing organosulfur compounds was interesting. Previous studies have found that garlic extracts inhibit *F. proliferatum* on culture media at pH 3 to 7 (Chen *et al.,* 2018). One hypothesis to explain pathogenicity is the production of desulfurization enzymes (sulfatases) by some *F. proliferatum* strains (Shvetsova *et al.,* 2015). This overcoming of host resistance could also be linked to glutathione metabolism (Leontiev *et al.,* 2018). Another example of fungi being able to grow in the presence of organosulfur is *Coriolus versicolor* known to degrade this type of compound in wood (Linder 2018). One hypothesis about the emergence of root rot of garlic is that some pathogen strains may have acquired resistance to garlic compounds. In further studies, we will assess the impacts of garlic extracts on *in vitro* development of several *F. proliferatum* strains, and evaluate the ability of *F. proliferatum* strains, collected from other crops, to develop disease symptoms on garlic.

Like most *Fusarium* spp., *F. proliferatum* has a soil-borne phase. The present study showed that this fungus can penetrate garlic cloves at the outline/contour of their basal plates when the roots emerge. This indicates that *F. proliferatum* remains dormant in the soil, is attracted to germinating garlic cloves (at early stages of their development), and then penetrates through wounds without generating visible symptoms. Airborne phases cannot be excluded. *Fusarium proliferatum* is a prolifically sporulating species, and in Spain, conidia collected in rainwater were shown to be aggressive on garlic (Gil-Serna *et al.,* 2016). In the field, sprouting garlic leaves take funnel shapes, and rainwater is directly led to germinated cloves where the epidermis is weakened. In further experiments, it could be interesting to test independent inoculation of shoots and of the basal plates could be investigated. Knowledge of the origin of inoculum that induces rot on garlic is crucial for development of efficient, sustainable and environmentally-friendly root rot management strategies.

Through of French and European actions, French garlic producers are encouraged to reduce their use of phytosanitary products (European Directive 2009/128/EC). There is a need for efficient alternative disease control methods, among which are aimed at management of garlic root rot. Soil solarization could be explored to control the soil-borne population of *Fusarium* spp. In Japan, this method was efficient for control *Fusarium* wilt of strawberry caused by *F. oxysporum*, in fields and greenhouses (Koike and Gordon 2015). Results could be linked to heat alone or to selection of antagonistic soil microorganisms. In another research, solarization with *Medicago sativa* amendment was shown to be an efficient, non-chemical, method for control of Fusarium wilt of cucumber caused by *F. oxysporum* (Yao *et al.,* 2016). Although soil solarization has proved to be efficient against species other than *F. proliferatum*, it would be worth testing this method for garlic crops. The use of biocontrol agents such as bacteria applied on garlic cloves may also be promising. Four strains of *B. subtilis* have been shown to reduce severity of disease caused by *F. proliferatum* strains on garlic (Bjelic *et al.,* 2018).

Biocontrol and solarization need to be applied at the right time, in optimum conditions, to have appropriate activity during or before crop planting. To this end, some of our current studies are focusing on the impacts of abiotic factors on *F. proliferatum* mycelium growth and sporulation.

ACKNOWLEDGEMENTS

This research was supported by the microscopy facilities of the Platform 3A, funded by the European Regional Development Fund, the French Ministry of Research, Higher Education and Innovation, the Provence-Alpes-Côte d'Azur region, the Departmental Council of Vaucluse and the Urban Community of Avignon. The authors thank M. Duffaud for her work in the purification of strains included in the laboratory fungal collection. We thank Top'Alliance Alinéa for providing the garlic cloves.

LITERATURE CITED

Agrios GN, 2005. *Plant Pathology*. 5th edition. Elsevier.

Alberti I., Prodi A., Montanari M., Paglia G., Asioli C., Nipoti P., 2017. First report of *Fusarium proliferatum* associated with *Allium fistulosum* L. in Italy. *Journal of Plant Diseases and Protection* 125: 231–233.

Basallote-Ureba M.J., Melero-Vara J.M., 1993. Control of garlic white rot by soil solarization. *Crop Protection* 12: 219–223.

Bjelić D., Ignjatov M., Marinković J., Milošević D., Nikolić Z., Gvozdanović-Varga J., Karaman M., 2018. *Bacillus* isolates as potential biocontrol agents of *Fusarium* clove rot of garlic. *Zemdirbyste-Agriculture* 105: 369–376.

Borrero C., Capote N., Gallardo M.A., Avilés M., 2019. First report of vascular wilt caused by *Fusarium proliferatum* on strawberry in Spain. *Plant Disease* 103: 581.

Clark G., 1981. Staining Procedures. 4th Edition. Williams & Wilkins. Baltimore.

Chen C., Liu C.-H., Cai J., Zhang W., Qi W.-L., … Yang Y., 2018. Broad-spectrum antimicrobial activity, chemical composition and mechanism of action of garlic (*Allium sativum*) extracts. *Food Control* 86: 117–125.

Curtis H., Noll U., Störmann J., Slusarenko A.J., 2004. Broad-spectrum activity of the volatile phytoanticipin allicin in extracts of garlic (*Allium sativum* L.) against plant pathogenic bacteria, fungi and oomycetes. *Physiological and Molecular Plant Pathology* 65: 79–89.

Delgado-Ortiz J.C., Ochoa-Fuentes Y.M., Cerna-Chávez E., Beltrán-Beache M., Rodríguez-Guerra R., Aguirre-Uribe L.A., Vázquez-Martínez O., 2016. Patogenicidad de especies de *Fusarium* asociadas a la pudrición basal del ajo en el centro norte de México. *Revista Argentina de Microbiologia* 48: 222–228.

Díaz Arias M.M., Munkvold G.P., Leandro L. F., 2011. First Report of *Fusarium proliferatum* causing root rot on soybean (*Glycine max*) in the United States. *Plant Disease* 95: 1316.

Dugan F.M., Hellier B.C., Lupien S. L., 2003. First report of *Fusarium proliferatum* causing rot of garlic bulbs in North America. *Plant Pathology* 52: 426.

El Maâtaoui M., Pichot C., 1999. Nuclear and cell fusion cause polyploidy in the megagametophyte of common cypress, *Cupressus sempervirens* L. *Planta* 208: 345–351.

European Parliament. Establishing a framework for Community action to achieve the sustainable use of pesticides. DIRECTIVE 2009/128/EC.

Hernández Fernaud J.R., Marina A., González K., Vázquez J., Falcón M.A., 2006. Production, partial characterization and mass spectrometric studies of the extracellular laccase activity from *Fusarium proliferatum*. *Applied Microbiology and Biotechnology* 70: 212–221.

FAOSTAT, 2018. Production/Yield quantities of Garlic in World + (Total). Available at: http://www.fao.org/faostat/en/#data/QC/visualize. Accessed September 6, 2018.

Gil-Serna J., Gálvez L., París M., Palmero D., 2016. *Fusarium proliferatum* from rainwater and rooted garlic show genetic and pathogenicity differences. *European Journal of Plant Pathology* 146: 199–206.

Ignjatov M., Bjelić D., Nikolić Z., Milošević D., Gvozdanović-Varga J., Marinković J., Ivanović Ž., 2017. First report of *Fusarium acuminatum* causing garlic bulb rot in serbia. *Plant Disease* 101: 1047.

INAO, 2019. Les signes officiels de la qualité et de l'origine, SIQO. Available at: https://www.inao.gouv.fr/Les-signes-officiels-de-la-qualite-et-de-l-origine-SIQO. Accessed June 6, 2019.

Keshri G., Magan N., 2000. Detection and differentiation between mycotoxigenic and non-mycotoxigenic strains of two *Fusarium* spp. using volatile production profiles and hydrolytic enzymes. *Journal of Applied Microbiology* 89: 825–833.

Koike S.T., Gordon T.R., 2015. Management of *Fusarium* wilt of strawberry. *Crop Protection* 73: 67–72.

Koleva K., 2004. Variety of species and spread of fungi of genus *Fusarium* related to rotting of garlic. *Bulgarian Journal of Agricultural Science* 10: 177–180.

Lebiush-Mordechai S., Erlich O., Maymon M., Freeman S., Ben-David T., … Tsror Lahkin L., 2014. Bulb and root rot in lily (*Lilium longiflorum*) and onion (*Allium cepa*) in Israel. *Journal of Phytopathology* 162: 466–471.

Leontiev R., Hohaus N., Jacob C., Gruhlke M.C.H., Slusarenko A.J., 2018. A comparison of the antibac-

terial and antifungal activities of thiosulfinate analogues of allicin. *Scientific Reports* 8: 1–19.

Leyronas C., Chrétien P.L., Troulet C., Duffaud M., Villeneuve F., Morris C.E., Hunyadi H., 2018. First Report of *Fusarium proliferatum* causing garlic clove rot in France. *Plant Disease* 102: 2658.

Linder T., 2018. Assimilation of alternative sulfur sources in fungi. *World Journal of Microbiology and Biotechnology* 34: 51.

Moharam M.H.A., Farrag E.S.H., Mohamed M.D.A., 2013. Pathogenic fungi in garlic seed cloves and first report of *Fusarium proliferatum* causing cloves rot of stored bulbs in upper Egypt. *Archives of Phytopathology and Plant Protection* 46: 2096–2103.

Ndambi B., Cadisch G., Elzein A., Heller A., 2012. Tissue specific reactions of sorghum roots to the mycoherbicide *Fusarium oxysporum* f. sp. *strigae* versus the pathogenic *F. proliferatum*. *Biocontrol Science and Technology* 22: 135–150.

Nelson P.E., 1981. Chapter 3: Life cycle and epidemiology of *Fusarium oxysporum*. In: Fungal Wilt Diseases of Plants. M.E. Mace, A.A. Bell & C.H. Beckman, eds. Academic press, New York, U.S., p. 51–80.

Ochoa Fuentes Y.M., Cerna Chávez E., Gallegos Morales G., Landeros Flores J., Delgado Ortiz J.C., … Olalde Portugal V., 2012. Identificación de especies de *Fusarium* en semilla de ajo en Aguascalientes, México. *Revista Mexicana de Micologia* 36: 27–32.

O'Donnell K., Rooney A.P., Proctor R.H., Brown D.W., McCormick S.P., … Aoki T., 2013. Phylogenetic analyses of RPB1 and RPB2 support a middle Cretaceous origin for a clade comprising all agriculturally and medically important fusaria. *Fungal Genetics and Biology* 52: 20–31.

Regalado V., Perestelo F., Rodríguez A., Carnicero A., Sosa F.J., De la Fuente G., Falcón M.A., 1999. Activated oxygen species and two extracellular enzymes: laccase and aryl-alcohol oxidase, novel for the lignin-degrading fungus *Fusarium proliferatum*. *Applied Microbiology and Biotechnology* 51: 388–390.

Ricard P., 2017. Les premiers pas vers l'étiologie et l'épidémiologie d'une maladie multifactorielle et en expansion : la fusariose de l'ail (*Allium sativum* L.). https://dumas.ccsd.cnrs.fr/dumas-01618306. Accessed 14 Oct 2019.

Roberts P.A., Matthews W.C., 1995. Disinfection alternatives for control of *Ditylenchus dipsaci* in garlic seed cloves. *Journal of Nematology* 27: 448–456.

Sankar N.R., Babu G.P., 2012. First Report of *Fusarium proliferatum* causing rot of garlic bulbs (*Allium sativum*) in India. *Plant Disease* 96: 290.

Seefelder W., Gossmann M., Humpf H.-U., 2002. Analysis of fumonisin B(1) in *Fusarium proliferatum*-infected asparagus spears and garlic bulbs from Germany by liquid chromatography-electrospray ionization mass spectrometry. *Journal of Agricultural and Food Chemistry* 50: 2778–2781.

Shvetsova S.V., Zhurishkina E.V., Bobrov K.S., Ronzhina N.L., Lapina I.M., … Kulminskaya A.A., 2015. The novel strain *Fusarium proliferatum* LE1 (RCAM02409) produces α- L -fucosidase and arylsulfatase during the growth on fucoidan: Alfa-L-fucosidase and arylsulfatase from the novel strain *Fusarium proliferatum*. *Journal of Basic Microbiology* 55: 471–479.

Stankovic S., Levic J., Petrovic T., Logrieco A., Moretti A., 2007. Pathogenicity and mycotoxin production by *Fusarium proliferatum* isolated from onion and garlic in Serbia. *European Journal of Plant Pathology* 118: 165–172.

Toit L.J., Inglis D.A., Pelter G.Q., 2003. *Fusarium proliferatum* pathogenic on onion bulbs in Washington. *Plant Disease* 87: 750.

Tonti S., Prà M.D., Nipoti P., Prodi A., Alberti I., 2012. First Report of *Fusarium proliferatum* causing rot of stored garlic bulbs (*Allium sativum* L.) in Italy. *Journal of Phytopathology* 160: 761–763.

This H., 2006. Molecular gastronomy: exploring the science of flavor. Columbia University Press.

Totelin L., 2015. When foods become remedies in ancient Greece: The curious case of garlic and other substances. *Journal of Ethnopharmacology* 167:3 0–37.

Tridge, 2019. Garlic (*Allium sativum*) – Garlic Price Trend. Available at: https://www.tridge.com/products/garlic. Accessed August 10, 2019.

Xie S.H., Zhang C., Chen M.S., Wei Z.P., Jiang Y.B.., Lin X., Zheng Y.Q., 2018. *Fusarium proliferatum* : a new pathogen causing fruit rot of peach in Ningde, China. *Plant Disease* 102: 1858.

Yamazaki M., Morita Y., Kashiwa T., Teraoka T., Arie T., 2013. *Fusarium proliferatum*, an additional bulb rot pathogen of Chinese chive. *Journal of General Plant Pathology* 79: 431–434.

Yao Y., Xue Z., Hong C., Zhu F., Chen X., … Yang X., 2016. Efficiency of different solarization-based ecological soil treatments on the control of *Fusarium* wilt and their impacts on the soil microbial community. *Applied Soil Ecology* 108: 341–351.

Phytopathologia Mediterranea
The international journal of the
Mediterranean Phytopathological Union

Firenze University Press
www.fupress.com/pm

Research Papers

Determining intra-host genetic diversity of *Citrus tristeza virus*. What is the minimal sample size?

Silvija ČERNI[1,*], Zlatko ŠATOVIĆ[2,3], Jelena RUŠČIĆ[4], Gustavo NOLASCO[5], Dijana ŠKORIĆ[1]

[1] *University of Zagreb, Faculty of Science, Department of Biology, Division of Microbiology, Marulićev trg 9a, 10000 Zagreb, Croatia*
[2] *University of Zagreb, Faculty of Agriculture, Department for Seed Science and Technology, Svetošimunska 25, 10000 Zagreb, Croatia*
[3] *Centre of Excellence for Biodiversity and Molecular Plant Breeding (CoE CroP-BioDiv), Svetošimunska cesta 25, 10000 Zagreb, Croatia*
[4] *Autolus Therapeutics plc, Forest House, 58 Wood Lane, White City, London, W12 7RZ*
[5] *Universidade do Algarve, Campus de Gambelas, Building 8, DCBB, 8005-139 Faro, Portugal (retired)*
*Corresponding author: silvija.cerni@biol.pmf.hr

Summary. Intra-host populations of plant RNA viruses are genetically diverse. Due to frequent reinfections, these populations often include phylogenetically distant variants that may have different biological properties. Random selection of variants, which occurs during host-to-host virus transmission, may affect isolate pathogenicity. Accurate characterization of genetic variants in intra-host virus populations is therefore epidemiologically important. In routine molecular characterization of *Citrus tristeza virus* (CTV) isolates, common practice is to analyze only a few cDNA clones per isolate. In the present study, based on the characterization of CTV populations displaying different levels of genetic diversity, we evaluated if analyzing large numbers of clones increased diversity parameters. A sequential sampling approach, based on analysis of genetic richness. is proposed for determining the minimal sample size required to obtain reliable information on levels of CTV genetic diversity.

Keywords. Cloning, CTV, population structure, sequencing, SSCP.

OPEN ACCESS

Citation: S. Černi, Z. Šatović, J. Ruščić, G. Nolasco, D. Škorić (2020) Determining intra-host genetic diversity of *Citrus tristeza virus*. What is the minimal sample size?. *Phytopathologia Mediterranea* 59(2): 295-302. DOI: 10.14601/Phyto-11276

Accepted: June 4, 2020

Published: August 31, 2020

Data Availability Statement: All relevant data are within the paper and its Supporting Information files.

Competing Interests: The Author(s) declare(s) no conflict of interest.

Editor: Anna Maria D'Onghia, CIHEAM/Mediterranean Agronomic Institute of Bari, Italy.

INTRODUCTION

High error rate of RNA dependent RNA polymerases is the main contributor in generating heterogenic populations of genetically related variants, attributed to all RNA viruses (Ojosnegros *et al.*, 2011; Domingo *et al.*, 2012). While this benefits virus populations, enabling adaptation to variable environmental conditions and different selective regimes (Domingo *et al.*, 1997; Schneider and Roossinck, 2001), the variation complicates study of virus isolate genetic structure and understanding of effects on the symptom expression. All evidence

suggests that mutant spectra can hide components that in isolation would display dissimilar biological properties (Domingo *et al*., 2012). Due to frequent reinfections, some long-living hosts can also accumulate highly heterogenic virus variants, some of which are phylogenetically distant. As a result of repeated genetic bottlenecks occurring during virus host-to-host transmission events (Li and Roossinck, 2004; Ali *et al*., 2006), virus populations are subjected to fitness reduction and biological alterations (Domingo *et al*., 2012). Minor population variants may influence the symptom expression (Domingo *et al*., 2006; Cerni *et al*., 2008), so it is important to have an efficient tool for accurate characterization of virus isolates, both for gaining insights into isolate epidemiology, and for understanding virus pathogenicity.

For isolates of *Citrus tristeza virus* (CTV), the most important virus pathogen of citrus, the relationships between population structure of an isolate and its biological expression remain neither well documented nor understood. This is also the case for many other viruses. Based on coat protein (CP) gene sequences, CTV variants are grouped into seven phylogenetic clusters between which the representatives of at least four clusters clearly differ in pathogenic potential (Nolasco *et al*., 2009; Hančević *et al*., 2013). Several authors have not fully characterized the extent of CTV variants composing individual isolates. Consequently, there are inconsistencies between phylogenetic data and isolate biological characteristics. Much understanding of viral pathogenesis derives from studies of single viral clones, which may not reveal many of the most important aspects of natural infections (Lauring and Andino, 2011). Gao *et al.* (2005) proposed the hypothesis that the level of intra-host virus population diversity can easily be missed. They showed that for obtaining good population structure of *Hepatitis virus C* isolates, it was necessary to analyze up to 40 separated genomic variants (clones). As CTV infects long-living hosts subjected to frequent reinfections, with genetic bottlenecks often occurring during virus transmission by the aphid vectors or grafting (Nolasco *et al*., 2008; Cerni *et al*., 2008), CTV variants belonging to diverse phylogenetic lineages are expected to coexist.

The probability of sampling at least one sequence of genomic variant x is given by the formula $Pr = 1-(1-p)^n$, where p is the frequency of the genetic variant x, and n is the sample size. Thus, the minimal sample size can be calculated as: $n = \log(1-Pr)/\log(1-p)$ (Ott, 1992). Therefore, the sample size of n = 59 should be adequate to detect a genetic variant whose frequency in the population is greater than 5%, with the probability of 95%. Further, if k variants present at frequency p are to be detected with a probability of Pr, the equation becomes: $n = \log(1-Pr^{1/k})/\log(1-p)$, and, similarly, the sample size of n = 72 would be needed to detect two genetic variants with frequencies greater than 5%.

Bulk virus clone analysis is time consuming and expensive, and not always required. Our goal was to investigate to what extent analysis of increased numbers of clones, based on a range of diversity parameters, enhanced information quality on CTV genomic variants within a virus population. We also assessed if an approach based on analyses of genetic richness could determine optimum sample size.

MATERIALS AND METHODS

Citrus tristeza virus *isolates*

All samples used in this study were previously confirmed to be CTV positive, by DAS-ELISA (Loewe). Samples were taken randomly from seven citrus hosts including: the *Citrus unshiu* Mac. Mark. varieties Aoshima, Chahara and Zorica Rana (isolates AO, CH and ZR), *C. sinensis* (L.) Osbeck variety Fukumoto Navel (isolate FN), and three *C. wilsonii* Tanaka plants (isolates CwS1, CwS2, CwS3). Two additional samples were created by pooling tissue of isolates AO, CH and ZR (sample P1) and isolates CwS1, CwS2 and CwS3 (sample P2), to create samples having high genetic diversity. Total RNA was extracted from each sample of infected tissue collected from different plant sections (Cerni *et al*., 2008), using the RNeasy Plant Mini Kit (Qiagen).

Separation and characterization of Citrus tristeza virus *variants*

Coat protein (CP) genes of CTV variants present in the sample populations were amplified by one-step RT-PCR (Cerni *et al*., 2008), using primers corresponding to both ends of the CP gene (Gillings *et al*., 1993). Resulting products (672 bp) were separated by electrophoresis in 1% agarose gel, and visualized in UV-light after ethidium bromide staining. To separate different CTV variants, amplicons were TA-cloned into the pTZ57R/T vector, followed by the transformation of competent *Escherichia coli* INVαF' cells, as described by the manufacturer (Fermentas). Transformed colonies were selected by α-complementation, and the presence of the insert was confirmed by PCR using the same primers and PCR reaction conditions as described above.

Identification of different genomic variants was performed by Single-Strand Conformation Polymorphism (SSCP) analysis (Rubio *et al*., 1996). For each virus iso-

late, the PCR products from 40 transformed colonies were analyzed sequentially in groups of ten, and different patterns were visualized by silver staining (Beidler *et al.*, 1982). PCR products displaying different SSCP patterns were considered different genomic variants (Kong *et al.*, 2000), and these were chosen for sequencing. Plasmids containing different genomic variants of each isolate were purified using a PureLink™ Quick Plasmid Miniprep Kit (Invitrogen), and were sequenced in both directions (Macrogen Inc.) using a pair of M13-pUC universal primers. Different genomic variants and their phylogenetic clustering were determined by using MEGA 5.5 (Tamura *et al.*, 2011), applying the neighbour-joining method and Kimura 2-parameter evolutionary model. The sequences of reference isolates were the same as those described in a previous study (Cerni *et al.*, 2009).

Data analyses

Genetic diversity of CTV isolates was assessed at genomic variant and phylogenetic group levels.

For each isolate the following parameters were calculated: (1) the total numbers (N_{Total}) of genomic variants and phylogenetic groups detected; (2) the equivalent numbers (N_E) of genomic variants/phylogenetic groups; (3) genomic variant/phylogenetic group diversity, as measured by Shannon's information index (H) (Lewontin, 1972); (4) genomic variant/phylogenetic group diversity, expressed as a maximum diversity (H_{Max}) for a given number of genomic variants/phylogenetic groups achieved in the case of equal frequencies of all genomic variants/phylogenetic groups in a sample (isofrequency situation); (5) the proportion of genomic variant/phylogenetic group diversity within and among four sets of ten clones (H_{avg}/H_{Total}); and (6) the statistical significance (Fisher's exact test) for differences in number of clones per genomic variant/phylogenetic group among four sets of ten clones (P). All the parameters are explained below in terms of genomic variants. The same approach was used in the assessment of phylogenetic group diversity.

Equivalent number of genomic variants (N_E) represents the number of equally frequent genomic variants for a given level of diversity, thus allowing comparison of isolates where the numbers and distributions of genomic variants differ greatly. N_E was calculated as:

$$N_E = \frac{1}{\sum_{i=1}^{I} p_i^2}$$

where, p_i is the frequency of the ith genomic variant, and I is the total number of genomic variants of the isolate.

The proportion of genomic variant diversity within and among four sets of ten clones was calculated based on Shannon's information index. This was calculated as:

$$H = -\sum_{i=1}^{I} (p_i \log_2 p_i)$$

where, p_i is the frequency of the ith genomic variant, and I is the total number of genomic variants of the isolate.

Shannon's information index was used to measure the total genomic variant diversity (H_{Total}) of a complete set of 40 clones, as well as the average diversity (H_{Avg}), over four sets of ten clones. The proportions of diversity within (H_{Avg}/H_{Total}) and among sets [(H_{Total}–H_{Avg})/H_{Total}] were calculated.

Fisher's exact test in SAS (SAS Institute Inc., 2004) was used to test for differences in number of clones in each genomic variant among four sets of ten clones. The number of genomic variants detected in a first set of ten clones and the number of additional genomic variants detected in incremental sets of ten clones were determined for each permutation of four sets of clones (n! = 4! = 24 possible orders), and averaged.

An approach for determining the optimum sample size to obtain the maximum information on CTV genomic variants present in an isolate was based on the formula proposed by Hurlbert (1971) for the assessment of species richness. In this method, the expected number of species (species richness) is calculated for the collection to be compared after all collections are scaled down to the same number of individuals, namely that of the smallest collection. This scaling is necessary because large collections would have more species than small ones, even if they were drawn from the same community (Heck *et al.*, 1975). This approach, called rarefaction, has been adopted (Hughes *et al.*, 2001) for estimation and comparison of species richness among sites, treatments, or habitats that have been unequally sampled. The same formula was introduced by Petit *et al.* (2008) for the calculation of haplotype richness, as the measure of the number of haplotypes per population independent of sample size, while the modified version, described by El Mousadik and Petit (1996), estimates allelic richness, i.e. the number of alleles per population comprised of diploid organisms.

In the present case, Hurlbert's formula was used to calculate genomic variant richness (N_r) as:

$$N_r = \sum_{i=1}^{I} \left[1 - \frac{\binom{N - N_i}{n}}{\binom{N}{n}} \right]$$

where, N is the sample size, n is the subsample size, N_i is the count of genomic variant i, and I is the total number of genomic variants.

The approach used in the present study included sequential sampling coupled with calculation of genomic variant richness for increasing numbers of samples. The principle was to estimate the expected number of genomic variants in a subsample of n individuals (n < N), given that N individuals were sampled. As explained above, genomic variant richness is a measure of genomic variant numbers independent of sample size. This allows comparison of this quantity between different sample sizes. In the present case, the genomic variant richness of samples of N = 20, 30 and 40 was equal to the expected number of genomic variants that a sample would have had if the sample size had been n individuals instead of N, n being equal to N - 10. Genomic variant richness (N_r; n = N - 10) was compared to the observed number of genomic variants in a sample of size n, and the difference (ΔI) between these two parameters was calculated. The procedure was repeated for all possible sampling orders, and the differences (ΔI) between genomic variant richness (N_r) and the observed number of genomic variants in a sample of size n were averaged. This approach can be applied for any number of individuals given that n > 1.

RESULTS

Molecular characterization of Citrus tristeza virus isolates

RT-PCR gave strong amplification signals corresponding to 672 bp length products of the CTV coat protein gene in all isolates. After the separation of different genomic variants by TA-cloning, 40 PCR products, representing separated variants of each isolate, were subjected to SSCP analysis in groups of ten. For each isolate, clones displaying different SSCP patterns were sequenced in a number approximately proportional to its frequency in the population. It was verified that the sequenced clones of each isolate displaying the same SSCP pattern had no significant nucleotide differences, validating the assumption that each SSCP pattern corresponded to a single genomic variant as suggested by Kong *et al.* (2000). For each isolate, all clones displaying distinct SSCP patterns had different nucleotide sequences. The phylogenetic analysis (results not presented) of the obtained sequences showed that all analyzed variants of isolates CH and ZR clustered into one phylogenetic group, while for all the other isolates, a mixture of genomic variants were detected, belonging to different phylogenetic groups (Supplementary Table 1). Variants of isolates AO, CwS2 and in sample P1 clustered into two different phylogenetic groups, and variants of isolates FN, CwS1, CwS3 and in sample P2 clustered into three different phylogenetic groups.

Genomic variant diversity

Total number of genomic variants (N_{Total}) detected across isolates varied from three to ten, but the equivalent number (N_E) was much smaller, exceeding three variants per isolate in case of three out of nine isolates (Table 1). The most frequent genomic variant (f_{Max}) had a frequency greater than 75% in five out of nine isolates; in only two cases (isolates AO and sample P1) the frequency of the most frequent variant did not exceed 50%. Variant diversity (H_{Total}) was generally low; in seven out of nine isolates H_{Total} was less than 75% of the H_{Max}, and frequencies of the variants were far from being equal. Generally, the greatest diversity (H_{avg}/H_{Total}) was attributable to within-sample diversity. Different sets of ten clones were not significantly different ($P > 0.05$) in number of clones per variant, except in the case of sample P1.

Table 1. Genomic variant diversity of nine *Citrus tristeza virus* isolates, based on SSCP analyses.

Isolate	N_{Total}	N_E	N_{Range}	f_{Max}	H_{Total}	$\%H_{Max}$	H_{Avg}/H_{Total}	P
AO	4	3.00	3-4	42.5	1.679	83.94	0.951	0.971
CH	3	1.29	1-3	87.5	0.634	39.99	0.833	0.726
CwS1	7	1.74	2-5	75.0	1.442	51.36	0.749	0.500
CwS2	5	1.30	2-3	87.5	0.784	33.76	0.743	1.000
CwS3	6	1.73	2-5	75.0	1.342	51.91	0.842	0.958
FN	5	2.40	2-4	57.5	1.570	67.60	0.824	0.269
ZR	4	1.17	1-2	92.5	0.503	25.16	0.699	1.000
P1	7	3.60	3-5	40.0	2.156	76.81	0.652	<0.001
P2	10	3.45	3-7	50.0	2.454	73.88	0.761	0.196

N_{Total}, Total number of genomic variants detected.
N_E, Equivalent number of genomic variants.
N_{Range}, Range of genomic variants detected in sets of ten clones.
f_{Max}, Frequency of the most frequent variant.
H_{Total}, Genetic diversity, as measured by Shannon's information index.
$\%H_{Max}$, Genetic diversity expressed as percent of the maximum diversity for a given number of variants achieved in case of equal frequencies of all the variants in an isolate (isofrequency situation).
H_{avg}/H_{Total}, Proportion of genomic variant diversity within four sets of ten clones.
P, Probability (Fisher's exact test) of differences in number of clones per variant among four sets of ten clones.

The average number of genomic variants detected in the first set of ten clones ranged from 1.75 (ZR) to 4.75 (P2), as obtained by permutations (Figure 1). Thus, the proportion (%) of variants detected in the first set varied between 43.75% (isolate ZR) to 82.25% (isolate AO). The analysis of an additional set of ten clones (second) yielded on average more than a quarter of the total number of variants in only one case (isolate CwS1), while in both third and fourth sets of ten clones, the number of additional variants detected did not exceed a fifth of the total number of variants.

Analyses of ΔI values in relation to increasing numbers of sampled clones (Figure 2) showed that ten clones would represent the existing CTV diversity of isolates AO, CH, CwS2, CwS3 and ZR, so additional sets did not increase the genetic richness over the number of variants already detected in a first set of ten clones. Additional sets (second, third or fourth) of ten clones yielding higher genetic richness (N_r) over the number of variants (n) detected in the first set of ten clones (i.e. $\Delta I > 0$; Figure 2 indicated in red) were needed in case of four out of nine isolates. In the case of samples of isolates CwS1, FN and sample P1, at least three sets were needed, but for sample P2, the analysis of the fourth set still increased the genetic richness over the number of variants detected in previous three sets, so more sets should be analysed.

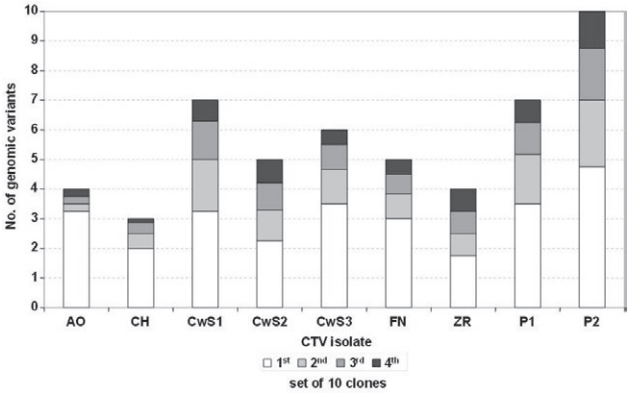

Figure 1. The number of genomic variants detected in a 1st set of 10 clones of nine *Citrus tristeza virus* isolates based on the results of the SSCP analysis and the number of additional variants detected in incremental sets of ten clones averaged over 24 possible sampling orders of four sets.

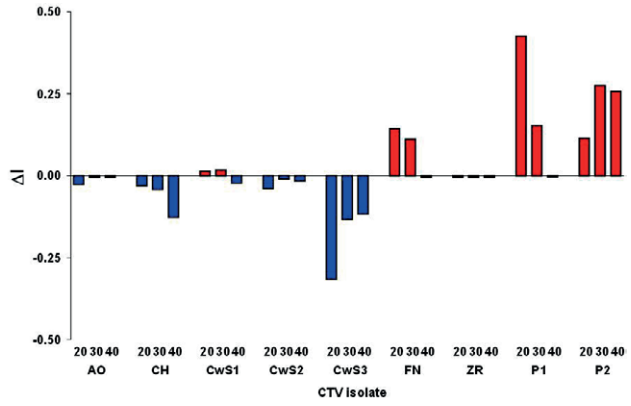

Figure 2. ΔI values of genomic variant richness in relation to increasing number of sampled clones averaged over 24 possible sampling orders of four sets based on the results of the SSCP analysis of nine *Citrus tristeza virus* isolates.

Phylogenetic group diversity

Total numbers of phylogenetic groups (N_{Total}) detected across isolates varied from 1 to 3, but the equivalent numbers (N_E) were below two in all the cases (Table 2). The most frequent (f_{Max}) phylogenetic group had a frequency greater than 75% in five out of seven isolates in

Table 2. Phylogenetic group diversity of nine *Citrus tristeza virus* isolates based on the results of the SSCP analysis and the classification, as proposed by Nolasco *et al.* (2009).

Isolate	N_{Total}	N_E	N_{Range}	f_{Max}	H_{Total}	$\%H_{Max}$	H_{Avg}/H_{Total}	P
AO	2	1.72	2-2	70.0	0.881	88.13	0.980	0.963
CH*	1	-	-	-	-	-	-	-
CwS1	3	1.23	1-2	90.0	0.569	35.90	0.729	0.408
CwS2	2	1.05	1-2	97.5	0.169	16.87	0.695	1.000
CwS3	3	1.36	2-3	85.0	0.748	47.17	0.930	1.000
FN	3	1.83	2-3	67.5	1.037	65.42	0.872	0.266
ZR*	1	-	-	-	-	-	-	-
P1	2	1.34	2-2	85.0	0.610	60.98	0.938	0.684
P2	3	1.59	2-3	77.5	0.976	61.57	0.879	0.456

N_{Total}, Total number of phylogenetic groups detected.
N_E, Equivalent number of phylogenetic groups.
N_{Range}, Range of phylogenetic groups detected in sets of ten clones.
f_{Max}, Frequency of the most frequent phylogenetic group.
H_{Total}, Genetic diversity, as measured by Shannon's information index.
$\%H_{Max}$, Genetic diversity, expressed as percent of the maximum diversity for a given number of phylogenetic groups achieved in the case of equal frequencies of all the groups in an isolate (isofrequency situation).
H_{avg}/H_{Total}, Proportion of phylogenetic group variant diversity within four sets of ten clones.
P, Probability (Fisher's exact test) for differences in number of clones in each phylogenetic group among four sets of ten clones.
* For samples CH and ZR, all the clones belonged to the same phylogenetic group.

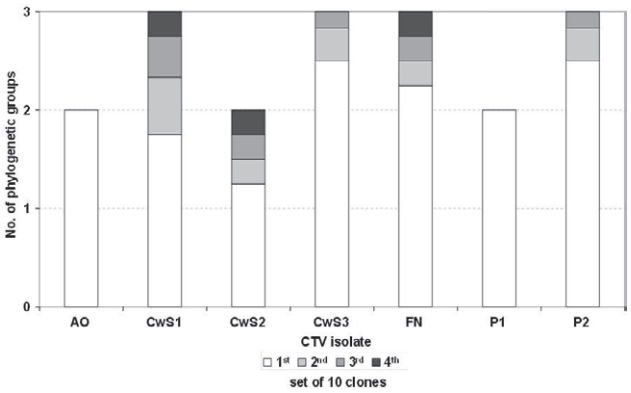

Figure 3. Number of phylogenetic groups detected in a first set of ten clones of seven *Citrus tristeza virus* isolates, based on the classification proposed by Nolasco *et al*. (2009), and number of additional variants detected in incremental sets of ten clones, averaged over 24 possible sampling orders of four sets.

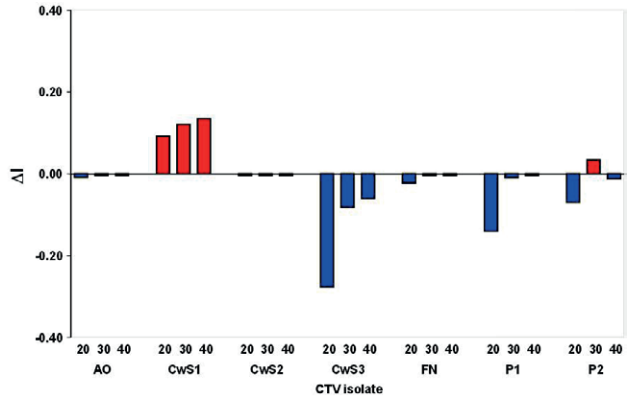

Figure 4. ΔI values of phylogenetic group richness in relation to increasing number of sampled clones averaged over 24 possible sampling orders of four sets based on the results of the classification proposed by Nolasco *et al*. (2009).

which more than one phylogenetic group was detected. Phylogenetic group diversity (H_{Total}) was generally low; in six out of seven isolates this was less than 75% of the H_{Max}; frequencies of the phylogenetic groups were far from being equal. Generally, the isolates tended to be comprised of genomic variants belonging predominantly to the same phylogenetic group. Most of the phylogenetic group diversity was attributable to within-sample diversity. The among-sample component was greater than 0.30 in just one case (isolate CwS2). Different sets of ten clones were not significantly different in number of clones per phylogenetic group.

The average number of phylogenetic groups (Figure 3) detected in the first set of ten clones ranged from 58.33% (isolate CwS1) to 100.00% (isolate AO and sample P1), as obtained by permutations. In the second, third and fourth sets of ten clones, the numbers of additional phylogenetic groups detected did not exceed a fifth of the total number of phylogenetic groups.

Analyses of ΔI values in relation to increasing number of sampled clones (Figure 4) showed that ten clones adequately represented the existing CTV diversity of isolates AO, CwS2, CwS3, and FN, and sample P1. Additional sets did not increase the genetic richness over the number of phylogenetic groups already detected in the first set of ten clones. Additional sets (up to four) of ten clones yielding greater phylogenetic group richness than the number of phylogenetic groups (n) detected in the first set (i.e. $\Delta I > 0$; Figure 4 marked in red), were required for isolate CwS1 and sample P2.

DISCUSSION

Accurate characterization and systemic monitoring of intra-host virus population diversity is important, as demonstrated from increasing numbers of studies (Domingo *et al*., 2012). In epidemiological research, this information is essential for identification of risk factors and surveillance of diseases. In evolutionary studies characterization aids understanding of how evolutionary forces shape virus populations, and in the studies of virus pathogenesis it improves understanding of how genetically different variants contribute to particular viral phenotypes.

Cloning and sequencing are the standard molecular procedures used for the detection and quantification of genetic variants present in virus quasispecies. Although sampling theory gives strict guidelines for numbers of clones that should be analyzed to detect genetic variants having particular population frequencies, extensive clone analyses are often unnecessary. Cloning and sequencing are time consuming and expensive, and genetic diversity of virus isolates may range from very low to high. Therefore, our aim was to develop an approach that could be applied to individual samples, regardless of their diversity levels, and to provide the information of adequate sample size.

In the case of CTV (Nolasco *et al*., 2009) and *Grapevine leafroll associated virus -3* (Gouveia *et al*., 2011), PCR-ELISA based typing tool (APET) has been developed, which allows rapid identification of the phylogenetic groups present in a sample, without the need for cloning. Use of this tool for initial analyses would allow identifying *a priori* how many groups are present, and would provide indication of when to stop cloning and sequencing. Nevertheless, for quantification and identification of variants from the same phylogenetic groups, cloning and sequencing remains the only suitable tool.

There is an increasing number of reports using next-generation sequencing for virus quasispecies characterisation (Barbezange *et al*., 2018, Yu *et al*., 2018). Although promising, next-generation sequencing approaches that enable rapid detection of single-nucleotide polymorphisms within different haplotypes is still challenging for virus quasispecies reconstruction. This requires bioinformatics support, and tools are not always well adapted, especially when sequence divergence is low or rare haplotypes are present (Schirmer *et al*., 2012). Therefore, cloning-based approaches may serve as good alternatives, and also as biological controls in results obtained after next-generation sequencing.

The present study, based on comprehensive characterization of genetic diversity of nine intra-host CTV populations displaying different diversity levels, revealed the following at genomic variant and phylogenetic group levels: (i) the equivalent number of genetic variants was much smaller than the total number of genetic variants detected; (ii) the most frequent genetic variant had frequency greater than 50% in almost all cases; (iii) variant diversity was generally low and frequencies of the variants were far from being equal; (iv) most of the diversity was attributed to within-sample variation; and (v) there were no significant differences between sets of clones. These results are similar to those of Chare and Holmes (2004) and García-Arenal *et al*. (2001), who reported that pairwise nucleotide sequence diversity among plant virus populations is usually low. García-Arenal *et al*. (2001) also reported that the most common composition of plant virus populations was differing numbers of haplotypes, separated only by small genetic distances that exhibit L-shaped rank-abundance curves; that is, one or a few major haplotypes plus many minor haplotypes.

Although the most abundant variants of CTV would most probably be detected in the first set of ten clones, the question still remains of "How many clones should be analyzed to adequately provide new information on population diversity?". The answer is given by an approach based on the calculation of genetic richness. Sequential sampling based on genetic richness gives the optimal sample size, and enables termination of the analysis when sufficient information regarding genetic diversity of the population is reached. Sequential sampling, as proposed, is suitable for genomic variant and phylogenetic group analyses, and consists of the following steps: (i) analyze two sets of ten clones each; (ii) calculate allelic richness (N_r) of a sample of N = 20, equal to the expected number of genetic variants that a sample would have had if the sample size had been ten; (iii) compare the genetic variant richness (N_r) to the average number of genetic variants detected in two sets of ten clones, and calculate the difference (ΔI); (iv) if $\Delta I < 0$, the number of sequenced clones is sufficient to represent the genetic variant diversity of the isolate; and (v) if $\Delta I > 0$, there is need for sequencing an additional set of ten clones, and for the procedure to be repeated.

The proposed approach is advantageous especially in cases when multiple factors influencing the structure of plant virus populations are to be assessed, such as geographic locations, hosts or duration of infections. While in such cases hierarchical sampling and/or randomized complete block studies are required (D'Urso *et al*., 2003; Moury *et al*., 2006), sequential sampling could be useful. This can provide information about the unexplored diversity at each sampling stage, and can aid comparisons of diversity in populations (or strata) with unequal sampling effort.

The experimental system proposed here is readily applicable to other host/virus systems, independently of population diversity, and can be used to track virus variants.

LITERATURE CITED

Ali A., Li H., Schneider W.L., Sherman D.J., Gray S., Roossinck M.J., 2006. Analysis of genetic bottlenecks during horizontal transmission of Cucumber mosaic virus. *Journal of Virology* 80: 8345–8350.

Beidler J.L., Hilliard P.R., Rill R.L., 1982. Ultrasensitive staining of nucleic acids with silver. *Analytical Biochemistry* 126: 374–380.

Barbezange C., Jones L., Blanc H., Isakov O., Celniker G., van der Werf S., 2018. Seasonal Genetic Drift of Human Influenza A Virus Quasispecies Revealed by Deep Sequencing. *Frontiers in Microbiology* 9: 2596.

Cerni S., Ruscic J., Nolasco G., Gatin Z., Krajacic M., Skoric D., 2008. Stem pitting and seedling yellows symptoms of Citrus tristeza virus infection may be determined by minor sequence variants. *Virus Genes* 36: 241–249.

Cerni S., Skoric D., Ruscic J., Krajacic M., Papic T., Nolasco G., 2009. East Adriatic—a reservoir region of severe Citrus tristeza virus strains. *European Journal of Plant Pathology* 124: 701–706.

Chare E.R., Holmes E.C., 2004. Selection pressures in the capsid genes of plant RNA viruses reflect mode of transmission. *The Journal of General Virology* 85: 3149–3157.

D'Urso F., Sambade A., Moya A., Guerri J., Moreno P., 2003. Variation of haplotype distributions of two genomic regions of Citrus tristeza virus populations from eastern Spain. *Molecular Ecology* 12: 517–526.

Domingo E., Menéndez-Arias L., Holland J., 1997. RNA virus fitness. *Reviews in Medical Virology* 7: 87–96.

Domingo E., Martin V., Perales C., Grande-Pérez A., García-Arriaza J., Arias A, 2006. Viruses as quasispecies: biological implications. *Current Topics in Microbiology and Immunology* 299: 51–82.

Domingo E., Sheldon J., Perales C., 2012. Viral quasispecies evolution. *Microbiology and Molecular Biology Reviews: MMBR* 76: 159–216.

El Mousadik A., Petit R.J., 1996. High level of genetic differentiation for allelic richness among populations of the argan tree [*Argania spinosa* (L.) Skeels] endemic to Morocco. *TAG. Theoretical and Applied Genetics* 92: 832–839.

Gao G., Stuver S.O., Okayama A., Tsubouchi H., Mueller N.E., Tabor E., 2005. The minimum number of clones necessary to sequence in order to obtain the maximum information about hepatitis C virus quasispecies: a comparison of subjects with and without liver cancer. *Journal of Viral Hepatitis* 12: 46–50.

García-Arenal F., Fraile A., Malpica J.M., 2001. Variability and genetic structure of plant virus populations. *Annual Review of Phytopathology* 39: 157–186.

Gillings M., Broadbent P., Indsto J., Lee R., 1993. Characterisation of isolates and strains of citrus tristeza closterovirus using restriction analysis of the coat protein gene amplified by the polymerase chain reaction. *Journal of Virological Methods* 44: 305–317.

Gouveia P., Santos M.T., Eiras-Dias J.E., Nolasco G., 2011. Five phylogenetic groups identified in the coat protein gene of grapevine leafroll-associated virus 3 obtained from Portuguese grapevine varieties. *Archives of Virology* 156: 413–420.

Hančević K., Černi S., Nolasco G., Radić T., Djelouah K., Škorić D., 2013. Biological characterization of Citrus tristeza virus monophyletic isolates with respect to p25 gene. *Physiological and Molecular Plant Pathology* 81: 45–53.

Heck K.L., van Belle G., Simberloff D., 1975. Explicit Calculation of the Rarefaction Diversity Measurement and the Determination of Sufficient Sample Size. *Ecology* 56: 1459–1461.

Hughes J.B., Hellmann J.J., Ricketts T.H., Bohannan B.J., 2001. Counting the uncountable: statistical approaches to estimating microbial diversity. *Applied and Environmental Microbiology* 67: 4399–4406.

Hurlbert S.H., 1971. The nonconcept of species diversity: a critique and alternative parameters. *Ecology* 52: 577–586.

Kong P., Rubio L., Polek M., Falk B.W., 2000. Population structure and genetic diversity within California Citrus tristeza virus (CTV) isolates. *Virus Genes* 21: 139–145.

Lauring A.S., Andino R., 2011. Exploring the fitness landscape of an RNA virus by using a universal barcode microarray. *Journal of Virology* 85: 3780–3791.

Lewontin R.C., 1972. The apportionment of human diversity. *Evolutionary Biology* 6: 381–398.

Li H, Roossinck M.J., 2004. Genetic bottlenecks reduce population variation in an experimental RNA virus population. *Journal of Virology* 78: 10582–10587.

Moury B., Desbiez C., Jacquemond M., Lecoq H., 2006. Genetic diversity of plant virus populations: towards hypothesis testing in molecular epidemiology. *Advances in Virus Research* 67: 49–87.

Nolasco G., Fonseca F., Silva G., 2008. Occurrence of genetic bottlenecks during citrus tristeza virus acquisition by Toxoptera citricida under field conditions. *Archives of Virology* 153: 259–271.

Nolasco G., Santos C., Silva G., Fonseca F., 2009. Development of an asymmetric PCR-ELISA typing method for citrus tristeza virus based on the coat protein gene. *Journal of Virological Methods* 155: 97–108.

Ojosnegros S., Perales C., Mas A., Domingo E., 2011. Quasispecies as a matter of fact: viruses and beyond. *Virus Research* 162: 203–215.

Ott J. 1992 Strategies for characterizing highly polymorphic markers in human gene mapping. *American Journal of Human Genetics* 51: 283–290.

Petit R.J., El Mousadik A., Pons O., 2008. Identifying Populations for Conservation on the Basis of Genetic Markers. *Conservation Biology* 12: 844–855.

Rubio L., Ayllonl M.A., Guerri J., Pappu H., Niblett C., Moreno P., 1996. Differentiation of citrus tristeza closterovirus (CTV) isolates by single-strand conformation polymorphism analysis of the coat protein gene. *Annals of Applied Biology* 129: 479–489.

SAS Institute Inc. 2004. SAS/INSIGHT® 9.1 User's Guide, Volumes 1 and 2. Cary, NC

Schirmer M., Sloan W.T., Quince C., 2012. Benchmarking of viral haplotype reconstruction programmes: an overview of the capacities and limitations of currently available programmes. *Briefings in Bioinformatics*.

Schneider W.L., Roossinck M.J., 2001. Genetic diversity in RNA virus quasispecies is controlled by host-virus interactions. *Journal of Virology* 75: 6566–6571.

Tamura K., Peterson D., Peterson N., Stecher G., Nei M., Kumar S., 2011. MEGA5: molecular evolutionary genetics analysis using maximum likelihood, evolutionary distance, and maximum parsimony methods. *Molecular Biology and Evolution* 28: 2731–2739.

Yu F., Wen Y., Wang J., Gong Y., Feng K., Qiu M., 2018. The Transmission and Evolution of HIV-1 Quasispecies within One Couple: a Follow-up Study based on Next-Generation Sequencing. *Scientific Reports* 8: 1404.

Phytopathologia Mediterranea
The international journal of the
Mediterranean Phytopathological Union

Firenze University Press
www.fupress.com/pm

Research Papers

Emerging leafy vegetable crop diseases caused by the *Fusarium incarnatum-equiseti* species complex

Slavica MATIĆ[1,2,*], Giulia TABONE[1], Vladimiro GUARNACCIA[1,2], Maria Lodovica GULLINO[1,2], Angelo GARIBALDI[1]

[1] *AGROINNOVA – Centre of Competence for the Innovation in the Agro-environmental Sector, University of Torino, Largo P. Braccini 2, 10095 Grugliasco (TO), Italy*
[2] *Dept. Agricultural, Forestry and Food Sciences (DISAFA), University of Torino, Largo P. Braccini 2, 10095 Grugliasco (TO), Italy.*
*Corresponding author: slavica.matic@unito.it

Summary. *Fusarium equiseti*, a member of the *Fusarium incarnatum-equiseti* species complex (FIESC), has recently been reported in Italy as the causal agent of a leaf spot diseases on previously unrecorded plant hosts. This emerging disease has affected leafy vegetable hosts including lettuce, lamb's lettuce, wild rocket, cultivated rocket, spinach and radish, and has caused symptoms that have not been previously described on those plants. Fifty-two fungal isolates obtained from symptomatic plants and different plant organs were identified according to their morphology as belonging to the FIESC. The present study aimed to characterize these isolates by identifying their FIESC phylogenetic species, and to evaluate their pathogenicity and host ranges. Six phylogenetically different species of FIESC were identified using MLST analyses of four loci (*tef1*, *cmdA*, *tub2*, and IGS). Most of the isolates were found to belong to *F. compactum* or *F. clavum*, while the other four FIESC species were represented by only a few isolates. All the fungal isolates were capable of inducing leaf spot diseases as single isolates with fulfilling Koch's postulates for these fungi. The intraspecies diversity of the FIESC, the seed-originated isolates of four FIESC identified species, and enhanced range of experimental hosts were observed in the FIESC emerging diseases of these vegetable hosts in Italy. Strict seed inspection procedures, and suitable alteration of environmentally friendly fungicides and biological control agents should achieve efficient management of the FIESC leaf spot diseases on vegetable crops, and prevent further spread of these pathogens to new hosts and new geographical areas.

Keywords. FIESC leaf spot diseases, multi-locus sequence typing, phylogenetic analyses, pathogenicity assays.

OPEN ACCESS

Citation: S. Matić, G. Tabone, V. Guarnaccia, M.L. Gullino, A. Garibaldi (2020) Emerging leafy vegetable crop diseases caused by the *Fusarium incarnatum*-equiseti species complex. *Phytopathologia Mediterranea* 59(2): 303-317. DOI: 10.14601/Phyto-10883

Accepted: June 29, 2020

Published: August 31, 2020

Data Availability Statement: All relevant data are within the paper and its Supporting Information files.

Competing Interests: The Author(s) declare(s) no conflict of interest.

Editor: Juan A. Navas-Cortes, Spanish National Research Council (CSIC), Cordoba, Spain.

INTRODUCTION

Members of the *Fusarium incarnatum-equiseti* species complex (FIESC) are generally associated with diseases of agricultural crops, particularly cereals (Kristensen *et al*., 2005; Castellá and Cabañes, 2014; Villani *et al*., 2016; Maryani *et al*., 2019; Wang *et al*., 2019). Like many *Fusarium* species com-

plexes, the FIESC contains plant pathogens and species that cause human opportunistic infections, generally of immunocompromised individuals (O' Donnell *et al*., 2009; Riddell *et al*., 2010; van Diepeningen *et al*., 2015; Santos *et al*., 2019). Species in the FIESC also have the ability to produce mycotoxins, including type A and type B trichothecenes, fusaric acid, and the estrogenic mycotoxin zearalenone, posing potential risks for human and animal health (Langseth *et al*., 1999; Desjardins, 2006; Goswami *et al*., 2008; Botha *et al*., 2014; Villani *et al*., 2016; Shi *et al*., 2017; Avila *et al*., 2019).

FIESC species have pronounced homoplasious morphological characteristics and cryptic speciation (O'Donnell *et al*., 2009; Avila *et al*., 2019; Wang *et al*., 2019). Multi-locus sequence typing (MLST) based on modern taxonomic concepts is therefore necessary for precise identification of FIESC species. The FIESC has been resolved into two clades, the *Equiseti* clade and the *Incarnatum* clade, containing more than 40 phylogenetically different species, and was separated from the phylogenetically close *F. camptoceras* species complex (FCAMSC) (O'Donnell *et al*., 2009; Short *et al*., 2011; Villani *et al*., 2016, 2019; O'Donnell *et al*., 2018; Avila *et al.,* 2019; Hartman *et al*., 2019; Maryani *et al*., 2019; Santos *et al*., 2019; Wang *et al*., 2019; Xia *et al.,* 2019). Each of these phylogenetic species is assigned an alphanumeric designation, and almost all species have assigned Latin binomial names, with exception of the species FIESC 8, FIESC 22, FIESC 27, FIESC 30, FIESC 31 and FIESC 32 (Xia *et al.,* 2019).

FIESC members are common soil inhabiting fungi which colonize the roots of plants and injured plant tissue. They occur very widely in cool to dry and warm regions (Leslie and Summerell, 2006). FIESC species are sporadic causal agents of plant diseases, including wheat head blight, maize ear and stalk rot, rice bakanae disease, asparagus crown and root rot, and sorghum head blight (Logrieco *et al*., 2003; Amatulli *et al*., 2010; Kelly *et al*., 2017). This complex has also been reported in Italy as an endophyte on chicory and fennel plants (D'Amico *et al*., 2008). The majority of FIESC reports have been based on morphological observations or sequencing of one gene, without precise species identification by means of MLST. Some MLST studies have reported the presence of different FIESC phylogenetic species on cereal grains, although no data have been provided on the symptomatic status of the grains during sampling (O'Donnell *et al*., 2009; Villani *et al*., 2016; Avila et al., 2019). These reports document major presences of *F. clavum* (FIESC 5), *F. flagelliforme* (FIESC 12), *F. equiseti* (FIESC 14a), *F. citri* (FIESC 29), and not yet assigned species (novel FIESC) in cereals from different European countries (Villani *et al*., 2016; 2019), and *F. hainanense* (FIESC 26) and novel FIESC phylogenetic species in cereals from Brazil (Avila *et al*., 2019). *Fusarium sulawesiense* (FIESC 16) and *F. tanahbumbuense* (FIESC 24) are predominant species on rice stubble in China, based on the *tef1* phylogeny (Yang *et al.,* 2018).

Unlike the frequent reports of FIESC in cereals, this species complex has recently been reported as the causal agent of different plant diseases in distinct geographical areas. Leaf spot, caused by FIESC, has been observed in different Italian areas on leafy vegetable hosts, including lettuce, lamb's lettuce, cultivated rocket, wild rocket, spinach and radish, grown in open fields and under intensive cultivation (Garibaldi *et al*., 2011; 2015; 2016a; 2017). Leafy vegetables are highly susceptible to FIESC fungi at high temperatures (25 to 35°C), and the recent increased temperature climate scenario are probably particularly favourable for spread of these pathogens in Italy (Garibaldi *et al*., 2016b; Gullino *et al*., 2017a; 2019). There is also risk of a further spread of these pathogens to new geographical areas and hosts as they are transmitted by seeds (Gilardi *et al*., 2017).

Additional newly described diseases associated with FIESC have also been reported on: onion in Serbia (Ignjatov *et al*., 2015), bell pepper in Trinidad (Ramdial *et al*., 2017), mustard and peanut in India (Prasad *et al*., 2017; Thirumalaisamy *et al*., 2019), *Nopalea cochenillifera* in Brasil (Santiago *et al*., 2018), cotton in Pakistan (Chohan and Abid, 2019), banana in Indonesia (Maryani *et al*., 2019), and various plant hosts in China (Hu *et al*., 2018; Cao *et al*., 2019; Wang *et al*., 2019; Jiang *et al*., 2019). These reports provide evidence that different FIESC species are the causal agents of plant disease.

The objective of the present study was to perform molecular characterization of fungal isolates identified as FIESC species in previous studies, using morphological observation or single gene sequencing. These isolates have been found to be the causal agents of leaf spot diseases on leafy vegetables originating from six plant hosts. The specific objectives were: (i) to identify the FIESC species of 52 fungus isolates associated with leaf spot diseases, and evaluate their genetic diversity by means of MLST analysis, ii) to evaluate their disease severity through pathogenicity assays, and (iii) to identify any possible new hosts by performing cross inoculation tests.

MATERIALS AND METHODS

Fungus isolates

Fifty-two fungus isolates from the Agroinnova collection (Grugliasco, Italy), previously identified as FIESC

on the basis of their morphological characteristics, were used in this study. Four of the isolates were also identified by *tef1* sequencing as *F. equiseti* (Garibaldi *et al*., 2011; 2015; 2016a; 2017). Approximately 95% of the isolates maintained in the Agroinnova collection, originating from leafy vegetable hosts, were analyzed during this study. These isolates were collected from six leafy vegetable hosts (lettuce, lamb's lettuce, spinach, wild rocket, cultivated rocket or radish) (Table 1), from 2011 to 2018, from greenhouses in different locations (Northern and Southern Italy).

DNA extraction from fungi, PCR and sequencing

Total DNA was extracted using the E.Z.N.A.® Fungal DNA Mini Kit (Omega Bio-Tek) according to the manufacturer's protocol. One hundred mg of fresh fungal mycelium grown on PDA plates was used for each isolate. Portions of the following genes were PCR amplified: translation elongation factor 1 α (*tef1*; O'Donnell *et al*., 1998), calmodulin (*cmdA*; Carbone and Kohn, 1999; Groenewald *et al*., 2013), β-tubulin (*tub2*; Glass and Donaldson, 1995), and the intergenic spacer region of the rDNA (IGS; Appel and Gordon, 1995). All the primer sets used for PCR are listed in Supplementary Table 1. The PCR products were purified using a QIAquick PCR purification kit (Qiagen) in accordance with the manufacturer's instructions, and were sequenced in both directions at the BMR Genomics Centre (Padua, Italy). The obtained sequences were deposited in the NCBI GenBank database under the following accession numbers: MK922189-MK922238 for *tef1*, MK937861-MK937912 for *cmdA*, MN078811-MN078862 for *tub2*, and MN078863-MN078914 for IGS (Table 1).

Sequence analyses of isolates

The *tef1* sequences of 52 isolates were aligned with the sequences available at the Fusarium-ID database, and all *tef1* sequences shared high similarity (99-100%) with the FIESC species (Geiser *et al*., 2004). To place the studied isolates within the correct phylogenetic species, phylogenetic analyses were performed on a concatenated dataset of two loci (*tef1* and *cmdA*) including 59 reference sequences of 33 distinct FIESC phylogenetic species (Table 1; O'Donnell *et al*., 2009; 2012; Villani *et al*., 2016; Gebru *et al*., 2019, Maryani *et al*., 2019; Torbati *et al.,* 2019; Wang *et al*., 2019; Xia *et al*., 2019). The additional phylogenetic analyses consisted of the single locus and concatenated sequences (*tef1*, *cmdA*, *tub2* and IGS), which were performed with 52 study isolates and eight FIESC reference strains (*F. clavum* ITEM 11348, *F. flagelliforme* ITEM 11294, *F. equiseti* CS581 and ITEM 11363, *F. irregulare* NRRL 31160, *F. citri* MOD1 FUNGI17 and ITEM 10392, and novel FIESC ITEM 11401). This was to confirm the assignment of the study isolates to the determined phylogenetic species. The eight reference strains were the only strains having the IGS sequence available at NCBI database, beside the *tef1*, *cmdA*, and *tub2* sequences, due to availability of their whole-genome sequence data (Gebru *et al*., 2019; Villani *et al.,* 2019). Few additional reference strains were included in the *tub2* phylogenetic analyses (Table 1). *Fusarium concolor* (NRRL 13459) sequences were used as the outgroup.

Phylogenetic analyses were carried out on the bases of the Maximum Parsimony (MP), Maximum Likelihood (ML) and Bayesian inference (BI). The MP analysis was carried out using Phylogenetic Analysis Using Parsimony (PAUP. v. 4.0b10; Swofford, 2003) for the concatenated dataset of *tef1* and *cmdA*. Phylogenetic relationships were estimated by heuristic searches with 100 random addition sequences. Tree bisection-reconnection was used, with the branch swapping option set on 'best trees' only, with all characters weighted equally and alignment gaps treated as fifth state. Tree length (TL), consistency index (CI), retention index (RI) and rescaled consistence index (RC) were calculated for parsimony, and the bootstrap analyses (Hillis and Bull, 1993) were based on 1000 replications. The BIs for all the analyses were conducted using MrBayes v. 3.2.5 (Ronquist *et al*., 2012) to generate a phylogenetic tree under optimal criteria per partition. The Markov Chain Monte Carlo (MCMC) analysis used four chains and started from a random tree topology. The heating parameter was set to 0.2 and trees were sampled every 1000 generations. The analyses ceased once the average standard deviation of split frequencies was < 0.01. The best evolutionary model for each partition was determined using MrModeltest v. 2.3 (Nylander, 2004), and incorporated into the analysis. The ML analyses were performed with 1000 bootstrap replications, using MEGA software 7 (Kumar *et al*., 2016) for the single locus analyses.

Morphological characterization of isolates

Monoconidium cultures, stored as conidium suspensions in a 30% glycerol solution at -80°C, were used for each isolate. The cultures were then grown on potato dextrose agar plates (PDA, Merck®) amended with streptomycin (Applichem) at 50 mg L^{-1}. Microscope

Table 1. List of *Fusarium* isolates used in the study with their corresponding origin, plant host and isolation source.

No	Isolate	Host	Locality	Country	Tissue	Clade	Species	Species complex	*tef1*	*cmdA*	*tub2*	IGS
1	Feq 12/14	Lettuce	Veneto	Italy	Leaf	*Equiseti*	*F. clavum*	FIESC 5	*KT149290*[a]	MK937861	MN078811	MN078863
2	Zarina	Lettuce	Veneto	Italy	Stem	*Equiseti*	*F. compactum*	FIESC 3	MK922189	MK937862	MN078812	MN078864
3	LBY Feq1	Lettuce	Unknown	Italy	Seed	*Equiseti*	*F. compactum*	FIESC 3	MK922190	MK937863	MN078813	MN078865
4	LBY Feq2	Lettuce	Unknown	Italy	Seed	*Equiseti*	*F. clavum*	FIESC 5	MK922191	MK937864	MN078814	MN078866
5	LBY Feq3	Lettuce	Unknown	Italy	Seed	*Equiseti*	*F. compactum*	FIESC 3	MK922192	MK937865	MN078815	MN078867
6	LBY Feq4	Lettuce	Unknown	Italy	Seed	*Equiseti*	*F. clavum*	FIESC 5	MK922193	MK937866	MN078816	MN078868
7	LBY Feq5	Lettuce	Unknown	Italy	Seed	*Equiseti*	*F. clavum*	FIESC 5	MK922194	MK937867	MN078817	MN078869
8	LBY Feq6	Lettuce	Unknown	Italy	Seed	*Equiseti*	*F. ipomoeae*	FIESC 1	MK922195	MK937868	MN078818	MN078870
9	LBY Feq6R	Lettuce	Unknown	Italy	Seed	*Equiseti*	*F. clavum*	FIESC 5	MK922196	MK937869	MN078819	MN078871
10	LBY Feq7	Lettuce	Unknown	Italy	Seed	*Incarnatum*	*F. citri*	FIESC 29	MK922197	MK937870	MN078820	MN078872
11	LBY Feq7R	Lettuce	Unknown	Italy	Seed	*Incarnatum*	*F. citri*	FIESC 29	MK922198	MK937871	MN078821	MN078873
12	LBY Feq8	Lettuce	Unknown	Italy	Seed	*Equiseti*	*F. compactum*	FIESC 3	MK922199	MK937872	MN078822	MN078874
13	LBY Feq8R	Lettuce	Unknown	Italy	Seed	*Equiseti*	*F. compactum*	FIESC 3	MK922200	MK937873	MN078823	MN078875
14	Feq A	Lamb's lettuce	Veneto	Italy	Leaf	*Equiseti*	*F. clavum*	FIESC 5	MK922201	MK937874	MN078855	MN078876
15	Feq B	Lamb's lettuce	Veneto	Italy	Leaf	*Equiseti*	*F. clavum*	FIESC 5	MK922202	MK937875	MN078824	MN078877
16	Feq C	Lamb's lettuce	Veneto	Italy	Leaf	*Equiseti*	*F. clavum*	FIESC 5	MK922203	MK937876	MN078825	MN078878
17	Feq 7/10	Cultivated rocket	Piedmont	Italy	Leaf	*Equiseti*	*F. compactum*	FIESC 3	MK922204	MK937877	MN078826	MN078879
18	5A, Feq 1/15	Wild rocket	Campania	Italy	Leaf	*Incarnatum*	*F. citri*	FIESC 29	MK922205	MK937878	MN078827	MN078880
19	Feq 1/14	Wild rocket	Campania	Italy	Leaf	*Incarnatum*	*F. citri*	FIESC 29	MK922206	MK937879	MN078828	MN078881
20	Feq 2/14 c1	Wild rocket	Veneto	Italy	Leaf	*Equiseti*	*F. clavum*	FIESC 5	MK922207	MK937880	MN078856	MN078882
21	Feq 2/14 c3	Wild rocket	Veneto	Italy	Leaf	*Equiseti*	*F. lacertarum*	FIESC 4	MK922208	MK937881	MN078857	MN078883
22	Feq 2/14 c6	Wild rocket	Veneto	Italy	Leaf	*Equiseti*	*F. longifundum*	FIESC 11	MK922209	MK937882	MN078858	MN078884
23	Feq 6/14	Wild rocket	Unknown	Italy	Seed	*Equiseti*	*F. compactum*	FIESC 3	MK922210	MK937883	MN078829	MN078885
24	Feq 7/14 M	Wild rocket	Veneto	Italy	Leaf	*Equiseti*	*F. compactum*	FIESC 3	MK922211	MK937884	MN078830	MN078886
25	Feq 8/14 M	Wild rocket	Veneto	Italy	Leaf	*Equiseti*	*F. compactum*	FIESC 3	MK922212	MK937885	MN078831	MN078887
26	Feq 9/14 M	Wild rocket	Veneto	Italy	Leaf	*Equiseti*	*F. compactum*	FIESC 3	MK922213	MK937886	MN078832	MN078888
27	Feq 13/14	Wild rocket	Campania	Italy	Leaf	*Equiseti*	*F. clavum*	FIESC 5	MK922214	MK937887	MN078833	MN078889
28	Feq 16/14 M	Wild rocket	Veneto	Italy	Leaf	*Equiseti*	*F. compactum*	FIESC 3	MK922215	MK937888	MN078834	MN078890
29	Feq 21/14.7	Wild rocket	Veneto	Italy	Leaf	*Equiseti*	*F. compactum*	FIESC 3	MK922216	MK937889	MN078835	MN078891
30	Feq 21/14.8	Wild rocket	Veneto	Italy	Leaf	*Equiseti*	*F. compactum*	FIESC 3	MK922217	MK937890	MN078836	MN078892
31	Feq 21/14.9	Wild rocket	Veneto	Italy	Leaf	*Equiseti*	*F. clavum*	FIESC 5	MK922218	MK937891	MN078837	MN078893
32	Feq 21/14.12	Wild rocket	Veneto	Italy	Leaf	*Equiseti*	*F. clavum*	FIESC 5	MK922219	MK937892	MN078838	MN078894
33	Feq 28/14 M	Wild rocket	Veneto	Italy	Leaf	*Equiseti*	*F. clavum*	FIESC 5	MK922220	MK937893	MN078859	MN078895
34	Feq5	Wild rocket	Unknown	Italy	Seed	*Equiseti*	*F. clavum*	FIESC 5	MK922221	MK937894	MN078839	MN078896
35	Feq 1A	Spinach	Lombardy	Italy	Root	*Equiseti*	*F. clavum*	FIESC 5	MK922222	MK937895	MN078860	MN078897

(Continued)

Table 1. (Continued).

No	Isolate	Host	Locality	Country	Tissue	Clade	Species	Species complex	*tef1*	*cmdA*	*tub2*	IGS
36	Feq 1AR	Spinach	Lombardy	Italy	Root	*Equiseti*	*F. clavum*	FIESC 5	MK922223	MK937896	MN078861	MN078898
37	Feq 2	Spinach	Lombardy	Italy	Leaf	*Equiseti*	*F. clavum*	FIESC 5	MK922224	MK937897	MN078862	MN078899
38	Feq 3	Spinach	Lombardy	Italy	Leaf	*Equiseti*	*F. clavum*	FIESC 5	MK922225	MK937898	MN078840	MN078900
39	Feq 3R	Spinach	Lombardy	Italy	Leaf	*Equiseti*	*F. clavum*	FIESC 5	MK922226	MK937899	MN078841	MN078901
40	Feq 52A	Spinach	Lombardy	Italy	Root	*Equiseti*	*F. clavum*	FIESC 5	MK922227	MK937900	MN078842	MN078902
41	Feq 11/14	Spinach	Piedmont	Italy	Stem	*Equiseti*	*F. compactum*	FIESC 3	MK922228	MK937901	MN078843	MN078903
42	Feq 11/14R	Spinach	Piedmont	Italy	Stem	*Equiseti*	*F. compactum*	FIESC 3	MK922229	MK937902	MN078844	MN078904
43	B63	Spinach	-	Italy	-	*Equiseti*	*F. clavum*	FIESC 5	MK922230	MK937903	MN078845	MN078905
44	SPI	Spinach	-	Italy	Stem	*Equiseti*	*F. compactum*	FIESC 3	MK922231	MK937904	MN078846	MN078906
45	Feq 1/18	Spinach	Piedmont	Italy	Stem	*Equiseti*	*F. clavum*	FIESC 5	MK922232	MK937905	MN078847	MN078907
46	Feq 2/18	Spinach	Piedmont	Italy	Stem	*Equiseti*	*F. compactum*	FIESC 3	MK922233	MK937906	MN078848	MN078908
47	Feq 3/18	Spinach	Piedmont	Italy	Stem	*Equiseti*	*F. compactum*	FIESC 3	MK922234	MK937907	MN078849	MN078909
48	Feq 4/18	Spinach	Piedmont	Italy	Stem	*Equiseti*	*F. compactum*	FIESC 3	MK922235	MK937908	MN078850	MN078910
49	Feq 5/18	Spinach	Piedmont	Italy	Stem	*Equiseti*	*F. compactum*	FIESC 3	MK922236	MK937909	MN078851	MN078911
50	Feq 7/18	Spinach	Piedmont	Italy	Stem	*Equiseti*	*F. clavum*	FIESC 5	MK922237	MK937910	MN078852	MN078912
51	Feq 8/18	Spinach	Piedmont	Italy	Root	*Equiseti*	*F. compactum*	FIESC 3	MK922238	MK937911	MN078853	MN078913
52	IT26	Radish	Piedmont	Italy	Leaf	*Equiseti*	*F. ipomoeae*	FIESC 1	*KY688192*	MK937912	MN078854	MN078914
53	CBS 135762	*Miscanthus giganteus*	-	USA	-	*Equiseti*	*F. ipomoeae*	FIESC 1	MN170478	MN170344	-	-
54	CBS 140909	Tomato	Vladistok	Russia	Fruit	*Equiseti*	*F. ipomoeae*	FIESC 1	MN170479	MN170345	-	-
55	NRRL 43637	Dog	-	PA, USA	-	*Equiseti*	*F. ipomoeae*	FIESC 1	GQ505664	GQ505575	-	-
56	NRRL 36401	Cotton	Maputo	Mozambique	-	*Equiseti*	*F. duofalcatisporum*	FIESC 2	GQ505651	GQ505563	-	-
57	NRRL 36448^{T}	Common bean	Nile Province	Sudan	Seed	*Equiseti*	*F. duofalcatisporum*	FIESC 2	GQ505652	GQ505564	-	-
58	NRRL 36323^{T}	Cotton yarn	-	England	-	*Equiseti*	*F. compactum*	FIESC 3	GQ505648	GQ505560	-	-
59	NRRL 28029	Human	-	CA, USA	Eye	*Equiseti*	*F. compactum*	FIESC 3	GQ505602	GQ505514	-	-
60	NRRL 36318	Unknown	-	Unknown	-	*Equiseti*	*F. compactum*	FIESC 3	GQ505646	GQ505558	-	-
61	NRRL 36123	Unknown	-	Unknown	-	*Equiseti*	*F. lacertarum*	FIESC 4	GQ505643	GQ505555	-	-
62	NRRL 20423^{T}	Lizard	-	India	Skin	*Equiseti*	*F. lacertarum*	FIESC 4	GQ505593	GQ505505	-	-
63	ITEM 10393	Wheat	-	Italy	-	*Equiseti*	*F. clavum*	FIESC 5	LN901566	LN901586	-	-
64	CBS 126202^{T}	Soil	Maltahohe	Namibia	-	*Equiseti*	*F. clavum*	FIESC 5	MN170456	MN170322	-	-
65	CBS 131015	*Phalaris minor*	Aziz abad	Iran	-	*Equiseti*	*F. clavum*	FIESC 5	MN170458	MN170324	-	-
66	CBS 131448	*Secale montanum*	Parsabad	Iran	-	*Equiseti*	*F. clavum*	FIESC 5	MN170459	MN170325	-	-
67	NRRL 34037	Human	-	CO, USA	Abscess	*Equiseti*	*F. clavum*	FIESC 5	GQ505638	GQ505550	-	-
68	NRRL 34032	Human	-	TX, USA	Abscess	*Equiseti*	*F. clavum*	FIESC 5	GQ505635	GQ505547	-	-
69	ITEM 7633	-	-	-	-	*Equiseti*	*F. clavum*	FIESC 5	-	-	LN901628	-

(Continued)

Table 1. (Continued).

No	Isolate	Host	Locality	Country	Tissue	Clade	Species	Species complex	*tef1*	*cmdA*	*tub2*	IGS
70	ITEM 10787	Wheat	-	Spain	-	*Equiseti*	*F. clavum*	FIESC 5	-	-	LN901620	-
71	ITEM 10789	Wheat	-	Spain	-	*Equiseti*	*F. clavum*	FIESC 5	-	-	LN901621	-
72	ITEM 11348	Oat	-	Canada	-	*Equiseti*	*F. clavum*	FIESC 5	QGEC00000000	QGEC00000000	QGEC00000000	QGEC00000000
73	NRRL 43638^{T}	Manatee	-	FL, USA	-	*Equiseti*	*F. brevicaudatum*	FIESC 6	GQ505665	GQ505576	-	-
74	NRRL 32997	Human	-	CO, USA	Toenail	*Equiseti*	*F. arcuatisporum*	FIESC 7	GQ505624	GQ505536	-	-
75	NRRL 5537	Fescue hay	-	MO, USA	-	*Equiseti*	*Fusarium* sp.	FIESC 8	GQ505588	GQ505500	-	-
76	NRRL 36478^{NT}	Pasture soil	-	Australia	-	*Equiseti*	*F. scirpi*	FIESC 9	GQ505654	GQ505566	-	-
77	ITEM 7621	-	-	-	-	*Equiseti*	*F. scirpi*	FIESC 9	-	-	LN901632	-
78	NRRL 26922	Soil	-	France	-	*Equiseti*	*F. neoscirpi*	FIESC 9n	GQ505601	GQ505513	-	-
79	CBS 131777^{T}	*Triticum* sp.	-	Iran	-	*Equiseti*	*F. croceum*	FIESC 10	MN170463	MN170329	-	-
80	CBS 131788	*Triticum* sp.	-	Iran	-	*Equiseti*	*F. croceum*	FIESC 10	MN170464	MN170330	-	-
81	NRRL 36372	Air	Antilles,	Netherlands	-	*Equiseti*	*F. longifundum*	FIESC11n	GQ505649	GQ505561	-	-
82	NRRL 36269	*Pinus nigra*	-	Croatia	Seedling	*Equiseti*	*F. flagelliforme*	FIESC 12	GQ505645	GQ505557	-	-
83	NRRL 36392	Unknown plant	-	Germany	Seedling	*Equiseti*	*F. flagelliforme*	FIESC 12	GQ505650	GQ505562	-	-
84	ITEM 11294	Oat	-	Canada	-	*Equiseti*	*F. flagelliforme*	FIESC 12	LN901571	QHHI00000000	QHHI00000000	QHHI00000000
85	ITEM 11296	Oat	-	Canada	-	*Equiseti*	*F. flagelliforme*	FIESC 12	-	-	LN901622	-
86	NRRL 43635^{T}	Horse	-	NE, USA	-	*Equiseti*	*F. gracilipes*	FIESC 13	GQ505662	GQ505573	-	-
87	NRRL 26419^{T}	Soil	-	Germany	-	*Equiseti*	*F. equiseti*	FIESC 14a	GQ505599	GQ505511	-	-
88	NRRL 36136	Unknown	-	Unknown	-	*Equiseti*	*F. equiseti*	FIESC 14a	GQ505644	GQ505556	-	-
89	ITEM 10675	-	-	-	-	*Equiseti*	*F. equiseti*	FIESC 14a	-	-	LN901623	-
90	ITEM 13585	Maize	-	Netherlands	-	*Equiseti*	*F. equiseti*	FIESC 14a	-	-	LN901624	-
91	ITEM 11363	Oat	-	Canada	-	*Equiseti*	*F. equiseti*	FIESC 14a	LN901574	QGEB00000000	QGEB00000000	QGEB00000000
92	CS581	Wheat		Australia	-	*Equiseti*	*F. equiseti*	FIESC 14a	MTPY00000000	MTPY00000000	MTPY00000000	MTPY00000000
93	NRRL 43636	Dog	-	TX, USA	-	*Equiseti*	*F. toxicum*	FIESC 14b	GQ505663	GQ505574	-	-
94	CBS 219.63	Soil	-	Germany	-	*Equiseti*	*F. toxicum*	FIESC 14b	MN170507	MN170373	-	-
95	CBS 119880	Unknown	-	Unknown	-	FIESC	*F. serpentinum*	Novel	MN170499	MN170365	-	-
96	CBS 150.25	Unknown	-	Unknown	-	FIESC	*F. cateniforme*	Novel	MN170451	MN170317	-	-
97	CBS 123.73	Unknown	-	Unknown	-	FIESC	*F. longicaudatum*	Novel	MN170481	MN170347	-	-
98	NRRL 31160	Human lung	-	TX, USA	-	*Incarnatum*	*F. irregulare*	FIESC 15	GQ505607	GQ505519	QGEA00000000	QGEA00000000
99	ITEM 7547	*Musa sampientum* var. *robusta*	-	Bahamas	-	*Incarnatum*	*F. sulawesiense*	FIESC 16	-	-	LN901629	-
100	NRRL 32522	Human	-	USA, IL	Diabetic cellulitis	*Incarnatum*	*F. luffae*	FIESC 18	GQ505612	GQ505524	-	-
101	NRRL 43639^{T}	Manatee	-	FL, USA	-	*Incarnatum*	*F. multiceps*	FIESC 19	GQ505666	GQ505577	-	-
102	NRRL 34003	Human	-	TX, USA	Sputum	*Incarnatum*	*F. caatingaense*	FIESC 20	GQ505627	GQ505539	-	-

(Continued)

Table 1. (Continued).

No	Isolate	Host	Locality	Country	Tissue	Clade	Species	Species complex	*tef1*	*cmdA*	*tub2*	IGS
103	NRRL 34002	Human	-	TX, USA	Ethmoid sinus	*Incarnatum*	*Fusarium* sp.	FIESC 22	GQ505626	GQ505538	-	-
104	NRRL 32866	Human	-	TX, USA	Cancer patient	*Incarnatum*	*F. incarnatum*	FIESC 23	GQ505615	GQ505527	-	-
105	ITEM 7155	-	-	-	-	*Incarnatum*	*F. incarnatum*	FIESC 23	-	-	LN901630	-
106	ITEM 6748	*Sorghum* sp.	-	Unknown	-	*Incarnatum*	*F. nanum*	FIESC 25	-	-	LN901631	-
107	NRRL 26417	Unknown plant	-	Cuba	Leaf litter	*Incarnatum*	*F. hainanense*	FIESC 26	GQ505598	GQ505510	-	-
108	CBS 635.76	Bermuda grass	-	New Zealand	-	Incarnatum	*F. coffeatum*	FIESC 28	MN120755	MN120696	-	-
109	CBS 621.87	*Medicago sativa*	-	Denmark	-	*Incarnatum*	*F. citri*	FIESC 29	MN170452	MN170318	-	-
110	CBS 678.77	Soil	-	Japan	-	*Incarnatum*	*F. citri*	FIESC 29	MN170453	MN170319	-	-
111	LC6896[T]	*Citrus reticulata*	Hunan	China	Leaf	*Incarnatum*	*F. citri*	FIESC 29	MK289617	MK289668	-	-
112	MOD1 FUNGI17	Peanut	Washington	DC, USA	-	*Incarnatum*	*F. citri*	FIESC 29	RBJE00000000	RBJE00000000	RBJE00000000	RBJE00000000
113	CBS 130905	*Triticum* sp.	-	Iran	-	*Incarnatum*	*F. citri*	FIESC 29	MN170454	MN170320	-	-
114	ITEM 10392	Wheat	-	Italy	-	*Incarnatum*	*F. citri*	FIESC 29	LN901576	LN901592	LN901625	QHHH00000000
115	CBS 143595	Ganoderma sp	Moghan-Ardabil	Iran	-	*Incarnatum*	*F. persicinum*	FIESC 29/30	LT970778	LT970731	-	-
116	CBS 143596	Stereum irsutum	Moghan-Ardabil	Iran	-	*Incarnatum*	*F. persicinum*	FIESC 29/30	LT970779	LT970732	-	-
117	CBS 102394	Cashew	-	El Salvador	-	*Equiseti*	*F. mucidum*	FIESC 30	MN170484	MN170350	-	-
118	CBS 102395[T]	Cashew	-	El Salvador	-	*Equiseti*	*F. mucidum*	FIESC 30	MN170485	MN170351	-	-
119	ITEM 11401	Oat	-	Canada	-	*Equiseti*	*Fusarium* sp.	Novel	LN901578	LN901594	LN901626	QHKN00000000
120	ITEM 13580	Maize	-	Netherlands	-	*Equiseti*	*Fusarium* sp.	Novel	-	-	LN901627	-
121	LC12158	Musa nana	Guangdong	China	Leaf	*Incarnatum*	*F. humuli*	FIESC 33	MK289592	MK289645	-	-
122	CBS 131382[T]	*Oryza australiensis*	-	Australia	-	*Incarnatum*	*F. fasciculatum*	Novel	MN170473	MN170339	-	-
123	NRRL 13459[T]	Plant debris	-	South Africa	-	FCONSC	*F. concolor*	FCONSC	GQ505674	GQ505585	-	-

[a] The accession numbers from reference isolates from the previous studies are indicated in bold (O'Donnell *et al*., 2009; Villani et al. 2016; Gebru et al., 2019; Maryani *et al*., 2019; Torbati *et al*., 2019; Wang *et al*., 2019; Xia *et al*., 2019). [T] = ex-type strain; [NT] = neotype strain. FIESC: *Fusarium incarnatum-equiseti* species complex, FCONSC: *Fusarium concolor* species complex.

observations of conidial shape and size for 52 isolates were carried out as described by Leslie and Summerell (2006).

Pathogenicity assays

Seedlings of five different plant hosts were used for the pathogenicity assays: spinach cv. Crocodile (Rijk Zwaan), lettuce cv. Gentilina (Maraldi sementi), lamb's lettuce cv. Palace (Meilland Richardier), cultivated rocket cv. Rucola coltivata (La Semiorto), and wild rocket cv. Frastagliata Mazzocchi (Casalpusterlengo). Seeds were sown in 2 L capacity plastic pots containing a sterilized mixture of 80% peat and 20% perlite, at nine seeds/pot. The pots were arranged in a randomized block design with three replicates. The resulting seedlings were grown in a greenhouse at 22 to 24°C until inoculation.

Fifty-two isolates of FIESC were grown on PDA supplemented with 50 mg L^{-1} of streptomycin sulfate for 10 d at 22°C and a photoperiod of 12 h. Three-week-old plants were artificially inoculated by spraying the above ground plant organs with spore suspensions of 1×10^5 conidia mL^{-1} (1 mL of suspension per pot). The plants were left for 5 d in a chamber enclosed by transparent polyethylene film, to achieve 100% relative humidity. The plants were then maintained under growth chamber conditions of 25°C (day), 23°C (night), 12 h photoperiod and with twice daily watering. Re-isolations were performed from the leaves of non-inoculated plants and plants inoculated with FIESC isolates, and by observing macro- and micromolecular characteristics of re-isolated fungi from the inoculated plants, completion of Koch's postulates was assessed.

Disease severity (percentage of affected leaf area) was assessed 7 d post-inoculation (dpi) using a 0-5 diagrammatic scale (Garibaldi *et al.*, 2016b), where: 0 = absence of symptoms; 1 = up to 5% leaf area affected; 2 = 6-10%; 3 = 11-25%; 4 = 26-50%; and 5 = 51 -100% leaf area affected. Small, circular and brown leaf spot symptoms were searched for and recorded on 100 leaves per pot. Disease severity (DS) was calculated as DS = Σ(no. of leaves × X_{0-5})/(no. of recorded leaves), using an approximate class midpoint (X_{0-5}): $X_0 = 0$, $X_1 = 5\%$, $X_2 = 10\%$, $X_3 = 25\%$, $X_4 = 50\%$ and $X_5 = 75\%$.

Statistical analyses used in this study were carried out using SPSS software (version 24.0, SPSS Inc.). Differences in disease severity between FIESC isolates were analyzed by a one-way ANOVA followed by the Turkey HSD used for mean separation when ANOVA results were significant ($P < 0.05$).

RESULTS

Molecular identification of pathogen species and phylogenetic analyses

Phylogenetic analyses were carried out, after alignment of the *tef1* sequences of 52 isolates with those available at the Fusarium-ID database resulting in high similarity (99–100%) of all isolates with the FIESC species. A total of 1174 characters (*cmdA*: 1–573, *tef1*: 580–1174) were included in the two locus phylogenetic analyses, 295 characters were parsimony-informative, 195 were variable and parsimony-uninformative, and 678 were constant. A maximum of 1000 equally most parsimonious trees were saved (Tree length = 1169, CI = 0.592, RI = 0.845, and RC = 0.5). Bootstrap support values from the parsimony analyses are plotted on the Bayesian phylogenies in Figure 1.

In the Bayesian analysis, the *cmdA* partition had 168 unique site patterns and the *tef1* partition had 278 unique site patterns. The analysis ran for 3,555,000 generations, resulting in 7112 trees of which 5334 trees were used to calculate the posterior probabilities included in the Figure 1. The consensus tree obtained from the Bayesian analysis agreed with the tree topology obtained from the MP analyses, and Bayesian posterior probability values were mainly in accordance with the ML bootstrap values (Figure 1).

Phylogenetic analyses based on concatenated *tef1* and *cmd*A gene sequences of the study isolates and reference isolates of 33 FIESC phylogenetic species grouped 23 isolates with *F. clavum*, 21 with *F. compactum*, four with *F. citri*, two with *F. ipomoeae*, one with *F. lacertarum*, and one isolate with *F. longifundum* (Figure 1). All the tested isolates, except four of *F. citri* (LBY Feq7 and LBY Feq7R from lettuce, and Feq 1/14 and Feq 5A from wild rocket), grouped in the *Incarnatum* clade, were included in the *Equiseti* clade.

Phylogenetic analyses were then performed for four single-locus sequences. The results of the *tef1*, *cmdA* and IGS analyses were in agreement, and the isolates were grouped into six phylogenetically distinct species. Conversely, the *tub2* phylogenetic tree did not permit clear separation of all the FIESC species (Supplementary Figure 1A), in contrast to the IGS region (Supplementary Figure 1B).

Concatenated phylogenetic analyses for all four loci (*tef1*, *cmdA*, *tub2* and IGS) were carried out, and the results obtained were similar with those of the previous phylogenetic analyses, whereby the study isolates were grouped into six phylogenetically distinct FIESC species. The bootstrap score supporting this analysis was greater, indicating better separation of the phylogenetic species

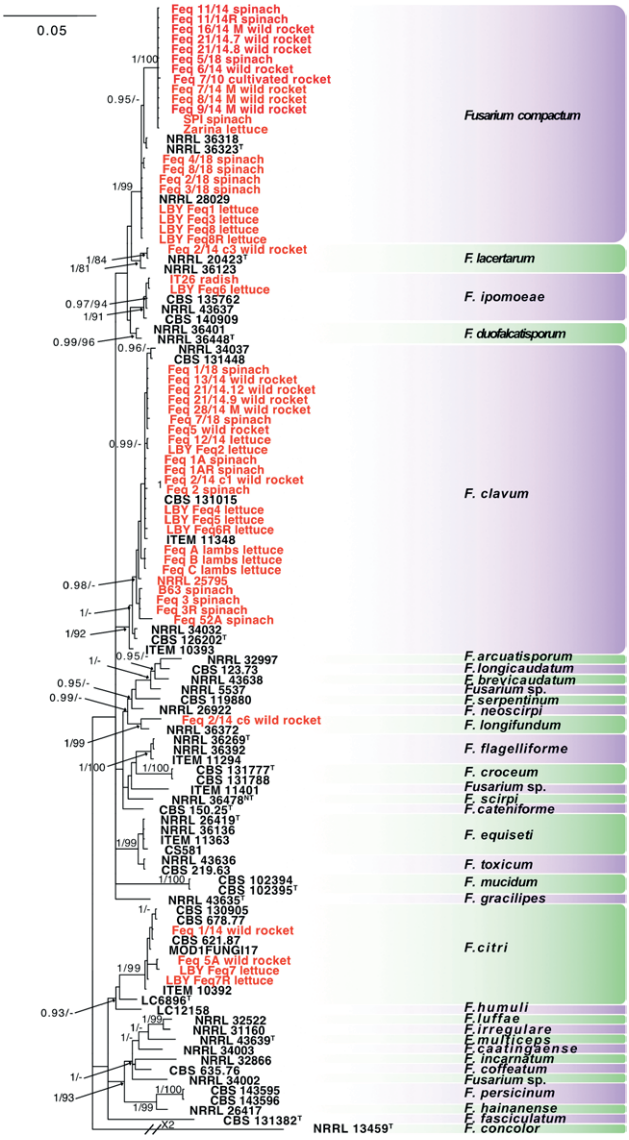

Figure 1. Consensus phylogram of 5334 trees resulting from a Bayesian analysis of the combined *tef1* and *cmdA* sequences from different isolates of the *Fusarium incarnatum-equiseti* species complex (FIESC). The isolate designation, host affiliation and fungal species of the 52 isolates used in this study are shown in red. Bayesian posterior probability (> 0.95) and bootstrap support values (> 70%) are shown at the nodes. The tree was rooted to *Fusarium concolor* (NRRL 13459). Ex-type and neotype strains are indicated with ^{T} and ^{NT}, respectively.

(bootstrap value = 100% for the *Equiseti* clade and 79% for the *Incarnatum* clade; Supplementary Figure 2).

Intraspecies molecular diversity was observed in isolates from this study in which distinct phylogenetic subgroups were demonstrated; two for *F. compactum* (bootstrap values = 99%), three for *F. clavum* (bootstrap values = 99 and 91%) and one for *F. citri* (bootstrap value = 90%) (Supplementary data, Figure 2). No clustering was observed within the study isolates on the basis of plant host. For geographical sampling location, *F. compactum* was identified among isolates from Northern Italy (the Piedmont and Veneto regions), *F. clavum* was found among isolates from Northern and Southern regions, while *F. citri* was represented by only in two isolates from Southern Italy (the Campania region). Additionally, these three species all included seed-originated isolates from unknown locations (Table 1).

When plant host/pathogen range was considered, wild rocket was a natural host for *F. compactum*, *F. clavum*, *F. citri, F. lacertarum* and *F. longifundum*, lettuce a host for *F. compactum*, *F. clavum*, *F. citri* and *F. ipomoeae,* and spinach a host for *F. compactum* and *F. clavum*. The other studied plant hosts were not representative due to limited number of fungal isolates.

Morphological species identification

The size and shape of conidia were similar among all study isolates, and they corresponded to those described for FIESC (Leslie and Summerell, 2006; Wang *et al.*, 2019). The macroconidia measured 25 to 35 × 3 to 5 µm, with 3-5 septa. They were spindle-shaped with slight curvature, and frequent apical tapering, which had almost a needle form in *F. compactum*. No macroconidia were observed in the isolates of the species identified by phylogeny as *F. clavum*. When present, the microconidia were non-septate, and ellipsoidal to ovoid.

Pathogenicity assays

The initial symptoms on inoculate plants consisted of tiny, brown spots on leaves of all five plant species (lettuce, lamb's lettuce, cultivated rocket, wild rocket, and spinach) at 4 dpi. Necrotic spots then enlarged, sometimes surrounded by yellow halos, and the plants progressed to wilt at 14 dpi (Supplementary Figure 3). All tested isolates of six FIESC species (*F. clavum*, *F. compactum*, *F. citri*, *F. ipomoeae*, *F. lacertarum* and *F. longifundum*) reproduced the leaf necrosis symptoms on their corresponding isolation hosts, but they were also capable for infections of experimental hosts causing specific symptoms, with exceptions of *F. compactum* Feq C and *F. clavum* Feq 13/14 isolates on lamb's lettuce (Supplementary Table 2).

One-way ANOVA tests on disease severity data between different FIESC isolates on inoculated plant species showed statistically significant differences between the isolates (Figure 2). FIESC isolates were more

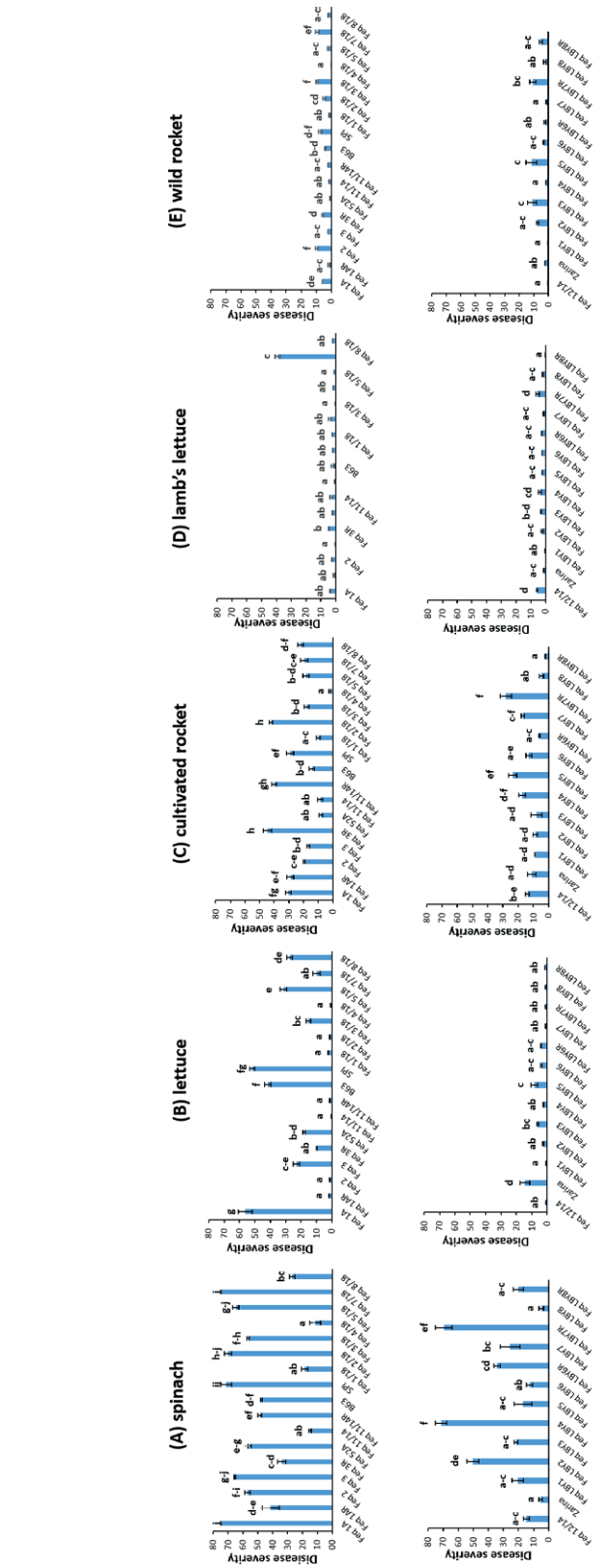

Figure 2. Mean disease severities (and standard deviations: nine replicates) on artificially inoculated leafy vegetable hosts 1 week after inoculation with different isolates of the *Fusarium incarnatum-equiseti* species complex (FIESC). The following FIESC species and their corresponding isolates were used in simple and cross-pathogenicity assays: *F. clavum* (Feq 1A, Feq 1AR, Feq 2, Feq 3, Feq 3R, Feq 52A, B63, Feq 1/18, Feq 7/18) and *F. compactum* (Feq 11/14, Feq 11/14R, SPI, Feq 2/18, Feq 3/18, Feq 4/18, Feq 5/18, Feq 8/18) from spinach; *F. clavum* (Feq 12/14, LBY Feq2, LBY Feq4, LBY Feq5, LBY Feq6R), *F. compactum* (Zarina, LBY Feq1, LBY Feq3, LBY Feq8, LBY Feq8R), *F. ipomoeae* (LBY Feq6) and *F. citri* (LBY Feq7, LBY Feq7R) from lettuce; *F. clavum* (Feq 2/14 c1, Feq 13/14, Feq 21/14.9, Feq 21/14.12, Feq5), *F. compactum* (Feq 6/14 , Feq 7/14 M, Feq 8/14 M, Feq 16/14 M, Feq 21/14.7, Feq 21/14.8), *F. citri* (5A, Feq 1/14), *F. lacertarum* (Feq 2/14 c3) and *F. longifundum* (Feq 2/14 c6) from wild rocket. The plant hosts inoculated with the FIESC isolates were: (A) spinach, (B) lettuce, (C) cultivated rocket, (D) lamb's lettuce and (E) wild rocket. The values present the means and standard deviations of 9 replicates.

harmful to plant vigor on experimental hosts, including lamb's lettuce and cultivated rocket, compared to the original hosts of isolation. Thus, the most aggressive isolates were found on alternative hosts: *F. clavum* Feq3R on cultivated rocket (mean DS = 44.8%), and *F. clavum* Feq 7/18 on lamb's lettuce (mean DS = 37.9%). For spinach and wild rocket, the most aggressive isolates were from the original plant host: *F. clavum* Feq 1A and Feq 7/18 on spinach (mean DS = 75.0%), and *F. compactum* Feq 7/14 M on wild rocket (mean DS = 39.4%) (Figure 2). The most virulent species on most leafy vegetable hosts was *F. clavum*.

In general, the most susceptible vegetable hosts were spinach and cultivated rocket, followed by the lettuce, while lamb's lettuce and wild rocket were not greatly affected. The greatest plant mortality after inoculation was for spinach (> 70%), while only occasional inoculated plants of the other plant hosts died after inoculations (data not shown).

DISCUSSION

Fifty-two fungus isolates originating from diverse geographical locations in Northern and Southern Italy, isolated in different years over an 8 year range, from six different leafy vegetable hosts, and different isolation sources (seeds and other plant tissues) have been characterized in this research as members of FIESC. These fungi have also been shown to be causal agents of leaf spot diseases of leafy vegetables.

The single locus (*tef1, cmdA* or IGS) phylogenetic analyses identified six phylogenetically distinct species. These were *F. clavum*, *F. compactum*, *F. citri*, *F. ipomoeae*, *F. lacertarum* and *F. longifundum*. The most frequently isolated fungi were *F. clavum* and *F. compactum*. This confirmed the *tef1* barcoding marker as the most informative for the separation of FIESC species (O'Donnell *et al*., 2009). The *cmdA* and IGS loci were phylogenetically informative, allowing separation of 52 isolates into six FIESC species. The *btub* gene was the least discriminative locus, probably due to the presence of paralogous or xenologous *btub* sequences (O'Donnell *et al*., 2009). The *tef1* gene cannot provide precise species identification within FIESC in some cases (O' Donnell *et al*., 2009; Villani *et al*., 2016; Torbati *et al.,* 2019), and the use of MLST analyses is recommended, due to its higher resolution capacity and sensitivity. Use of MLST in the present study allowed increased sensitivity in the bootstrap score support between two clades, based on concatenated two-locus (*tef1* and *cmdA*) and four-locus (*tef1*, *cmdA*, *tub2* and IGS) sequences.

The greater resolution of MLST mirrored the results of previous FIESC multi-locus studies based on *cmdA, tef1, tub2* and *rpb2* genes (Villani *et al*., 2016), and on *cmdA, tef1, rpb1* and *rpb2* genes (Wang *et al*., 2019). However, for improved FIESC comparisons, it will be useful to include additional molecular markers, such as *rpb1* and *rpb2*. In this study, robust molecular analyses (the use of MLST and the Fusarium ID database) made it possible to improve the species identification in four isolates, assigning them as *F. compactum* (Feq 7/10 and Feq 9/14 M), *F. ipomoeae* (IT26), and *F. clavum* (Feq 12/14), instead of *F. equiseti*, identified previously by single locus sequencing (Garibaldi *et al*., 2011; 2015; 2016a; 2017).

All the isolates examined in this study were also identified morphologically as FIESC. However, it was not possible to identify precise species based on morphological observations, because of their high cryptic speciation. This has been reported for previous FIESC morphological descriptions (Leslie and Summerell, 2006; O'Donnell *et al*., 2009; Avila *et al*., 2019; Wang *et al*., 2019).

Identification of the presence of FIESC on wild rocket in Italy was based exclusively on the ITS sequencing of one isolate (Garibaldi *et al*., 2015), but the use of MLST in the present study has permitted identification of four FIESC species within 17 wild rocket isolates. These were *F. compactum*, *F. lacertarum*, *F. citri* and *F. longifundum*. Furthermore, this study reports, for the first time, that four FIESC species, *F. ipomoeae*, *F. compactum*, *F. citri* and *F. clavum* were the causal agents of the leaf spot disease of lettuce, whereas *F. ipomoeae* caused this disease on radish. This study is also the first report of *F. clavum* on lamb's lettuce, and of *F. compactum* and *F. clavum* on spinach.

The diversity of FIESC in leafy vegetable hosts was shown in the present study, and six phylogenetically distinct species were differentiated among the 52 isolates. *Fusarium compactum* and *F. clavum* were the most commonly isolated species, with the greatest number of isolates of the different phylogenetic subgroups, comprising different hosts and isolation sources (leaves, stems, roots and seeds). This is consistent with the results of previous FIESC studies (Marín *et al*., 2012; Castellá and Cabañes, 2014; Villani *et al*., 2016; Wang *et al*., 2019; Xia *et al*., 2019; Avila *et al*., 2019) on other plant hosts in different geographical locations. Comparing the FIESC prevalence in this and the study of Villani *et al.* (2016), *F. clavum* and *F. citri* were present in cereals and leafy vegetables, in Italy, while *F. compactum* was found exclusively in vegetable hosts. Furthermore, *Fusarium compactum* was previously identified from plant hosts originating from England (O' Donnell *et al*., 2009). The six FIESC phylogenetic species identified in the present study were

single isolates from individual plants, and all caused leaf spot diseases on test plants as single isolates. Additional research involving greater numbers of fungal isolates, single hosts and fields are necessary to evaluate if mixed infections of FIESC species could also be involved in leaf spot diseases.

The recent emergence of FIESC on leafy vegetable hosts in Italy could be related to changes in pathogenicity of this fungal complex. These fungi may have shifted from endophytic or sporadic and weak plant pathogenic status to principal plant pathogens, as has been reported in other fungi (Sacristán and García-Arenal, 2008; Bamisile *et al*., 2018). Moreover, its natural plant host range has extended, and different phylogenetic species are able to cause similar leaf spot symptoms on individual plant host species. This host expansion is likely to continue, since each identified FIESC species was able to infect leafy vegetable species different of original host of isolation. This has also been recently reported for other necrotrophic fungal pathogens of *Paramyrothecium*, *Albifimbria* and *Alternaria* (Matić *et al*., 2019; 2020).

The emergence of these fungi on new hosts could be associated with environmental changes. Gullino *et al.* (2017a) reported increases in disease incidence and severity caused by *F. equiseti* on wild rocket and radish, as a result of increases in average temperatures and CO_2 concentrations. Furthermore, additional necrotrophic pathogens which cause similar leaf spot diseases, including *Alternaria alternata, Paramyrothecium* spp., *Albifimbria verrucaria, Plectosphaerella cucumerina* and *Allophoma tropica,* have emerged on vegetables in Italy. All of these fungi are favoured by elevated temperature or CO_2 (Gullino *et al*., 2014; 2017b; Siciliano *et al*., 2017, Bosio *et al*., 2017; Matic *et al*., 2019). FIESC emergence was observed on the plants, and in undisturbed soils of the grassland biome. The recent poisoning of animals, caused by feeding with FIESC-infected grass (containing different species of FIESC), and associated with environmental changes, has been reported (Botha *et al*., 2014; Jacobs *et al*., 2018).

Another epidemiological aspect that should be taken into consideration is the ability of FIESC to be transmitted by seeds of wild rocket, onion, bean, and other hosts (Ignjatov *et al*., 2015; Marcenaro and Valkonen, 2016; Gilardi *et al*., 2017; Gullino *et al*., 2019). The globalization of seed markets and inefficient seed health inspections, along with climate changes, may be additional causes of the recent outbreaks of seed-borne fungal pathogens.

Epidemiological facet which may also be of crucial importance is the polyphagousness of FIESC. This low host specificity may have assisted the emergence of FIESC, along with seed transmission and climatic changes. Low host specificity has also allowed different plant- and animal-originating isolates of FIESC to be grouped within the same fungus haplotypes (Ramdial *et al*., 2017).

In summary, the present study has shown that the emerging leaf spot diseases of leafy vegetable hosts in Italy are caused by members of FIESC. The polyphagous nature of this species complex, which affects plant hosts of different monocot and dicot families, is an important disease management consideration. Rigorous seed inspection measures, and suitable choice of eco-sustainable fungicides and biological control agents should also be implemented. These measures, together with crop rotation, the use of resistant cultivars and the alternation of products, may lead to efficient management of FIESC leaf spot diseases on vegetable crops.

ACKNOWLEDGMENTS

The research reported in this paper was funded from the European Union Horizon 2020 research and innovation program under grant agreement numbers: 634179 "Effective Management of Pests and Harmful Alien Species-Integrated Solutions" (EMPHASIS), and 633999 "EU-CHINA Lever for IPM Demonstration" (EUCLID). The authors thank Dr G. Gilardi (Agroinnova, Grugliasco (TO), Italy) for isolating the FIESC strains, and Marguerite Jones for language revision of the manuscript of this paper.

LITERATURE CITED

Amatulli M.T., Spadaro D., Gullino M.L., Garibaldi A., 2010. Molecular identification of *Fusarium* spp. associated with bakanae disease of rice in Italy and assessment of their pathogenicity. *Plant Pathology* 59: 839–844.

Appel D.J., Gordon T.R., 1995. Intraspecific variation within populations of *Fusarium oxysporum* based on RFLP analysis of the intergenic spacer region of the rDNA. *Experimental Mycology* 19: 120–128.

Avila C.F., Moreira G.M., Nicolli C.P., Gomes L.B., Abreu L.M., … Del Ponte E.M., 2019. *Fusarium incarnatum-equiseti* species complex associated with Brazilian rice: Phylogeny, morphology and toxigenic potential. *International Journal of Food Microbiology* 306: 108267.

Bamisile B.S., Dash C.K., Akutse K.S., Keppanan R., Wang L., 2018. Fungal Endophytes: Beyond Herbivore Management. *Frontiers in Microbiology* 9: 544.

Botha C.J., Truter M., Jacobs A., 2014. *Fusarium* species isolated from *Pennisetum clandestinum* collected during outbreaks of kikuyu poisoning in cattle in South Africa. *Onderstepoort Journal of Veterinary Research* 81: e1–e8.

Bosio P., Siciliano I., Gilardi G., Gullino M.L., Garibaldi A., 2017. Verrucarin A and roridin E produced on rocket by *Myrothecium roridum* under different temperatures and CO_2 levels. *World Mycotoxin Journal* 10: 229–236.

Cao P., Li C., Xiang W., Wang X., Zhao J., 2019. First report of *Fusarium incarnatum-equiseti* species complex causing fruit rot on muskmelon (*Cucumis melo*) in China. *Plant Disease* 103: 1768.

Carbone I., Kohn L.M., 1999. A method for designing primer sets for speciation studies in filamentous ascomycetes. *Mycologia* 91: 553–556.

Castellá G., Cabañes F.J. 2014. Phylogenetic diversity of *Fusarium incarnatum-equiseti* species complex isolated from Spanish wheat. *Antonie Van Leeuwenhoek* 106: 309–317.

Chohan S., Abid M., 2019. First report of *Fusarium incarnatum-equiseti* species complex associated with boll rot of cotton in Pakistan. *Plant Disease* 103: 151.

D'Amico M., Frisullo S., Cirulli M., 2008. Endophytic fungi occurring in fennel, lettuce, chicory, and celery d commercial crops in southern Italy. *Mycological Research* 112: 100–107.

Desjardins A.E., 2006. *Fusarium* mycotoxins. Chemistry, genetics, and biology. APS Press, St. Paul, MN, USA.

Garibaldi A., Gilardi G., Bertoldo C., Gullino M.L., 2011. First report of leaf spot of rocket (*Eruca sativa*) caused by *Fusarium equiseti* in Italy. *Plant Disease* 95: 1315.

Garibaldi A., Gilardi, G., Ortu G., Gullino M.L., 2015. First report of leaf spot of wild rocket (*Diplotaxis tenuifolia*) caused by *Fusarium equiseti* in Italy. *Plant Disease* 99: 118.

Garibaldi A., Gilardi G., Ortu G., Gullino M.L., 2016a. First report of leaf spot of lettuce (*Lactuca sativa*) caused by *Fusarium equiseti* in Italy. *Plant Disease* 100: 531.

Garibaldi A., Gilardi G., Berta F., Gullino M.L., 2016b. Temperature and leaf wetness affect the severity of leaf spot on lettuce and wild rocket incited by *Fusarium equiseti*. *Phytoparasitica* 44: 681–687.

Garibaldi A., Gilardi G., Matic S., Gullino M.L., 2017. Occurrence of *Fusarium equiseti* on radish (*Raphanus sativus*) seedlings in Italy. *Plant Disease* 101: 1548.

Gebru S.T., Mammel M.K., Gangiredla J., Tournas V.H., Lampel K.A., Tartera C., 2019. Draft Genome sequences of 12 isolates from 3 *Fusarium* species recovered from moldy peanuts. *Microbiology Resource Announcements* 8: e01642–18.

Geiser D.M., del Mar Jiménez-Gasco M., Kang S., Makalowska I., Veeraraghavan N., …O'Donnell K., 2004. FUSARIUM-ID v. 1.0: A DNA sequence database for identifying *Fusarium*. *European Journal of Plant Pathology* 110: 473–479.

Gilardi G., Pintore I., Gullino M.L., Garibaldi A., 2017. Occurence of *Fusarium equiseti* as a contaminant of *Diplotaxis tenuifolia* seeds. *Journal of Plant Pathology* 99: 245–248.

Glass N.L., Donaldson G., 1995. Development of primer sets designed for use with PCR to amplify conserved genes from filamentous ascomycetes. *Applied and Environmental Microbiology* 61: 1323–1330.

Goswami R.S., Dong Y., Punja Z.K., 2008. Host range and mycotoxin production by *Fusarium equiseti* isolates originating from ginseng fields. *Canadian Journal of Plant Pathology* 30: 155–160.

Groenewald J.Z., Nakashima C., Nishikawa J, Shin H.D., Park, J. H., … Crous P.W., 2013. Species concepts in *Cercospora*: spotting the weeds among the roses. *Studies in Mycology* 75: 115–170.

Gullino M.L., Gilardi G., Garibaldi A., 2014. Seed-borne pathogens of leafy vegetable crops. In: *Global Perspectives on the Health of Seeds and Plant Propagation Material* (M. L. Gullino, G. Munkvold, ed.) Springer, Dordrecht, the Netherlands, 47–53.

Gullino M.L., Gilardi G., Garibaldi A., 2017a. Effect of a climate change scenario on *Fusarium equiseti* leaf spot on wild rocket and radish under phytotron simulation. *Phytoparasitica* 45: 293–298.

Gullino M.L., Gilardi G., Garibaldi A., 2017b. Evaluating severity of leaf spot of lettuce, caused by *Allophoma tropica*, under a climate change scenario. *Phytopathologia Mediterranea* 56: 235–241.

Gullino M.L., Gilardi G., Garibaldi A., 2019. Ready-to-Eat Salad Crops: A Plant Pathogen's Heaven. *Plant Disease* 103: 2153–2170.

Hartman G.L., McCormick S.P., O'Donnell K., 2019. Trichothecene-Producing Fusarium Species Isolated from Soybean Roots in Ethiopia and Ghana and their Pathogenicity on Soybean. *Plant Disease* 103: 2070–2075.

Hillis D.M., Bull J.J., 1993. An empirical test of bootstrapping as a method for assessing confidence in phylogenetic analysis. *Systematic Biology* 42: 182–192.

Hu J., Ren H.Y., Gao T., Yang J.Y., Li J., …Yang G.W., 2018. First report of Fusarium patch on *Festuca arundinacea* caused by *Fusarium incarnatum-equiseti* species complex (FIESC 1) in China. *Plant Disease* 102: 1035.

Ignjatov M., Milošević D., Nikolić Z., Tamindžić G., Gvozdanović-Varga J., … Popović T., 2015. First report of *Fusarium* sp. FIESC 3 on onion seed in Serbia. *Plant Disease* 99: 1277.

Jacobs A., Mojela L., Summerell B., Venter E., 2018. Characterisation of members of the *Fusarium incarnatum-equiseti* species complex from undisturbed soils in South Africa. *Antonie van Leeuwenhoek* 111: 1999–2008.

Jiang S., Jin Y., Jiang X., 2019. First report of *Stachys sieboldii* angular leaf spot caused by *Fusarium incarnatum–equiseti* species complex in Guizhou Province, China. *Journal of Plant Pathology* 101: 1225–1226.

Kelly L.A., Tan Y.P., Ryley M.J., Aitken E.A.B., 2017. *Fusarium* species associated with stalk rot and head blight of grain sorghum in Queensland and New South Wales, Australia. *Plant Pathology* 66: 1413–1423.

Kristensen R., Torp M., Kosiak B., Holst-Jensen A., 2005. Phylogeny and toxigenic potential is correlated in *Fusarium* species as revealed by partial translation elongation factor 1 alpha gene sequences. *Mycological Research* 109: 173–186.

Kumar S., Stecher G., Tamura K., 2016. MEGA7: Molecular Evolutionary Genetics Analysis Version 7.0 for Bigger Datasets. *Molecular Biology and Evolution* 33: 1870–1874.

Langseth W., Bernhoft A., Rundberget T., Kosiak B., Gareis M., 1999. Mycotoxin production and cytotoxicity of *Fusarium* strains isolated from Norwegian cereals. *Mycopathologia* 144: 103–113.

Leslie J.F., Summerell B.A., 2006. The Fusarium Laboratory Manual, 1st edn. Blackwell Publishing, Ames, Iowa.

Logrieco A., Bottalico A., Mulé G., Moretti A., Perrone G., 2003. Epidemiology of toxigenic fungi and their associated mycotoxins for some Mediterranean crops. *European Journal of Plant Pathology* 109: 645–667.

Marcenaro D., Valkonen J.P.T., 2016. Seedborne Pathogenic Fungi in Common Bean (*Phaseolus vulgaris* cv. INTA Rojo) in Nicaragua. *PLoS One* 11: e0168662.

Marín P., Moretti A., Ritieni A., Jurado M., Vázquez C., González-Jaén M.T., 2012. Phylogenetic analyses and toxigenic profiles of *Fusarium equiseti* and *Fusarium acuminatum* isolated from cereals from Southern Europe. *Food Microbiology* 31: 229–237.

Maryani N., Sandoval-Denis M., Lombard L., Crous P.W., Kema G.H.J. 2019. New endemic *Fusarium* species hitch-hiking with pathogenic *Fusarium* strains causing Panama disease in small-holder banana plots in Indonesia. *Persoonia* 43: 48–69.

Matić S., Gilardi G., Gullino M.L., Garibaldi A., 2019. Emergence of leaf spot disease on leafy vegetable and ornamental crops caused by *Paramyrothecium* and *Albifimbria* species. *Phytopathology* 109: 1053–1061.

Matić S., Tabone G., Garibaldi A., Gullino M.L., 2020. *Alternaria* leaf spot caused by *Alternaria* species: an emerging problem on ornamental plants in Italy. *Plant Disease*. DOI: 10.1094/PDIS-02-20-0399-RE.

Nylander J.A.A., 2004. MrModeltest v. 2. Program distributed by the author. Evolutionary Biology Centre, Uppsala University.

O'Donnell K., Kistler H.C., Cigelnik E., Ploetz R.C., 1998. Multiple evolutionary origins of the fungus causing Panama disease of banana: concordant evidence from nuclear and mitochondrial gene genealogies. *Proceedings of the National Academy of Sciences of the United States of America* 95: 2044–2049.

O'Donnell K., Sutton D.A., Rinaldi M.G., Gueidan C., Crous P.W., Geiser D.M., 2009. Novel multilocus sequence typing scheme reveals high genetic diversity of human pathogenic members of the *Fusarium incarnatum-F. equiseti* and *F. chlamydosporum* species complexes within the United States. *Journal of Clinical Microbiology* 47: 3851–3861.

O'Donnell K., Humber R.A., Geiser D.M., Kang S., Park B., … Rehner, S.A., 2012. Phylogenetic diversity of insecticolous fusaria inferred from multilocus DNA sequence data and their molecular identification via FUSARIUM-ID and *Fusarium MLST*. *Mycologia* 104: 427–445.

O'Donnell K., McCormick S.P., Busman M., Proctor R.H., Ward T.J., … Rheeder J.P., 2018. Marasas et al. 1984 "Toxigenic *Fusarium* Species: Identity and Mycotoxicology" revisited. *Mycologia* 110: 1058–1080.

Prasad L., Kamil D., Singh N., Singh O.W., Yadava D.K., Prameela Devi T. 2017. First report of *Fusarium equiseti* causing stem and root rot on *Brassica juncea* in India. *Journal of Plant Pathology* 99: 799–818.

Ramdial H., Latchoo R.K., Hosein F.N., Rampersad S.N., 2017. Phylogeny and haplotype analysis of fungi within the *Fusarium incarnatum-equiseti* species complex. *Phytopathology* 107: 109–120.

Riddell J.IV., Woodside K.J., Leavitt M.A., Newton D.W., Punch J.D., 2010. *Fusarium incarnatum/equiseti* hemodialysis graft infection. *Infectious Disease Reports* 2: e14.

Ronquist F., Teslenko M., van der Mark P., Ayres D.L., Darling A., Höhna S., … Huelsenbeck J.P., 2012. MrBayes 3.2: Efficient Bayesian phylogenetic inference and model choice across a large model space. *Systematic Biology* 61: 539–542.

Santiago M.F., Santos A.M.G., Inácio C.P., Neto A.C.L., Assis T.C., … Laranjeira D., 2018. First report of

Fusarium lacertarum causing cladode rot in *Nopalea cochenellifera* in Brazil. *Journal of Plant Pathology* 100: 611.

Santos A.C.D.S., Trindade J.V.C., Lima C.S., Barbosa R.D.N., da Costa, A.F., … de Oliveira N.T., 2019. Morphology, phylogeny, and sexual stage of *Fusarium caatingaense* and *Fusarium pernambucanum*, new species of the *Fusarium incarnatum-equiseti* species complex associated with insects in Brazil. *Mycologia* 111: 244–259.

Sacristán S., García-Arenal F., 2008. The evolution of virulence and pathogenicity in plant pathogen populations. Molecular Plant Pathology 9: 369–384.

Shi W., Tan Y., Wang S., Gardiner D.M., De Saeger S., Liao Y., … Wu A., 2017. Mycotoxigenic potentials of *Fusarium* species in various culture matrices revealed by mycotoxin profiling. *Toxins* 9: 6.

Short D.P.G., O'Donnell K., Zhang N., Juba J.H., Geiser, D.M., 2011. Widespread occurrence of diverse human pathogenic types of the fungus *Fusarium* detected in plumbing drains. *Journal of Clinical Microbiology* 49: 4264–4272.

Siciliano I., Bosio P., Gilardi G., Gullino M.L., Garibaldi A., 2017. Verrucarin A and roridin E produced on spinach by *Myrothecium verrucaria* under different temperatures and CO_2 levels. *Mycotoxin Research* 33: 139–146.

Swofford D.L., 2003. PAUP*. Phylogenetic analysis using parsimony (*and other methods), v. 4.0b10. Sinauer Associates, Sunderland, Massachusetts.

Torbati M., Arzanlou M., Sandoval-Denis M., Crous P.W., 2019. Multigene phylogeny reveals new fungicolous species in the *Fusarium tricinctum* species complex and novel hosts in the genus *Fusarium* from Iran. *Mycological Progress* 18: 119–133.

Thirumalaisamy P.P., Dutta R., Jadon K.S., Nataraja M.V., Padvi R.D., … Yusufzai S., 2019. Association and characterization of the *Fusarium incarnatum-F. equiseti* species complex with leaf blight and wilt of peanut in India. *Journal of General Plant Pathology* 85: 83–89.

van Diepeningen A.D., Feng P., Ahmed S., Sudhadham M., Bunyaratavej S., de Hoog G.S., 2015. Spectrum of *Fusarium* infections in tropical dermatology evidenced by multilocus sequencing typing diagnostics. *Mycoses* 58: 48–57.

Villani A., Moretti A., De Saeger S., Han Z., Di Mavungu J.D., … Susca A., 2016. A polyphasic approach for characterization of a collection of cereal isolates of the *Fusarium incarnatum-equiseti* species complex. *International Journal of Food Microbiology* 234: 24–35.

Villani A., Proctor R.H., Kim H.S., Brown, D.W., Logrieco, A.F, … Susca A., 2019. Variation in secondary metabolite production potential in the *Fusarium incarnatum-equiseti* species complex revealed by comparative analysis of 13 genomes. *BMC genomics* 20: 314.

Wang M.M., Chen Q., Diao Y.Z., Duan W.J., Cai L., 2019. *Fusarium incarnatum-equiseti* complex from China. *Persoonia* 43: 70–89.

Xia J.W., Sandoval-Denis M., Crous P.W., Zhang X.G., Lombard L., 2019. Numbers to names - restyling the *Fusarium incarnatum-equiseti* species complex. *Persoonia* 43: 186–221.

Yang M., Zhang H., Kong X., van der Lee T., Waalwijk C., … Feng, J., 2018. Host and Cropping System Shape the *Fusarium* Population: 3ADON-Producers Are Ubiquitous in Wheat Whereas NIV-Producers Are More Prevalent in Rice. *Toxins* (Basel): 10: 115.

Phytopathologia Mediterranea
The international journal of the
Mediterranean Phytopathological Union

Firenze University Press
www.fupress.com/pm

Research Papers

Postharvest application of hot water and putrescine treatments reduce brown rot and improve shelf life and quality of apricots

Mehdi HOSSEINIFARAHI[1,*], Seyedeh Marzieh MOUSAVI[2], Mohsen RADI[2], Mohammad Mahdi JOWKAR[3], Gianfranco ROMANAZZI[4,*]

[1] *Department of Horticultural Science, Yasooj Branch, Islamic Azad University, Yasooj, Iran*
[2] *Department of Food Science and Technology, Yasooj Branch, Islamic Azad University, Yasooj, Iran*
[3] *Department of Horticultural Science, Kermanshah Branch, Islamic Azad University, Kermanshah, Iran*
[4] *Department of Agricultural, Food and Environmental Sciences, Marche Polytechnic University, Via Brecce Bianche, 60131 Ancona, Italy*
*Corresponding authors. E-mails: m.h.farahi@iauyasooj.ac.ir (MHF), g.romanazzi@univpm.it (GR)

Summary. Iran is an important apricot production and export country. Postharvest losses of apricots from brown rot (caused by *Monilinia* spp.) are major concerns for producers. Effects were assessed of postharvest hot water, putrescine and acetic acid treatments on apricot quality and shelf life. After treatment applications, fruit were cold stored at 5°C and 80% (±5%) relative humidity for 40 d. During this period, physical and physiological properties of the apricots were evaluated at 10-d intervals. Parameters assessed were fruit weight, decay, firmness, total soluble solids, titratable acidity, and skin colour values (L^*, a^*, b^*). The 55°C hot water and 2.0 mM putrescine treatments gave the least fruit weight loss, brown rot incidence, and firmness loss after 40 of storage. For all treatments, fruit total soluble solids increased during storage, and these were greatest for the control (untreated) apricots. Apricots treated with hot water and putrescine had the greatest titratable acidity. The skin colour of all untreated and treated apricots improved throughout storage (from red to deep yellow). These data support the use of postharvest hot water and putrescine treatments for improved quality of apricots during storage. The scaling up of these treatments to packinghouse situations is important for evaluation of their technical and economic feasibility.

Key words. Decay, fruit firmness, *Monilinia* spp., skin colour.

Citation: M. Hosseinifarahi, S.M. Mousavi, M. Radi, M.M. Jowkar, G. Romanazzi (2020) Postharvest application of hot water and putrescine treatments reduce brown rot and improve shelf life and quality of apricots. *Phytopathologia Mediterranea* 59(2): 319-329. DOI: 10.14601/Phyto-10751

Accepted: August 24, 2020

Published: August 31, 2020

Data Availability Statement: All relevant data are within the paper and its Supporting Information files.

Competing Interests: The Author(s) declare(s) no conflict of interest.

Editor: Lluís Palou, Valencian Institute for Agricultural Research, Valencia, Spain.

INTRODUCTION

Apricot (*Prunus armeniaca* L.) is one of the most important fruits cultivated in Iran since ancient times. Iran is the second largest producer of apricots in the world, after Turkey, with an annual production of more than 400,000 MT (Salehi *et al.*, 2018). Apricots can provide many benefits for

human health and well-being. These are due to the antiseptic, antipyretic, ophthalmic, and emetic properties of apricots (Ghasemnezhad *et al*., 2010). Apricots contain sugars, saccharides, organic acids, mineral nutrients (e.g., Fe, B, K, Ca), vitamins (e.g., B group, C), and polyphenols, and also contain high levels of antioxidant compounds and phytochemicals, such as flavonoids, carotenoids, lycopene, and carotenes (Hajilou *et al*., 2013).

Due to poor postharvest management, including poor handling, packaging, and storage, a lot of fruit and vegetables are wasted every year due to postharvest diseases, which result in greatly increased production costs. Preharvest and postharvest application of synthetic fungicides is an effective strategy for controlling postharvest fruit and vegetable decay, although these applications may have harmful environmental or human health effects. Many studies have focused on replacing synthetic fungicides with natural compounds and biocontrol agents as postharvest treatments (Spadaro and Droby, 2016).

Brown rot is a major stone fruit postharvest disease, and it is especially prevalent in apricot. Brown rot is caused by *Monilinia* spp., and it can result in severe fruit losses and economic damage to producers and consumers (Oliveira Lino *et al*., 2016; Landi *et al*., 2018, 2020; De Miccolis Angelini *et al*., 2019). Apricots are also very sensitive to storage conditions; they are climacteric fruit and undergo accelerated ripening under uncontrolled conditions. Due to these drawbacks, apricots are particularly sensitive to decay and softening during storage, handling and transport, and they cannot be kept at low temperatures for extended periods (Siddiq, 2007). Furthermore, apricots have high rates of postharvest climacteric respiration and high water contents, and are thus highly susceptible to decay, which results in short shelf life (Zokaee-Khosroshahi and Esna-Ashari, 2008). Therefore, slowing ripening rates to delay senescence of apricots is important for increased fruit shelf life.

Compounds such as polyamines can delay fruit ripening and thus improve shelf life and quality characteristics of various climacteric fruit (Valero *et al*., 2002). Polyamines are ubiquitous biogenic amines that are recognized as having important roles in biological processes, including cell growth, division, proliferation, apoptosis/senescence, embryogenesis, organ development, and responses to abiotic and biotic stressors (Mattoo and Handa, 2008). Putrescine, spermidine, and spermine are the main polyamines found in plant tissues (Valero and Serrano, 2010).

Application of polyamines to peaches to delay ripening and aging was reported by Bregoli *et al.* (2002), and Serrano *et al.* (2003) reported beneficial effects of polyamine application to plums. The effects of hot water, ethanol and acetic acid vapour on the physicochemical and sensory properties of peaches have also been investigated (Sharayei and Ganji Moghadam, 2013). Acetic acid vapour helped to maintain the quantitative, qualitative, and sensory characteristics of peaches (Zokaee-Khosroshahi and Esna-Ashari, 2008). Postharvest application of 1 mM putrescine to peaches increased their firmness and resistance to mechanical damage, while decreasing their respiration rates and delaying senescence (Martínez-Romero *et al*., 2000).

On kiwifruit, application of putrescine and spermidine provided improved postharvest quality (Assar *et al*., 2012). On strawberries, postharvest applications of putrescine and UV light increased firmness, vitamin C, anthocyanin, phenolic contents, and antioxidant capacity (Siruieneja *et al*., 2013). On Granny Smith apples, preharvest and postharvest treatments with putrescine and salicylic acid reduced weight loss and increased firmness (Asgarpour *et al*., 2016). Similarly, on broccoli florets, putrescine prevented chlorophyll degradation, promoted maintenance of antioxidant compounds, and delayed senescence (Jafarpour *et al*., 2014).

Hot water treatments after harvest are physical nondestructive methods for the control of postharvest decay in fruit and vegetables (Larrigaudière *et al*., 2002; Usall *et al*., 2016), with no residues left on produce after treatment. Therefore, hot water can be used in packinghouses as a simple way to reduce infections by postharvest fruit pathogens. Hot water treatments have numerous advantages, which include ease of application and short treatment times, with consistent monitoring of the water and fruit temperatures. These treatments can also disinfect fruit skins by removal of surface-borne decay microorganisms (Fallik, 2004). As heat transfer in water is efficient, fruit immersion in hot water is preferred over other heat treatments, with hot water treatment now accepted as a commercial method to maintain postharvest quality of certain fruit commodities (Paull and Jung Chen, 2000). Casals *et al.* (2010) reported that on nectarines and peaches, hot water treatment at 60°C for 40 s controlled brown rot. Shorter treatments (20 s) at 60°C also reduced brown rot by 80% when these fruit were drenched with water while passing through rotating brushes (Karabulut *et al*., 2002).

Acetic acid has been shown to be a potent natural antimicrobial agent that can also be used for disinfection of fruit surfaces. Radi *et al.* (2010) reported that treatment of apples with warm acetic acid solution controlled postharvest decay mostly caused by *Penicillium expansum*. Sholberg and Gaunce (1995, 1996) reported

that application of acetic acid vapour to stone fruit controlled Rhizopus rot and brown rot, and to application table grapes controlled gray and blue molds.

The aim of the present study was to evaluate the effects of hot water, putrescine, and acetic acid treatments of apricots on postharvest quality and decay development during storage.

MATERIALS AND METHODS

Plant materials

Apricots cv. Shahrodi at their commercially mature stage were picked early in the morning in a local orchard in the suburb of Yasooj City, Iran, and were immediately transferred to the Laboratory of Food Science. Damaged fruit were discarded, and 1,080 fruit that had uniform colour, shape, and size were selected.

Treatments

The selected apricots were randomly divided into ten groups. Treatments consisted of different water temperatures (25, 45, and 55°C), different putrescine concentrations (0.5, 1.5, and 2.0 mM; Sigma Aldrich Chemicals Co.) and different acetic acid concentrations (1, and 2%; Merck). Ten apricots of each replicate were used to evaluate the fruit characteristics at harvest. The fruit treatments were carried out by immersion for 5 min, followed by 30 min drying at room temperature. The apricots were then kept in polyethylene macroperforated fruit packs, at 5°C and 80% (±5%) relative humidity for 40 d. Fruit characteristics were evaluated immediately before storage and at 10-d intervals during the storage period (i.e., after 10, 20, 30, and 40 d of storage).

Fruit weight loss

To determine weight loss, the apricots were individually weighed before storage and at 10-d intervals during storage.

Fruit decay

The proportion of apricots showing decay was determined by counting the number showing decay symptoms during storage. The causal pathogens were identified according to their morphological properties (Abdipour *et al.*, 2019).

Fruit firmness

The firmness of the apricots was measured by the puncturing test before and during storage, using a texture analyzer (CT3; Brookfield Engineering). This used a flat-tipped, cylindrical, 5 mm diam. stainless steel probe, with permeation depth 2 mm and rate 5 mm s^{-1}.

Fruit titratable acidity and pH

The pH of the juice from the apricots was determined using a pH meter (Knick), and titratable acidity (TA, as malic acid) of the juice was determined by titration of 50 mL juice with 0.1 N NaOH to an endpoint of pH 8.1. pH and titration data were recorded before and during storage, with the titrations converted to g kg^{-1} malic acid (Radi *et al.*, 2010).

Fruit total soluble solids

Total soluble solids (TSS) of fruit were determined before and during storage using a refractometer (NAR-3T; Abbe) and are expressed as °Brix.

Fruit colour determinations

Fruit colour parameters were determined before and during storage using a digital colorimeter (CR400; Konika-Minolta) in three points on the surface of each apricot, with mean values determined for each fruit. The parameters measured were: L^* for lightness; a^* for redness; b^* for yellowness; C^* for chroma; and H^* for hue angle. C^*, H^*, and total colour difference (ΔE^*) were calculated, respectively, according to Equations (1), (2) and (3) (Huang *et al.*, 2013).

$$C^* = [a^{*2} + b^{*2}]^{1/2} \quad (1),$$

$$H^* = \arctan[b^*/a^*] \quad (2),$$

$$\Delta E^* = [(L^* - L_o^*)^2 + (a^* - a_o^*)^2 + (b^* - b_o^*)^2]^{1/2} \quad (3),$$

where L_0^*, a_0^*, and b_0^* are the control values for the untreated apricots.

Experimental design and data analyses

A completely randomized experimental design was used, with factorial arrangement that included the nine treatments each with three replications, with each rep-

lication consisting of ten observations (separate fruit). All trials were repeated at least twice. The data generated underwent analysis of variance (ANOVA) using the SPSS 21 statistical software. Significant differences were defined at $P \leq 0.05$, and the means were separated using least significant differences (LSD) tests.

RESULTS AND DISCUSSION

Fruit weight loss

All apricots lost weight throughout the storage period (Figure 1). The smallest weight losses after 40 d of storage were for the fruit treated with 55°C hot water (mean loss = 6.3%) and with 2.0 mM putrescine (7.3%). These hot water and putrescine treatments gave significantly less weight losses ($P < 0.05$) compared with that for the untreated control fruit (mean = 15.5%), and also less ($P < 0.05$) than for 2% acetic acid (10.7%), which still provided less ($P < 0.05$) weight loss than the control. Thus, the greatest weight loss after 40 d of storage was recorded for the control fruit.

Loss of weight of apricots due to water loss (evaporation from the fruit surface) is an important fruit quality factor. Water loss during storage results in apricots with shrivelled and dry appearance, and these symptoms increase with increases in storage duration and temperature.

Serrano *et al.* (2004) reported that for mechanically damaged plums, 45°C hot water treatment for 10 min reduced weight loss through reductions in ripening-related membrane changes. Useful effects of hot water to reduce fruit weight loss have also been reported for melons (Lamikanra and Watson, 2007), blueberries (Fan *et al.*, 2008), pears (Hosseini *et al.*, 2015), and Mexican limes (Obeed and Harhash, 2006). The mechanism by which hot water treatments reduce fruit weight loss may involve the melting of the fruit epicuticular waxes, which cover and seal cracks and lenticels in the fruit surfaces, preventing water vapour losses through these openings (Valero and Serrano, 2010). Hot water treatments may also reduce respiration rate and ethylene evolution, and postpone fruit ripening (Zoran *et al.*, 2001; Fallik, 2004).

Putrescine binds to cell membranes and protects the cuticle wax layers, and probably reduced water evaporation from apricots in the present study. Similar positive effects of putrescine for reducing water loss have been described for other fruit, including plums (Serrano *et al.*, 2003), courgettes (Palma *et al.*, 2015), and pears (Hosseini *et al.*, 2015).

Similar to the findings in the present study, previous reports have shown that acetic acid treatment of fruit, including apples, grapes, tomatoes, and kiwifruit, can also reduce weight loss and postharvest decay (Sholberg and Gaunce, 1995). However, in the present study, acetic acid treatment was not as effective as the other treatments that were applied.

Fruit decay

Decay caused by fungal pathogens are one of the most important factors for economic losses of fresh horticultural crops (Palou *et al.*, 2016). Postharvest brown rot was observed for the apricots in the present study. Incidence of brown rot (as the proportion of apricots affected) increased during the storage period (Figure 2). By day 40 of storage, the greatest protection for the apri-

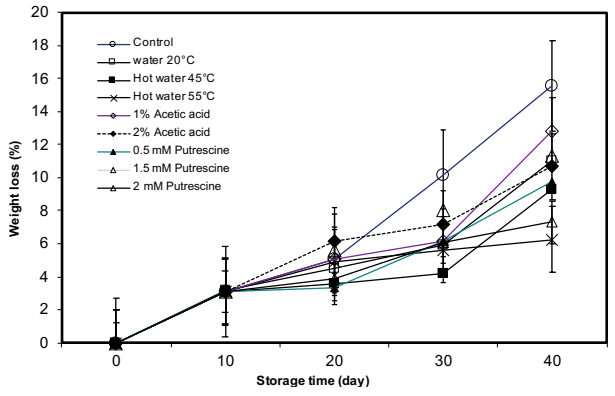

Figure 1. Mean weight loss (± standard deviation; n = 3) of cv. Shahrodi apricots before and during storage for 40 d at 5°C following different treatments.

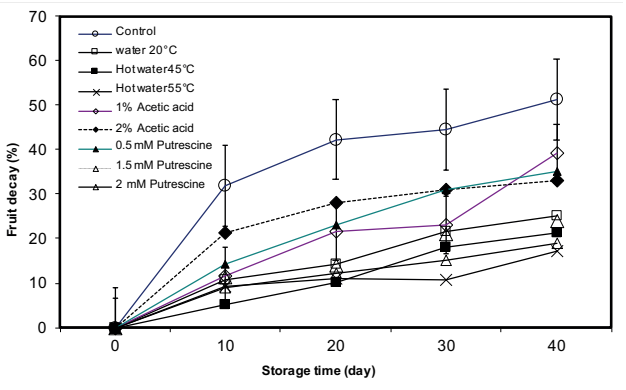

Figure 2. Mean incidence (± standard deviation; n = 3) of decay due to brown rot for cv. Shahrodi apricots before and during storage for 40 d at 5°C following different treatments.

cots against brown rot was obtained from the treatments with 55°C hot water (mean = 19.0% decay) or 2.0 mM putrescine (17.3% decay), which were significantly less ($P < 0.05$) than for the untreated (control) apricots (mean = 51.3% decay). The 2% acetic acid treatment (33.2% decay) was not as effective as hot water or putrescine ($P < 0.05$), although it reduced ($P < 0.05$) decay during storage compared to the untreated fruit. Similar data for acetic acid treatments have been reported for other fruit, including apples, grapes, tomatoes, and kiwifruit (Sholberg and Gaunce, 1995).

Decay is one of the main limiting factors that determines the shelf life of fresh agricultural and horticultural products, with losses reported to be 20 to 50% in developing countries and 5 to 25% in developed countries (Valero and Serrano, 2010). Many studies on postharvest hot water treatments showed that they are commonly used for quality maintenance of fruit crops, including peaches, nectarines (Sisquella *et al.*, 2013; Spadoni *et al.*, 2014), limes (Kaewsuksaeng *et al.*, 2015), and pears (Hosseini *et al.*, 2015).

Some studies have shown that fruit ripening can be delayed by applying hot water treatments, and at the same time fungal decays can be reduced without major changes in fruit quality (Fattahi Moghadam and Ebadi, 2012). According to Kou *et al.* (2007), the use of 45°C hot water for 8 min for table grapes was the most effective treatment. When strawberries were treated with 63°C hot water for 12 s and kept under a controlled atmosphere with 15 kPa CO_2, they showed low amounts of decay (Wszelaki and Mitcham, 2003). Pavoncello *et al.* (2001) reported that on grapefruit, resistance to green mold was achieved with water at 62°C applied for 20 s. Kiwifruit quality after storage was also improved by hot water treatments at 55 and 60°C for 1.5 min, which provided extended fruit shelf life and good preservation (Koukounaras *et al.*, 2008). The impacts of such hot water treatments for prevention of pathogen establishment and spread may be related to the initiation of host defense mechanisms that can be activated in the outer layers of fruit epicarps that can kill pathogens on fruit surfaces (Ben-Yehoshua *et al.*, 2000).

Khosroshahi *et al.* (2007) reported that application of putrescine (1-2 mM) increased the storage life of strawberries compared to untreated control fruit. Mangoes treated with 2.0 mM putrescine retained particularly good quality with a good blend of acidity, TSS, high 'deliciousness' ratings, and low physiological spoilage and weight loss (Jawandha *et al.*, 2012). Postharvest application of polyamines has also been reported to improve the quality and shelf life of fruit, including pomegranates (Mirdehghan *et al.*, 2007), plums (Pérez-Vicente *et al.*, 2002; Serrano *et al.*, 2003; Khan *et al.*, 2008), peaches (Martínez-Romero *et al.*, 2000; Bregoli *et al.*, 2002), mangoes (Malik and Singh, 2005), and apricots (Martínez-Romero *et al.*, 2002).

Fruit firmness

Firmness under all of the apricot treatments decreased during the storage period (Figure 3). At the end of the 40 d of storage, greatest firmness was recorded for the apricots treated with 55°C hot water (mean = 2859 mN) or with 2.0 mM putrescine (2841 mN), while least firmness was for the untreated (control) apricots (mean = 2196 mN; $P < 0.05$). The 2% acetic acid treatment also significantly maintained fruit firmness of the apricots (mean = 2570 mN; $P < 0.05$).

Apricots have short postharvest shelf lives compared to most other fruits, with fruit firmness being an important indicator for increased shelf life, processing, and marketing (Kakkar and Rai, 1993). The maintenance of the flesh firmness is one of the main effects of postharvest polyamine applications for vegetables and fruit. The softness of fruit tissues results from changes in the cell wall structure, including reductions in hemicellulose and pectin de-polymerization, due to the activities of cell wall-hydrolyzing enzymes. Maintenance and improvement of fruit firmness (and thus delayed ripening) using pre- and postharvest putrescine treatments have been reported for fruit, including courgettes (Palma *et al.*, 2015), pears (Hosseini *et al.*, 2015), plums (Serrano *et al.*, 2003; Khan *et al.*, 2008), peaches and nectarines (Bregoli *et al.*, 2002), strawberries (Zokaee Khosroshahi *et al.*, 2007), and apricots (Martínez-Romero *et al.*, 2001).

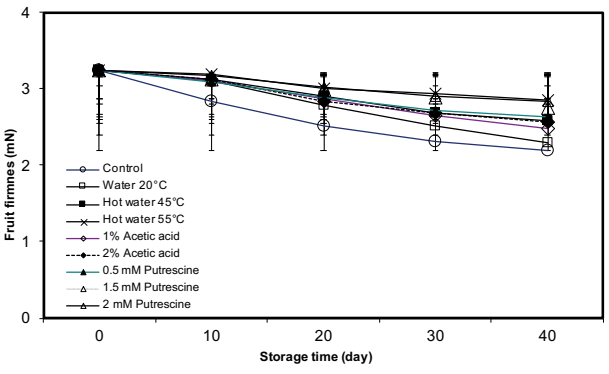

Figure 3. Mean firmness (± standard deviation; n = 3) of cv. Shahrodi apricots before and during storage for 40 d at 5°C following different treatments.

Several mechanisms have been suggested to explain maintenance of fruit firmness after putrescine treatments. One suggested mechanism was decreased activities of the ethylene biosynthetic enzymes 1-aminocyclopropane-1-carboxylate synthase and oxidase, and inhibition of endo- and exo-polygalacturonases, endo-β-1,4-glucanases, and pectin methylesterase related to cell-wall degradation (and thus to fruit softening). An additional mechanism may involve polyamine cross-linking of pectic substances in cell walls, which would help to maintain fruit firmness (Martínez-Romero *et al.*, 2002; Pérez-Vicente *et al.*, 2002). This binding would also prevent the access of degrading enzymes, which decrease softening rates during storage (Valero *et al.*, 2002).

In the present study, the hot water treatments increased apricot firmness throughout the 40 d of storage. Beneficial effects of hot water treatments for maintenance of fruit firmness have been reported for other fruit, including pears (Hosseini *et al.*, 2015), kiwifruit (Beirão-da-Costa *et al.*, 2006), melons (Lamikanra and Watson, 2007), peaches (Koukounaras *et al.*, 2008), and mangoes (Djioua *et al.*, 2009). Heat treatments may protect cell wall integrity, and thus maintain fruit firmness (Valero and Serrano, 2010). Heat treatments can also activate endogenous calcium to form calcium pectate, which delays activities of mainly the polygalacturonase and pectin methylesterase cell wall-degrading enzymes (Serrano *et al.*, 2004; Valero and Serrano, 2010). Direct consequences of heat treatments on the inactivation of these enzymes were suggested by Paull and Jung Chen (2000) and Serrano *et al.* (2004).

Fruit total soluble solids

The changes in the TSS of the apricots during storage are shown in Figure 4. In general, there were gradual increases in the TSS during the storage period. The untreated (control) fruit had the greatest TSS from about day 10 onwards, while all the other treatments gave less TSS. The 55°C hot water and 2.0 mM putrescine treatments resulted in the least TSS (respectively, mean = 6.1% ±0.2% and 5.2% ±0.02%). The general increase in TSS of stored fruit was probably due to increased fruit respiration and weight reduction during the storage period. Several studies have reported improved maintenance of TSS from putrescine treatments, mainly due to the impact that putrescine has on respiration, ethylene production, and delayed ripening (Martínez-Romero *et al.*, 2002; Serrano *et al.*, 2003; Zokaee Khosroshahi *et al.*, 2007).

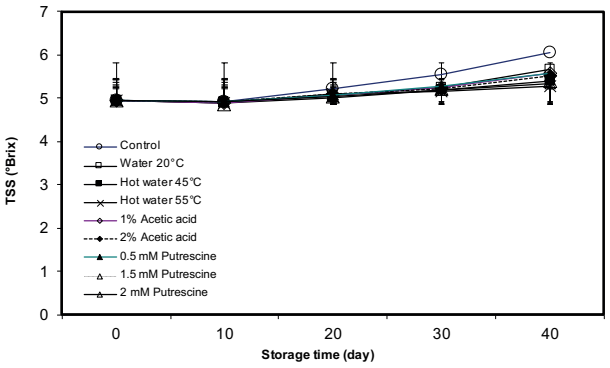

Figure 4. Mean total soluble solids (TSS; ± standard deviation; n = 3) of cv. Shahrodi apricots before and during storage for 40 d at 5°C following different treatments.

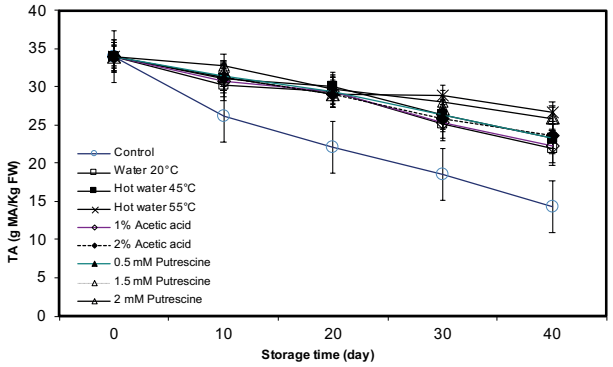

Figure 5. Mean titratable acidity (TA; ± standard deviation; n = 3) of the cv. Shahrodi apricots before and during storage for 40 d at 5°C following different treatments

Fruit titratable acidity

TA decreased during the storage period for all of the apricot treatments (Figure 5). These data showed that after 40 d of storage, the greatest TA was in the apricots treated with 55°C hot water (mean = 26.7 g MA kg^{-1} FW) or with 2.0 mM putrescine (25.8 g MA kg^{-1} FW), which were both greater ($P < 0.05$) than that in the control apricots. The untreated apricots had the lowest TA at the end of the 40 d of storage (mean = 14.3 g MA kg^{-1} FW). TA is directly influenced by the levels of organic acids in fruit (Ghasemnezhad *et al.*, 2010). The decreases in TA during storage may have been due to metabolic changes in the fruit or to the degradation of organic acids during respiration. Similar protection against reductions in TA during storage have been observed on pears treated with hot water and putrescine (Hosseini *et al.*, 2015), strawberries treated with putrescine (Zokaee Khosroshahi *et al.*, 2007), limes treated with hot water (Kaewsuksaeng *et*

al., 2015), and apricots coated with chitosan (Ghasemnezhad *et al*., 2010).

Fruit skin colour changes

The L^* (brightness) of the apricots for all of the treatments generally increased during the first 30 d of storage, and then remained essentially unchanged to 40 d (Table 1). Increased L^* indicated that the fruit changed to brighter colour during most of the storage period. The greatest final L^* (after 40 d storage) was in the untreated (control) apricots and the least L^* was in the fruit subjected to the acetic acid and putrescine treatments.

The a^* (green to red) increased after all of the treatments during the first 10 d of storage (Table 1). This indicated that initially the skin colour showed diminished green tints (change from negative to zero a^*), and then shifted further from pale green to pale red (change from negative to positive a^*). After 40 d storage, the greatest a^* was in the untreated (control) apricots (mean = 5.11) and the least a^* was in the apricots treated with 55°C hot water (mean = 0.18) or with 1.5 mM putrescine (mean = 0.20; $P < 0.05$). These changes in colour from green to red (as in the control samples) are a good indication of apricot fruit ripening.

The b^* (blue to yellow) after all of the fruit treatments continued to increase during the 40 d of storage (Table 1). Increased b^* indicated a deeper yellow colour. The data showed that, as for a^*, the greatest b^* after 40 d storage was in the untreated (control) (mean = 34.13), although the increase was similar ($P > 0.05$) for most of the other treatments. The least b^* after 40 d was in the apricots treated with 45°C hot water (mean = 28.21) or with 0.5 mM and 2.0 mM putrescine (respectively, 28.10 and 28.25), which were less ($P < 0.05$) than on all of the other treatments.

The C^* and H^* after these treatments showed different changes during 40 d of storage. The C^* generally increased by day 40, although this was almost exclusively during the first 10 d, and then remained essentially unchanged. The greatest C^* after 40 d was in the untreated (control) apricots (mean = 7.76) and the least C^* was in the fruit treated with 45°C or 55°C hot water (respectively, 5.45 and 5.44), 2.0 mM putrescine (5.43), or 1% acetic acid (5.41) (Table 2). In contrast, H^* showed little or no initial increase to day 10, and then generally increased to day 40 for these treatments. The least H^* at 40 d was for the untreated (control) apricots (mean = 81.48), which also showed the overall lowest H^* at day 20 of storage (74.75). In the fruit treated with water at different temperatures, the H^* initially declined at day 10, but then generally increased to day 40, as similarly recorded

Table 1. Mean L^*, a^*, and b^* colour parameters of cv. Shahrodi apricots during storage for 40 d at 5°C after application of different treatments.

Treatment		Mean colour parameters after different periods (d) of storage															
		0			10			20			30			40			
		L^*	a^*	b^*	L^*	a^*	b^*	L^*	a^*	b^*	L^*	a^*	b^*	L^*	a^*	b^*
Control	---	34.20 aA	-3.00 aA	12.10 aA	46.42 dB	4.00 aB	17.32 bB	55.44 eE	6.33 dC	23.22 aC	53.23 dD	3.61 bB	33.19 cD	51.11 dC	5.11 bC	34.13 bD
Water	20°C	34.20 aA	-3.00 aA	12.20 aA	46.12 cB	5.10 aD	15.23 aB	50.11 cCD	2.43 bC	23.11 aC	51.23 bD	1.22 aB	25.13 abD	49.12 cC	2.10 aBC	29.11 abE
	45°C	34.20 aA	-3.00 aA	12.10 aA	46.63 eB	4.47 aC	17.22 bB	49.21 bCD	2.11 bB	24.12 abC	50.11 abD	1.39 aB	23.38 aC	48.12 bC	1.20 aB	28.21 aD
	55°C	34.20 aA	-3.00 aA	12.10 aA	45.52 bB	5.23 aD	16.11 abB	46.61 aB	3.44 cC	24.17 abC	49.21 aC	2.44 abC	24.11 abC	48.1 bBC	0.18 aB	29.51 abD
Putrescine	0.5 mM	34.20 aA	-3.00 aA	12.10 aA	46.28 cdB	4.21 aC	17.92 bB	51.45 cdC	1.31 aB	25.11 bC	50.23 abC	1.00 aB	25.70 bC	47.19 abB	1.17 aB	28.10 aD
	1.5 mM	34.20 aA	-3.00 aA	12.10 aA	46.11 cB	5.21 aD	16.89 abB	52.76 dC	3.11 bcC	22.81 aC	53.10 dC	1.10 aB	25.90 bD	46.79 aB	0.20 aB	29.19 abE
	2.0 mM	34.20 aA	-3.00 aA	12.10 aA	46.12 cB	4.41 aC	16.89 abB	52.11 dC	1.29 aB	22.81 aC	52.19 cC	0.31 aB	22.71 aC	47.36 abB	1.41 aB	28.25 aD
Acetic acid	1%	34.20 aA	-3.00 aA	12.10 aA	45.11 aB	4.21 aC	17.34 bB	47.10 aC	2.12 bB	22.31 aC	50.10 abD	1.22 aB	25.99 bD	47.12 abC	1.22 aB	29.11 abE
	2%	34.20 aA	-3.00 aA	12.10 aA	46.62 eB	4.44 aC	17.21 bB	52.66 dC	3.43 cC	22.71 aC	51.11 bC	1.21 aB	23.22 aC	46.27 aB	1.82 aB	29.67 abD

Means accompanied by different lower case letters in each column are significantly different ($P < 0.05$; LSD tests).
Means accompanied by different capital letters in each row within each treatment are significantly different between days of storage ($P < 0.05$; LSD tests).

Table 2. Mean H^*, C^*, and ΔE^* colour parameters of the cv. Shahrodi apricots during storage for 40 d at 5°C after application of different treatments.

Treatment		Mean colour parameters after different periods (d) of storage													
		0			10			20			30			40	
		C^*	H^*	ΔE^*	C^*	H^*	ΔE^*	C^*	H*	ΔE^*	**C***	H^*	ΔE^*	C^*	**H***	ΔE^*
Control	--	4.59 p	76.08 ij	36.40	5.77 ei	77.00 gi	49.71	7.96 a	74.75 ij	60.44	6.80 b	83.79 cf	62.83	7.76 a	81.48 fh	61.67
Water	20 °C	4.59 p	76.08 ij	36.40	6.42 bd	71.49 j	48.84	5.39 in	84.00 cf	55.24	5.16 ko	87.22 ad	57.07	5.79 ei	85.87 af	57.14
	45 °C	4.59 p	76.08 ij	36.40	6.10 ce	75.45 ij	49.91	5.35 in	85.00 af	54.84	5.03 lp	86.60 ae	55.31	5.45 hm	87.56 ac	55.79
	55 °C	4.59 p	76.08 ij	36.40	6.59 bc	72.01 ij	48.57	6.00 df	81.90 eg	52.62	5.48 gl	84.22 cf	54.85	5.44 hn	89.65 a	56.43
Putrescine	0.5 mM	4.59 p	76.08 ij	36.40	5.92 eh	76.35 ij	48.51	5.18 ko	84.57 bf	52.16	5.24 jo	87.31 ac	56.45	5.53 fk	87.60 ac	55.40
	1.5 mM	4.59 p	76.08 ij	36.40	6.08 dg	75.53 ij	49.89	4.77 op	89.82 a	57.35	4.97 mp	87.02 ad	56.15	5.74 ei	86.49 ac	55.00
	2.0 mM	4.59 p	76.08 ij	36.40	5.97 dg	76.78 hi	49.81	5.18 ko	87.01 ab	57.27	5.17 ko	87.77 ac	56.43	5.43 hn	87.62 ac	54.94
Acetic acid	1%	4.59 p	76.08 ij	36.40	6.64 b	72.86 ij	49.38	5.70 ej	82.24 df	57.56	5.21 jo	87.57 ac	59.09	5.41 in	89.61 a	55.15
	2%	4.59 p	76.08 ij	36.40	6.03 de	75.37 ij	49.31	4.95 np	86.76 ae	56.90	4.78 op	89.22 ab	56.92	5.50 gl	87.14 ac	55.16

Means for each treatment accompanied by different letters are significantly different between days of storage ($P < 0.05$; LSD tests).

for the acetic acid treatments. For the putrescine treatments, H^* was initially unchanged (at day 10), before increasing to day 30, with no change to day 40 (Table 2).

The total colour difference (ΔE^*) indicated the magnitude of colour difference between untreated and treated apricots. The untreated (control) fruit had the greatest ΔE^* from day 20 (mean = 60.44) to day 40 (61.67), while the other treatments all gave similar ΔE^* by day 40 (Table 2).

Polyamines have been reported to inhibit chlorophyll degradation and reduce colour changes in cucumber (Jia *et al.*, 2018), table grapes (Champa *et al.*, 2014), strawberries (Zokaee Khosroshahi *et al.*, 2007), and apricots (Martínez-Romero *et al.*, 2002). Similarly (Zheng *et al.*, 2019) reported that treatment with putrescine reduced L^* in broccoli.

The impacts of temperature on apricot injury were studied by Demartino *et al.* (2002). They reported discolouration of bruised cv. San Castrese apricots as loss of yellow pigment. The L^* (lightness) and b^* (yellowness) of bruised apricots were decreased by keeping them at 18°C. In contrast, in the present study, the b^* of apricots increased for all of the treatments during the 40 d storage period (Table 2). Dong *et al.* (2002) investigated the effects of 1-methylcyclopropene on ripening of cv. Canino apricots. They reported that the H^* of these fruit decreased after 30 d of storage. They also reported that during ripening, H^* decreased for both the untreated fruit and those treated with 1-methylcyclopropene, although this treatment slowed the decrease in H^* compared to the control. Similarly, we observed that treatments that improved apricot quality also reduced the H^* decline. Martínez-Romero *et al.* (2002) also reported that with putrescine application, the colour index (a*/b*) of cv. Mauricio apricots increased during storage.

In conclusion, this study has shown that hot water and putrescine treatments, and to a lesser extent those with acetic acid, can maintain the postharvest quality of apricots by reducing the fresh weight loss, brown rot incidence, and fruit softening. Postharvest use of treatments with 55°C hot water or 2.0 mM putrescine for postharvest quality improvements of apricots in cold storage is recommended. Whether these treatments can be scaled up to the fruit packinghouse level is an important issue that requires of the evaluation of the technical and economic feasibility of these treatments.

LITERATURE CITED

Abdipour M., Hosseinifarahi M., Naseri N., 2019. Combination method of UV-B and UV-C prevents post-

harvest decay and improves organoleptic quality of peach fruit. *Scientia Horticulturae* 256: 108564. DOI: 10.1016/j.scienta.2019.108564.

Asgarpour A., Babalar M., Ali M., Sarcheshmeh A., 2016. The effect of preharvest spray of putrescine and salicylic acid solutions on some qualitative properties of 'Granny Smith' apple fruit. *Iranian Journal of Horticultural Science* 47: 445–456.

Assar P., Rahemi M., Taghipour L., 2012. Effect of postharvest treatments of spermidine and putrescine on 'Hayward' kiwifruit quality during storage. *Iranian Journal of Horticultural Science* 43: 331–336.

Beirão-da-Costa S., Steiner A., Correia L., Empis J., Moldão-Martins M., 2006. Effects of maturity stage and mild heat treatments on quality of minimally processed kiwifruit. *Journal of Food Engineering* 76: 616–625. DOI: 10.1016/j.jfoodeng.2005.06.012.

Ben-Yehoshua S., Peretz J., Rodov V., Nafussi B., Yekutieli O., … Regev R., 2000. Postharvest application of hot water treatment in citrus fruits: the road from the labratory to the packing-house. *Acta Horticulturae* 518: 19–28.

Bregoli A.M., Scaramagli S., Costa G., Sabatini E., Ziosi V., … Torrigiani P., 2002. Peach (*Prunus persica*) fruit ripening: aminoethoxyvinylglycine (AVG) and exogenous polyamines affect ethylene emission and flesh firmness. *Physiologia Plantarum* 114: 472–481. DOI: 10.1034/j.1399-3054.2002.1140317.x.

Casals C., Teixidó N., Viñas I., Silvera E., Lamarca N., Usall J., 2010. Combination of hot water, Bacillus subtilis CPA-8 and sodium bicarbonate treatments to control postharvest brown rot on peaches and nectarines. *European Journal of Plant Pathology* 128: 51–63. DOI: 10.1007/s10658-010-9628-7.

Champa H.A.H., Gill M.I.S., Mahajan B.V.C., Arora N.K., 2014. Postharvest treatment of polyamines maintains quality and extends shelf-life of table grapes (*Vitis vinifera* L.) cv. Flame Seedless. *Postharvest Biology and Technology* 91: 57–63. DOI: 10.1016/j.postharvbio.2013.12.014.

De Miccolis Angelini R.M., Romanazzi G., Pollastro S., Rotolo C., Faretra F., Landi L., 2019. New high-quality draft genome of the brown rot fungal pathogen *Monilinia fructicola*. *Genome Biology and Evolution* 11: 2850–2855. DOI: 10.1093/gbe/evz207.

De Martino G., Massantini R., Botondi R., Mencarelli F., 2002. Temperature affects impact injury on apricot fruit. *Postharvest Biology and Technology* 25: 145–149. DOI: 10.1016/S0925-5214(01)00165-X

Djioua T., Charles F., Lopez-Lauri F., Filgueiras H., Coudret A., … Sallanon H., 2009. Improving the storage of minimally processed mangoes (*Mangifera indica* L.) by hot water treatments. *Postharvest Biology and Technology* 52: 221–226. DOI: 10.1016/j.postharvbio.2008.10.006.

Dong L., Lurie S., Zhou H.W., 2002. Effect of 1-methylcyclopropene on ripening of "Canino" apricots and "Royal Zee" plums. *Postharvest Biology and Technology* 24: 135–145. DOI: 10.1016/S0925-5214(01)00130-2.

Fallik E., 2004. Prestorage hot water treatments (immersion, rinsing and brushing). *Postharvest Biology and Technology* 32: 125–134. DOI: 10.1016/j.postharvbio.2003.10.005.

Fan L., Forney C.F., Song J., Doucette C., Jordan M.A., … Walker B.A., 2008. Effect of hot water treatments on quality of highbush blueberries. *Journal of Food Science* 73. DOI: 10.1111/j.1750-3841.2008.00838.x.

Fattahi Moghadam J., Ebadi H., 2012. The effect of hot water treatments on gray mold and physicochemical quality of kiwi fruit during storage. *Journal of Ornamental and Horticultural Plants* 2: 73–82.

Ghasemnezhad M., Shiri M.A., Sanavi M., 2010. Effect of chitosan coatings on some quality indices of apricot (*Prunus armeniaca* L.) during cold storage. *Caspian Journal of Environmental Sciences* 8: 25–33.

Hajilou J., Fakhim Rezaei S., Dehghan G.R., 2013. Comparison of the quality attributes and antioxidant capacity of plum-apricot interspecific hybrid with some plum and apricots cultivars in harvesting time. *Journal of Food Research* 23: 107–119.

Hosseini M.S., Babalar M., Askari M.A., Davarpanah S., 2015. Comparison of putrescine application and heat treatment on storage quality of "Shahmiveh" and "Spadona" pears. *Iranian Journal of Horticultural Science* 45: 234–225.

Huang W., Bi X., Zhang X., Liao X., Hu X., Wu J., 2013. Comparative study of enzymes, phenolics, carotenoids and color of apricot nectars treated by high hydrostatic pressure and high temperature short time. *Innovative Food Science and Emerging Technologies* 18: 74–82. DOI: 10.1016/j.ifset.2013.01.001.

Jafarpour F., Bakhshi D., Ghasemnezhad M., Sajedi R.., 2014. Effect of putrescine on postharvest quality, and phenolic compounds and antioxidant capacity of Broccoli (*Brassica oleracea* L. cv. Italica) florets. *Journal of Horticulture Science* 28: 303–311.

Jawandha S.K., Gill M. S., Singh N., Gill P.P.S., Singh N., 2012. Effect of post-harvest treatments of putrescine on storage of mango cv. Langra. *African Journal of Agricultural Research* 7: 6432–6436. DOI: 10.5897/AJAR12.1425.

Jia B., Zheng Q., Zuo J., Gao L., Wang Q., … Shi J., 2018. Application of postharvest putrescine treatment to maintain the quality and increase the activity of anti-

oxidative enzyme of cucumber. *Scientia Horticulturae* 239: 210–215. DOI: 10.1016/j.scienta.2018.05.043.

Kaewsuksaeng S., Tatmalaa N., Srilaong V., Pongprasert N., 2015. Postharvest heat treatment delays chlorophyll degradation and maintains quality in Thai lime (*Citrus aurantifolia* Swingle cv. Paan) fruit. *Postharvest Biology and Technology* 100: 1–7. DOI: 10.1016/j.postharvbio.2014.09.020.

Kakkar R.K., Rai V.K., 1993. Plant polyamines in flowering and fruit ripening. *Phytochemistry* 33: 1281–1288. DOI: 10.1016/0031-9422(93)85076-4.

Karabulut O.A., Cohen L., Wiess B., Daus A., Lurie S., Droby S., 2002. Control of brown rot and blue mold of peach and nectarine by short hot water brushing and yeast antagonists. *Postharvest Biology and Technology* 24: 103–111. DOI: 10.1016/S0925-5214(01)00132-6.

Khan A. s, Singh Z., Abbasi N.A., Swinny E.E., 2008. Pre- or post-harvest applications of putrescine and low temperature storage affect fruit ripening and quality of 'Angelino' plum. *Journal of the Science of Food and Agriculture* 88: 1686–1695. DOI: 10.1002/jsfa.

Kou L., Luo Y., Wu D., Liu X., 2007. Effects of mild heat treatment on microbial growth and product quality of packaged fresh-cut table grapes. *Journal of Food Science* 72: 567–573. DOI: 10.1111/j.1750-3841.2007.00503.x.

Koukounaras A., Diamantidis G., Sfakiotakis E., 2008. The effect of heat treatment on quality retention of fresh-cut peach. P*ostharvest Biology and Technology* 48: 30–36. DOI: 10.1016/j.postharvbio.2007.09.011.

Lamikanra O., Watson M.A., 2007. Mild heat and calcium treatment effects on fresh-cut cantaloupe melon during storage. *Food Chemistry* 102: 1383–1388. DOI: 10.1016/j.foodchem.2006.05.060.

Landi L., Angelini R.M.D.M., Pollastro S., Abate D., Faretra F., 2018. Genome sequence of the brown rot fungal pathogen *Monilinia fructigena*. *BMC Research Notes* 11, 758. DOI: 10.1186/s13104-018-3854-z.

Landi L., Pollastro S., Rotolo C., Romanazzi G., Faretra F., de Miccolis Angelini R.M., 2020. Draft genomic resources for the brown rot fungal pathogen *Monilinia laxa*. *Molecular Plant-Microbe Interactions* 33: 145–148. DOI: 10.1094/MPMI-08-19-0225-A.

Larrigaudière C., Pons J., Torres R., Usall J., 2002. Storage performance of clementines treated with hot water, sodium carbonate and sodium bicarbonate dips. *Journal of Horticultural Science and Biotechnology* 77: 314–319. DOI: 10.1080/14620316.2002.11511499.

Malik A.U., Singh Z., 2005. Pre-storage application of polyamines improves shelf-life and fruit quality of mango. *Journal of Horticultural Science and Biotechnology* 80: 363–369. DOI: 10.1080/14620316.2005.11511945.

Martínez-Romero D., Serrano M., Carbonell A., Burgos L., Riquelme F., Valero D., 2002. Effects of postharvest putrescine treatment on extending shelf life and reducing mechanical damage in apricot. *Journal of Food Science*, 1706–1712. DOI: 10.1111/j.1365-2621.2002.tb08710.x.

Martínez-Romero D., Valero D., Riquelme F., Zuzunaga M., Serrano M., … Carbonell A., 2001. Infiltration of putrescine into apricots hepls handling and storage. *Acta Horticulturae* 553: 189–192. DOI: 10.17660/ActaHortic.2001.553.41.

Martínez-Romero D., Valero D., Serrano M., Burló F., Carbonell A., … Riquelme F., 2000. Exogenous polyamines and gibberellic acid effects on peach (*Prunus persica* L.) storability improvement. *Journal of Food Science* 65: 288–294. DOI: 10.1111/j.1365-2621.2000.tb15995.x.

Mattoo A.K., Handa A.K., 2008. Higher polyamines restore and enhance metabolic memory in ripening fruit. *Plant Science* 174: 386–393. DOI: 10.1016/j.plantsci.2008.01.011.

Mirdehghan S.H., Rahemi M., Martínez-Romero D., Guillén F., Valverde J.M., … Valero D., 2007. Reduction of pomegranate chilling injury during storage after heat treatment: Role of polyamines. *Postharvest Biology and Technology* 44: 19–25. DOI: 10.1016/j.postharvbio.2006.11.001.

Obeed R.S., Harhash M.M., 2006. Impact of postharvest treatments on storage life and quality of "Mexican" lime. *Journal of Advanced Agricultural Technologies* 11: 533–549.

Oliveira Lino L., Pacheco I., Mercier V., Faoro F., Bassi D., … Quilot-Turion B., 2016. Brown rot strikes prunus fruit: An ancient fight almost always lost. *Journal of Agricultural and Food Chemistry* 64: 4029–4047. DOI: 10.1021/acs.jafc.6b00104.

Palma F., Carvajal F., Ramos J.M., Jamilena M., Garrido D., 2015. Effect of putrescine application on maintenance of zucchini fruit quality during cold storage: Contribution of GABA shunt and other related nitrogen metabolites. *Postharvest Biology and Technology* 99: 131–140. DOI: 10.1016/j.postharvbio.2014.08.010.

Palou L., Ali A., Fallik E., Romanazzi G., 2016. GRAS, plant- and animal-derived compounds as alternatives to conventional fungicides for the control of postharvest diseases of fresh horticultural produce. *Postharvest Biology and Technology* 122: 41–52. DOI: 10.1016/j.postharvbio.2016.04.017.

Paull R.E., Jung Chen N., 2000. Heat treatment and fruit ripening. *Postharvest Biology and Technology* 21: 21–37. DOI: 10.1016/S0925-5214(00)00162-9.

Pavoncello D., Lurie S., Droby S., Porat R., 2001. A hot water treatment induces resistance to *Penicillium digitatum* and promotes the accumulation of heat shock and pathogenesis-related proteins in grapefruit flavedo. *Physiologia Plantarum* 111: 17–22. DOI: 10.1034/j.1399-3054.2001.1110103.x.

Pérez-Vicente A., Martınez-Romero D., Carbonell Á., Serrano M., Riquelme F., … Valero D., 2002. Role of polyamines in extending shelf life and the reduction of mechanical damage during plum (*Prunus salicina* Lindl.) storage. *Postharvest Biology and Technology* 25: 25–32. DOI: 10.1016/S0925-5214(01)00146-6.

Radi M., Jouybari H.A., Mesbahi G., Farahnaky A., Amiri S., 2010. Effect of hot acetic acid solutions on postharvest decay caused by *Penicillium expansum* on Red Delicious apples. *Scientia Horticulturae*, 421–425. DOI: 10.1016/j.scienta.2010.06.023.

Salehi M., Salehi E., Siampour M., Quaglino F., Bianco P.A., 2018. Apricot yellows associated with '*Candidatus* Phytoplasma phoenicium' in Iran. *Phytopathologia Mediterranea* 57: 269–283. DOI: 10.14601/Phytopathol_Mediterr-22588.

Serrano M., Martínez-Romero D., Castillo S., Guillén F., Valero D., 2004. Role of calcium and heat treatments in alleviating physiological changes induced by mechanical damage in plum. *Postharvest Biology and Technology* 34: 155–167. DOI: 10.1016/j.postharvbio.2004.05.004.

Serrano M., Martinez-Romero D., Guillén F., Valero D., 2003. Effects of exogenous putrescine on improving shelf life of four plum cultivars. *Postharvest Biology and Technology* 30: 259–271. DOI: 10.1016/S0925-5214(03)00113-3.

Sharayei P., Ganji Moghadam E., 2013. Effect of hot water, ethanol and acetic acid vapor on physical, chemical and organoleptic characteristics of peaches (*Prunus persica* batsch cv. Elberta). *Journal of Agricultural Engineering Research* 14: 59–72.

Sholberg P.L., Gaunce A.P., 1995. Fumigation of fruit with acetic-acid to prevent postharvest decay. *HortScience* 30: 1271–1275.

Sholberg P.L., Gaunce A.P., 1996. Fumigation of stonefruit with acetic acid to control postharvest decay. *Crop Protection* 15: 681–686. DOI: 10.1016/s0261-2194(96)00039-7.

Siddiq M., 2007. Plums and Prunes. In: *Handbook of Fruits and Fruit Processing*, (Y.H. Hui ed.). DOI: 10.1002/9780470277737.ch29

Siruieneja B., Mortazavi S.M.H., Moalemmi N., Eshghi S., 2013. The effect of postharvest application of putrescine and UV-C irradiation on strawberry (*Fragaria* × *ananassa* cv. Selva) fruit quality. *Journal of Plant Production* 36: 117–127.

Sisquella M., Casals C., Viñas I., Teixidó N., Usall J., 2013. Combination of peracetic acid and hot water treatment to control postharvest brown rot on peaches and nectarines. *Postharvest Biology and Technology* 83: 1–8. DOI: 10.1016/j.postharvbio.2013.03.003.

Spadaro D., Droby S., 2016. Development of biocontrol products for postharvest diseases of fruit: The importance of elucidating the mechanisms of action of yeast antagonists. *Trends in Food Science and Technology* 47: 39–49. DOI: 10.1016/j.tifs.2015.11.003.

Spadoni A., Guidarelli M., Sanzani S.M., Ippolito A., Mari M., 2014. Influence of hot water treatment on brown rot of peach and rapid fruit response to heat stress. *Postharvest Biology and Technology* 94: 66–73. DOI: 10.1016/j.postharvbio.2014.03.006.

Usall J., Ippolito A., Sisquella M., Neri F., 2016. Physical treatments to control postharvest diseases of fresh fruits and vegetables. *Postharvest Biology and Technology* 122: 30-40. DOI: 10.1016/j.postharvbio.2016.05.002.

Valero D., Martínez-Romero D., Serrano M., 2002. The role of polyamines in the improvement of the shelf life of fruit. *Trends in Food Science and Technology* 13: 228–234. DOI: 10.1016/S0924-2244(02)00134-6.

Valero D., Serrano M., 2010. *Postharvest Biology and Technology for Preserving Fruit Quality*. CRC-Taylor & Francis, Boca Raton, USA, 287 pp.

Wszelaki A.L., Mitcham E.J., 2003. Effect of combinations of hot water dips, biological control and controlled atmospheres for control of gray mold on harvested strawberries. *Postharvest Biology and Technology* 27: 255–264. DOI: 10.1016/S0925-5214(02)00095-9.

Zheng Q., Zuo J., Gu S., Gao L., Hu W., … Jiang A., 2019. Putrescine treatment reduces yellowing during senescence of broccoli (*Brassica oleracea* L. var. italica). *Postharvest Biology and Technology* 152: 29–35. DOI: 10.1016/j.postharvbio.2019.02.014.

Zokaee-Khosroshahi M., Esna-Ashari M., 2008. Effect of putrescine application on post-harvest life and physiology of strawberry, apricot, peach and sweet cherry fruits. *Journal of Crop Production and Processing* 12: 219–230.

Zokaee Khosroshahi M.R.Z., Esna-Ashari M., Ershadi A., 2007. Effect of exogenous putrescine on post-harvest life of strawberry (*Fragaria ananassa* Duch.) fruit, cultivar Selva. *Scientia Horticulturae* 114: 27–32. DOI: 10.1016/j.scienta.2007.05.006.

Zoran I., Yulita P., Sharon A.T., Azica C., Elazar F., 2001. Short prestorage hot water rinse and brushing reduces decay development in tomato, while maintaining its quality. *Tropical Agricultural Research and Extention* 4: 1–6.

Phytopathologia Mediterranea
The international journal of the
Mediterranean Phytopathological Union

Firenze University Press
www.fupress.com/pm

Research Papers

Origanum vulgare essential oil vapour impedes *Botrytis cinerea* development on grapevine (*Vitis vinifera*) fruit

Andrea BURGGRAF, Markus RIENTH*

University of Sciences and Art Western Switzerland, Changins College for Viticulture and Oenology, route de duillier 50, 1260 Nyon, Switzerland
*Corresponding author. E-mail: markus.rienth@changins.ch

Summary. *Botrytis cinerea* infections of *Vitis* spp. fruits cause major economic losses, and grape producers rely on synthetic and copper-based fungicides for control of this pathogen. These pesticides present risks for human health and the environment. Implementation of low-impact disease management solutions is important for improving sustainability of viticulture industries. This study investigated the effects of *Origanum vulgare* (oregano) essential oil (EO) as an antifungal agent. *In vitro* and *in vivo* experiments with *B. cinerea* were carried out using a vaporization system to circumvent drawbacks of direct EO application. *In vitro* experiments confirmed the effectiveness of EO vapour treatments, which gave 100% inhibition of *B. cinerea* growth. Treatment of *V. vinifera* cv. Chasselas berries resulted in a 73% reduction in fungal growth, confirming the efficacy of the oregano EO vapour for control of grey mould caused by *B. cinerea*. This study has demonstrated the efficacy of EOs in the vapour phase on grape berries, which provides new possibilities for development of in-field or greenhouse vaporization systems that can reduce the use of synthetic and copper-based fungicides.

Keywords. Postharvest disease, grape grey mould, volatile organic compounds, sustainable viticulture, biopesticides, essential oils.

OPEN ACCESS

Citation: A. Burggraf, M. Rienth (2020) *Origanum vulgare* essential oil vapour impedes Botrytis cinerea development on grapevine (*Vitis vinifera*) fruit. *Phytopathologia Mediterranea* 59(2): 331-344. DOI: 10.14601/Phyto-11605

Accepted: August 25, 2020

Published: August 31, 2020

Data Availability Statement: All relevant data are within the paper and its Supporting Information files.

Competing Interests: The Author(s) declare(s) no conflict of interest.

Editor: Lluís Palou, Valencian Institute for Agricultural Research, Valencia, Spain.

INTRODUCTION

Fungicides represent 49% of the pesticides utilized in the European Union (European Commission Eurostat, 2007). The viticulture industry contributes to this high fungicide use via efforts to control vineyard diseases caused by fungi, including *Botrytis cinerea, Plasmopara viticola* and *Erysiphe necator*. This is a growing problem, due to the possible negative impacts on consumer and producer health and on the surrounding ecosystems and soils (Komárek *et al*., 2010; Aminifard and Mohammadi, 2012). *Botrytis cinerea* is an important fungal pathogen in viticulture and in other crops. This pathogen causes grey mould (Naegele, 2018) and Botrytis bunch rot. *Botrytis cinerea* infections cause major economic losses (Elmer and Michailides, 2007) due to reductions in grape yields and quality (Jacometti *et al*., 2010; Paňitrur-De La Fuente *et al*., 2018). Due to the high frequency of usage and possible detrimental health

and environmental impacts of pesticides, alternative disease management strategies are required to reduce pesticide use for sustainable agriculture.

Alternatives to pesticides include measures to increase plant and fruit resistance to *B. cinerea* and other fungal diseases, and cultural practices to encourage the maintenance of unfavourable habitats for pathogen development. Cultural practices in viticulture include maintenance of good vine canopy structure, the growing of cover crops and mulching to reduce excessive vine vigour. However, these practices can be challenging and only marginally effective. Other alternatives include the use of biological control agents and plant extracts, all of which have shown some efficacy for control of *B. cinerea*, and are typically applied in conjunction with other control methods (Jacometti *et al.*, 2010). Interspecific crossbreeding of naturally disease-resistant varieties is also a very cost-effective, environmentally-friendly solution for the control of fungal diseases. However, challenges regarding the marketing of disease-resistant varieties, such as labelling concerns and varietal reputation, are important when assessing the economic viability and future of new varieties (Fuller *et al.*, 2014). Recent research suggests that essential oils (EOs), with antifungal capacities and low environmental impacts, could be alternatives for control of fungal fruit pathogens. Development of EO treatments for fungal disease management could solve the environmental and human health issues caused by pesticide-based disease management.

EOs naturally present in plants can protect against infections by pathogenic microorganisms (Mohammadi *et al.*, 2013; Nazzaro *et al.*, 2017). These materials are generally recognized as safe (GRAS) by the United States of America Food and Drug Administration (FDA), and are widely accepted as alternatives to synthetic chemicals because of their natural origins (Nazzaro *et al.*, 2017).

The antifungal properties of EOs are primarily linked to terpenes (monoterpenes and sesquiterpenes), terpenoids (isoprenoids), alipathic and aromatic compounds such as aldehydes and phenols. Terpenes are naturally occurring hydrocarbons with various chemical and biological properties, and constitute up to 90% of most EO components (Sakkas and Papadopoulou, 2017).

The active antifungal properties of EOs are mainly attributed to disruption of cell wall formation and interference with phospholipid bilayers of cell membranes. Their high lipophilicity allows absorption by fungal mycelium (Soylu *et al.*, 2007). They also have low molecular weights, allowing cell death and inhibition of fungal sporulation and germination (Nazzaro *et al.*, 2017), or deformation of cell structure and functional disruption (Mohammadi *et al.*, 2013; Sakkas and Papadopoulou, 2017). Furthermore, the antifungal compounds in EOs have been shown to prevent fungal pectinases from hydrolyzation and invasion of host plant cells (Soylu *et al.*, 2010; Aminifard and Mohammadi, 2012).

EOs can also debilitate mitochondria of fungal pathogens (Nazzaro *et al.*, 2017). Effects of EOs on mitochondria and fungal plasma membranes cause inhibition of the synthesis of ergosterol and activities of mitochondrial ATPase, malate dehydrogenase, and succinate dehydrogenase (Hu *et al.*, 2017). Carvacrol, a monoterpene present in many EOs, including those from oregano and thyme, may also inhibit fungal growth by stimulating pathogen responses similar to calcium stress and inhibition of the target of rapamycin (TOR) pathway. This suggests that antifungal properties of carvacrol include activation of specific signalling pathways within fungi, causing debilitation (Rao *et al.*, 2010).

Numerous studies have confirmed the efficacy of EOs for inhibiting growth of fungal pathogens, including *B. cinerea, Rhizopus stolonifer, Fusarium* spp., *Clavibacter michiganensis, P. viticola*, and *Sclerotinia sclerotiorum*. Mohammadi *et al.* (2013) found through gas chromatography-mass spectrometry (GC/MS) analyses of black caraway, fennel, peppermint and thyme oils that they were mainly composed of monoterpenes and terpenes. They confirmed that all four EOs inhibited *B. cinerea* and *R. stolonifer* under *in vitro* conditions, with black caraway and fennel oils showing the greatest efficacy for reducing growth of the fungi. In a study of the efficacy of EOs for inhibition of *in vitro* and *in vivo* growth of *B. cinerea*, Aminifard and Mohammadi (2012) found that the EO of black caraway and fennel completely inhibited the growth of the fungus at, respectively, 400 and 600 µL L^{-1}. Daferera *et al.* (2003) demonstrated, under *in vivo* conditions, that black caraway, fennel, and peppermint oils inhibited the growth of *B. cinerea*. EOs of oregano, thyme, dictamnus and marjoram completely inhibited the growth of *B. cinerea, Fusarium* sp. and *C. michiganesis* at 85 to 300 µg mL^{-1}, and the main antifungal components in the EOs were identified as thymol and carvacrol.

The antifungal effects of the EOs of oregano and fennel were studied for inhibitory effects on *S. sclerotiorum* by Soylu *et al.* (2007). Similar to *B. cinerea, S. sclerotiorum* produces overwintering sclerotia, which make the fungus particularly difficult to control. Their results showed that both EOs in volatile and liquid phases inhibited fungal growth, reducing mycelium growth and germination of sclerotia. Soylu *et al.* (2010) evaluated the effectiveness of oregano, lavender, and rosemary (Lamiaceae), and showed that the EO of oregano was the most effective at low concentrations in vapour (0.2 µg mL^{-1} air) and contact (12.8 µg mL^{-1}) phases under *in vitro* and *in vivo* conditions for

inhibiting the growth of *B. cinerea*. Oregano oil was also shown to possess strong antifungal properties by Vitoratos *et al.* (2013), who observed complete inhibition of fungal growth by oregano EO at 0.30 μL mL^{-1}. Lemon oil was also shown to reduce growth of *B. cinerea*. *Salvia officinalis* (sage) EO was studied for efficacy in control of *P. viticola* by Dagostin *et al.* (2010). The EO had inhibition potential similar to copper hydroxide, showing that sage extract was another promising alternative to copper fungicides in viticulture. However, the rainfastness of the EO was very low, indicating potential complications associated with its practical efficacy (Daferera *et al.*, 2003; Soylu *et al.*, 2010; Mohammadi *et al.*, 2013).

Several studies have shown that application of EOs can be very effective in vapour phase at lower concentrations than in liquid phase (Edris and Farrag, 2003; Soylu *et al.*, 2010; Babalık *et al.*, 2020). In addition to being more effective at lower doses than contact applications, vapour treatments could be efficient due to lack of direct contact between EOs and host plants, reducing phytotoxicity and circumventing the drawbacks of direct applications (low rainfastness, UV degradation, poor mixability with water and/or other products) (Edris and Farrag, 2003). Drawing upon results from previous studies, the present research aimed to investigate whether continuous fumigation with EO vapour from *Origanum vulgare* could reduce *B. cinerea* development *in vitro* and *in vivo* on grape berries, thereby circumventing the drawbacks of direct applications.

MATERIALS AND METHODS

Isolation and culture of Botrytis cinerea

Botrytis cinerea conidia used for *in vivo* and *in vitro* tests were harvested from decaying strawberries. Conidia were removed from berries with forceps and plated on potato dextrose agar (PDA) in Petri dishes, using a sterile inoculation loop. The Petri dishes were incubated at 22.5°C under continuous light for 14 d to encourage conidium production. Actively growing *B. cinerea* cultures on PDA were maintained through conidium transfer onto freshly prepared Petri dishes every 7–14 d throughout experimentation.

After successful growth of *B. cinerea* on PDA, conidia were collected from cultures and suspended in Ringer's solution. The solution was added to the dishes and the culture surfaces were then rubbed with an inoculation loop to dislodge conidia. Solutions and spores were removed from the Petri dishes and passed through 100 mm diam. filter paper (Schleicher & Schuell; pore size 11 μm) to remove agar pieces and mycelia. The suspensions were then vortexed before quantification using a vortex mixer (Bender & Hobein Vortex Genie 2, 1410). Conidia concentration was calculated using a microscope (Carl Zeiss, Lab A1 AXIO) with an A-Plan 10x/0.25 Ph1 lens, and a 0.100 mm depth 0.0025 mm^2 Thoma counting chamber. The conidial suspension concentrations were adjusted to the range of 5×10^5 to 1×10^6 conidia mL^{-1} recommended by Guetsky *et al.* (2001) throughout the experiment.

In vitro *fumigation with oregano essential oil*

Petri dishes were assigned to treatment and control groups and were placed inside a climate chamber (Percival Scientific; Intellus Ultra C8), which was customized to allow simultaneous treatment and control fumigation to be carried out inside airtight plexiglass chambers (dimensions: 67 × 67 × 108 cm). The customized two-chamber pump mechanism included two plastic boxes, one treatment box containing EO and one empty box assigned to the control group. EO vapour and air (control) treatments were transferred by a pump system to the climate chamber containing the petri dishes. These were left inside the chamber with the lids off, facing upward during treatment. Mycelium growth in the dishes was quantified until fungus colonies in a majority of the control dishes had reached full capacity. The increases in the diameter of *B. cinerea* colonies in the Petri dishes were determined by tracing the radial growth on the underside of each dish. The proportion of mycelium growth inhibition was calculated using the following equation:

$$\left(\frac{DC-DT}{DC}\right) \times 100$$

where DC = the average colony diameter on the control dishes, and DT = the average colony diameter on the treatment dishes (Badawy and Abdelgaleil, 2014).

Three different experiments were carried out. A diurnal climate chamber programme was run during each experiment, with a daily regime of 12 h light, 20°C, 70% relative humidity (RH) / 12 h dark, 15°C, 50% RH. Each Petri dish was inoculated at the centre with 10 μL of *B. cinerea* conidial suspension, which was allowed to dry before measuring the initial colony diameter. EO of oregano (Origan Vert, Companie des Sens, France), was placed in a glass dish inside the treatment chamber of the customized fumigation system.

Specifications for the individual experiments are shown in Table 1. EO composition was determined by GC with flame ionization detection (GC-FID; Agilent GC system 7890B/7010 Agilent GC-TQ).

Table 1. Specifications for three *in vitro* experiments (T = Treatment, C = Control).

Experiment	Sample size	Conidial solution concentration (conidia mL^{-1})	Dosage and parameters	Duration
Trial I	11 (T) 11 (C)	9.11×10^5	4 mL EO inside pump chamber	4 d
Trial II	10 (T) 10 (C)	7.49×10^5	5 mL EO inside pump chamber	3 d
Trial III	10 (T) 10 (C)	7.71×10^5	5 mL EO inside pump chamber 5 mL EO inside climate chamber	3 d

In vivo *treatment of grape berries with oregano essential oil*

Four trials were carried out with detached *Vitis vinifera* cv. Chasselas berries. The different parameters of the experiments are summarized in Table 2. Ripe grape berries were collected from the vineyards at Changins, Haute Ecole de Viticulture et Oenologie (Nyon, Switzerland). Total soluble solids (TSS, expressed in °Brix) were measured with a Wine Line HI96811 0-50°Brix wine refractometer. Thirty healthy berries were each punctured once using a 0.5 mm diam. sterile pin with a puncture depth of 3 mm. All berries were inoculated with *B. cinerea* by individual submersion for 5 s in a conidial suspension prepared as described above.

The grape berries were placed into 90 mm diam. sterile Petri dishes, which were placed inside the climate chamber for treatment. A diurnal climate chamber programme was run during each experiment, with a daily regime of 12 h light, 25°C, 90% RH / 12 h dark, 17°C, 50% RH. Five milliliters of EO were placed in a glass dish on top of a heating pad inside the treatment chamber of the fumigation system. The air pump was turned on at maximum air flow intensity, transferring air into the treatment and control chambers.

Quantification of grey mould severity on cv. Chasselas berries

At the end of each treatment, three replicates each of five berries from the treatment and control groups were placed into 50 mL capacity sterile centrifuge tubes each containing 25 mL of reverse osmosis water. Each centrifuge tube was agitated for 2 min with a vortex (Bender & Hobein Vortex Genie 2) to dislodge conidia from berries. After vortexing, the berries were removed from the solution by filtering through a 100 mm diam. filter paper (Schleicher & Schuell). Conidia concentrations in the solutions were quantified with a microscope with an A-Plan ×10/0.25 Ph1 lens (Carl Zeiss Lab A1 AXIO), using a 0.100 mm depth 0.0025 mm^2 Thoma counting chamber.

Table 2. Specifications for four fumigation treatment trials applied to detached cv. Chasselas grape berries.

Experiment	Berry collection site	°Brix	Spore suspension concentration (conidia mL^{-1})	Duration
Trial I	Changins Vineyard	20.7	9.98×10^5	10 d
Trial II	Changins Vineyard	17.4	1.96×10^6	7 d
Trial III	Supermarket	25.5	1.05×10^6	7 d
Trial IV	Changins Vineyard	17.6	1.02×10^6	7 d

Quantification and identification of the active compounds present during treatment

Analysis was carried out using the saturation point of activated charcoal (Supelco Activated Coconut Charcoal; 20-40 mesh) to capture oil vapours for analysis of vapour concentrations during treatment. This was used to determine the appropriate quantity to be used in subsequent experiments. Tissue bags filled with 500 mg, 1 g, or 1.5 g of the charcoal were hung in the treatment and control chambers at the beginning of treatment. At the end of the 7-d treatment, samples were analyzed with GC-FID on a gas chromatograph (Agilent 7890B) with an autosampler (Agilent 7693). The charcoal samples in which the volatile compounds were trapped were eluted by dichloromethane. Two milliliters of dichloromethane was used for extraction of the 500 mg and 1 g samples. Four milliliters of dichloromethane were used for extraction of the 1.5 g sample. Additionally, an internal standard of 10 µL of 1,6-heptendiol at 50 mg L^{-1} was added during sample preparation. Samples were incubated and mixed for 1 h at room temperature. The supernatant from each sample was then collected and transferred into a sterile vial for analysis. The sample was injected directly for component determination by GC using hydrogen as the carrier gas at a constant flow of 4 mL min^{-1}. Separation of the compounds was performed using a capillary column (60 m, 0.25 mm ID, 1.4 µm; Rtx®-1301) and detection was carried out by flame ionization. P-cymene, thymol, and carvacrol were identified, quantified and expressed in mg L^{-1}. The limit of quantification (LOQ) for all three molecules was set at 3.50 mg L^{-1}, and the limit of detection

Table 3. Saturation point analysis of activated charcoal.

Sample	Charcoal control 0.5 g	Charcoal control 1.0 g	Charcoal control 1.5 g	Charcoal treatment 0.5 g	Charcoal treatment 1.0 g	Charcoal treatment 1.5 g
P-cymene (mg L^{-1})	31.513	48.059	60.22	471.85	834.55	816.73
Thymol (mg L^{-1})	3.825	4.274	13.49	32.27	34.62	38.21
Carvacrol (mg L^{-1})	5.358	4.821	8.60	665.26	770.89	1012.94
Extraction measurement	2 mL	2 mL	4 mL	2 mL	2 mL	4 mL

Table 4. Dose and treatment parameters for individual trials with corresponding conidial suspension solution.

Parameter	Trial 1	Trial 2	Trial 3	Trial 4	Trial 5
EO dose parameters	CONTROL No EO Treatment	2 mL EO in pump chamber No heat application	2 mL EO in pump chamber Heat application	3 mL EO in pump chamber Heat application	3 mL EO in pump chamber 3 mL EO in treatment chamber Heat application
Conidium suspension concentration	9.5×10^5	9.33×10^5	9.33×10^5	9.75×10^5	9.75×10^5

(LOD) for all three molecules was 2.5 mg L^{-1}. Five hundred milligrams was shown to be the saturation point during the treatment period. Saturation was not reached in the 1 g samples; therefore, 1 g was determined to be the appropriate quantity to be used for vapour quantification in subsequent experiments (Table 3).

Analysis of essential oil residual surface contamination on berry skins and in berry flesh

Evaluation of p-cymene, thymol, and carvacrol present on the surfaces of berry skins and in berry flesh after treatment with EO of oregano was carried out twice during each fumigation experiment. Nine berries were assigned to each treatment group and nine berries were assigned to each control group. Healthy and intact berries were placed on standard 90 mm diam. sterile Petri dishes inside of the treatment and control fumigation chambers. After 7 d of treatment, the berries were placed into 50 mL capacity sterile centrifuge tubes, each containing 25 mL of reverse osmosis water, and these were each vortexed for 1 min. The berries remained in each solution until GC-FID analysis and the solution was prepared for GC-FID analysis following the procedure outlined above using 2 mL of dichloromethane for extraction. For berry flesh analyses, a second experiment was carried out, and at the end of 7 d of treatment, berries were rinsed under lukewarm water for 2 min to remove surface residues. The berries were left to dry and then placed inside 50 mL capacity sterile centrifuge tubes for storage until quantification. GC-FID was carried out on the berries by pressing the whole berries to extract juice from the flesh, which was then prepared as described above for GC-FID using 2 mL of dichloromethane for each extraction.

Conidium suspension preparation and essential oil dose parameters for dose-dependent in vitro *treatments*

Conidial suspensions were prepared as described above. One suspension was individually prepared for the control trial I harvesting conidia from actively growing *B. cinerea* colonies. One suspension was prepared for experimental treatment trials 2 and 3, which were carried out simultaneously. One suspension was prepared for experiments 4 and 5, which were also carried out simultaneously. Conidial suspension concentrations had little variation during the three phases of experimentation. The five trials were carried out using different concentrations, placements, and modes of diffusion of oregano oil (Table 4). The conidial suspension concentrations and the corresponding EO dosage parameters are outlined in Table 4.

During each treatment, eight Petri dishes were placed in the climate chamber and each was inoculated with 10 µL of conidial suspension. Fumigation parameters were the same for all five trials. A diurnal climate chamber programme was run during each experiment, with a daily regime of 12 h light, 25°C, 90% RH / 12 h dark, 17°C, 50% RH. Treatments were carried out over 3 d.

Statistical analysis and data presentation

Statistical analyses (Welch's two sample t-test and two-way ANOVA) were carried out using R Studio. Graphical presentation of data was performed with MS Excel and OriginPro.

RESULTS

Chemical composition of essential oils

Chemical composition as determined by GC-FID showed that the oregano EO used in this study contained 68.60% carvacrol, 11.27% p-cymene, 5.91% γ-terpinene, and 1.93% thymol (Table 5). This composition is similar to that from other studies, which have reported 58.1% carvacrol and 11.4% p-cymene as the composition of *O. vulgare* EO (Bouchra *et al.*, 2003; Daferera *et al.*, 2003; Teixeira *et al.*, 2013; Rienth *et al.*, 2019). Variation in active compounds and the presence of additional components can be attributed to source plant genotype and nutritional status, and to environmental conditions and geographical location (Badawy and Abdelgaleil, 2014).

Table 5. Composition of the oregano essential oil determined by GC-FID.

Retention time (min)	Composition	Percent probability	Percent measured	Theoretical percentage
18.43	Carvacrol	93.2	68.60	21–63%
7.59	Paracymène	96.6	11.27	6–20%
8.72	Gamma-terpinene	94.8	5.91	9-26%
23.11	Caryophyllène	96.6	2.46	
18.10	Thymol	95.3	1.93	3–28%
7.34	Alpha-terpinene	85.4	1.44	
6.58	Beta-myrcene	90.4	0.94	
5.11	Alpha-pinene	93.5	0.90	
10.28	Linalool	82.5	0.61	≤2%
7.73	D-limonene	80.8	0.58	≤1%
4.94	Alpha-thujene	89.4	0.40	
5.47	Camphene	86.3	0.21	

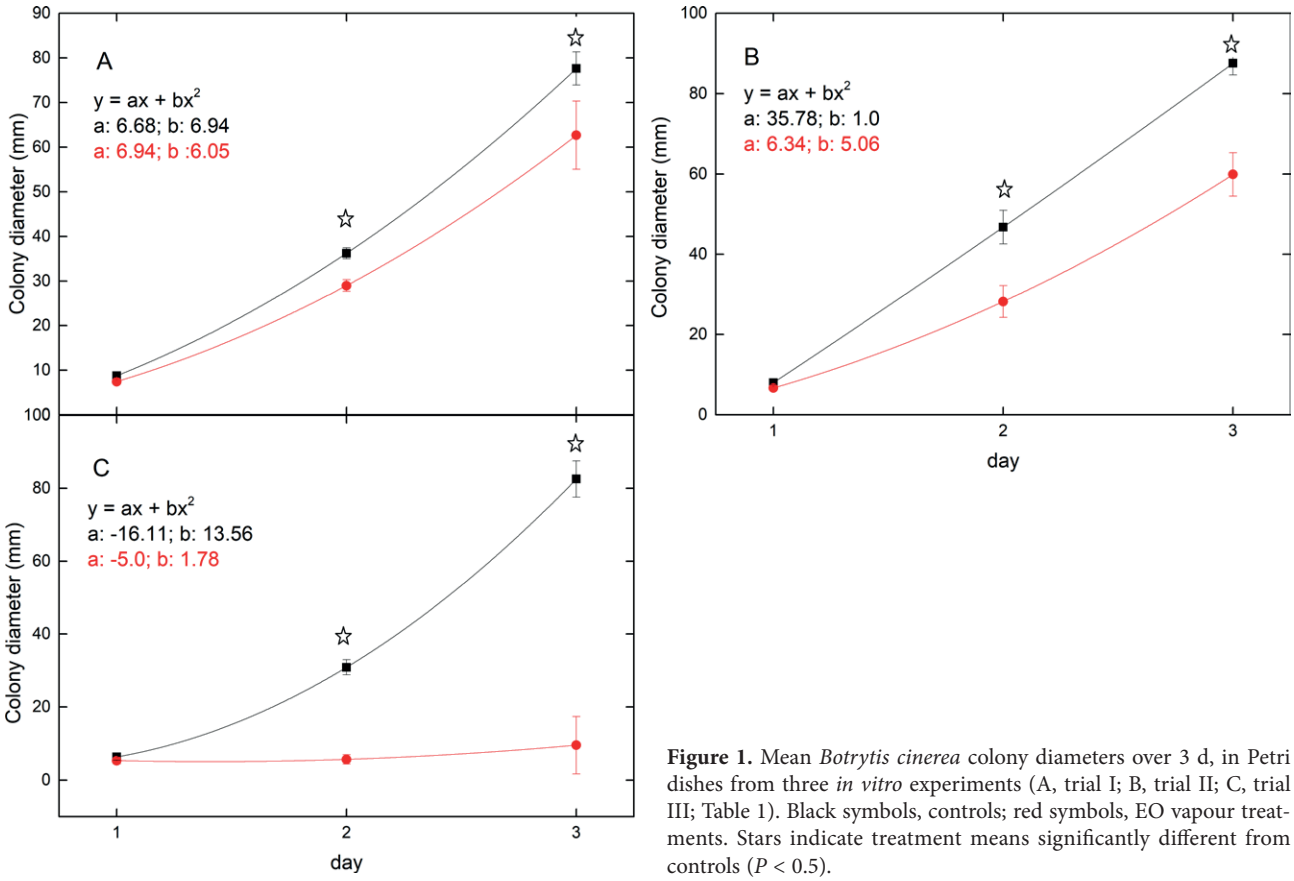

Figure 1. Mean *Botrytis cinerea* colony diameters over 3 d, in Petri dishes from three *in vitro* experiments (A, trial I; B, trial II; C, trial III; Table 1). Black symbols, controls; red symbols, EO vapour treatments. Stars indicate treatment means significantly different from controls ($P < 0.5$).

Effects of in vitro *fumigation with essential oil on* Botrytis cinerea

The average colony radial growth difference between *B. cinerea*-inoculated Petri plates dishes treated with EO vapour and control samples is illustrated in Figure 1. Treatment with EO vapour inhibited the growth of *B. cinerea* in all three experiments.

Effects of essential oil vapour on Botrytis cinerea *growth on grape berries*

Treatment with oregano oil vapour on detached cv. Chasselas berries reduced *B. cinerea* infections in all four trials, with the results from trials II and IV showing the greatest proportional inhibition, as indicated by the conidial suspension concentrations from the control and treatments (Figure 2).

An example of cv. Chasselas berries before and after treatment for the control and essential oil treatment samples is shown in Figure 3. EO vapour-treated berries developed browning due to the puncture wounds made at inoculation, but low levels of *B. cinerea* conidia were present on the berries. Control berries browned significantly after the 7 d treatments and showed significant amounts of mycelial growth and decay of berry flesh.

GC-FID analyses of fumigation residues in grape berries

GC-FID analyses of berries that underwent EO treatments identified the oil components p-cymene, thymol, and carvacrol (Table 6 and Table 7). Thymol and carvacrol were shown to be absorbed by berries during treatments, with greatest absorption of carvacrol in the treated samples. For the berry surface residues, p-cymene was the least persistent of the active compounds, which was less than the LOQ in trial III, compared to thymol and carvacrol. Thymol was present in the surface residue samples of both the treatment and control samples during both rounds of GC-FID analyses, demonstrat-

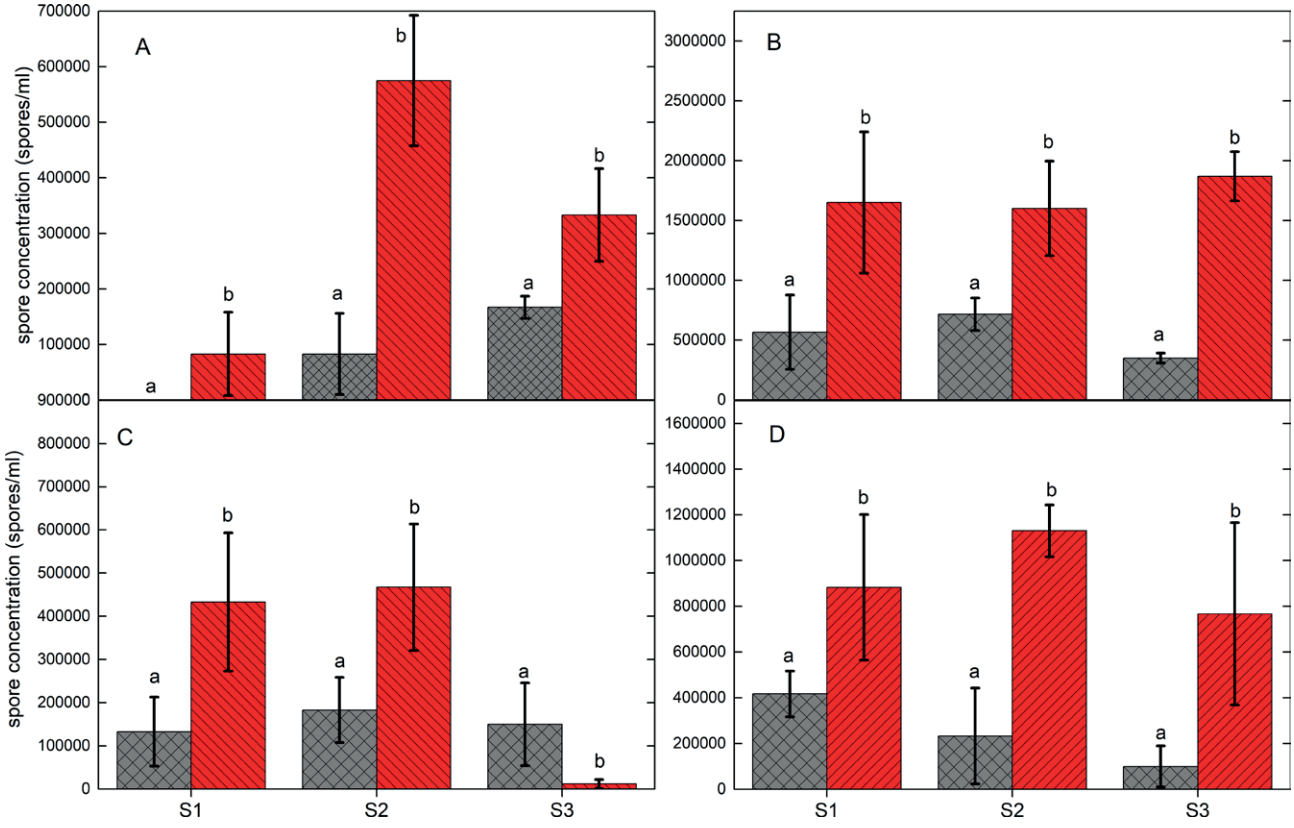

Figure 2. Mean numbers of *Botrytis cinerea* conidia from controls (gray histograms) and essential oil treatments (red histograms) for samples (S1, S2, S3) in four *in vivo* experiments (Table 2); trial I (A), trial II (B), trial III (C) and trial IV (D). Different letters for each experiment indicate significant differences between treatments and controls ($P < 0.5$), and bars indicate standard errors of the means.

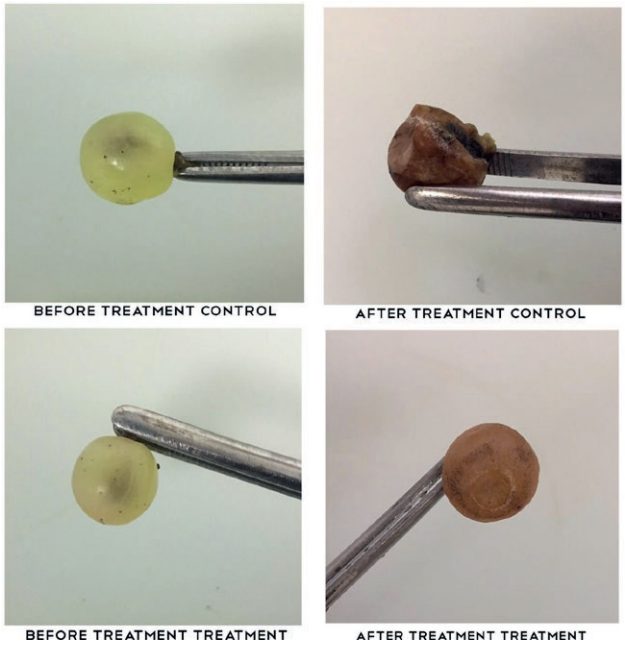

Figure 3. Visual differences in mycelium growth and fruit desiccation of detached cv. Chasselas berries for control berries (top), and treatment berries (bottom) after 7 d of treatment. These images were captured at the end of *in vivo* trial IV.

ing its strong persistence after treatment. Thymol was not quantifiable in the berry absorption analyses of the control group during the trial II GC-FID analysis, but was present in trial III, where carvacrol and p-cymene were not measurable. Carvacrol was not measurable in the surface residue samples for the control groups during both rounds of GC-FID analysis and was present at concentrations less than those of thymol during both rounds of analysis in the treatment samples. For berry absorption, carvacrol was at substantially different concentrations in the treatment group during trials II and III. For p-cymene, average berry absorption in the treatment sample was less than the LOQ and the measured surface residue concentration was 4.54 mg L^{-1}. For thymol, the average berry absorption for the treated berries was 7.57 mg L^{-1} and the surface residue concentration was 11.36 mg L^{-1}. For carvacrol, the average berry absorption level was 11.06 mg L^{-1} and the surface residue concentration was 6.81 mg L^{-1}.

Table 6. Mean inhibition (%) of *Botrytis cinerea* radial colony growth after treatment with essential oil vapour. In each trial, radial colony growth was reduced ($P < 0.05$) by treatment.

	Inhibition after 36 h	Inhibition after 48 h
Trial I	19.3%	20.2%
Trial II	31.8%	39.9%
Trial III	89.0%	81.7%

Effects essential oil dose on in vitro *growth inhibition of* Botrytis cinerea

Treatment parameters and dosages of EO vapour were modified during five *in vitro* trials to assess the impacts of different concentrations of the active components on growth inhibition of *B. cinerea*. The inhibition

Table 7. Essential oil component residues in grape berries and on berry surfaces in trials I and II. C1, C2, and C3 are three experimental controls: T1, T2 and T3 are three treatments with essential oil.

Component	Berry absorption Trial I						Surface residue Trial I					
	C1	C2	C3	T1	T2	T3	C1	C2	C3	T1	T2	T3
p-cymene	<LOQ	<LOQ	<LOQ	<LOQ	<LOQ	<LOQ	5.4	6.3	4.73	4.94	6.31	5.47
Thymol (mg L^{-1})	<LOQ	<LOQ	<LOQ	5.90	9.38	5.74	10.9	11.29	11.69	9.76	11.29	11.95
Carvacrol (mg L^{1})	<LOQ	<LOQ	<LOQ	20.29	35.68	12.23	<LOQ	<LOQ	<LOQ	4.44	6.65	6.26
	Berry absorption Trial II						Surface residue Trial II					
	C1	C2	C3	T1	T2	T3	C1	C2	C3	T1	T2	T3
p-cymene	<LOQ	<LOQ	<LOQ	<LOQ	<LOQ	<LOQ	<LOQ	<LOQ	<LOQ	<LOQ	<LOQ	<LOQ
Thymol (mg L^{-1})	8.37	8.18	7.63	6.54	6.89	10.95	11.39	9.57	9.915	11.98	12.33	10.82
Carvacrol (mg L^{1})	<LOD	<LOD	<LOD	5.06	4.78	6.28	<LOD	<LOD	<LOD	7.95	6.39	9.17

LOQ = limit of quantification
LOD = Limit of detection

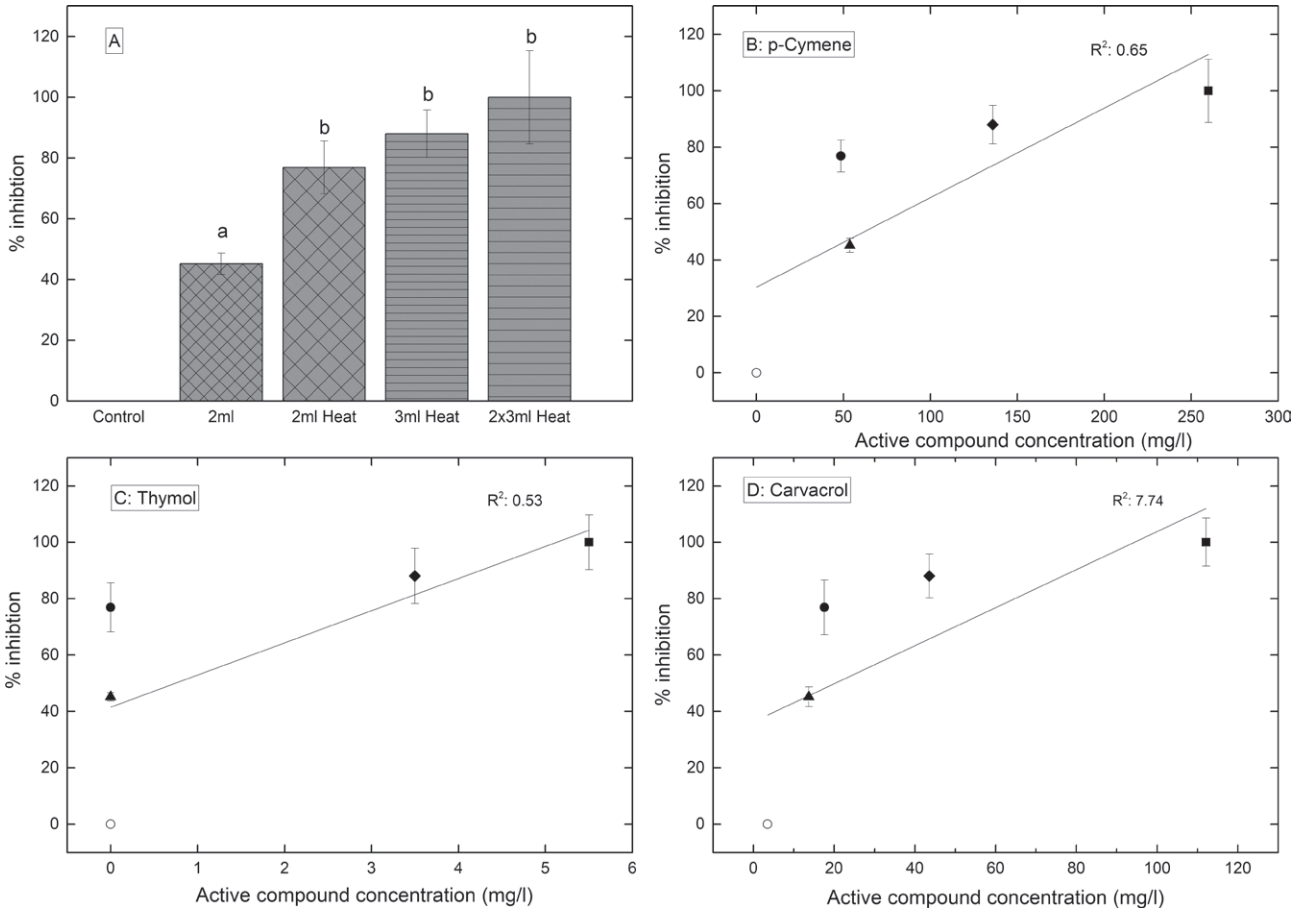

Figure 4. A) Mean growth inhibition proportions (%) for *Botrytis cinerea* on individual grape berries after 48 h exposure to different oregano EO exposure treatments. B), C) and D), mean growth inhibition of *B. cinerea* colonies exposed for 48 h to different concentrations of three EO components at different concentrations. Individual analyses of the relationships between each active component and percent growth inhibition are indicated. Scatter plot point shapes correspond to the same shape shown below each treatment parameter on the bar graph. Different letters indicate significant differences ($P < 0.05$) between treatments and controls.

proportions for the treatment parameters are shown in Table 8. For the controls (no oil treatment) and for treatments including heat, the dish containing oil was placed on top of a heating pad. In the treatment including two oil dishes, one was placed in the pump chamber with a heating pad, and the other was placed in the treatment chamber directly under the Petri dishes, resulting in an 100% inhibition of growth (Figure 4).

EO component compounds measured with GC-FID are indicated in Figure 4, which shows the concentrations of the active compounds p-cymene, thymol, and carvacrol in relation to the different dosage parameters. Components with concentrations less than the LOQ (3.50 mg L^{-1}) and LOD (2.50 mg L^{-1}) were plotted with a baseline value of zero.

The active component p-cymene was present at the greatest concentrations in all the trials, with concentrations of 53.7 mg L^{-1}, 48.5 mg L^{-1}, 135.9 mg L^{-1}, and 259.9 mg L^{-1}, where 259.9 mg L^{-1} corresponded to 100% inhibition of *B. cinerea* growth. Carvacrol was present at the second greatest concentrations throughout all the experimental trials, with concentrations of 13.7 mg L^{-1}, 17.6 mg L^{-1}, 43.6 mg L^{-1}, and 112.1 mg L^{-1}, where 112.1 mg L^{-1} corresponded to 100% inhibition. Thymol was present at low concentrations during all the trials, with concentrations of <LOQ, <LOQ, 3.5 mg L^{-1}, and 5.2 mg L^{-1}, where 5.2 mg L^{-1} corresponded to 100% inhibition. In this case, the concentrations of active compounds giving 50% inhibition of mycelial growth (EC_{50}; Badawy and Abdelgaleil, 2014), could be estimated using the concentrations obtained by GC-FID analysis after trial I, where 45.2% inhibition of mycelium growth inhibition was achieved. These estimated EC_{50} values in the vapour states were: for p-cymene, 53.7 mg

Table 8. Percent *Botrytis cinerea* colony growth inhibition and corresponding treatment parameters and EO dosages.

	Control	2 mL no heat	2 mL heat	3 mL heat	2 × 3 mL heat
Mycelium growth inhibition (%)	0	45.2	76.9	88	100

L^{-1}; for carvacrol, 13.70 mg L^{-1}; and for thymol, <3.50 mg L^{-1}.

Two-way ANOVA of the relationship between concentration of active compounds and percent inhibition of radial growth of *B. cinerea* showed significant relationships ($P < 0.05$) for all three compounds.

DISCUSSION

There is urgent need in global food production for natural alternatives to synthetic fungicides. The results of the present study confirm the findings of previous studies which have reported effectiveness of EOs and their major components, specifically that of oregano and particularly in the vapour state, as alternatives for management of fungal diseases (Dagostin *et al.*, 2010; Soylu *et al.*, 2010; Matusinsky *et al.*, 2015; Rienth *et al.*, 2019; Babalık *et al.*, 2020). However, direct treatment with EOs has several drawbacks, which probably explains why the observed inhibition of fungal development is often inconsistent in field experiments (Dagostin *et al.*, 2010). In the present study, we developed an innovative experimental approach that enabled applications of EO vapour continuously to Petri dishes and to grape berries inoculated with *B. cinerea*.

In vitro *treatment with essential oil vapour against* Botrytis cinerea

Three experiments were carried out to evaluate the effectiveness of vapour from the oregano EO for inhibition of radial colony growth of *B. cinerea*. All treatments reduced the growth of the fungus, with the greatest inhibition in trial III, where an additional dish containing the EO was placed directly under inoculated Petri dishes inside the fumigation treatment chamber. These results are consistent with previous findings (Daferera *et al.*, 2003; Aminifard and Mohammadi, 2012; Vitoratos *et al.*, 2013), where oregano EO and EOs of thyme, dictamnus, marjoram, lemon, and black caraway, completely inhibited the growth of *B. cinerea* under *in vitro* conditions. The present results highlight that the vapour phase of EOs has direct antifungal effects against *B. cinerea*, in a dose-dependent manner, and is not only through stimulation of innate plant immunity as shown in previous studies (Rienth *et al.*, 2019).

In vivo *treatment of grape berries with essential oil vapour*

In vivo experimentation was carried out on detached grape berries to determine the effectiveness of vapour treatments. Treatments were applied in four trials, each of which resulted in inhibition of *B. cinerea* growth. The extent of fungal growth in cultures and inhibition of fungal growth on berries varied during the different trials, with the most consistent growth and inhibition patterns observed in trials II and IV. These results are consistent with the findings of other studies carried out on harvested fruits and vegetables, as well as on growing plants. For example, in *V. vinifera* cv. Chasselas vines, Rienth *et al.* (2019) found 95% inhibition of the growth of *P. viticola* after treatment with vapour of oregano EO. Efficacy was mainly associated with stimulation of grapevine innate immunity by the EO. Aminifard and Mohammadi (2012) demonstrated reduced decay caused by *B. cinerea* on plum fruit treated with EO of black caraway. Soylu *et al.* (2010) demonstrated the ability of EOs of oregano, lavender and rosemary, applied as contact and vapour phases, to reduce disease on *B. cinerea*-infected tomatoes. These EOs inhibited fungal growth in dose-dependent manners, with the vapour phase treatments being more effective at low dosages than the contact phase treatments. Soylu *et al.* (2007) showed the effectiveness of soil amendments with the EOs of oregano and fennel for protection of tomato seedlings against *S. sclerotiorum*. The antifungal effects of oregano EO were also observed by Vitoratos *et al.* (2013), where treatments with the EO completely inhibited the growth of *B. cinerea* in tomato plants. The present study highlighted the effective inhibition of fungal growth and emphasized the efficacy of the volatile phase against fungal pathogens, which is of interest for development of sustainable treatment strategies. These could rely on EO vapour diffusion systems or encapsulated EOs to circumvent commonly encountered drawbacks of direct application and decrease phytotoxicity. The present results confirm the direct effects of EO vapour on the fungus hyphae since treatments were applied to detached fruits. This was also shown with the scanning electron microscope analysis carried out in a similar experiment by Soylu *et al.* (2010).

Residues on berry skins and in berry flesh after treatment with essential oil vapour

An important question regarding the persistence of aroma compounds on fruit after treatment has not been reported in previous research. In the present study, consideration of the impacts of residual active molecules on cv. Chasselas berries was a fundamental question, because of the importance of aroma compounds in winegrapes. GC-FID analyses of the active compounds present in the residues left on berry skins, and those absorbed into berry flesh, showed consistently low concentrations of p-cymene in both trials. Carvacrol was present at high concentrations in the berry flesh, but at low concentrations on berry skins during trial II, but during trial III, this compound was at low concentrations on berry flesh and surfaces. Thymol was consistently present at slightly greater concentrations than the other two compounds on the berry surfaces and in berry flesh during both rounds of treatment.

The persistence of the different active molecules can be determined by comparing the total concentrations of the molecules present during treatment in the chamber with the residual concentrations left on the berries after treatment. P-cymene had the greatest concentration in the chamber during treatment but the lowest residual concentrations after treatment, showing its persistence to be low. Marchese *et al.* (2017) reported a short half-life for p-cymene, resulting in rapid absorption and rapid *in vivo* elimination. Carvacrol was also present at high concentrations in the chamber during treatment and at low residual concentrations, with the exception of the berry absorption levels, in trial II. This also showed that carvacrol had low persistence on berries after treatment. Thymol showed very high persistence, with high residual concentrations on berry skins and in berry flesh after treatment. The concentrations of thymol were also greater, in some cases, in the control samples than in the treatment samples for both surface residues and berry absorption. This could be due to the presence of residual concentrations of thymol left in the chamber from previous trials that involved EO treatments. As demonstrated in a previous study, lemons treated with carvacrol and thymol for postharvest fungal protection exhibited persistence of these compounds directly after application, which disappeared shortly thereafter, leaving aroma and taste of the fruit unaffected (Castillo *et al.*, 2014).

Continued research on the concentrations of active compounds present in wine grapes treated with EOs is important before moving forward with the next research steps, primarily using sensory analyses. It must be determined that the berries are safe for human consumption. According to the National Cancer Institute, most EOs are considered to be safe and without adverse side effects. Only natural substances with EC_{50} > 20 µg m L^{-1} are considered toxic to human cells (Puškárová *et al.*, 2017). In the present study, all of the total concentrations of p-cymene, thymol, and carvacrol left on the berries after treatment were below this threshold, with the exception of the concentration of carvacrol in berry flesh after the trial II treatments. The concentrations used for comparisons correspond to the total concentrations present during treatment, not specifically to the EC_{50} dosages. For the samples in question, the total concentration of carvacrol (35.68 mg L^{-1}) present in berry flesh after treatment gave 70.9% inhibition of mycelium growth. Although sensory analysis was not carried out in this experiment, compared to the average sensory threshold reported for panelists by Bitar *et al.* (2008), we observed that the average concentration of carvacrol in berry flesh was 11.06 mg L^{-1}, which was greater than the sensory threshold of 3.1 mg L^{-1} for this compound. The equivalent thymol concentration in berry flesh was 7.57 mg L^{-1}, which is less than the sensory threshold of 12.4 mg L^{-1}. The p-cymene concentration was <LOQ and was considerably less than the sensory threshold of 79.4 mg L^{-1} reported by Bitar *et al.* (2008). Because of the probability of sensory detection of carvacrol in treated berries as well as the potential for damage to berries after treatment, it is important that the EO dosages are applied at quantities that are efficient at impeding fungal growth without causing undesirable secondary effects.

Impacts of vapour concentrations on Botrytis cinerea *growth inhibition*

Five experiments were carried out to assess the relationships between the concentration of active EO compounds and inhibition of *B. cinerea* mycelium growth. Doses and treatment parameters were adjusted for each trial to increase the concentration of vapour in the fumigation chamber. Fumigation with the oregano EO inhibited the radial growth of *B. cinerea* in a dose-dependent manner.

After the end of the 3-d treatment period, test dishes were observed for an additional 4-d period, during which no fumigation was applied. For dishes treated with p-cymene at 135.9 mg L^{-1} or 259.9 mg L^{-1}, carvacrol at 43.6 mg L^{-1} or 112.1 mg L^{-1} or thymol at 3.5 or 5.2 mg L^{-1}, no additional growth was seen during the post-treatment observations. This indicated that the greater dosages killed *B. cinerea* conidia. Dishes treated with p-cymene (53.7 mg L^{-1}, 48.5 mg L^{-1}), carvacrol (13.7 mg L^{-1}, 17.6 mg L^{-1}), and thymol (<LOQ, <LOQ), exhibited slow, minimal growth after the 3-d treatment period, but

the growth never reached the total Petri plate diameter of 90 mm. All of the control sample plates that were not treated with any EO had reached this diameter after the 3 d treatment period, and continued vigorous growth was observed throughout the 4-d observation period. These observations indicate that the three analyzed terpenic components of oregano EO interacted with fundamental *B. cinerea* cell functions, rendering the pathogen incapable of growing. Prediction of the antifungal mechanisms of EOs and interpretation of the results in the present study indicated that damage to the cell structure of *B. cinerea* had occurred, resulting in inhibition of vigorous growth after treatments with low dosages of the oil, and total inhibition of growth after treatment with greater dosages.

The EC_{50} values for p-cymene (53.7 mg L^{-1}), carvacrol (13.7 mg L^{-1}) and thymol (<3.50 mg L^{-1}) were similar to those reported in previous studies, where the EO of oregano was used for control of fungal pathogens (Badawy and Abdelgaleil, 2014). The oregano EO gave the lowest EC_{50} compared to the EOs of *P. graveolens, S. cumini* and *V. agnus-castus*. This was the reason for focusing on the oregano EO in the present experiments. The EC_{50} values for the oregano EO against *B. cinerea* (44 mg L^{-1} for the vapour phase and 241 mg L^{-1} for the contact phase) reported by Soylu *et al.* (2010) also correspond to those reported in the present study, and demonstrate the improved effectiveness of EO treatments in volatile phases. Figure 4 shows the low concentration of thymol compared to the concentrations of carvacrol and p-cymene. However, it cannot be concluded how the different terpenes contributed individually to the antifungal activity of EO vapour due to the importance of their synergistic effects.

Although significant alterations to hyphal morphology and cell structure have been observed in numerous studies, the specific mechanisms of antifungal activity of EOs have not been fully elucidated (Soylu *et al.*, 2010). Recent research indicates that inhibition of fungal pathogens can be partly due to immune responses triggered within host plants after treatment with EOs, which activate genes responsible for syntheses of compounds involved in plant immune systems and defense response pathways (Rienth *et al.*, 2019). Priming of these defense response mechanisms in plants after treatment with oregano EO has been shown in *V. vinifera* cv. Chasselas (Rienth *et al.*, 2019), in apples after treatment with the EO of thyme (Banani *et al.*, 2018), in strawberries after treatment with tea tree and thyme EOs (Liu *et al.*, 2016), and in *Arabidopsis thaliana* after treatment with the EO of *Gaultheria procumbens* (Vergnes *et al.*, 2014).

CONCLUSION

The present study has highlighted the remarkable capability of EOs, specifically that of *O. vulgare*, as effective antifungal agents. The study confirmed the ability of the EO to completely inhibit the *in vitro* growth of *B. cinerea*, and to inhibit the pathogen development on grapevine berries. The study also demonstrated the efficacy of the EO in vapour phase using innovative experimental procedures. These results emphasize that EOs are promising alternatives to synthetic and copper-based fungicides currently being used in agriculture and food industries. The results of vapour phase efficacy indicate potential for development of disease management systems using vapor diffusion in crops. These could be more efficient than direct applications since they could circumvent commonly encountered problems due to poor rain fastness, mixability or degradation of fungicide compounds.

Botrytis cinerea causes considerable economic losses in agriculture, and is one of the most damaging pathogens in vineyards. Finding environmentally sustainable treatments against this pathogen is, therefore, very important.

Further research is required to fully understand the effects of EOs on fungal diseases and the mechanisms of the antifungal activity. To fully implement the practical usage of EOs as viable alternatives to the fungicides on which agriculture heavily relies, further research is also required to determine the impacts of these materials on living plants and particularly on harvested fruits.

AUTHOR CONTRIBUTIONS

AB and MR designed the experiments. AB carried out the experiments. MR and AB analyzed the data. AB and MR wrote the paper.

ACKNOWLEDGEMENTS

The authors thank Marilyn Cleroux for conducting the GC-FID analyses, Arnaut Pernet for technical support with the climate chamber vaporization system, and Jean-Philppe Burdet for fruitful discussions. This research was part of the project IZCOZ0_189896 financed by the Swiss National Science Foundation (SNF).

LITERATURE CITED

Aktar M.W., Sengupta D., Chowdhury A., 2009. Impact of pesticides use in agriculture: their benefits and hazards. *Interdisciplinary Toxicology* 2: 1–12.

Alleweldt G., Possingham J.V., 1988. Progress in grapevine breeding. *Theoretical and Applied Genetics* 75: 669–673.

Aminifard M.H., Mohammadi S., 2012. Essential oils to control *Botrytis cinerea* in vitro and in vivo on plum fruits. *Journal of the Science of Food and Agriculture* 93: 348–353.

Babalık Z., Onursal C.E., Erbaş D., Koyuncu M.A., 2020. Use of carvacrol helps maintain postharvest quality of Red Globe table grape. *Journal of Animal and Plant Sciences* 30: 655–662.

Badawy M.E.I., Abdelgaleil S.A.M., 2014. Composition and antimicrobial activity of essential oils isolated from Egyptian plants against plant pathogenic bacteria and fungi. *Industrial Crops and Products* 52: 776–782.

Banani H., Olivieri L., Santoro K., Garibaldi A., Gullino M.L., Spadaro D., 2018. Thyme and savory essential oil efficacy and induction of resistance against *Botrytis cinerea* through priming of defense responses in apple. *Foods* 7: 11.

Bitar A., Ghaddar T., Malek A., Haddad T., Toufeili I., 2008. Sensory thresholds of selected phenolic constituents from thyme and their antioxidant potential in sunflower oil. *Journal of the American Oil Chemists' Society* 85: 641–646.

Bouchra C., Achouri M., Idrissi Hassani L.M., Hmamouchi M., 2003. Chemical composition and antifungal activity of essential oils of seven Moroccan Labiatae against *Botrytis cinerea* Pers: Fr. *Journal of Ethnopharmacology* 89: 165–169.

Bowman S.M., Free S.J., 2006. The structure and synthesis of the fungal cell wall. *BioEssays* 28: 799–808.

Castillo S., Pérez-Alfonso C.O., Martínez-Romero D., Guillén F., Serrano M., Valero D., 2014. The essential oils thymol and carvacrol applied in the packing lines avoid lemon spoilage and maintain quality during storage. *Food Control* 35: 132–136.

Ciliberti N., Fermaud M., Roudet J., Languasco L., Rossi V., 2016. Environmental effects on the production of *Botrytis cinerea* conidia on different media, grape bunch trash, and mature berries. *Australian Journal of Grape and Wine Research* 22: 262–270.

Daferera D.J., Ziogas B.N., Polissiou M.G., 2003. The effectiveness of plant essential oils on the growth of *Botrytis cinerea*, *Fusarium* sp. and *Clavibacter michiganensis* subsp. michiganensis. *Crop Protection* 22: 39–44.

Dagostin S., Formolo T., Giovannini O., Pertot I., Schmitt A., 2010. *Salvia officinalis* extract can protect grapevine against *Plasmopara viticola*. *Plant Disease* 94: 575–580.

Edris A.E., Farrag E.S., 2003. Antifungal activity of peppermint and sweet basil essential oils and their major aroma constituents on some plant pathogenic fungi from the vapor phase. *Nahrung/Food* 47: 117–121.

Elad Y., Vivier M., Fillinger S., 2016. *Botrytis*, the good, the bad and the ugly. In: *Botrytis – the Fungus, the Pathogen and its Management in Agricultural Systems* (S. Fillinger, Y. Elad, ed.), Springer International Publishing, Cham, Switzerland, 1–15.

Elmer P.A.G., Michailides T.J., 2007. Epidemiology of *Botrytis cinerea* in orchard and vine crops. In: *Botrytis: Biology, Pathology and Control* (Y. Elad, B. Williamson, P. Tudzynski, N. Delen, ed.), Springer, Dordrecht, Netherlands, 243–272.

European Commission Eurostat, 2007. *The Use of Plant Protection Products in the European Union: Data 1992-2003*. Publications Office of the European Union, Luxembourg, Europe.

Fischer B.M., Salakhutdinov I., Akkurt M., Eibach R., Edwards K.J., … Zyprian E.M., 2004. Quantitative trait locus analysis of fungal disease resistance factors on a molecular map of grapevine. *Theoretical and Applied Genetics* 108: 501–515.

Fuller K.B., Alston J.M., Sambucci O.S., 2014. The value of powdery mildew resistance in grapes: evidence from California. *Wine Economics and Policy* 3: 90–107.

Gog L., Berenbaum M.R., DeLucia E.H., Zangerl A.R., 2005. Autotoxic effects of essential oils on photosynthesis in parsley, parsnip, and rough lemon. *Chemoecology* 15: 115–119.

Guetsky R., Shtienberg D., Elad Y., Dinoor A., 2001. Combining biocontrol agents to reduce the variability of biological control. *Phytopathology* 91: 621–627.

Hu Y., Zhang J., Kong W., Zhao G., Yang M., 2017. Mechanisms of antifungal and anti-aflatoxigenic properties of essential oil derived from turmeric (*Curcuma longa* L.) on *Aspergillus flavus*. *Food Chemistry* 220: 1–8.

Jacometti M.A., Wratten S.D., Walter M., 2010. Review: alternatives to synthetic fungicides for *Botrytis cinerea* management in vineyards. *Australian Journal of Grape and Wine Research* 16: 154–172.

Komárek M., Čadková E., Chrastný V., Bordas F., Bollinger J.C., 2010. Contamination of vineyard soils with fungicides: a review of environmental and toxicological aspects. *Environment International* 36: 138–151.

Liu S., Shao X., Wei Y., Li Y., Xu F., Wang H., 2016. *Solidago canadensis* L. essential oil vapor effectively inhibits *Botrytis cinerea* growth and preserves postharvest quality of strawberry as a food model system. *Frontiers in Microbiology* 7: 1179–1179.

Marchese A., Arciola C.R., Barbieri R., Silva A.S., Nabavi S.F., … Nabavi S.M., 2017. Update on monoterpenes as antimicrobial agents: a particular focus on p-cymene. *Materials* 10: 947.

Matusinsky P., Zouhar M., Pavela R., Novy P., 2015. Antifungal effect of five essential oils against important pathogenic fungi of cereals. *Industrial Crops and Products* 67: 208–215.

Mohammadi S., Aroiee H., Aminifard M.H., Tehranifar A., Jahanbakhsh V., 2013. Effect of fungicidal essential oils against *Botrytis cinerea* and *Rhizopus stolonifer* rot fungus in vitro conditions. *Archives of Phytopathology and Plant Protection* 47: 1603–1610.

Naegele R.P., 2018. Evaluation of host resistance to Botrytis bunch rot in *Vitis* spp. and its correlation with Botrytis leaf spot. *HortScience* 53: 204–207.

Nazzaro F., Fratianni F., Coppola R., De Feo V., 2017. Essential oils and antifungal activity. *Pharmaceuticals* 10: 86.

Paňitrur-De La Fuente C., Valdés-Gómez H., Roudet J., Acevedo-Opazo C., Verdugo-Vásquez N., … Fermaud M., 2018. Classification of winegrape cultivars in Chile and France according to their susceptibility to *Botrytis cinerea* related to fruit maturity. *Australian Journal of Grape and Wine Research* 24: 145–157.

Puškárová A., Bučková M., Kraková L., Pangallo D., Kozics K., 2017. The antibacterial and antifungal activity of six essential oils and their cyto/genotoxicity to human HEL 12469 cells. *Scientific Reports* 7: 8211.

Rao A., Zhang Y., Muend S., Rao R., 2010. Mechanism of antifungal activity of terpenoid phenols resembles calcium stress and inhibition of the TOR pathway. *Antimicrobial Aagents and Chemotherapy* 54: 5062–5069.

Rienth M., Crovadore J., Ghaffari S., Lefort F., 2019. Oregano essential oil vapour prevents *Plasmopara viticola* infection in grapevine (*Vitis vinifera*) and primes plant immunity mechanisms. *PLoS One* 14: e0222854.

Sakkas H., Papadopoulou C., 2017. Antimicrobial activity of basil, oregano, and thyme essential oils. *Journal of Microbiology and Biotechnology* 27: 429–438.

Soylu E.M., Kurt Ş., Soylu S., 2010. In vitro and in vivo antifungal activities of the essential oils of various plants against tomato grey mould disease agent *Botrytis cinerea*. *International Journal of Food Microbiology* 143: 183–189.

Soylu S., Yigitbas H., Soylu E.M., Kurt Ş., 2007. Antifungal effects of essential oils from oregano and fennel on *Sclerotinia sclerotiorum*. *Journal of Applied Microbiology* 103: 1021–1030.

Teixeira B., Marques A., Ramos C., Serrano C., Matos O., … Nunes M.L., 2013. Chemical composition and bioactivity of different oregano (*Origanum vulgare*) extracts and essential oil. *Journal of the Science of Food and Agriculture* 93: 2707–2714.

Vergnes S., Ladouce N., Fournier S., Ferhout H., Attia F., Dumas B., 2014. Foliar treatments with *Gaultheria procumbens* essential oil induce defense responses and resistance against a fungal pathogen in *Arabidopsis*. *Frontiers in Plant Science* 5: 477.

Vitoratos A., Bilalis D., Karkanis A., Efthimiadou A., 2013. Antifungal activity of plant essential oils against *Botrytis cinerea*, *Penicillium italicum* and *Penicillium digitatum*. *Notulae Botanicae Horti Agrobotanici* 41: 86–92.

Phytopathologia Mediterranea
The international journal of the
Mediterranean Phytopathological Union

Firenze University Press
www.fupress.com/pm

New or Unusual Disease Reports

Plenodomus biglobosus on oilseed rape in Hungary

Bianka BAGI[1], Csaba NAGY[2], Annamária TÓTH[1], László PALKOVICS[1], Marietta PETRÓCZY[1,*]

[1] *Department of Plant Pathology, Faculty of Horticultural Science, Szent István University, 44. Ménesi road, Budapest, Hungary H-1118*
[2] *KWS Hungary Ltd., 4. Gesztenyefa street, Győr (Industrial Park Service House), Hungary, H-9027*
*Corresponding author: petroczy.marietta@kertk.szie.hu

Summary. The commonly occurring blackleg is an economically important disease in oilseed rape cultivation. This disease is caused by a complex of two closely related species, *Plenodomus lingam* and *P. biglobosus*. To date, only *P. lingam* (syn.: *Leptosphaeria maculans*) has been known in Hungary as the cause of blackleg in oilseed rape crops. The present study aimed to determine if *P. biglobosus* (syn.: *Leptosphaeria biglobosa*) was present in Hungary. The two fungus pathogens are difficult to distinguish using conventional morphological criteria. Reliable detection and differentiation of the two species can only be achieved using molecular methods. This is the first report describing the pathogen, *P. biglobosus*, in Hungary.

Keywords. *Brassica napus*, blackleg, multiplex PCR, ITS region.

OPEN ACCESS

Citation: B. Bagi, C. Nagy, A. Tóth, L. Palkovics, M. Petróczy (2020) *Plenodomus biglobosus* on oilseed rape in Hungary. *Phytopathologia Mediterranea* 59(2): 345-351. DOI: 10.14601/Phyto-11099

Accepted: June 2 , 2020

Published: August 31, 2020

Data Availability Statement: All relevant data are within the paper and its Supporting Information files.

Competing Interests: The Author(s) declare(s) no conflict of interest.

Editor: Thomas A. Evans, University of Delaware, Newark, DE, United States.

INTRODUCTION

Blackleg or stem canker of oilseed rape is an internationally important disease of oilseed brassicas (oilseed rape, canola) (Rouxel and Balesdent, 2005). In Brassica-growing areas (especially in Australia, North America and Europe) this disease can cause severe yield losses (Henderson, 1918; Fitt *et al*., 2006). The disease is associated with two closely related fungi, *Plenodomus lingam* and *P. biglobosus* (Dilmaghani *et al*., 2009). These fungi have been referred to as *Leptosphaeria* species, but recent studies reveal that they belong in *Plenodomus* (de Gruyter *et al*., 2012; Wijayawardene *et al*., 2014). Co-existence of these two pathogens has been reported in different countries of Europe, including Poland (Kaczmarek and Jędryczka, 2011), Lithuania (Brazauskienė *et al*., 2011) and the Czech Republic (Mazáková *et al*., 2017).

Varga (2014) noted that the disease caused by *P. lingam* had become a significant factor in oilseed rape cultivation in the Carpathian Basin. Aggressive and non-aggressive isolates of *P. lingam* could be differentiated, based on restriction fragment length polymorphism (RFLP) analyses (Koch *et al*., 1991). Two groups of *P. lingam* isolates can be further separated, based on their abil-

ities to produce phytotoxins *in vitro* (Koch *et al*., 1989). The isolates producing phytotoxin were defined as Tox^+, while non-toxin-producing isolates were defined as Tox^0 (Balesdent *et al*., 1992). The weakly virulent Tox^0 isolates (designated as the new species *P. biglobosus* since 2001) can cause necrotic lesions on the upper stems of plants, and are less likely to cause stem cankers than Tox^+ isolates (Shoemaker and Brun, 2001; West *et al*., 2002).

In 2010, samples from *Brassica napus* stems from near Rimski Šančevi, Serbia, with symptoms of canker were cultured, and some of the resulting isolates were identified as *P. biglobosus* (Mitrović *et al*., 2016). Due to the proximity of this region to Hungary, there was reason to assume that *P. biglobosus* could also be present in Hungary. Therefore, the aim of the present study was to determine if *P. biglobosus* was present in this country.

MATERIALS AND METHODS

Plant samples, fungus isolation and morphology

Leaves and stems of oilseed rape plants showing symptoms of blackleg were collected from oilseed rape hybrids in fields from four counties in Hungary in 2017 and 2018. Samples were transferred to the laboratory of the Department of Plant Pathology, Szent István University. Unsterilized samples were placed in humidity chambers made from 30 cm diam. Petri dishes each containing a layer of filter paper moistened with sterile distilled water to induce the pycnidia to exude cirri of conidia. Three days later, conidia were collected with sterile handmade glass needles, using the method of Goh (1999), and were suspended in sterile distilled water. Size and shape of 50 conidia per sample were characterized. Conidium size data were evaluated using multivariate analysis of variance (MANOVA). Normality of residuals was checked using the Shapiro-Wilk test, homogeneity of variances was assessed using Levene's test. Multivariate differences between samples were determined using the Wilk's-lambda (Tabachnick and Fidell, 2013).

Conidium suspensions were transferred onto potato dextrose agar (PDA, BioLab Zrt.), distributed using a spread plate technique, and then incubated for 3–4 d in the dark at 24 ± 1°C. Hyphal tips from germinating conidia (observed under an inverted microscope) were aseptically transferred onto fresh PDA plates using sterile dissection needles. Monoconidial isolates were characterized after 28 d. Macroscopic traits (growth rates, colour of mycelia, colony shapes, edges and patterns, amounts of aerial mycelium, presence of fruiting bodies, and pigment secretion) and microscopic traits (colour, shape and sizes of conidia) of fungal isolates were recorded.

Within two years, 188 plant samples were collected, and 54 *Plenodomus lingam* isolates were obtained. Three putative *P. biglobosus* isolates were chosen for detailed comparison with four *P. lingam* isolates.

Pathogenicity tests

Pathogenicity of the isolates was tested by inoculating the stems of live seedlings and detached leaves of oilseed rape seedlings. The seedlings were grown in potting mix soil from seeds that were untreated by fungicides, and were kept in the greenhouse of the Department of Plant Pathology (Buda Campus) for 2 months at 26 ± 3°C. Five seedlings were each injured above the cotyledons in V shape, using a sterile dissection needle, and were then inoculated with hyphal tip mycelium from 7–10 d-old PDA colonies. Five detached leaves were each inoculated at the main vein on the upper surface without puncturing, with each of seven different isolates. The detached leaves were then placed in sterile glass vessels containing sterilized glass beads and sterile distilled water in order, to maintain 95 ± 3% relative humidity. Control seedlings and control detached leaves were treated as for inoculated specimens with sterile pieces of PDA. The inoculated seedlings and the glass vessels containing the detached leaves were incubated under natural light conditions at room temperature for 10 d. Re-isolations from symptomatic tissues were made onto PDA to fulfil Koch's postulates. The pathogenicity test was repeated once.

DNA extraction from fungi, amplification in multiplex PCR and sequencing

Genomic DNA was extracted from the growing margins of single conidium colonies on PDA, using the cetyl-trimethyl-ammonium-bromide (CTAB) method (Maniatis *et al*., 1983), followed by phenol-chloroform extraction and isoamyl alcohol (24:1) precipitation. The concentration and purity of the DNA were evaluated using a NanoDropTM Spectrophotometer.

The ribosomal RNA region incorporating the internal transcribed spacer (ITS) regions and the 5.8S rRNA gene from *Plenodomus* isolates were amplified by multiplex PCR. The reverse primer LmacR (5' GCAAAATGTGCTGCGCTCCAGG 3') specific for *P. lingam* and *P. biglobosus*, and two species-specific forward primers; LmacF (5' CTTGCCCACCAATTGGATCCCCTA 3', for *P. lingam*) and LbigF (5' ATCAGGGGATTGGTGTCAGCAGTTGA 3', for *P. biglobosus*) were used (Liu *et al*., 2006). Two different PCR products were reliably

detected: one of 331 bp from *P. lingam* isolates, and the other of 444 bp from *P. biglobosus* isolates.

PCR mixtures were prepared in a reaction volume of 50 µL, containing 15 ng genomic DNA, 0.2 µM forward and reverse primer, 200 µM dNTPs, 2.5 mM $MgCl_2$ and 0.4 U DreamTaq Polymerase (Thermo Scientific) in 10× Dream Taq Buffer (Fermentas). Amplifications were carried out in a GeneAmp PCR System 9700 thermal cycler (Applied Biosystems), using amplification conditions consisting of denaturation at 95°C for 3 min, followed by 30 cycles of the following steps: denaturation at 95°C for 15 sec, annealing at 70°C for 30 sec, and extension at 72°C for 60 sec, with a final extension step at 72°C for 10 min. PCR products specific for *P. lingam* and *P. biglobosus* were electrophoretically separated in 1% agarose gel run in 1× TBE buffer. The gel was stained with EcoSafe stain and the products were visualized and photographed under UV light. The amplicons were purified using the High Pure PCR Product Purification Kit (Roche). Fragments were sequenced in both directions using the same primers as for PCR, in an ABI Prism automatic sequencer (BaseClear B.V.). Nucleotide sequence identities were determined by BLAST analyses.

RESULTS AND DISCUSSION

In 2017 and 2018, leaf and stem spots were observed on oilseed rape plants as specific symptoms of blackleg. Greyish lesions containing numerous small, black pycnidia, appeared on lower leaves of affected plants. The symptoms were identical to those for blackleg of oilseed rape described in Western Australia (Bokor *et al*., 1975). The pathogens causing the disease were identified in 54 samples from the isolates examined in this study, using morphology and molecular biology methods. *Plenodomus biglobosus* was identified from leaf samples from Kétpó (47°04'S/20°28'W), and stem samples from Sza-

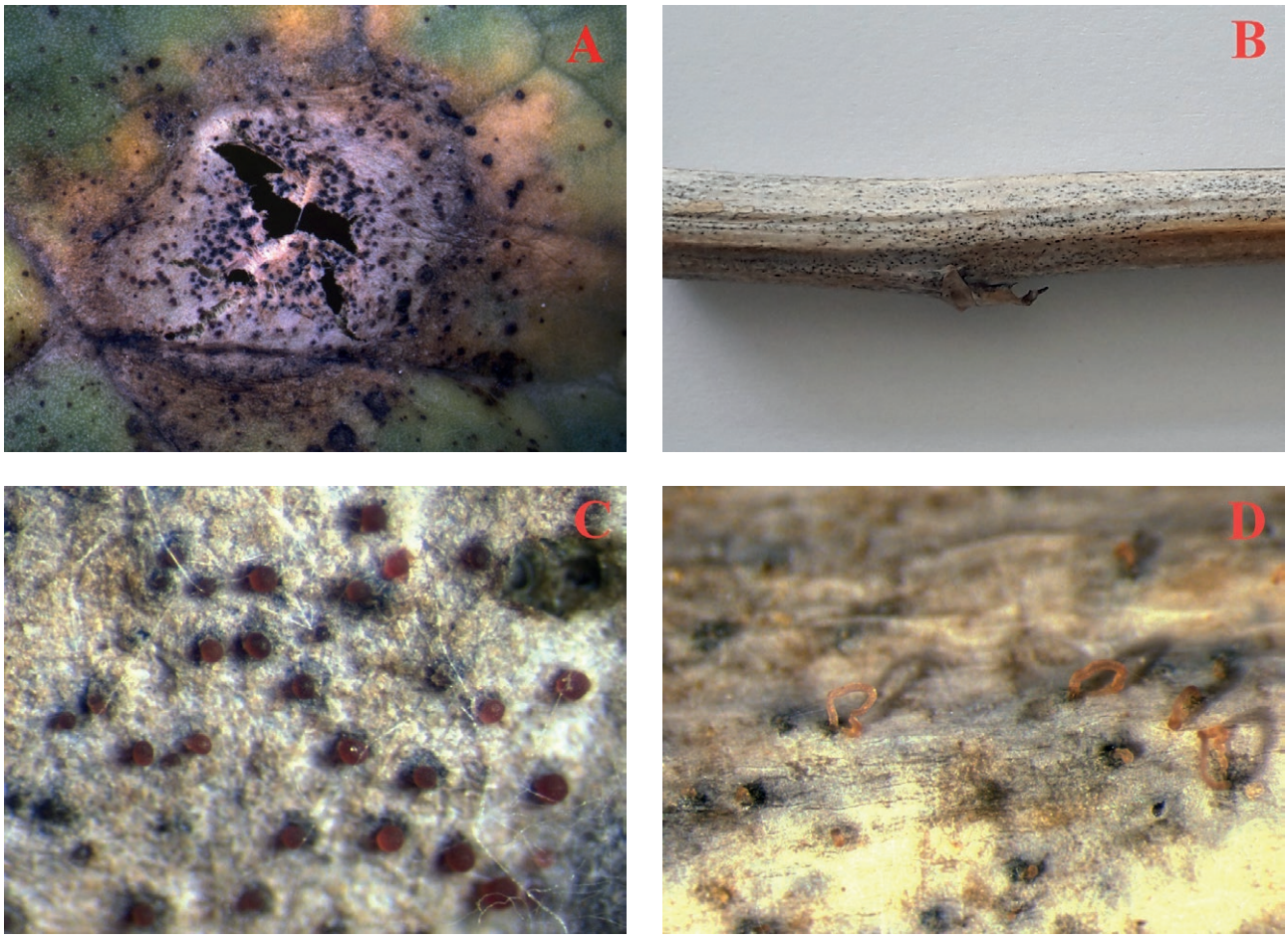

Figure 1. Leaf lesion on oilseed rape hybrid 'Marc KWS' (A), and stem necrosis with black pycnidia on hybrid 'Alvaro KWS' (B). Pycnidia on a leaf of hybrid 'Gordon KWS' (C) and a stem of hybrid 'Umberto KWS' (D).

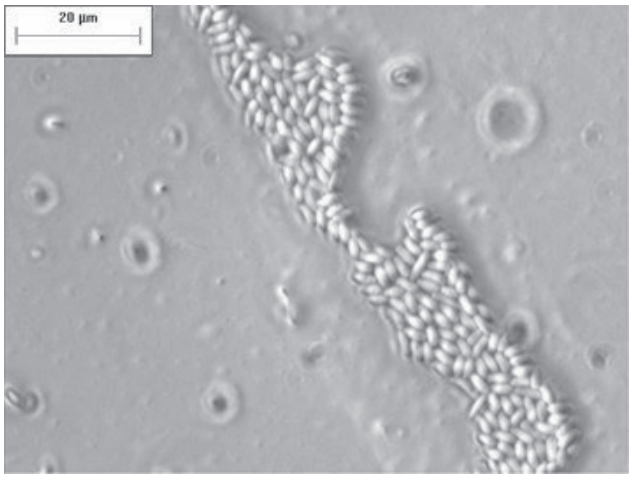

Figure 2. Conidia from *Plenodomus biglobosus*.

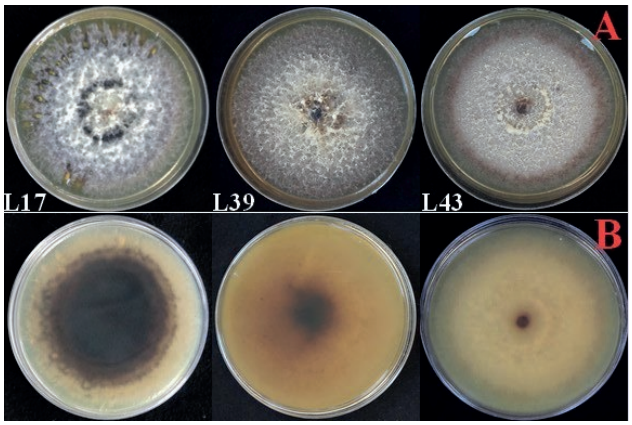

Figure 3. *Plenodomus biglobosus* colonies on PDA after 28 d. Upper surface (A) and lower surface (B).

lánta (45°93'S/18°23'W) and Tordas (47°33'S/18°76'W).

Plenodomus lingam and *P. biglobosus* caused small, circular patches on oilseed rape true leaves, that were 3–10 mm diam., with each lesion having a dark outer margin (Figure 1a). On diseased stems both pathogens produced broad, elongated necrotic lesions (Figure 1b). Dark pycnidia formed in leafspots. Conidial masses excreted from pycnidia, ranged in colour from claret to light brown (Figure 1c and d). It was not possible to distinguish the pathogens based on disease symptoms or morphology of pycnidia, as has been reported previously (Karolewski *et al*., 2007).

Conidia borne in pycnidia of *P. biglobosus* and *P. lingam* were hyaline, cylindrical, unicellular and were rounded at the ends (Figure 2). Dimensions of conidia are detailed in Table 1. Requirements were completed for the multivariate analysis of variance, Shapiro-Wilk test (P = 0.461 for conidium width; P = 0.745 for length) and Levene's test ($F_{(6;343)}$ = 0.568; P = 0.756 for width; $F_{(6;343)}$ = 1.198; P = 0.306 for length). Conidium dimensions for the different isolates did not differ significantly in length, or width (Wilk's-lambda = 0.96; P = 0.330), so conidium size was not reliable for identification of the isolates.

Eleven isolates out of the 54 samples were putatively identified on PDA medium as *P. biglobosus*, using the characteristics described by Mitrović *et al*. (2016) (Figure 3). The colour of colony upper surfaces was greyish, and the lower surfaces were dark greyish brown. Mitrović *et al*. (2016) detected yellow-brown pigments in substrate mycelia after 15 d. In the present study, yellow pigmentation was observed at the edges of the colonies and also in the PDA. In the middle of the colonies, there was abundant aerial mycelium. The colonies were round shape, with indeterminate edges. Calvert *et al*. (1949) described strains that were differed in production of pycnidia. In the present study, pycnidia were not observed in the colonies. Colony growth rates of the isolates are listed in Table 1. Colony form of *P. lingam* isolates was similar to that described by Mitrović and Marinković (2007).

Table 1. Host and plant organ sources, collection dates and regions of Hungary, average conidium dimensions and colony growth rates, for representative *Plenodomus* isolates assessed in this study.

Isolate	Host hybrid	Plant organ	Date of collection	Region of collection	Average conidium dimensions (µm)	Average colony growth rate (mm d^{-1})
L7	'Factor KWS'	stem	July 4th, 2017	Nagylózs	1.55×3.86	1.96
L17	'Marc KWS'	leaf	April 7th, 2018	Kétpó	1.57×3.73	2.71
L18	'Marc KWS'	leaf	April 7th, 2018	Kétpó	1.56×3.73	2.50
L26	'Hybrirock'	leaf	April 13th, 2018	Vadosfa	1.55×3.76	1.68
L34	'Hybrirock'	leaf	April 13th, 2018	Bősárkány	1.55×3.83	2.21
L39	'Umberto KWS'	stem	June 27th, 2018	Szalánta	1.57×3.75	2.64
L43	'Gordon KWS'	stem	June 28th, 2018	Tordas	1.55×3.78	2.67

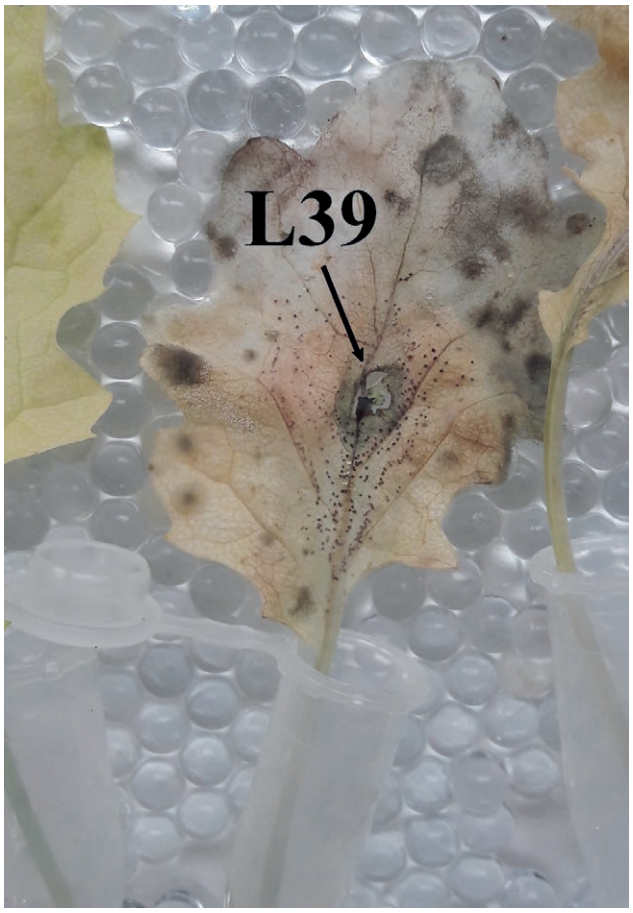

Figure 4. Necrotic lesion and pycnidia (arrow) caused by *Plenodomus biglobosus* (isolate L39) on an inoculated oilseed rape leaf after 10 d incubation.

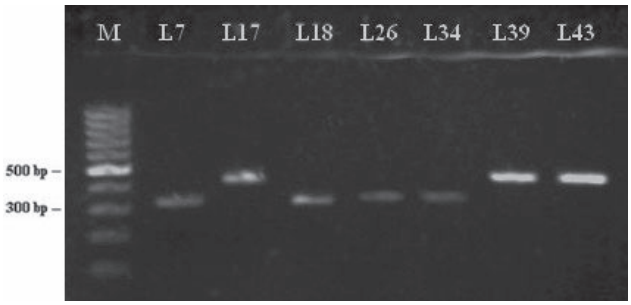

Figure 5. Gel electrophoresis pattern of some amplicons: a PCR product of 444 bp was amplified from *Plenodomus biglobosus* isolates L17, L39 and L43, and of 331 bp was amplified from *P. lingam* isolates L7, L18, L26 and L34. M indicates the GeneRuler 100 bp DNA ladder (Thermo Scientific).

In the pathogenicity tests *P. biglobosus* and *P. lingam* isolates caused browning and death of vascular bundles on oilseed rape seedlings at the inoculation points, after 2–3 d. After 10 d, necrosis was observed on inoculated seedlings, and on inoculated detached leaves. Pycnidia developed on some inoculated leaves (Figure 4). Control seedlings and control detached leaves did not show any symptoms. Koch's postulates were fulfilled by re-isolation of *P. biglobosus* from dark brown parts of the tissues of inoculated seedlings and detached leaves. The re-isolated isolates had the same cultural characteristics as the fungi used for the inoculations.

All of the samples were assessed by multiplex PCR with species specific primers: *P. biglobosus* was detected in 11 samples (20%), while *P. lingam* was detected in 43 samples (80%). Based on gel electrophoresis, the *P. biglobosus* isolates were clearly distinguishable from those of *P. lingam*, from their amplicon lengths (Figure 5). BLAST searches of the ITS sequences of the selected isolates matched the references with 99.7-100% similarity (Table 2).

The results presented here prove the presence of *P. biglobosus* associated with blackleg of oilseed rape

Table 2. Molecular identification and GenBank accession numbers of representative *Plenodomus* isolates assessed in this study.

Isolate	Molecular identification	DNA target[a]	GenBank accession No.	Blast match sequence		
				Reference accession No.	Coverage (%)	Identity (%)
L7	*Plenodomus lingam* (*Leptosphaeria maculans*)	ITS regions and the 5.8 rRNA gene	MK922353	*Leptosphaeria maculans* JF740234	100%	100%
L18			MK922979			
L26			MK922998			
L34			MK922973			
L17	*Plenodomus biglobosus* (*Leptosphaeria biglobosa*)		MK922972	*Leptosphaeria biglobosa* AJ542501	100%	99.7%
L39			MK922343			100%
L43			MK922971			

[a] ITS, internal transcribed spacer; rRNA, ribosomal RNA.

in Hungary. This pathogen has also been observed in neighbouring Serbia (Mitrovic *et al*., 2016). Further comprehensive monitoring and sampling is required to fully characterize distribution of this pathogen in Hungary. Both *Plenodomus* species initially infect the leaves of oilseed rape plants in autumn, leading to stem damage before harvest. However, little is known about role and the significance of *P. biglobosus* in the disease in Hungary, or the factors that influence host infection.

This is the first report of *P. biglobosus* infection of oilseed rape in Hungary.

ACKNOWLEDGEMENTS

This research was supported by the ÚNKP-18-2 New National Excellence Program of the Ministry of Human Capacities, Hungary, and by the Ministry for Innovation and Technology, Hungary, within the framework of the Higher Education Institutional Excellence Program (NKFIH-1159-6/2019) in the scope of plant breeding and plant protection researches of Szent István University.

LITERATURE CITED

Balesdent M.H., Gall C., Robin P., Rouxel T., 1992. Intraspecific variation in soluble mycelial protein and esterase patterns of *Leptosphaeria maculans* French isolates. *Mycological Research* 96: 677–684.

Bokor A., Barbetti M.J., Brown A.G.P., Mac Nish G.C., Wood P.McR., 1975. Blackleg of Rapeseed – Unless blackleg can be controlled there is little future for rapeseed as a major commercial crop in W. A. *Journal of Agriculture* 16: 7–10.

Brazauskienė I., Piliponytė A., Petraitienė E., Brazauskas G., 2011. Diversity of *Leptosphaeria maculans*/*L. biglobosa* species complex and epidemiology of phoma stem canker on oilseed rape in Lithuania. *Journal of Plant Pathology* 93: 577–585.

Calvert O.H., Pound G.S., Walker J.C., Stahmann M.A., Stauffer J.F., 1949. Induced variability in *Phoma lingam*. *Journal of Agricultural Research* 78: 571–588.

de Gruyter J., Woundenberg J.H.C., Aveskamp M.M., Verkley, G.J.M., Groenewald J.Z., Crous P.W., 2012. Redisposition of phoma-like anamorphs in *Pleosporales*. *Studies in Mycology* 75: 1–36.

Dilmaghani A., Balesdent M.H., Didier J.P., Wu C., Davey J., … T. Rouxel, 2009. The *Leptosphaeria maculans – Leptosphaeria biglobosa* species complex in the American continent. *Plant Pathology* 58: 1044–1058.

Fitt B.D.L., Brun H., Barbetti M.J., Rimmer S.R., 2006. World-wide importance of phoma stem canker (*Leptosphaeria maculans* and *L. biglobosa*) on oilseed rape (*Brassica napus*). *European Journal of Plant Pathology* 114: 3–15.

Goh T.K., 1999. Single-spore isolation using a hand-made glass needle. *Fungal Diversity* 2: 47–63.

Henderson M.P., 1918. The Black-leg disease of cabbage caused by *Phoma lingam* (Tode) Desmaz. *Phytopathology* 8: 379–431.

Kaczmarek J., Jędryczka M., 2011. Characterization of two coexisting pathogen populations of *Leptosphaeria* spp., the cause of stem canker of brassicas. *Acta Agrobotanica* 64: 3–14.

Karolewski Z., Walczak D., Kosiada T., Lewandowska D., 2007. Occurrence of *Leptosphaeria maculans* and *L. biglobosa* in oilseed rape leaves with different symptoms of stem canker. *Phytopathologia polonica* 44: 43–50.

Koch E., Badawy H.M.A., Hoppe H.H., 1989. Differences between aggressive and non-aggressive single spore lines of *Leptosphaeria maculans* in cultural characteristics and phytotoxin production. *Journal of Phytopathology* 124: 52–62.

Koch E., Song K., Osborn T.C., Williams P.H., 1991. Relationship between pathogenicity and phylogeny based on restriction fragment length polymorphism in *Leptosphaeria maculans*. *Molecular Plant-Microbe Interactions* 4: 341–349.

Liu S.Y., Liu Z., Fitt B.D.L., Evans N., Foster S.J., … Lucas J.A., 2006. Resistance to *Leptosphaeria maculans* (phoma stem canker) in *Brassica napus* (oilseed rape) induced by *L. biglobosa* and chemical defense activators in field and controlled environments. *Plant Pathology* 55: 401–412.

Maniatis T., Sambrook J., Fritsch E.F., 1983. *Molecular cloning: A laboratory manual*. New York: Cold Spring Harbor Laboratory, Cold Spring Harbor

Mazáková J., Urban J., Zouhar M., Ryšánek P., 2017. Analysis of *Leptosphaeria* species complex causing phoma leaf spot and stem canker of winter oilseed rape (*Brassica napus*) in the Czech Republic. *Crop & Pasture Science* 68: 254–264.

Mitrović P., Marinković R., 2007. *Phoma lingam* – a rapeseed parasite in Serbia. Proceedings – The 12th International Rapeseed Congress – IV. Sustainable Development in Cruciferous Oilseed Crops Production. Wuhan, China, *Plant Protection: Diseases* 217–219.

Mitrović P., Jeromela A.M., Trkulja V., Milovac Z., Terzic S., 2016. The First Occurrence of Stem Canker on Oilseed Rape Caused by *Leptosphaeria biglobosa* in Serbia. *Ratarstvo i povrtarstvo* 53: 53–60.

Rouxel T., Balesdent M.H., 2005. The stem canker (blackleg) fungus, *Leptosphaeria maculans*, enters the genomic era. *Molecular Plant Pathology* 6: 225–241.

Shoemaker R.A., Brun H., 2001. The teleomorph of the weakly aggressive segregate of *Leptosphaeria maculans*. *Canadian Journal of Botany* 79: 412–419.

Tabachnick B.G., Fidell L.S., 2013. *Using Multivariate Statistics*. 6th ed. Boston, Pearson

Varga Zs., 2014. Blackleg disease of oilseed rape (in Hungarian). *Agrofórum* 25: 40–45.

West J.S., Balesdent M.H., Rouxel T., Narcy J.P., Huang Y.J., … Schmit J., 2002. Colonization of winter oilseed rape tissues by A/Tox^{+} and B/Tox^{0} *Leptosphaeria maculans* (phoma stem canker) in France and England. *Plant Pathology* 51: 311–321.

Wijayawardene N.N., Crous P.W., Kirk P.M., Hawksworth D.L., Boonmee S., … Hyde K.D., 2014. Naming and outlike of *Dothideomycetes* - 2014 including proposals for the protection or suppression of generic names. *Fungal Diversity* 69: 1-55.

Phytopathologia Mediterranea
The international journal of the
Mediterranean Phytopathological Union

Firenze University Press
www.fupress.com/pm

New or Unusual Disease Reports

A new leaf spot disease of *Chamaerops humilis* caused by *Palmeiromyces chamaeropicola* gen. et sp. nov.

Diana S. PEREIRA, Alan J.L. PHILLIPS*

Universidade de Lisboa, Faculdade de Ciências, Biosystems and Integrative Sciences Institute (BioISI), Campo Grande, 1749-016 Lisbon, Portugal
*Corresponding author: alan.jl.phillips@gmail.com

Summary. In September 2018, a leaf spot disease was noticed on a European fan palm (*Chamaerops humilis* L.) in Oeiras, Portugal. The aim of this study was to identify and characterize the causative agent of this disease symptom. Morphological characters and phylogenetic data derived from ITS and LSU sequences revealed that the leaf spot was caused by a filamentous fungus in the *Mycosphaerellales*, as a unique lineage within the *Teratosphaeriaceae*. This pathogen is introduced here as a new genus and species, *Palmeiromyces chamaeropicola* D.S. Pereira & A.J.L. Phillips, the cause of a newly reported leaf disease on *Chamaerops humilis*.

Keywords. Fungus, new genus, new species, palm tree, plant pathogen.

OPEN ACCESS

Citation: D.S. Pereira, A.J.L. Phillips (2020) A new leaf spot disease of *Chamaerops humilis* caused by *Palmeiromyces chamaeropicola* gen. et sp. nov. *Phytopathologia Mediterranea* 59(2): 353-363. DOI: 10.14601/Phyto-11213

Accepted: June 17, 2020

Published: August 31, 2020

Data Availability Statement: All relevant data are within the paper and its Supporting Information files.

Competing Interests: The Author(s) declare(s) no conflict of interest.

Editor: Lizel Mostert, Faculty of AgriSciences, Stellenbosch, South Africa.

INTRODUCTION

Chamaerops humilis L. (*Arecaceae*), commonly known as the European fan palm or Mediterranean dwarf palm, is one of only two indigenous European palms, and the only one found in the Iberian Peninsula (Guzmán *et al*., 2017). This palm tree is distributed around the western Mediterranean Basin, occurring in Europe (Portugal, Spain, France and Italy), North Africa (Morocco, Algeria and Tunisia) and in Mediterranean islands (Balearic, Sicily, Sardinia and Malta) (Dransfield *et al*., 2008; Quattrocchi, 2017; Palmweb, 2020). These trees are used as sources of several products with commercial value, including textiles, food and seeds; they are also important ornamental trees (Guzmán *et al*., 2017). In Portugal, although these palms occur naturally, almost exclusively in the Algarve region (Carapeto *et al*., 2020), they are widely planted and used in gardening and landscaping due to their hardiness and aesthetic value.

Chamaerops humilis is generally free of diseases. No major diseases or pests have been reported for this palm, although it is a potential host for the red palm weevil and other harmful insects (Elliott, 2004). Some reports have shown that the principal fungal diseases on *C. humilis* are leaf spots. For example, this palm is a host for *Graphiola phoenicis*, a leaf spotting

Basidiomycete found exclusively on palms (Piepenbring *et al*., 2012). Fröhlich and Hyde (1998) listed six species of *Mycosphaerella* from leaf spots on different palms, including *M. chamaeropis* on *C. humilis*. More recently, Fusarium wilt and dieback were reported from young and adult *C. humilis* in Spain (Armengol *et al*., 2005), and *Pestalotiopsis chamaeropis* was described from leaves of this host in Italy (Maharachchikumbura *et al*., 2014).

In the present study, a leaf spot disease was noticed on a *C. humilis* palm growing as an ornamental. On the lesions, ascomata, asci and ascospores with characteristics of the *Mycosphaerellales* (Abdollahzadeh *et al*., 2019) were found. Therefore, the purpose of this paper was to characterize the fungus in terms of its morphology and phylogeny.

MATERIALS AND METHODS

Specimen collection and examination

Diseased leaf segments with leaf spots were collected from an ornamental *C. humilis* palm in Oeiras, near Lisbon, Portugal. Plant material was transported to a laboratory in paper envelopes, and examined with a Leica MZ9.5 stereo microscope (Leica Microsystems GmbH) for observations of lesion morphology and associated fungi.

Fungal isolation

A small piece of a leaf spot lesion bearing ascomata was placed on a drop of sterile water in the inverted lid of a Petri dish. The dish base, containing half-strength potato dextrose agar (1/2 PDA) (BIOKAR Diagnostics) was placed on top of the inverted lid. Ascospores were discharged upwards and impinged on the agar surface. After incubating overnight, single germinating ascospores were transferred to fresh plates of 1/2 PDA. Cultures were then incubated in ambient light at room temperature (18–20°C).

Isolations were also made directly from leaf spots. Pieces of leaf spot tissue 1–2 mm^2 were cut from the edge of each lesion, surface sterilized in 5% sodium hypochlorite for 1 min, rinsed in three times in sterile water, and then blotted dry on sterile filter paper. The fragments were plated onto 1/2 PDA containing 0.05% chloramphenicol, and incubated at room temperature until colonies developed.

Morphological observations and characterization

Microscopic structures of isolated fungi were mounted in 100% lactic acid and examined with differential interference contrast (DIC) microscopy. Observations of micromorphological features were made with Leica MZ9.5 and Leica DMR microscopes (Leica Microsystems GmbH), and digital images were recorded, respectively on the two microscopes, with Leica DFC300 and Leica DFC320 cameras (Leica Microsystems GmbH). Measurements were made with the measurement module of the Leica IM500 Image Management System (Leica Microsystems GmbH). Mean, standard deviation (SD) and 95% confidence intervals were calculated from n = total of measured structures. Measurements are presented as minimum and maximum dimensions with mean and SD in parentheses. Photographs were prepared with Adobe Photoshop CS6 (Adobe).

DNA extraction, PCR amplification and sequencing

Genomic DNA (gDNA) was extracted from mycelium of cultures grown on 1/2 PDA, following a modified and optimized version of the guanidium thiocyanate method described by Pitcher *et al*. (1989). PCR reactions were carried out with Taq polymerase, nucleotides, primers, PCR-water (ultrapure DNase/RNase-free distilled water) and buffers supplied by Invitrogen. Amplification reactions were performed in a TGradient Thermocycler (Biometra). Amplified PCR products were purified and sequenced by Eurofins (Germany).

The primers ITS5 (White *et al*., 1990) and NL-4 (O'Donnell, 1993) were used to amplify part of the cluster of rRNA genes, including the nuclear 5.8S rRNA gene and its flanking ITS1 and ITS2 regions, along with the first two domains of the large-subunit rRNA gene (ITS-D1/D2 rDNA region). The PCR reaction mixture consisted of 50–100 ng of gDNA, 1× PCR buffer, 50 pmol of each primer, 200 µM of each dNTP, 2 mM $MgCl_2$, 1 U Taq DNA polymerase, and was made up to a total volume of 50 µL with PCR water. The following cycling conditions were used: initial denaturation at 95°C for 5 min, followed by 40 cycles of denaturation at 95°C for 1 min, annealing at 52°C for 30 s and elongation at 72°C for 1.5 min, and a final elongation step at 72°C for 10 min.

The ITS region was sequenced only in the forward direction using the primer ITS5. The D1/D2 region (LSU) was sequenced only in the forward direction using the primers ITS5 and NL1 (O'Donnell, 1993). Consensus sequences were produced and edited with BioEdit version 7.0.5.3 (Hall, 1999).

Sequence alignment and phylogenetic analyses

ITS and LSU sequences of species in representative genera of *Teratosphaeriaceae* and *Neodevriesiaceae* in *Mycosphaerellales* were retrieved from GenBank by BLAST searches with the sequences generated in this study (Table 1). These were supplemented with taxa listed in recent literature (e.g. Quaedvlieg *et al*., 2014; Isola *et al*., 2016; Wang *et al*., 2017; Delgado *et al*., 2018). *Capnodium coffeae* Pat. was used as the outgroup taxon representative of a species in *Capnodiales*.

Sequences were aligned with ClustalX version 2.1 (Thompson *et al*., 1997) using the following parameters: pairwise alignment parameters (gap opening = 10, gap extension = 0.1), and multiple alignment parameters (gap opening = 10, gap extension = 0.2, DNA transition weight = 0.5, delay divergent sequences = 25%). Alignments were checked and manual adjustments were made where necessary with BioEdit. Terminal regions with data missing in some of the isolates were excluded from the analysis. The aligned ITS and LSU sequences were concatenated and combined in a single matrix.

Maximum Likelihood (ML) and Maximum Parsimony (MP) were used for phylogenetic inferences of single gene sequence alignments and the concatenated alignments. The individual gene trees were assessed for clade conflicts between the individual phylogenies by visually comparing the trees generated. ML and MP inferences were implemented on the CIPRES Science Gateway portal version 3.3 (Miller *et al*., 2010), using, respectively, RAxML-HPC2 version 8.2.12 (Stamatakis, 2014) and PAUP version 4.0a165 (Swofford, 2002). The resulting trees were visualized with TreeView version 1.6.6 (Page, 1996).

MP analyses were performed using the heuristic search option with 1000 random taxa additions and Tree Bisection and Reconnection (TBR) as the branch-swapping algorithm. All characters were unordered and of equal weight, and alignment gaps were treated as missing data. Maxtrees was set to 1000, branches of zero length were collapsed, and all multiple, equally parsimonious trees were retained. Clade stability and robustness of the most parsimonious trees were assessed using bootstrap analysis with 1000 pseudoreplicates, each with ten replicates of random stepwise addition of taxa (Felsenstein, 1985; Hillis and Bull, 1993). Descriptive tree statistics for parsimony included tree length (TL), homoplasy index (HI), consistency index (CI), retention index (RI) and rescaled consistency index (RC).

ML analyses were performed using a General Time Reversible (GTR) nucleotide substitution model including a discrete gamma distribution and estimation of proportion of invariable sites (GTR+G+I) to accommodate variable rates across sites. Clade stability and robustness of the branches of the best-scoring ML tree were estimated by conducting rapid bootstrap analyses with iterations halted automatically by RAxML.

RESULTS

Symptoms and isolations

Symptoms of the disease were found on a single *C. humilis* palm. These were leaf spots randomly distributed on segments of several leaves, which were frequently accompanied by yellowing of the leaf tips and generalized blight (Figure 1). The leaf spots were discrete, circular to ellipsoidal, amphigenous, initially yellowish to brown-grey, each with a wide dark-brown border. The leaf spot centre became progressively greyish and brittle. Each spot was surrounded by a conspicuous yellow or brown to red-brown halo. The discrete spots frequently coalesced, giving rise to blotches of grey necrotic plant tissue. In mature or older spots, the leaf epidermis often flaked off exposing dark ascomata immersed in the necrotic tissue. The bitunicate, obovate to pyriform asci contained eight hyaline, 1-septate ascospores (Figure 1). The lack of pseudoparaphyses suggested that the fungus was closely related to genera in *Teratosphaeriaceae* or *Mycosphaerellaceae*.

Ascospores ejected from ascomata germinated slowly on 1/2 PDA. After 6–12 h 1–2 additional septa formed in each ascospore (Figure 1k and l). After 24–48 h, 1–2 swellings developed on the middle cells and the ascospores became markedly curved (Figure 1m). Further septa developed and germ tubes emerged at right angles to the long axis of each ascospore, all from one side of the ascospore (Figure 1n). Ascospores and germ tubes remained hyaline. The fungus grew slowly forming a black, amorphous mass of mycelium on 1/2 PDA that attained a diameter of *ca*. 3 mm after 3 months of incubation (Figure 1o). No signs of sporulation were visible even after extended periods of incubation of up to 3 months. No other fungi were isolated, even from surface sterilized tissues taken from within the leaf lesions and plated on 1/2 PDA.

Phylogenetic analyses

Results of the BLAST search with ITS and LSU of the fungus isolated from *C. humilis* revealed that it was closely related to species in *Teratosphaeriaceae* and *Neodevriesiaceae*, and only distantly related to *Mycosphaerellaceae*. The available ITS and LSU sequences of 81 strains of *Teratosphaeriaceae* and *Neodevriesi-*

Table 1. Isolates used in the phylogenetic analyses of *Palmeiromyces chamaeropicola*.

Taxon	Strain number[a]	Status[b]	GenBank accession number[c]	
			ITS	LSU
Acrodontium pigmentosum	CBS 111111	T	KX287275	KX286963
Batcheloromyces alistairii	CBS 120035	T	DQ885901	KF937220
B. alistairii	CPC 18251		JX556227	JX556237
B. leucadendri	CBS 114146		–	EU707892
B. proteae	CBS 110696		JF746163	KF901833
B. sedgefieldii	CBS 112119	T	EU707893	KF937222
Camarosporula persooniae	CBS 112494		JF770448	JF770460
Capnodium coffeae	CBS 147.52		MH856967	MH868489
Devriesia staurophora	CBS 375.81		KF442532	KF442572
D. thermodurans	CBS 115878	T	MH862991	MH874549
Eupenidiella venezuelensis	CBS 106.75	T	KF901802	KF902163
Hortaea thailandica	CBS 125423	T	MH863702	MH875167
H. werneckii	CBS 107.67	T	AJ238468	EU019270
H. werneckii	CBS 359.66		MH858825	MH870461
Meristemomyces arctostaphylos	CBS 141290	T	KX228264	KX228315
M. frigidus	CBS 136109	T	KF309971	GU250401
Myrtapenidiella corymbia	CBS 124769	T	KF901517	KF901838
M. eucalypti	CBS 123246	T	KF901772	KF902130
M. tenuiramis	CBS 124993	T	KF937262	GQ852626
Neodevriesia agapanthi	CBS 132689	T	KJ564346	JX069859
N. coccolobae	CBS 145064	T	MK047432	MK047483
N. coryneliae	CBS 137999	T	KJ869154	KJ869211
N. hilliana	CBS 123187	T	MH863277	MH874801
N. imbrexigena	CAP 1373	T	JX915746	JX915750
N. imbrexigena	CAP 1375		JX915748	JX915752
N. knoxdaviesii	CBS 122898	T	EU707865	EU707865
N. knoxdaviesii	CPC 14905		EU707866	KJ564328
N. lagerstroemiae	CBS 125422	T	GU214634	KF902149
N. shakazului	CBS 133579	T	KC005776	KC005797
N. stirlingiae	CBS 133581	T	KC005778	KC005799
N. strelitziae	CBS 122379	T	EU436763	GU301810
N. tabebuiae	CBS 145065	T	MK047433	MK047484
N. xanthorrhoeae	CBS 128219	T	HQ599605	HQ599606
Neophaeothecoidea proteae	CBS 114129	T	MH862955	KF937228
Palmeiromyces chamaeropicola	CDP 001	T	MT068628	MT076194
Parapenidiella pseudotasmaniensis	CBS 124991	T	MH863440	MH874943
Para. tasmaniensis	CBS 111687	T	KF901521	KF901843
Penidiella carpentariae	CBS 133586	T	KC005784	KC005806
Pen. columbiana	CBS 486.80	T	KF901630	KF901965
Pseudotaeniolina globosa	CBS 109889	T	KF309976	KF310010
Pseudoteratosphaeria flexuosa	CBS 111012	T	KF901755	KF902110
Pseudo. flexuosa	CBS 111048		KF901643	KF901978
Pseudo. ohnowa	CBS 112896	T	KF901620	KF901946
Queenslandipenidiella kurandae	CBS 121715	T	KF901538	KF901860
Readeriella dendritica	CBS 120032	T	KF901543	KF901865
R. limoniforma	CBS 134745	T	KF901547	KF901869
R. mirabilis	CBS 125000	ET	KF901549	KF901871

(Continued)

Table 1. (Continued).

Taxon	Strain number[a]	Status[b]	GenBank accession number[c]	
			ITS	LSU
Stenella araguata	CBS 105.75	T	MH860897	MH872633
Zasmidium musae	CBS 122477	T	EU514291	–
Z. musae	CBS 121385		EU514293	–
Teratosphaeria alboconidia	CBS 125004	T	KF901558	KF901881
Ter. biformis	CBS 124578	T	KF901564	KF901887
Ter. blakelyi	CBS 120089	T	KF901565	KF901888
Ter. brunneotingens	CPC 13303	T	EF394853	EU019286
Ter. complicata	CBS 125216	T	MH863461	MH874961
Ter. complicata	CPC 14535		KF901781	KF902139
Ter. considenianae	CBS 120087	T	DQ923527	KF937238
Ter. considenianae	CPC 14057		KF901568	KF901892
Ter. cryptica	CBS 110975		KF901573	KF901897
Ter. cryptica	CBS 111679		KF901691	KF902037
Ter. dimorpha	CBS 120085		DQ923529	KF937240
Ter. dimorpha	CBS:124051		KF901575	KF901899
Ter. encephalarti	CBS 123540	T	FJ372395	FJ372412
Ter. encephalarti	CPC 15466		FJ372401	FJ372418
Ter. hortaea	CBS 124156	T	MH863358	MH874881
Ter. hortaea	CPC 15723		FJ790279	FJ790300
Ter. macowanii	CBS 122901	ET	MH863257	MH874781
Ter. macowanii	CPC 1488		AY260096	FJ493199
Ter. mareebensis	CBS 129529	T	JF951149	JF951169
Ter. maxii	CBS 120137	T	DQ885899	KF937243
Ter. maxii	CBS 112496		EU707871	KF937242
Ter. micromaculata	CBS 124582	T	MH863390	MH874909
Ter. profusa	CBS 125007	T	KF901592	KF901916
Ter. profusa	CPC 12821		FJ493196	FJ493220
Ter. rubidae	CBS 124579	T	MH863388	MH874907
Ter. rubidae	MUCC 659		EU300992	–
Ter. sieberi	CBS 144443	T	MH327816	MH327852
Ter. wingfieldii	CBS 112163	T	EU707896	–
Teratosphaericola pseudoafricana	CBS 114782	T	KF901737	KF902084
Terph. pseudoafricana	CBS 111168		KF901699	KF902045
Teratosphaeriopsis pseudoafricana	CBS 111171	T	KF901738	KF902085

[a]CAP = Culture Collection of Alan Phillips, housed at M&B-BioISI, Tec Labs, University of Lisbon, Lisbon, Portugal, CBS = Culture Collection of the Westerdijk Fungal Biodiversity Institute, Utrecht, The Netherlands, CDP = Culture Collection of Diogo Pereira, housed at M&B-BioISI, Tec Labs, University of Lisbon, Lisbon, Portugal, CPC = Culture Collection of Pedro Crous, housed at the Westerdijk Institute,, MUCC = Murdoch University Culture Collection, Murdoch, Australia.
[b]Status of the strains, T = ex-type, ET = ex-epitype.
[c]Newly generated sequences are in bold font.

aceae, either sequenced in this study or retrieved from GenBank, were included in the phylogenetic analysis (Table 1). The concatenated ITS and LSU alignment of 80 ingroup taxa and one outgroup taxon comprised 1152 characters (including alignment gaps), with 599 characters for ITS and 553 for LSU, after alignment. Tree topologies resulting from maximum parsimony and maximum likelihood analyses were similar, and both presented well-resolved clades for each genus included in the analyses, mostly supported by high bootstrap values (≥ 70%). The ML tree is shown in Figure 2.

Of the 1152 characters, 653 were constant and 139 variable characters were parsimony-uninformative. MP analysis of the remaining 364 parsimony-informative

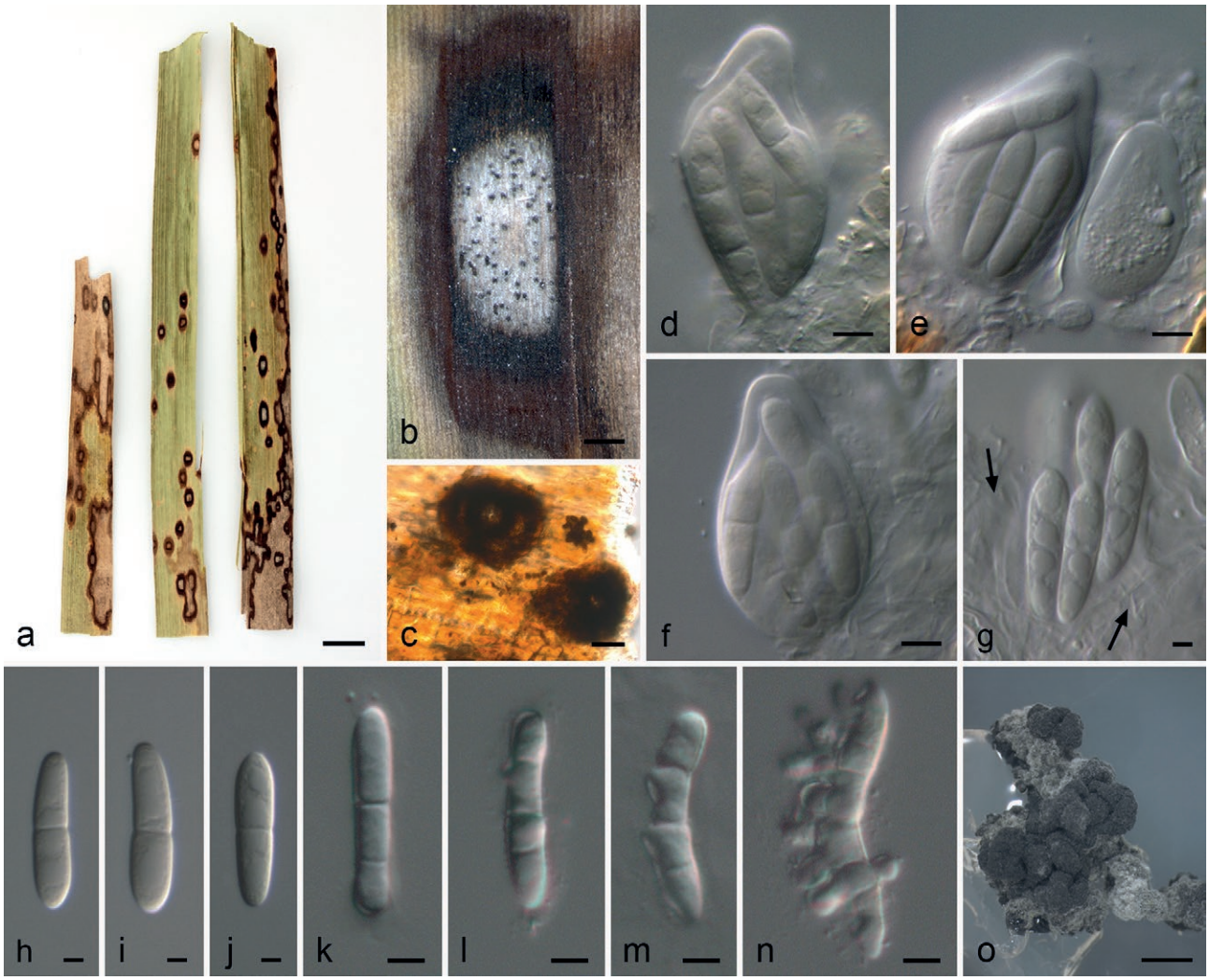

Figure 1. *Palmeiromyces chamaeropicola* (CDP 001, ex-type). a, Leaf spots on segments of *Chamaerops humilis*. b and c, Appearance of ascomata on host leaf surface. d, e and f, Asci and cellular hamathecium remnants. g, Immature ascospores (black arrows indicate remnants of cellular hamathecium). h, i and j, Mature ascospores. k, l, m and n, Germinating ascospores (k, after *ca.* 6 h incubation; l, after *ca.* 12 h incubation; m, after *ca.* 24 h incubation; n, after *ca.* 48 h incubation). o. Three-month-old colony on 1/2 PDA. Scale bars: a = 10 mm, b = 0.5 mm, c = 30 µm, d, e and f = 5 µm, g, h, i and j = 2.5 µm, k, l, m and n = 5 µm, o = 1 mm.

characters resulted in 140 equally parsimonious trees of 2181 steps and a moderately high level of homoplasy as indicated by a CI of 0.381, an RI of 0.693, an HI of 0.619 and an RC of 0.264. Topology of the trees differed from one another only in the position of the isolates within the terminal groupings of the *Teratosphaeria* clade. All other clades were consistent in their phylogenetic positions.

The final likelihood score for the ML tree was -11854.411424. The matrix had 560 distinct alignment patterns, with 15.85% undetermined characters or gaps. Estimated base frequencies were as follows: A = 0.222286, C = 0.271515, G = 0.286947 and T = 0.219253; substitution rates AC = 1.523961, AG = 1.983358, AT = 1.573616, CG = 1.073620, CT = 5.812546 and GT = 1.000000; gamma distribution shape parameter α = 0.554479; proportion of invariable sites = 0.384063.

Although well-resolved, internal nodes within *Teratosphaeriaceae* received low bootstrap support (≤ 50%). Nevertheless, *Teratosphaeriaceae* and *Neodevriesiaceae* were well-separated, insomuch that represented a clade with 100% bootstrap support, which confirms the phylogenetic difference that supports these two families.

The isolate obtained from *C. humilis* clustered in a separate and previously undescribed lineage among the selected genera in *Teratosphaeriaceae* and *Neodevriesiaceae*. Nevertheless, its placement between these two

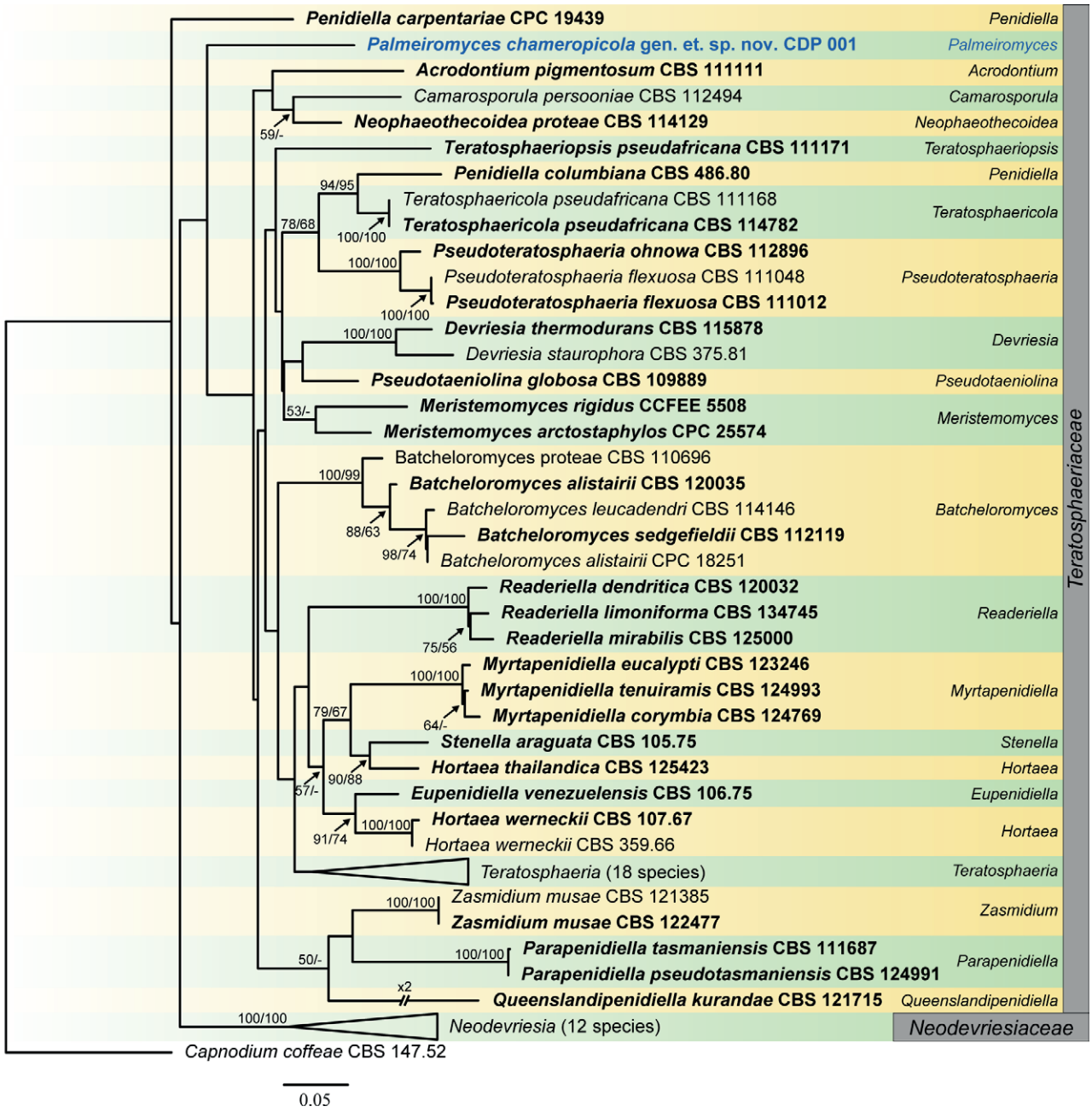

Figure 2. Maximum likelihood tree of *Teratosphaeriaceae* and *Neodevriesiaceae* based on combined ITS and LSU sequences. ML/MP bootstrap support values (> 50%) are shown above the branches. The isolate from *Chamaerops humilis* is indicated in blue font. The scale bar represents the expected number of nucleotide changes per site. Ex-type/ex-epitype isolates are in bold font.

families received low bootstrap support. Considering the results from both MP and ML analyses, this fungus clusters close to genera in *Teratosphaeriaceae*. A total of nine unique base pair differences in the ITS locus and five in the LSU locus among the 81 isolates included in the phylogenies confirms the novel lineage of the isolate as a new genus here introduced in *Mycosphaerellales*.

Taxonomy

Based on DNA phylogeny and morphology, the isolate collected from leaf spots on *C. humilis* was distinct from all other known species and genera in *Mycosphaerellales*. The data presented here indicate that this fungus resides in *Teratosphaeriaceae* as a new spe-

cies and a new genus. Descriptions of the fungus are provided below.

Palmeiromyces D.S. Pereira & A.J.L. Phillips, gen. nov.
MycoBank: MB 834638

Etymology: Named for the Portuguese word for palms (palmeiras), the host on which it was found.

Type species: *Palmeiromyces chamaeropicola* D.S. Pereira & A.J.L. Phillips, sp. nov.

Ascomata pseudothecial, amphigenous, subepidermal, immersed to erumpent, scattered or clustered, globose to subglobose, dark-brown, ostiolate. *Ostiole* circular, aperiphysate. *Peridium* thin-walled, composed of cells forming a *textura angularis*, outer layer composed of thick-walled, dark-brown to brown cells, inner layers composed of thin-walled, hyaline cells. *Pseudoparaphyses* absent. *Asci* bitunicate, fissitunicate, pyriform to obovoid, with well-developed ocular chamber, smooth-walled, hyaline, 8-spored. *Ascospores* biseriate, hyaline, broadly ellipsoidal to subcylindrical, with rounded ends, smooth- and thin-walled, medianly 1-septate, not constricted at the septum.

Palmeiromyces chamaeropicola D.S. Pereira & A.J.L. Phillips, sp. nov. (Figure 1)
MycoBank: MB 834639

Etymology: Named for *Chamaerops humilis*, the host genus from which it was collected.

Holotype: AVE-F-11

Leaf spots sunken, circular to broadly ellipsoidal, 3–7 × 2–3 mm (mean ± SD = 4.67 ± 1.06 × 2.52 ± 0.51 mm), identical on both leaf surfaces, brown-grey to yellowish centre, later becoming greyish and fragile, with a dark-brown border (*ca.* 1 mm wide), surrounded by a conspicuous yellow or brown to red-brown halo, occasionally coalescing, randomly distributed. Mature leaf spots contain several immersed ascomata. *Ascomata* pseudothecial, amphigenous, subepidermal, immersed to erumpent, scattered or clustered in groups of two or three, globose to subglobose, dark-brown, up to 90 µm diam., ostiolate. *Ostiole* circular, up to 21 µm diam., aperiphysate. *Peridium* thin-walled, composed of cells forming a *textura angularis*, outer layer composed of thick-walled, dark-brown to brown cells, inner layers composed of thin-walled, hyaline cells. *Pseudoparaphyses* absent, but pseudoparenchymatous, cellular hamathecium remnants present. *Asci* bitunicate, outer wall up to 2 µm thick, fissitunicate, pyriform to obovoid, slightly curved, broader at the base, well-developed ocular chamber, smooth-walled, hyaline, 8-spored, 21.4–57.9 × 8.2–19.1 µm (mean ± SD = 33.22 ± 9.69 × 14.20 ± 3.75 µm, n = 11). *Ascospores* biseriate, broadly ellipsoidal to subcylindrical, with rounded ends, occasionally slightly curved, hyaline, smooth- and thin-walled, guttulate, medianly 1-septate, not to slightly constricted at the septa, 9.5–21.9 × 2.8–5.5 µm (mean ± SD = 17.31 ± 3.23 × 4.05 ± 0.72 µm, n = 50); mean ± SD ascospore length/width ratio = 4.30 ± 0.58 (n = 50).

Material examined: PORTUGAL, Oeiras, National Sports Centre of Jamor, on leaf spots of *Chamaerops humilis* (*Arecaceae*), 20 September 2018, Alan J.L. Phillips (holotype AVE-F-11, ex-type living culture CDP 001).

GenBank Numbers: ITS: MT068628; LSU: MT076194.

Distribution: Oeiras, Portugal.

Host: *Chamaerops humilis*.

Notes: *Palmeiromyces chamaeropicola* was found associated with leaf spots of *C. humilis*, but pathogenicity has not been tested. Nevertheless, there is evidence that this species represents an obligate biotroph causing a previously undescribed disease on *C. humilis*. Phylogenetically, *P. chamaeropicola* is closely related to genera in *Teratosphaeriaceae* (Figure 2). Morphology of the sexual morph, ascospores with a peculiar mode of germination, lack of an asexual morph and very slow growth in culture correspond to genera in *Teratosphaeriaceae* (Crous *et al*., 2007). However, ascospores of *P. chamaeropicola* lack mucous sheaths, which is a characteristic of *Teratosphaeriaceae* (Crous *et al*., 2007; Quaedvlieg *et al*., 2014).

DISCUSSION

In this study, a new species in *Teratosphaeriaceae*, *Palmeiromyces chamaeropicola*, is described and a new genus is established to accommodate the fungus. Phylogenetic analyses based on ITS and LSU sequences revealed that *Palmeiromyces* represents a separate lineage close to several *Teratosphaeriaceae* genera, as well as to *Neodevriesiaceae*. The evidence gained from unique nucleotide differences among the several genera included in the phylogeny supports this novelty at genus-level. This species was associated with, and is considered to be the cause of, a leaf spot disease of the palm *C. humilis*.

Morphologically *Palmeiromyces chamaeropicola* resembles *Mycosphaerellaceae* and *Teratosphaeriaceae*, characterized by small, inconspicuous ascomata immersed in the host tissue, which produce pyriform asci with eight hyaline, ellipsoidal and medianly 1-septate ascospores. The presence of pseudoparenchymatal remnants in ascomata of *Palmeiromyces* and the absence of paraphyses place it within *Teratosphaeriaceae*, since Crous *et al*. (2007) used these characters to separate

Teratosphaeriaceae from *Mycosphaerellaceae*. Nevertheless, the low bootstrap support for the internal nodes and thus for the branches between *P. chamaeropicola* and the remaining taxa in the phylogenetic analyses suggest that future studies may reveal a different phylogenetic position for this taxon, possibly as a new family. Genera in *Teratosphaeriaceae* and *Mycosphaerellaceae* are often defined based on DNA sequence data, and on morphology of their asexual morphs. However, *P. chamaeropicola* barely grew in culture with no signs of asexual sporulation. This is common in *Teratosphaeria* species, which are cultivated with difficulty (Crous *et al*., 2007, 2009c). Morphologically *P. chamaeropicola* resembles *Mycosphaerella cocoës*, which was found associated with leaf spots on various palm hosts, such as *Calamus*, *Cocos* and *Mauritia* (Fröhlich and Hyde, 1998). However, no cultures linked to the holotype of *M. cocoës* are extant and thus no DNA data are available for this species. Comparison of species within *Mycosphaerellaceae* and *Teratosphaeriaceae* solely on the basis of morphology is unreliable (Hunter *et al*., 2006; Crous *et al*., 2008, 2009c). Crous *et al*. (2008) noted that the morphological species concept had in the past obscured the presence of novel taxa, which have been resolved by means of molecular analyses. Therefore, it was not possible to determine the phylogenetic relationship between *P. chamaeropicola* and *M. cocoës*.

The phylogenetic position of *P. chamaeropicola* within *Mycosphaerellales* is uncertain and no accurate nearest neighbours could be indicated in the present analyses. In addition, a high level of homoplasy was detected in the MP analysis. Most genera within *Teratosphaeria* are polyphyletic, and within *Capnodiales* are paraphyletic (Crous *et al*., 2007). Convergence is observed in several genera, especially with respect to the morphology of asexual morphs (Crous *et al*., 2007, 2009b; Ruibal *et al*., 2008; Quaedvlieg *et al*., 2014). *Capnodiales* was recently sub-divided into seven orders (Abdollahzadeh *et al*., 2019) with *Mycosphaerellaceae* and *Teratosphaeriaceae* accommodated in *Mycosphaerellales*.

The phylogenetic analyses in this study suggest that *Palmeiromyces* could represent a new family, although it is not regarded as such in the present study, mainly due to low taxon sampling for the new genus. Besides the DNA phylogenetic data, *P. chamaeropicola* lacks several morphological characters that are diagnostic for *Teratosphaeria*, the type genus of *Teratosphaeriaceae*. These characters include ascospores that turn brown and verruculose while still in the asci, as well as the presence of mucoid sheaths around the ascospores (Quaedvlieg *et al*., 2014), all of which are lacking in *Palmeiromyces*. In addition, the germination pattern of ascospores of *Palmeiromyces* is completely distinct from those reported in *Mycosphaerellaceae*, although this pattern is seen in some species in *Teratosphaeriaceae*. Thus, *Palmeiromyces* clearly represents a separate genus within *Mycosphaerellales* where several phylogenetic lineages remain poorly resolved due to limited taxon sampling (Quaedvlieg *et al*., 2014). However, its position within *Teratosphaeriaceae* cannot be established and it is possible that future studies with greater taxon sampling may split *Palmeiromyces* from *Teratosphaeriaceae*.

Palmeiromyces chamaeropicola was collected from diseased foliage of *C. humilis* and reveals a new insight into the *Teratosphaeriaceae* leaf diseases (TLD) and *Mycosphaerellaceae* leaf diseases (MLD). Although the pathogenicity of *P. chamaeropicola* has not been tested, the extremely slow growth rate in culture and almost complete lack of growth on agar suggests that this fungus has highly specific growth requirements and can be regarded as an obligate biotroph. The fungus barely grows in culture, attaining a colony diameter of only 1 mm after 1 month of incubation. Furthermore, this growth was a black, amorphous mass of sterile mycelium, which can hardly be regarded as a colony. This extremely slow growth rate is often reported in important leaf spotting fungi within *Capnodiales* (Crous *et al*., 2008), so *P. chamaeropicola* represents a new record of a phytopathogenic fungus. The report of a previously undescribed leaf spotting fungus in *Mycosphaerellales* represents a significant advance in the knowledge on TLD and MLD, since these fungi are important phytopathogens in various plant hosts, including *Eucalyptus* (Hunter *et al*., 2006; Crous *et al*., 2009a; Pérez *et al*., 2009; 2013; Taylor *et al*., 2012; Quaedvlieg *et al*., 2014). Furthermore, several species within *Mycosphaerellales* families, especially *Teratosphaeriaceae*, are of quarantine importance in many countries in Europe (Crous *et al*., 2009a; Quaedvlieg *et al*., 2012; Crous *et al*., 2019).

The present study has revealed a new disease of the ornamental, indigenous palm, *C. humilis*, caused by a fungal species in a previously unknown genus in the *Mycosphaerellales*. The geographical distribution of this fungus is, for now, confined to a single plant in the Lisbon district of Portugal. The survey conducted in this study can only be regarded as preliminary and it is likely that wider surveys will reveal more cases of this previously undescribed disease. Therefore, further sampling is essential to understand the geographical and ecological range of *P. chamaeropicola*. Future studies should also aim to elucidate the ecology and physiology of *Palmeiromyces* to assess its traits as a phytopathogen.

ACKNOWLEDGEMENTS

Work supported by UIDB/04046/2020 and UIDP/04046/2020 Centre grants from FCT, Portugal (to BioISI).

LITERATURE CITED

Abdollahzadeh, J., Groenewald, J.Z., Coetzee, M.P.A., Wingfield, M.J., Crous, P.W., 2019. Evolution of lifestyles in *Capnodiales*. *Studies in Mycology* (in press). DOI: 10.1016/j.simyco.2020.02.004

Armengol A., Moretti A., Perrone G., Vicent A., Bengoechea J.A., García-Jiménez J., 2005. Identification, incidence and characterization of *Fusarium proliferatum* on ornamental palms in Spain. *European Journal of Plant Pathology* 112: 123–131.

Carapeto A., Clamote F., Schwarzer U., Pereira A.J., Almeida J.D., *et al*., 2020. *Chamaerops humilis* L. - mapa de distribuição. Flora-On: Flora de Portugal Interactiva, Sociedade Portuguesa de Botânica. http://www.flora-on.pt/#wChamaerops+humilis. Accessed 25 February 2020.

Crous P.W., Braun U., Groenewald J.Z., 2007. *Mycosphaerella* is polyphyletic. *Studies in Mycology* 58: 1–32.

Crous P.W., Summerell B.A., Mostert L., Groenewald J.Z., 2008. Host specificity and speciation of *Mycosphaerella* and *Teratosphaeria* species associated with leaf spots of Proteaceae. *Persoonia* 20: 59–86.

Crous P.W., Groenewald J.Z., Summerell B.A., Wingfield B.D., Wingfield M.J., 2009a. Co-occurring species of *Teratosphaeria* on *Eucalyptus*. *Persoonia* 22: 38–48.

Crous P.W., Schoch C.L., Hyde K.D., Wood A.R., Gueidan C., … Groenewald J.Z., 2009b. Phylogenetic lineages in the *Capnodiales*. *Studies in Mycology* 64: 17–47.

Crous P.W., Summerell B.A., Carnegie A.J., Wingfield M.J., Groenewald J.Z., 2009c. Novel species of *Mycosphaerellaceae* and *Teratosphaeriaceae*. *Persoonia* 23: 119–146.

Crous P.W., Wingfield M.J., Cheewangkoon R., Carnegie A.J., Burgess T.I, … Groenewald J.Z., 2019. Foliar pathogens of eucalypts. *Studies in Mycology* 94: 125–298.

Delgado G., Miller A.N., Piepenbring M., 2018. South Florida microfungi: *Castanedospora*, a new genus to accommodate *Sporidesmium pachyanthicola* (Capnodiales, Ascomycota). *Cryptogamie Mycologie* 39: 109–127.

Dransfield J., Uhl N.W., Asmussen C.B., Baker W.J., Harley M.M., Lewis C.E., 2008. *Genera Palmarum – the Evolution and Classification of Palms*. 2nd ed. Royal Botanic Gardens, Kew, London, UK, 744 pp.

Elliott M.L., 2004. *Compendium of Ornamental Palm Diseases and Disorders*. 2nd ed. American Phytopathological Society Press, Saint Paul, Minnesota, USA, 69 pp.

Felsenstein J., 1985. Confidence limits on phylogenies: an approach using the bootstrap. *Evolution* 39: 783–791.

Fröhlich J., Hyde K.D., 1998. Fungi from palms. XXXVI-II. The genera *Mycosphaerella* and *Sphaerella*. *Sydowia* 50: 171–181.

Guzmán B., Fedriani J.M., Delibes M., Vargas P., 2017. The colonization history of the Mediterranean dwarf palm (*Chamaerops humilis* L., Palmae). *Tree Genetics & Genomes* 13: 24.

Hall T.A., 1999. BioEdit: a user-friendly biological sequence alignment editor and analysis program for Windows 95/98/NT. *Nucleic Acids Symposium Series* 41: 95–98.

Hillis D.M., Bull J.J., 1993. An empirical test of bootstrapping as a method for assessing confidence in phylogenetic analysis. *Systematic Biology* 42: 182–192.

Hunter G.C., Wingfield B.D., Crous P.W., Wingfield M.J., 2006. A multi-gene phylogeny for species of *Mycosphaerella* occurring on *Eucalyptus* leaves. *Studies in Mycology* 55: 147–161.

Isola D., Zucconi L., Onofri S., Caneva G., de Hoog G.S., Selbmann L., 2016. Extremotolerant rock inhabiting black fungi from Italian monumental sites. *Fungal Diversity* 76: 75–96.

Maharachchikumbura S.S.N., Hyde K.D., Groenewald J.Z., Xu J., Crous P.W., 2014. *Pestalotiopsis* revisited. *Studies in Mycology* 79: 121–186.

Miller M.A., Pfeiffer W., Schwartz T., 2010. Creating the CIPRES Science Gateway for inference of large phylogenetic trees. In: *Proceedings of the Gateway Computing Environments Workshop (GCE), 2010*, November 14, 2010, New Orleans, Los Angeles, USA, 1–8.

O'Donnell K., 1993. *Fusarium* and its near relatives. In: *The Fungal Holomorph: Mitotic, Meiotic and Pleomorphic Speciation in Fungal Systematics* (D.R. Reynolds, J.W. Taylor, ed.), CAB International, Wallingford, England, UK, 225–233.

Page R.D.M., 1996. TreeView: an application to display phylogenetic trees on personal computers. *Bioinformatics* 12: 357–358.

Palmweb, 2020. Palmweb: Palms of the World Online. http://www.palmweb.org/. Accessed 24 February 2020.

Pérez C.A., Wingfield M.J., Altier N.A., Blanchette R.A., 2009. *Mycosphaerellaceae* and *Teratosphaeriaceae* associated with *Eucalyptus* leaf diseases and stem cankers in Uruguay. *Forest Pathology* 39: 249–360.

Pérez C.A., Wingfield M.J., Altier N.A., Blanchette R.A., 2013. Species of *Mycosphaerellaceae* and *Teratosphaeriaceae* on native *Myrtaceae* in Uruguay: evidence of fungal host jumps. *Fungal Biology* 117: 94–102.

Piepenbring M., Nold F., Trampe T., Kirschner R., 2012. Revision of the genus *Graphiola* (*Exobasidiales, Basidiomycota*). *Nova Hedwigia* 94: 67–96.

Pitcher D.G., Saunders N.A., Owen R.J., 1989. Rapid extraction of bacterial genomic DNA with guanidium thiocyanate. *Letters in Applied Microbiology* 8: 151–156.

Quaedvlieg W., Groenewald J.Z., de Jesús Yáñez-Morales M., Crous P.W., 2012. DNA barcoding of *Mycosphaerella* species of quarantine importance to Europe. *Persoonia* 29: 101–115.

Quaedvlieg W., Binder M., Groenewald J.Z., Summerell B.A., Carnegie A.J., … Crous P.W., 2014. Introducing the consolidated species concept to resolve species in the *Teratosphaeriaceae*. *Persoonia* 33: 1–40.

Quattrocchi, F.L.S.U., 2017. *The CRC World Dictionary of Palms: Common Names, Scientific Names, Eponyms, Synonyms, and Etymology*. 1st ed. CRC Press, Taylor & Francis Group, Boca Raton, Florida, USA, 2753 pp.

Ruibal C., Platas G., Bills G.F., 2008. High diversity and morphological convergence among melanised fungi from rock formations in the Central Mountain System of Spain. *Persoonia* 21: 93–110.

Stamatakis A., 2014. RAxML version 8: a tool for phylogenetic analysis and post-analysis of large phylogenies. *Bioinformatics* 30: 1312–1313.

Swofford D.L., 2002. *PAUP*. Phylogenetic Analysis Using Parsimony (*and other methods)*. Version 4. 2nd ed. Sinauer Associates, Sunderland, Massachusetts, USA.

Taylor K., Andjic V., Barber P.A., Hardy G.E.S., Burgess T.I., 2012. New species of *Teratosphaeria* associated with leaf diseases on *Corymbia calophylla* (Marri). *Mycological Progress* 11: 159–169.

Thompson J.D., Gibson T.J., Plewniak F., Jeanmougin F., Higgins D.G., 1997. The ClustalX windows interface: flexible strategies for multiple sequence alignment aided by quality analysis tools. *Nucleic Acids Research* 25: 4876–4882.

Wang M.M., Shenoy B.D., Li W., Cai L., 2017. Molecular phylogeny of *Neodevriesia*, with two new species and several new combinations. *Mycologia* 109: 965–974.

White T.J., Bruns T., Lee S., Taylor J., 1990. Amplification and direct sequencing of fungal ribosomal RNA genes for phylogenetics. In: *PCR protocols: a Guide to Methods and Applications* (M.A. Innis, D.H. Gelfand, J.J. Sninsky, T.J. White, ed.), Academic Press, San Diego, California, USA, 315–322.

Phytopathologia Mediterranea
The international journal of the
Mediterranean Phytopathological Union

Firenze University Press
www.fupress.com/pm

New or Unusual Disease Reports

Stem rot caused by *Fusarium oxysporum* f. sp. *opuntiarum* on *Mammillaria painteri* in Italy

Domenico BERTETTI[1,*], Pietro PENSA[2], Slavica MATIĆ[1], Maria Lodovica GULLINO[1,3], Angelo GARIBALDI[1]

[1] *Centre of Competence AGROINNOVA, University of Torino, Largo Paolo Braccini 2, 10095 Grugliasco (TO), Italy*
[2] *ANT-NET s.r.l., Via Livorno 60, Torino, Italy*
[3] *DiSAFA, University of Torino, Largo Paolo Braccini 2, 10095 Grugliasco (TO), Italy*
*Corresponding author: domenico.bertetti@unito.it

Summary. Potted plants of *Mammillaria painteri* (*Cactaceae*) showing symptoms of stem rot were collected from a nursery in Imperia province, Liguria region, Italy. Isolations from internal rotting tissues allowed gave constantly similar fungal colonies. Morphological characteristics of the isolates identified them as *Fusarium oxysporum*. Molecular analyses of the elongation factor 1α (*EF1α*) and *RPB2* genes confirmed the identification. Analysis of part of the intergenic spacer (IGS) region of the ribosomal DNA identified the pathogen as *F. oxysporum* f. sp. *opuntiarum*. In pathogenicity tests, stems of *M. painteri* plants were inoculated with representative *F. oxysporum* f. sp. *opuntiarum* isolates. Approx. 30 d after the inoculation, yellowing appeared around the inoculated wounds. The inoculated stems then rotted developing symptoms similar to those observed in greenhouse-grown plants. This is the first report of *F. oxysporum* f. sp. *opuntiarum* on *M. painteri.*

Keywords. Ornamentals, cacti, Fusarium wilt.

OPEN ACCESS

Citation: D. Bertetti, P. Pensa, S. Matić, M.L. Gullino, A. Garibaldi (2020) Stem rot caused by *Fusarium oxysporum* f. sp. *opuntiarum* on *Mammillaria painteri* in Italy. *Phytopathologia Mediterranea* 59(2): 365-369. DOI: 10.14601/Phyto-11735

Accepted: August 3, 2020

Published: August 31, 2020

Data Availability Statement: All relevant data are within the paper and its Supporting Information files.

Competing Interests: The Author(s) declare(s) no conflict of interest.

Editor: Jean-Michel Savoie, INRA Villenave d'Ornon, France.

INTRODUCTION

In the Liguria region of Italy, production of ornamental plants is continuously enriched with genera, species and cultivars, including several succulent plants belonging to *Cactaceae*. Cacti are extensively grown in specialized nurseries, with risks of propagating pathogens that can cause severe economic losses.

Fusarium oxysporum f. sp. *opuntiarum* is an important fungal pathogen of succulent host species (Gerlach, 1972; Souza de *et al*., 2010), including *Mammillaria zeilmanniana* (Alfieri *et al*., 1984; French, 1989). In Italy, this fungus has been identified on several succulent plants, including *Echinocactus grusonii* (Polizzi and Vitale, 2004), *Schlumbergera truncata* (Lops *et al*., 2013), *Astrophytum myriostigma*, *Cereus marginatus* var. *cristata*, *C. peruvianus monstruosus* and *C. peruvianus florida* (Bertetti *et al*., 2017), and, more recently, on *Sulcorebutia heliosa* (Garibaldi *et al*., 2019a) and *S. rauschii* (Gar-

ibaldi *et al*., 2019b). This pathogen was also reported on *Euphorbia mammillaris* var. *variegata* (*Euphorbiaceae*) (Garibaldi *et al*., 2015). On affected plants, *F. oxysporum* f. sp. *opuntiarum* can cause root rot, stem rot and wilting, and the mycelium of the pathogen can appear at soil level. Sporodochia producing abundant macroconidia can also be observed on affected stem tissues.

Mammillaria painteri Rose (*Cactaceae*) is a small plant native to Mexico, which produces globose stems with pale rose flowers, and is commercialized as potted plants. The aim of the present study was to identify the causal agent of disease on *M. painteri*, detected during the summer of 2018, on plants grown in a specialized cactus nursery, located in Vallecrosia (Imperia province, Liguria region of Italy).

MATERIALS AND METHODS

Isolation and morphological characterization of the pathogen

Twenty 2-year-old potted plants of *M. painteri* with stem rot symptoms were collected for isolation of the possible causal agent of the disease. Small pieces of symptomatic stems were disinfected in sodium hypochlorite (1%) for 2 min, then washed in sterile water. Several stem pieces (approx. 3 × 3 × 3 mm) were taken from the borders of internal rotting tissues and plated onto potato dextrose agar (PDA) (Merck KGaA), and incubated at 25°C. Resulting colonies were transferred onto carnation leaf-piece agar (CLA) (Fisher *et al*., 1982), and incubated at 25°C. The morphological identification of the isolates was carried out according to colour, shape and pigmentation of the mycelia grown on PDA, and characteristics of microconidia, macroconidia and chlamydospores observed on CLA, observed using an optical microscope (Nikon Eclipse 55i). Since all the isolates were similar, one was selected for a pathogenicity test and for molecular characterization.

Molecular characterization

DNA of the isolate (coded DB18AGO01) was extracted using the E.Z.N.A. fungal DNA Mini Kit (Omega Bio-Tek) from mycelium of the fungus grown on PDA. For the molecular analyses, the following primers were used: EF1/EF2 (O'Donnell *et al*., 1998) for the elongation factor 1α gene (*EF1α*), 5F2/7CR (O'Donnell *et al*., 2007) for the *RPB2* gene encoding DNA-directed RNA polymerase II second largest subunit, and CNS1/CNL12 (Appel and Gordon, 1995) for the intergenic spacer (IGS) region of the ribosomal DNA. The resulting amplicons were sequenced, obtaining three sequences that were analyzed with the BLASTn (Altschul *et al*., 1997) to define similarities with the sequences listed in GenBank. Maximum Likelihood (ML) phylogenetic analyses were performed on IGS sequences, including the corresponding sequences of ten reference strains of *F. oxysporum* f. sp. *opuntiarum*. The *Fusarium proliferatum* (31X4) sequence was used as an outgroup.

Pathogenicity test

The isolate DB18AGO01, preserved in the Agroinnova collection (University of Torino, Italy), was used in the pathogenicity test. The isolate was tested on three 18-month-old healthy potted plants of *M. painteri*, using the method of Talgø and Stensvand (2013). Host stems were wounded (three lesions/stem) with previously sterilized needles. The inoculum consisted in a culture of the fungus grown on PDA for 5 d. Tufts of mycelium were taken from this culture and used to contaminate the tips of needles that were introduced into the lesions on stems. Three control plants were treated with needles without the inoculum. All plants were grown in a greenhouse, at 21 to 30°C.

RESULTS AND DISCUSSION

The initial symptoms on affected *M. painteri* plants were chlorosis and yellowing of stems that were followed by the browning of tissues. The exterior of stems later become blackish (Figure 1a), while the internal stem tissues were rotted (Figure 1b). The disease affected about 80% of 1,000 plants *M. painteri* in the nursery.

The isolates on PDA produced pale pink colonies generating pale pink pigments in the agar. On CLA, colonies produced microconidia, macroconidia in pale orange sporodochia, and chlamydospores. The unicellular, oval to elliptical microconidia were supported by short monophialides (Figure 1c), and measured 4.4–8.6 × 1.3–3.4 (mean = 6.0 × 2.3) µm (n = 50). The slightly falcate macroconidia had foot-shaped basal cells and short apical cells (Figure 1d), three (rarely four) septa, and measured 26.5-44.6 × 3.0–4.5 (mean = 33.5 × 3.6) µm (n = 50). The rough walled chlamydospores were intercalary or terminal, single or in pairs or chains (Figure 1e), and measured 6.2–12.3 (mean = 8.7) µm (n = 50). These morphological characteristics are typical of *Fusarium oxysporum* (Leslie and Summerell, 2006).

The morphological identification was confirmed by the molecular analyses that obtained three sequences

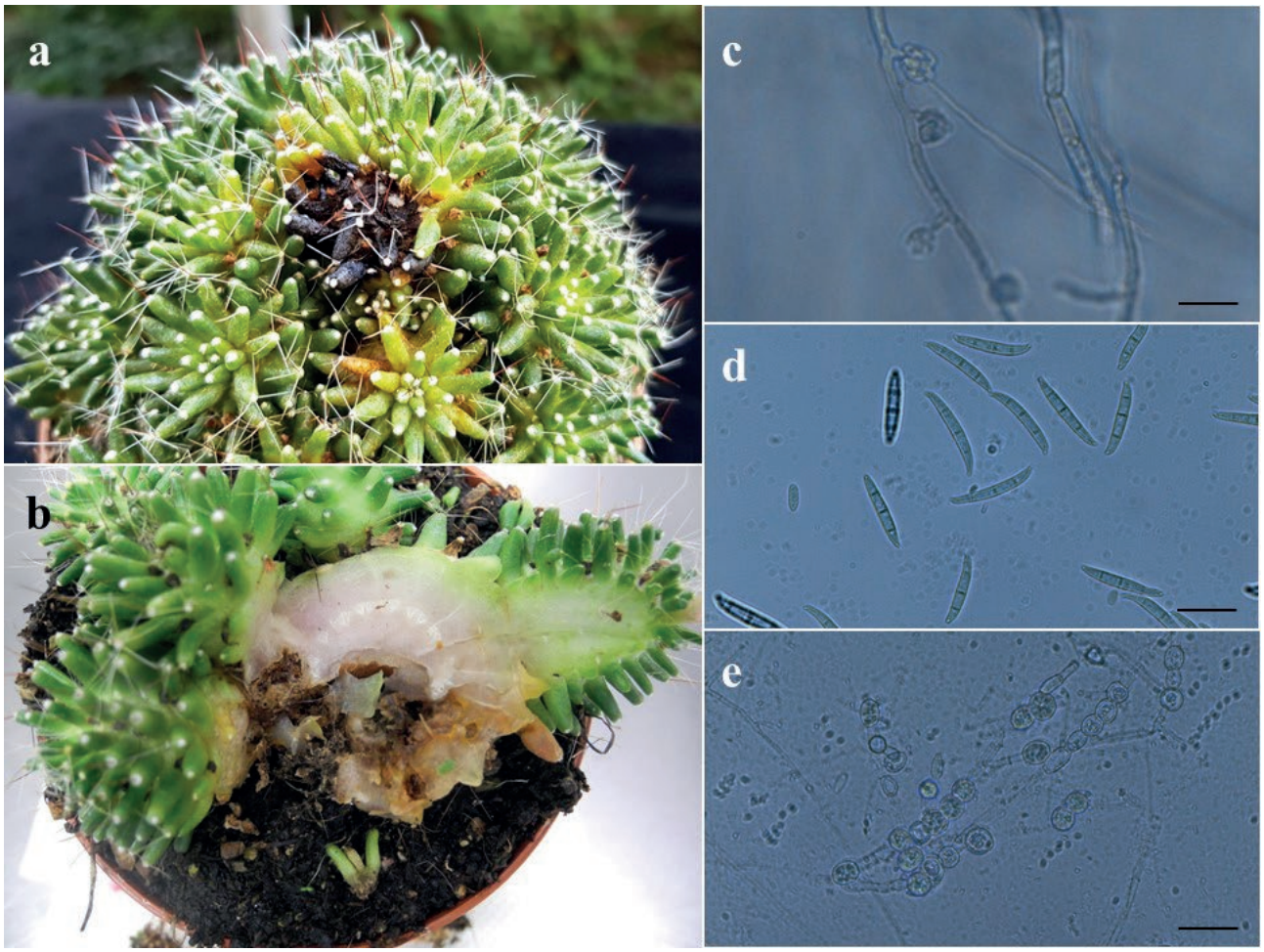

Figure 1. Disease symptoms caused by *Fusarium oxysporum* f. sp. *opuntiarum* on stems of *Mammillaria painteri* (a), and rot of the internal tissues (b). Microconidia (c), macroconidia (d) and chlamydospores (e) of the pathogen. Scale bars = 20 µm.

with, respectively, 676 (*EF1α*), 975 (*RPB2*), and 914 (IGS) base pairs. These sequences were deposited in GenBank (accession numbers, respectively, MT450439, MT450441, MT450440). The BLASTn analysis of these sequences showed 100% similarity with *Fusarium oxysporum* strain CBS 133.023 (accession no. KF255547) in the *RPB2* portion. Furthermore, 100% similarity was obtained with the reference strain of *F. oxysporum* f. sp. *opuntiarum* NRRL28368 (O'Donnell *et al*., 2009) in the *EF1α* portion (accession no. AF246871), and IGS region (accession no. FJ985530). Phylogenetic analysis of IGS sequences was performed, showing that the DB18AGO01 isolate grouped together with the reference NRRL_28368 strain and other strains of *F. oxysporum* f. sp. *opuntiarum* from different plant hosts (Figure 2) (Bertetti *et al*., 2017; Garibaldi *et al*., 2019a; Garibaldi *et al*., 2019b). Within the main cluster, three different phylogenetic subgroups were observed. The first subgroup comprised the DB18AGO01 isolate from *M. painteri*, and strains originating from *Disco placentiformis*, *Cereus peruvianus florida*, *C. marginatus*, *Sulcorebutia rauschii*, *S. heliosa*, and *Euphorbia mammillaris*. The second subgroup included strains from *C. peruvianus monstruosus, Zygocactus truncatus,* and the *F. oxysporum* f. sp. *opuntiarum* reference strain from *Echinocactus grusonii*. The DB14OTT05 M1 strain from *Astrophytum myriostigma* represented the third subgroup. These subgroups may indicate the presence of different physiological races within *F. oxysporum* f. sp. *opuntiarum*, which will require further molecular studies for adequate differentiation. Therefore, the fungus isolated from *M. painteri* was added in the *forma specialis opuntiarum* of *F. oxysporum*.

In the pathogenicity test, the first symptoms consisting of yellowing around the inoculated wounds appeared approx. 30 d after inoculation. As the disease progressed, stems became blackish around the

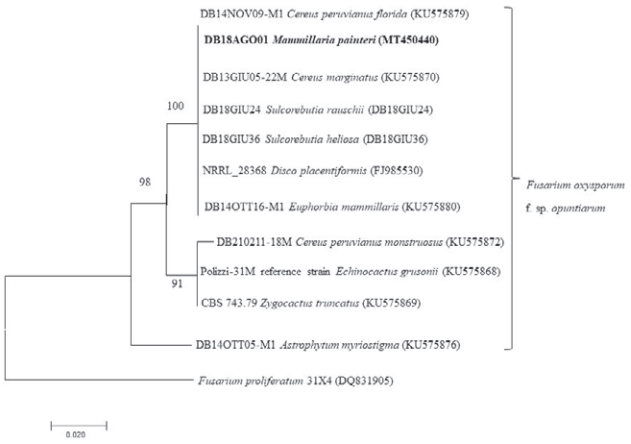

Figure 2. Phylogenetic analysis of a *Fusarium oxysporum* f. sp. *opuntiarum* isolate on the basis of intergenic spacer (IGS) sequences, inferred from maximum likelihood analysis. The values at the dendrogram nodes are bootstrap support values based on 1000 replicates. The strain DB18AGO01 from *Mammillaria painteri* is shown in bold font. The strain 31X4 of *Fusarium proliferatum* was used as an outgroup.

wounds, and the internal stem tissues rotted. Affected plants died. *Fusarium oxysporum* was constantly re-isolated from inoculated plants, whereas control plants remained symptomless. Most of the isolates reported in Figure 2 (DB14NOV09-M1, DB13GIU05-22M, DB14OTT16-M1, DB210211-18M, CBS 743.79, Polizzi-31M and DB14OTT05-M1) were previously inoculated onto *Schlumbergera truncata*, a species very susceptible to *F. oxysporum* f. sp. *opuntiarum*, and they all showed the same high virulence towards this host. Moreover, *C. peruvianus florida*, *C. marginatus*, *E. mammillaris*, *C. peruvianus monstruosus* and *A. myriostigma* were more or less susceptible to the *F. oxysporum* f. sp. *opuntiarum* reference isolates (CBS 743.79 and Polizzi-31M) (Bertetti *et al*., 2017). Further cross-pathogenicity assays should be performed. including to additional hosts of *F. oxysporum* f. sp. *opuntiarum*, in order to establish the host range of the DB18AGO01 isolate from *M. painteri*, and to investigate the occurrence of physiological races of *F. oxysporum* f. sp. *opuntiarum*.

Morphological and molecular identifications were in agreement, and Koch's postulates were satisfied, demonstrating that *F. oxysporum* f. sp. *opuntiarum* was the causal agent of the disease observed on *M. painteri*. This is the first report of this pathogen on *M. painteri*. Stem rot could cause significant economic losses in *M. painteri* cultivated in Italy. Commercial growing of succulent plants is increasing in Italy, and the evaluation of their susceptibility to *F. oxysporum* from *M. painteri* may provide useful information to avoid the spread of this pathogen.

LITERATURE CITED

Alfieri Jr. S.A., Langdon K.R., Wehlburg C., Kimbrough J.W., 1984. Index of Plant Diseases in Florida (Revised). *Florida Department of Agriculture and Consumer Service, Division of the Plant Industry Bulletin* 11: 1–389.

Altschul S.F., Madden T.L., Schaffer A.A., Zhang Z., Miller W., Lipman D.J., 1997. Gapped BLAST and PSI-BLAST: a new generation of protein database search programme. *Nucleic Acids Research* 25: 3389–3402.

Appel D.J., Gordon T.R., 1995. Intraspecific variation within populations of *Fusarium oxysporum* based on RFLP analysis of the intergenic spacer region of the rDNA. *Experimental Mycology* 19: 120–128.

Bertetti D., Ortu G., Gullino M.L., Garibaldi A., 2017. Identification of *Fusarium oxysporum* f. sp. *opuntiarum* on new hosts of the *Cactaceae* and *Euphorbiaceae* families. *Journal of Plant Pathology* 99: 347–354.

Fisher N.L., Burgess L.W., Toussoun T.A., Nelson P.E., 1982. Carnation leaves as a substrate and for preserving cultures of *Fusarium* species. *Phytopathology* 72: 151–153.

French A.M., 1989. California plant disease host index. California Dept. of Food and Agriculture, Division of Plant Industry, Sacramento, California, USA, 394 pp.

Garibaldi A., Bertetti D., Pensa P., Ortu G., Gullino M.L., 2015. First Report of *Fusarium oxysporum* Causing Wilt on *Euphorbia mammillaris* var. *variegata* in Italy. *Journal of Plant Pathology* 97 (4 Supplement): S68.

Garibaldi A., Bertetti D., Pensa P., Matić S., Gullino M.L., 2019a. First Report of stem rot caused by *Fusarium oxysporum* f. sp. *opuntiarum* on *Sulcorebutia heliosa* in Italy. *Plant Disease* 103: 2678.

Garibaldi A., Bertetti D., Pensa P., Matić S., Gullino M.L., 2019b. First report of stem wilt caused by *Fusarium oxysporum* f. sp. *opuntiarum* on *Sulcorebutia rauschii* in Italy. *Journal of Plant Pathology* 102: 577.

Gerlach W., 1972. Fusarium rot and other fungal diseases of horticulturally important cacti in Germany. *Phytopathologische Zeitschrift* 74: 197–217.

Leslie J.F., Summerell B.A., 2006. *The Fusarium Laboratory Manual*. Blackwell Professional, Ames, Iowa, USA, 388 pp.

Lops F., Cibelli F., Raimondo M.L., Carlucci A., 2013. First report of stem wilt and root rot of *Schlumbergera truncata* caused by *Fusarium oxysporum* f. sp. *opuntiarum* in southern Italy. *Plant Disease* 97: 846.

O'Donnell K., Kistler H.C., Cigelink E., Ploetz R.C., 1998. Multiple evolutionary origins of the fungus causing Panama disease of banana: concordant evidence from nuclear and mitochondrial gene genealogies. *Pro-*

ceedings of the National Academy of Science USA 95: 2044–2049.

O'Donnell K., Sarver B.A., Brandt M., Chang D.C., Noble-Wang J., … Ward T.J., 2007. Phylogenetic diversity and microsphere array-based genotyping of human pathogenic Fusaria, including isolates from the multistate contact lens-associated U.S. keratitis outbreaks of 2005 and 2006. *Journal of Clinical Microbiology* 45: 2235–2248.

O'Donnell K., Gueidan C., Sink S., Johnston P.R., Crous P.W., … Sarver B.A.J., 2009. A two-locus DNA sequence database for typing plant and human pathogens within the *Fusarium oxysporum* species complex. *Fungal Genetics and Biology* 46: 936–948.

Polizzi G., Vitale A., 2004. First report of basal stem rot of golden barrel cactus caused by *Fusarium oxysporum* f. sp. *opuntiarum* in Italy. *Plant Disease* 88: 85.

Souza de A.E.F., Nascimento L.C., Araújo E., Lopes E.B., Souto F.M., 2010. Occurrence and identification of the etiologic agents of plant diseases in cactus (*Opuntia ficus-indica* Mill.) in the semi-arid region of Paraiba. *Biotemas* 23: 11–20.

Talgø V., Stensvand A., 2013. A simple and effective inoculation method for *Phytophthora* and fungal species on woody plants. *OEPP/EPPO Bulletin* 43: 276–279.

Phytopathologia Mediterranea
The international journal of the
Mediterranean Phytopathological Union

Firenze University Press
www.fupress.com/pm

Short Notes

Identification and characterization of the first complete genome sequence of prune dwarf virus in China

Shuang SONG[1,†], Lei ZHANG[2,†], Qiang WANG[3], Jun-hua ZHANG[1], Zheng-nan LI[2,*]

[1] *College of Agriculture, Northeast Agricultural University, Harbin 150030, China*
[2] *College of Horticulture and Plant Protection, Inner Mongolia Agricultural University, Hohhot 010018, China*
[3] *Department of Plant Pathology, University of Florida, Gainesville FL 32611, USA*
† Shuang Song and Lei Zhang contributed equally to this work.
* Corresponding author: lizhengnan@imau.edu.cn

Summary. *Prune dwarf virus* (PDV; *Ilarvirus*, *Bromoviridae*), is a common virus infecting stone fruit trees (*Prunus* spp.). The complete genome sequence of a sweet cherry isolate of PDV (PDV-DL) from Dalian, Liaoning Province, China, was determined. The RNA1, RNA2 and RNA3 of PDV-DL are, respectively, 3,376 nt, 2,594 nt and 2,129 nt in size, and have the same genome organization as those previously reported. When compared to the available sequences of PDV, isolate PDV-DL shares pairwise identities between 91.1 to 97.4% for the RNA1, 87.2 to 99.0% for the RNA2, and 88.1 to 96.9% for the RNA3. Phylogenetic analyses based on near full-length RNA3 sequences clustered 14 PDV isolates into three groups, and PDV-DL showed the closest relationship with a peach isolate PCH4 from Australia and an experimental isolate CH137 from the United States of America. Nine recombination events were predicted in genomic RNA1-3 among all of the PDV isolates. This is the first report of the complete genome sequence of PDV from China, which provides the basis for further studies on the molecular evolution of PDV, and will assist help molecular diagnostics and management of the diseases caused by PDV.

Keywords. *Prunus*, stone fruit.

OPEN ACCESS

Citation: S. Song, L. Zhang, Q. Wang, J.-hua Zhang, Z.-nan Li (2020) Identification and characterization of the first complete genome sequence of prune dwarf virus in China. *Phytopathologia Mediterranea* 59(2): 371-376. DOI: 10.14601/Phyto-11492

Accepted: May 11, 2020

Published: August 31, 2020

Data Availability Statement: All relevant data are within the paper and its Supporting Information files.

Competing Interests: The Author(s) declare(s) no conflict of interest.

Editor: Arnaud G Blouin, New Zealand Institute for Plant and Food Research, Auckland, New Zealand.

Funding: This study was financially supported by the University Nursing Program for Young Scholars with Creative Talents in Heilongjiang Province (uNPYSCT- 2018157), and the Natural Science Foundation of Inner Mongolia, China (2019MS03021).

Ethical approval: This article does not contain any studies with human participants or animals performed by any of the authors.

Informed consent: Informed consent was obtained from all individual participants included in the study.

INTRODUCTION

Prune dwarf virus (PDV) is a species of *Ilarvirus* in the *Bromoviridae*, which has a tripartite positive-sense single-stranded RNA genome (Pallas *et al.*, 2012). RNA1 of PDV encodes the replicase protein P1, and RNA2 encodes the replicase protein P2 (Koonin, 1991; Rozanov *et al.*, 1992), whereas RNA3 encodes the movement protein (MP) in 5'-proximal half and the coat protein (CP) in 3'-proximal half (Codoñer and Elena, 2008; Pallas *et al.*, 2012). PDV is an economically important virus of stone fruits (*Prunus* spp.), causing losses especially in cherry, almond and peach (Çağlayan *et al.*, 2011;

Kinoti *et al*., 2018; Kamenova *et al*., 2019). The virus is distributed widely in the world, and can be transmitted by vegetative propagation materials and through pollen and seed (Mink, 1993).

In China, PDV was first detected on sweet cherry in 1996 (Zhou *et al*., 1996), and subsequently reported on cherry or peach from the main stone fruit planting districts of China, including Shaanxi, Liaoning, Beijing and Shandong (Ruan *et al*., 1998; Hou *et al*., 2005; Zhao *et al*., 2009; Zong *et al*., 2015). The virus has been regarded as a serious threat to the commercial production of cherry in China (Zong *et al*., 2015). No complete genomic sequence of Chinese PDV isolate was available. The present study determined the first complete genomic sequence of PDV in China, and compared this with other available PDV genomic sequences. This will provide the basis for further research on the molecular evolution of PDV, and assist molecular diagnostics and management of the diseases caused by PDV.

MATERIALS AND METHODS

Virus source

In July 2019, sweet cherry (*Prunus avium* L.) 'Meizao' trees with symptoms of leaf mosaic and crinkle, indicative of virus infection, were observed in an orchard in Dalian, Liaoning Province, China. Leaf samples were collected from a symptomatic tree, frozen in liquid nitrogen, and then transferred to -80°C for further research.

RNA extraction, small RNA sequencing and analysis

High-throughput sequencing (HTS) of small RNAs was used to identify viruses in the samples. Total RNA was extracted from leaf samples using TRIzol reagent (Invitrogen, 15596) according to the manufacturer's instructions. A library of small RNAs was constructed using a TruSeq Small RNA Sample Preparation Kit (IIIumina, RS-200-0024), and was sequenced using IIIumina HiSeq2000 platform at Biomarker Technologies (Beijing, China). The obtained raw reads were cleaned by trimming adapter sequences and eliminating reads less than 18 nt or more than 35 nt, using an in-house Perl script from Biomarker Technologies. The clean reads were assembled *de novo* into contigs using Velvet Software (Zerbino and Birney, 2008). The contigs were used for Blast analysis against the GenBank Virus RefSeq Nucleotide and Virus RefSeq Protein databases, with e-values of 10^{-5} (Wu *et al*., 2010).

RT-PCR validation of candidate viruses

To validate the occurrence of HTS-detected viruses in the samples, RT-PCR was carried out using specific primers designed based on the obtained viral contigs and conserved regions of the published genome from GenBank (Table S1). Single-stranded cDNA was synthesized from the total RNA using M-MLV Reverse Transcriptase (Promega, M1701) with random hexamer primer following the manufacturer's instructions. PCR was performed in a volume of 25 µL containing 1.0 µL cDNA, 12.5 µL Premix *LA Taq* DNA polymerase Mix (TaKaRa, RR900A), 1.0 µL 10 µM corresponding upstream and downstream primers, with 35 cycles of 94°C for 30 s, 54°C for 30 s and 72°C for 1 min. The PCR products were examined by 1% agarose gel electrophoresis and ethidium bromide staining.

Cloning and sequencing of PDV genome

The primer pairs PDV-F1/PDV-R, PDV-F2/PDV-R and PDV-F3/PDV-R (Table S1) were selected to amplify, respectively, the near full-length sequences of RNA1, RNA2 and RNA3. PCR was performed as described above, except that the elongation time was increased from 1 min to 3 min at 72°C. The 5' and 3' terminal sequences were obtained from the total RNA, which had been treated with Poly(A) polymerase (TaKaRa, D2180A), using SMARTer^{TM} RACE cDNA Amplification Kit (Clontech, 634923). All of the amplicons were gel-purified using Gel Extraction Kit (CWBIO, CW2302M), cloned into pMD18-T simple vector (TaKaRa, D103A) and sequenced. Three independent clones were sequenced for each amplicon.

Sequence, phylogenetic and recombination analyses

The genomic sequences were assembled from the near full-length sequences and 5' and 3' terminal sequences using Vector NTI based on overlapping regions of 127-723 nt, and the ORFs were identified using ORFfinder (https://www.ncbi.nlm.nih. gov/orffinder). Blast analysis was performed online (http://blast.ncbi.nlm.nih.gov/ Blast.cgi). Only four full genomes of PDV are available in GenBank (sweet cherry isolate 1046C from Slovakia, sweet cherry isolate Niagara D5 from Canada, and peach isolates PCH4 and NS9 from Australia). In addition, one full-length RNA1 from sweet cherry isolate Salmo BC from Canada, one full-length RNA2 from an unknown isolate (AF277662), and one full-length RNA3 from experimental isolate

CH137 maintained in squash from the United States of America were available. SDT 1.0 software (Muhire *et al.*, 2014) was used to calculate the pairwise identities of nucleotide and amino acid sequences by the ClustalW algorithm. Multiple sequence alignment was performed using the ClustalW algorithm of MEGA 6.0 (Tamura *et al.*, 2013), with gap opening penalty of 15 and gap extension penalty of 6.66. Phylogenetic trees were constructed using the neighbor-joining (NJ) method with 1,000 bootstrap replicates, and genetic distance was calculated by the Tamura three-parameter model which was determined as the best-fitting model of substitution using MEGA 6.0. Recombination events were predicted by seven methods in RDP3 Software (Heath *et al.*, 2006), including RDP, Geneconv, Chimera, BootScan, MaxChi, SiScan and 3Seq, with default settings. Only the recombination events predicted by at least five methods with P values <0.01 were accepted.

RESULTS AND DISCUSSION

A total of 16,858,859 raw reads were obtained by HTS of small RNAs. After removing adapter sequences, a total of 15,488,787 clean reads with lengths of 18-35 nt were assembled into 3,742 contigs with N50 of 66 nt using Velvet Software. Blast analysis against the GenBank database showed that 11 out of the 3,742 contigs with lengths of 53-204 nt were mapped to the genome sequence of PDV, seven mapped to cherry virus A (CVA) with lengths of 46-189 nt, five to prunus necrotic ringspot virus (PNRSV) with lengths of 49-230 nt, one of 42 nt to papaya ringspot virus (PRSV) and one of 43 nt mapped to pepper chlorotic spot virus (PCSV). RT-PCR detection with specific primers derived from the contigs and sequencing of the amplicons confirmed the occurrence of PDV, CVA and PNRSV. However, PRSV or PCSV were RT-PCR negative, which might indicate false positive results of HTS considering the limited numbers and lengths of contigs. Previous research showed that virus detection based on HTS of small RNAs could be 10 times more sensitive than RT-PCR (Santala and Valkonen, 2018). Therefore, it cannot be excluded that the low titres of PRSV and PCSV were below the sensitivity of RT-PCR.

The complete genomic sequence of the PDV isolate PDV-DL was determined and submitted to GenBank with accession numbers MT013233-MT013235. It shares the same genome organization as those previously reported. The RNA1 of PDV-DL is 3,376 nt, encoding P1 of 1,055 aa from 39 to 3,206 nt. This contains the methyltransferase domain at N-terminal and the NTPase/helicase-like domain at C-terminal (Rozanov *et al.*, 1992; Gorbalenya and Koonin, 1993). The RNA2 is 2,594 nt, encoding the RNA-dependent RNA polymerase (P2) of 788 aa from 32 to 2,398 nt. The RNA3 is 2,129 nt, encoding MP of 293 aa from 261 to 1,142 nt and CP of 218 aa from 1,215 to 1,871 nt.

Compared to available full-length genomic sequences, PDV-DL shares pairwise nucleotide sequence identities of 91.1–97.4% for RNA1, 87.2–99.0% for RNA2, and 88.1–96.9% for RNA3 (Figure 1). The P1 of PDV-DL shares the highest amino acid sequence identity of 97.7% with that of isolate Salmo BC (YP_611154). The P2 shares the highest amino acid sequence identity of 98.9% with that of isolate Niagara D5 (QGA70956). The MP shares the highest amino acid sequence identity of 98.3% with that of isolate CH137 (AAA46818), and the CP of PDV-DL shares the highest amino acid sequence identity of 99.5% with that of a cherry isolate PD6 from Turkey (ABQ96001).

There are only two records of CP genes of Chinese PDV isolates available from sweet cherry in GenBank, HSY4-1 (KC965106) and DJ1-2 (JF333587). The CP gene of PDV-DL shares 93.5% nucleotide and 96.3% amino acid identities with that of HSY4-1, and 92.7% nucleotide and 95.4 amino acid identities with that of DJ1-2.

The phylogenetic NJ trees based on RNA1, RNA2 and RNA3 showed different topological structures. PDV-DL in this study clustered together with isolate Niagara D5 in the RNA2 tree, and together with isolates PCH4 and CH137 in the RNA3, both of which were supported by high bootstrap values, but PDV-DL did not form a distinct clade with any other isolates in the RNA1 tree (Figure 1). The different clustering of RNA1, RNA2 and RNA3 may be related with the potential recombination and segment re-assortment during the evolutionary history of PDV, which are common for the family *Bromoviridae* (Codoñer and Elena, 2008; Song *et al.*, 2019). However, this is difficult to confirm because of the limited number of published PDV genome records. Therefore, the information of genome sequences from more PDV isolates are needed to confirm the evolutionary history of this virus.

Recombination and segment reassortment are two of the important mechanisms for driving the evolution of RNA plant viruses, which mainly occur during mixed infections (Codoñer and Elena, 2008). The present study has shown that a total of nine recombination events were predicted by RDP3, and three events were identified in each of genomic RNA1, RNA2 and RNA3 (Table 1).

Due to limited number of PDV complete genomes and in order to eliminate the potential effects of recombination events on phylogenetic analysis, the near full-

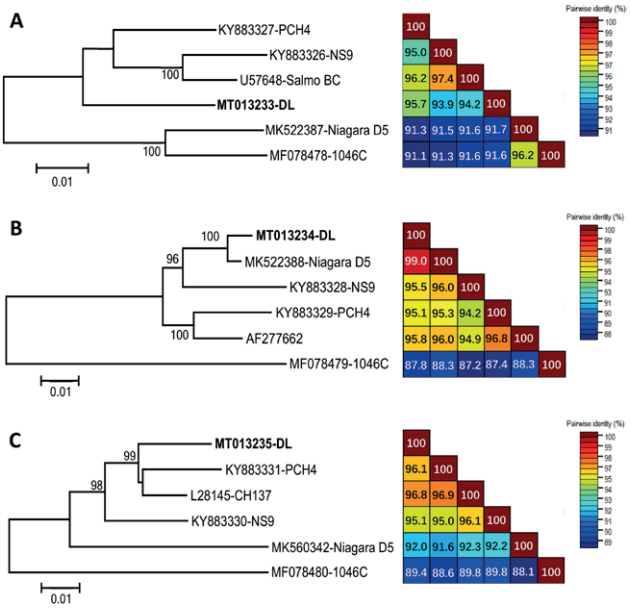

Figure 1. Phylogenetic analyses and matrix of pairwise identities based on prune dwarf virus (PDV) full-length genomic sequences of RNA1 (A), RNA2 (B) and RNA3 (C). The PDV-DL isolate examined in this study is marked in bold. Phylogenetic trees were constructed by the neighbor-joining (NJ) method with 1,000 bootstrap replicates, and genetic distance was calculated by the Tamura three-parameter model using MEGA 6.0. The pairwise identities were calculated by the ClustalW algorithm using SDT 1.0 software.

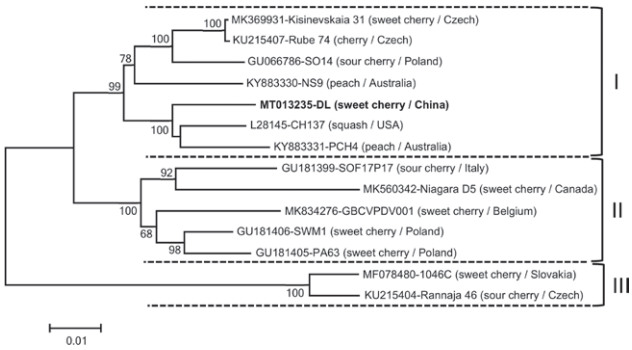

Figure 2. Phylogenetic analysis based on the near full-length sequence of RNA3, covering the complete coding regions of movement protein (MP) and coat protein (CP) genes and the intergenic region (IGR), of the prune dwarf virus (PDV) isolate examined in this study (PDV-DL), and 13 other PDV isolates available in GenBank, without recombination events detected. The accession number, isolate names, hosts and countries for each isolate are indicated, and PDV-DL examined in this study is marked in bold. Phylogenetic tree was constructed by the neighbor-joining (NJ) method with 1,000 bootstrap replicates, and genetic distance was calculated by the Tamura three-parameter model using MEGA 6.0.

length sequence of RNA3 of PDV-DL, covering the complete coding regions of MP and CP genes and the intergenic region (MP-IGR-CP), was used for phylogenetic analysis with 13 PDV isolates from GenBank where no recombination events were detected. The obtained NJ tree based on the MP-IGR-CP regions clustered the 14 PDV isolates into three groups supported by high bootstrap values, and PDV-DL showed the closest evolutionary relationship with isolates PCH4 and CH137 (Figure 2). The phylogenetic grouping showed no clear correlation to host or geographic origin. Individual phylogenetic analysis of the CP and the MP confirmed the same clustering, although this was not supported by high bootstrap values (62 for CP and 69 for MP) (Figure S1).

Previous studies of PDV genetic diversity mostly focused on the CP gene of RNA3, and showed different results. Ulubaş Serçe *et al.* (2009) reported the existence of four distinct phylogenetic groups of PDV isolates based on the CP gene, while Predajňa *et al.* (2017) identified only two groups of PDV isolates based on MP and CP phylogenetic trees. In the present study, three distinct phylogenetic groups were observed in phylogenetic NJ tree based on the near full-length RNA3 sequences,

Table 1. Recombination events in genomic RNA1, RNA2 and RNA3 of prune dwarf virus (PDV) predicted by RDP3.

	Recombinant	Major parent	Minor parent	Region (nt)	RDP	Geneconv	BootScan	MaxChi	Chimaera	SiScan	3Seq
RNA1	PCH4	Salmo BC	DL	1134-1517	5.96E-08	1.06E-05	3.10E-08	1.63E-05	4.33E-06	1.84E-06	3.77E-05
	PCH4	Salmo BC	DL	1757-2145	2.57E-06	1.26E-05	8.92E-07	1.05E-04	9.85E-05	3.31E-10	2.59E-06
	PCH4	Salmo BC	DL	2369-2727	9.47E-09	1.27E-07	4.34E-09	3.03E-08	4.67E-06	1.48E-08	3.28E-05
RNA2	Niagara D5	PCH4	NS9	55-671	7.90E-03	-	6.68E-03	4.64E-03	-	2.01E-03	7.68E-03
	1046C	PCH4	NS9	399-754	7.90E-03	-	6.68E-03	4.64E-03	-	2.01E-03	7.68E-03
	AF277662	NS9	PCH4	436-697	7.90E-03	-	6.68E-03	4.64E-03	-	2.01E-03	7.68E-03
RNA3	PA78	PA63	SWM1	16-1006	-	1.65E-04	2.23E-06	7.26E-08	1.46E-07	3.86E-11	3.77E-13
	SOF15P11	SWM1	SOF17P17	1-933	1.76E-05	1.05E-03	1.78E-05	4.53E-09	2.15E-03	2.47E-12	3.25E-07
	PE247	SOF17P17	Rannaja 46	12-957	-	2.38E-12	9.39E-14	7.74E-17	2.76E-16	2.11E-23	1.20E-36

which was consistent with results from Australia (Kinoti *et al*., 2018) and Bulgaria (Kamenova *et al*., 2019).

PDV is one of the most common viruses infecting stone fruit trees, especially sweet cherry trees (Predajňa *et al*., 2017). Symptom expression induced by PDV is highly variable, ranging from symptomless to leaf yellowing, chlorosis, mosaic, ringspot, necrosis, malformations and fruit reduction, depending on environmental conditions, virus isolate, host species and cultivar (Fonseca *et al*., 2005; Predajňa *et al*., 2017). Stone fruit trees with mixed infections of PDV with other viruses are common in nature and these infections can also affect symptom expression (Gao *et al*., 2016). In the present study, PDV was detected in a sweet cherry tree with symptoms of leaf mosaic and crinkle. However, PNRSV and CVA were also detected in the same tree, so there is no clear evidence supporting the correlation of the observed symptoms to infection by PDV. However, this is the first report of the complete genomic sequence of PDV from China, which provides the basis for further studies on genetic evolution in this virus, and for molecular diagnostics and potential disease management of PDV in this country.

ACKNOWLEDGEMENTS

This study was funded by the University Nursing Program for Young Scholars with Creative Talents in Heilongjiang Province (uNPYSCT-2018157), and the Natural Science Foundation of Inner Mongolia, China (2019MS03021).

LITERATURE CITED

Çağlayan K., Serçe Ç.U., Gazel M., Varveri C., 2011. *Prune dwarf virus*. In: Virus and Virus Like Diseases of Pome and Stone Fruits (A. Hadidi, M. Barba, T. Candresse, W. Jelkmann, ed.), APS Press, St. Paul, MN, USA, 281–287.

Codoñer F.M., Elena S.F., 2008. The promiscuous evolutionary history of the family *Bromoviridae*. *Journal of General Virology* 89: 1739-1747.

Fonseca F., Neto J.D., Martins V., Nolasco G., 2005. Genomic variability of prune dwarf virus as affected by agricultural practice. *Archives of Virology* 150: 1607–1619.

Gao R., Li S., Lu M., 2016. Complete nucleotide sequences of two isolates of *Cherry virus A* from sweet cherry in China. *Journal of Integrative Agriculture* 15: 1667–1671.

Gorbalenya A.E., Koonin E.V., 1993. Helicases: amino acid sequence comparisons and structure-function relationships. *Current Opinion in Structural Biology* 3: 419–429.

Heath L., van der Walt E., Varsani A., Martin D.P., 2006. Recombination patterns in aphthoviruses mirror those found in other picornaviruses. *Journal of Virology* 80: 11827–11832.

Hou Y., Yang J., Li C., 2005. Establishment and application of detection of *Prune dwarf virus* (PDV) by RT-PCR. *Scientia Agricultura Sinica* 38: 425–427 (In Chinese).

Kamenova I., Borisova A., Popov A., 2019. Incidence and genetic diversity of *Prune dwarf virus* in sweet and sour cherry in Bulgaria. *Biotechnology & Biotechnological Equipment* 33: 980–987.

Kinoti W.M., Constable F.E., Nancarrow N., Plummer K.M., Rodoni B., 2018. The incidence and genetic diversity of Apple mosaic virus (ApMV) and Prune dwarf virus (PDV) in *Prunus* species in Australia. *Viruses* 10: 136.

Koonin E.V., 1991. The phylogeny of RNA-dependent RNA polymerase of positive-strand RNA viruses. *Journal of General Virology* 72: 2197–2206.

Mink G.I., 1993. Pollen- and seed-transmitted viruses and viroids. *Annual Review of Phytopathology* 31: 375–402.

Muhire B.M., Varsani A., Martin D.P., 2014. SDT: A virus classification tool based on pairwise sequence alignment and identity calculation. *PLoS One* 9: e108277.

Pallas V., Aparicio F., Herranz M.C., Amari K., Sanchez-Pina M.A., Sanchez-Navarro J.A., 2012. Ilarviruses of *Prunus* spp.: a continued concern for fruit trees. *Phytopathology* 102: 1108–1120.

Predajňa L., Sihelská N., Benediková D., Šoltys K., Candresse T., Glasa M., 2017. Molecular characterization of *Prune dwarf virus* cherry isolates from Slovakia show their substantial variability and reveals recombination events in PDV RNA3. *European Journal of Plant Pathology* 147: 877–885.

Rozanov M., Koonin E.V., Gorbalenya A.E., 1992. Conservation of the putative methyltransferase domain: a hallmark of the 'Sindbis-like' supergroup of positive-strand RNA viruses. *Journal of General Virology* 73: 2129–2134.

Ruan X., Zhou Y., Ma S., Yang Y., 1998. Research on virus survey and detection in peach. Acta *Agriculturae Boreali-occidentalis Sinica* 7: 59–62 (In Chinese).

Santala J., Valkonen J.P.T., 2018. Sensitivity of small RNA-based detection of plant viruses. *Frontiers in Microbiology* 9: 939.

Song S., Sun P., Chen Y., Ma Q., Wang X., … Li Z., 2019. Complete genome sequences of five prunus necrotic

ringspot virus isolates from Inner Mongolia of China and caparison to other PNRSV isolates around the world. *Journal of Plant Pathology* 101: 1047–1054.

Tamura K., Stecher G., Peterson D., Filipski A., Kumar S., 2013. MEGA6: Molecular evolutionary genetics analysis version 6.0. *Molecular Biology & Evolution* 30: 2725–2729.

Ulubaş Serçe Ç., Ertunç F., Öztürk A., 2009. Identification and genomic variability of *Prune dwarf virus* variants infecting stone fruit trees in Turkey. *Journal of Phytopathology* 157: 298–305.

Wu Q., Luo Y., Lu R., Lau N., Lai E.C., Palese P., 2010. Virus discovery by deep sequencing and assembly of virus-derived small silencing RNAs. *Proceeding of the National Academy of Sciences of the United States of America* 107: 1606–1611.

Zerbino D.R., Birney E., 2008. Velvet: Algorithms for *de novo* short read assembly using de Bruijn graphs. *Genome Research* 18: 821–829.

Zhao S., Wang J., Li M., Li G., Ma J., Gou J., 2009. Detection and identification of prune dwarf virus in Huairou district in Beijing. *China Plant Protection* 29: 5-7 (In Chinese).

Zhou Y.Y., Ruan X.F., Wu C.L., 1996. First report of sweet cherry virus in China. *Plant Disease* 80: 1429.

Zong X., Wang W., Wei H., Wang J., Yan X., Liu Q., 2015. Incidence of sweet cherry viruses in Shandong Province, China and a case study on multiple infection with five viruses. *Journal of Plant Pathology* 97: 61–68.

Phytopathologia Mediterranea
The international journal of the
Mediterranean Phytopathological Union

Firenze University Press
www.fupress.com/pm

Short Notes

Protective effects of mycorrhizal association in tomato and pepper against *Meloidogyne incognita* infection, and mycorrhizal networks for early mycorrhization of low mycotrophic plants

Melvin RODRIGUEZ-HEREDIA[1,*], Caroline DJIAN-CAPORALINO[2], Michel PONCHET[2], Laurent LAPEYRE[3], Renaud CANAGUIER[3], Ariane FAZARI[2], Nathalie MARTEU[2], Benoit INDUSTRI[2], Marie OFFROY-CHAVE[4,*]

[1] *School of Chemical and Biological Sciences, Queen Mary University of London, London, E1 4NS, United Kingdom*
[2] *INRAE, Université Côte d'Azur, CNRS, Institut Sophia Agrobiotech, 06903 Sophia-Antipolis, France*
[3] *NIXE Laboratoire, 80 route des lucioles-Bât O-Sophia-Antipolis, 06905 Valbonne, France*
[4] *INRAE, AgroSystèmes TROpicaux, 97170 Petit-Bourg, Guadeloupe, France*
*Corresponding authors: m.rodriguez-heredia@qmul.ac.uk; Marie.Chave@inra.fr

Summary. Root knot nematodes are obligate phytoparasites that invade the roots of important crop plants causing severe economic losses. Arbuscular Mycorrhizal Fungi (AMF) are soil borne microorganisms that establish mutualistic associations with the roots of most plants. AMF have been frequently indicated to help their host to attenuate the damage caused by pathogens and predators. In this study, the effects of a commercial inoculum of AMF against *Meloidogyne incognita* on tomato and pepper were evaluated under controlled conditions. Mycorrhizal association decreased *M. incognita* development in pepper, and improved tolerance to nematode infection in tomato plants. Rapid plant mycorrhization is critical for delivering protective effects against biotic stress. A novel mycorrhization technique using AMF from the highly mycotrophic plant sorghum was applied to tomato. More rapid mycorrhization was achieved in tomato plants grown in soil containing mycorrhized roots of sorghum than in plants directly inoculated with the commercial AMF.

Keywords. Crop pests, symbiosis, agricultural management.

Citation: M. Rodriguez-Heredia, C. Djian-Caporalino, M. Ponchet, L. Lapeyre, R. Canaguier, A. Fazari, N. Marteu, B. Industri, M. Offroy-Chave (2020) Protective effects of mycorrhizal association in tomato and pepper against *Meloidogyne incognita* infection, and mycorrhizal networks for early mycorrhization of low mycotrophic plants. *Phytopathologia Mediterranea* 59(2): 377-384. DOI: 10.14601/Phyto-11637

Accepted: May 28, 2020

Published: August 31, 2020

Data Availability Statement: All relevant data are within the paper and its Supporting Information files.

Competing Interests: The Author(s) declare(s) no conflict of interest.

Editor: Isabel Abrantes, University of Coimbra, Portugal.

INTRODUCTION

Phytoparasite nematodes are part of the soil microfauna with life cycles that are totally or partially within plants. Root-knot nematodes (RKNs) of the genus *Meloidogyne* are obligate endoparasites affecting a large number of plant species (Sasser and Freckman, 1987). They form characteristic galls in roots and block host plant conductive tissues, causing moisture stress

(Meon *et al*. 1978), poor root development and growth, and significantly reduce crop productivity (Hussey, 1985; Melakeberhan and Webster, 1993).

RKNs are present in most farmlands, and can infect more than 5500 plant species, including vegetables, fruit crops, cereals and ornamentals (Blok *et al*., 2008). Economic losses due to RKN are estimated at tens of billions of euros per year (Jones *et al.,* 2013). For example, more than 40% of economic crops in the southeast of France are affected by *Meloidogyne* spp. (Djian-Caporalino, 2010, 2012). The usual methods for controlling RKNs included use of bromide/chloride/phosphorus-based products which are very concerning for the environment and human health, and therefore have been phased out in the European Union since 2009 (Council of the European Union, 2009). Physical approaches include prophylaxis, steam disinfection and solarisation, which are not always effective. Biological approaches for controlling RKNs are based on resistant plant varieties, nematode parasitic bacteria, toxins from nematicidal plants, biofumigation from plant oil cakes, and fungi that alter nematode life cycles (Djian-Caporalino *et al.,* 2009).

Arbuscular mycorrhizal fungi (AMF) are obligate biotrophs that exclusively colonise plant roots. These fungi form hyphae connections between roots from one or several host species to establish the Common Mycorrhizal Networks (CMNs) (Simard *et al.,* 2012). Plants associated with CMNs have improved assimilation of phosphate, macronutrients such as N, K and Mg, and some micronutrients (Bhatia *et al.,* 1998; Montaño *et al.,* 2007). Colonising AMF receive organic carbon from the host plants (Sanders and Tinker, 1971). The review of Veresoglou and Rilling (2012) indicated that AMF have capacity to decrease losses caused by diverse plant pathogens, with the interaction between AMF and RKNs representing 28% of the listed reports. For example, early mycorrhization by mixtures of AMF species is effective against *Meloidogyne* spp. and *Pratylenchus* spp. (Vos *et al.,* 2012). Sikora and Schönbeck (1975) reported that *Funneliformis mosseae* and *Rhizophagus fasciculatus* decreased *M. incognita* infection on tomato by, respectively, 13% and 50%. In pepper, Peregrin *et al.,* (2012) assessed effects of AMF and *Bacillus megaterium* (simultaneously and individually) on *Meloidogyne incognita*, although the bioprotection conferred by the AMF was not clearly demonstrated.

Tomato and pepper have been frequently reported as mycotrophic plants (Cress *et al.,* 1979; Al-Karaki, 2000; Schroeder and Janos, 2004; Schroeder-Moreno and Janos, 2008; Gashua *et al.,* 2015; Chialva *et al.,* 2019). Nevertheless, tomato plants do not rapidly develop intensive mycorrhization compared to highly mycotrophic species (Schroeder and Janos, 2004; Kubota, 2005; Thougnon Islas *et al.,* 2014). This can be inconvenient for horticultural applications, as any probable benefit from AMF against RKN may only be obtained through early mycorrhization (Jaizme-Vega *et al.,* 1997; Molinari and Leonetti, 2019). Interconnection from mature plants by CMNs could improve establishment and growth of seedlings (van der Heijden and Horton, 2009). Derelle *et al.,* (2012) reported enhanced mycorrhization of *Silene vulgaris* (weakly mycotrophic) by mycorrhizal networks (MNs) previously developed by *Medicago truncatula* (highly mycotrophic) under *in vitro* conditions. Therefore, examining new strategies for tomato mycorrhization involving MNs could provide worthwhile new and practically valuable knowledge.

To test bioprotection of AMF against RKNs, the effect of mycorrhizal colonisation against development of *M. incognita* was examined in tomato and pepper, as two economically important crop plants. Additionally, the potential of MNs for accelerating mycorrhization was demonstrated on tomato plants using MNs previously established by a suitable highly mycotrophic host such as sorghum.

MATERIALS AND METHODS

Plant material

RKN-susceptible seedlings of tomato (*Solanum lycopersicum* 'Saint Pierre') and pepper (*Capsicum annuum* 'Doux long des Landes') were transplanted into 9 cm × 9 cm pots containing sterilised soil, and were inoculated with AEGIS powder from NIXE® (AMF inoculum containing *Rhizophagus irregularis*). Unless otherwise stated, all the plant cultures were in a growth chamber at 25°C (± 1°C) with a 16 h light / 8 h dark illumination cycle. A nutrient solution adapted for AMF development (200 mg L^{-1} $Ca(NO_3)_2$, 300 mg L^{-1} KNO_3, 25 mg L^{-1} KH_2PO_4, 150 mg L^{-1} $MgSO_4$ 7 H_2O, 1.5 mg L^{-1} H_3BO_3, 0.05 mg L^{-1} $(NH_4)_6Mo_7O_{24}$, 1 mg L^{-1} $ZnSO_4$ 7 H_2O, 2 mg L^{-1} $MnSO_4$ H_2O, 0.25 mg L^{-1} $CuSO_4$ 5 H_2O, 225 mg L^{-1} Fe EDTA) was added every 3 d to the plants, at 1 mL per application for the first week of culture, then increased by 1 mL every week from the second to the fifth weeks. After 6 weeks of culture, the root mycorrhization rates were assessed for three plants of each species, and 5000 freshly hatched J2s of *M. incognita* suspended in water were inoculated onto each plant. The number of nematode egg masses was assessed on each plant at 6 weeks after J2 inoculation, by acid eosin staining. The same experiment was performed simultaneously with non-AMF treated plants as experimental controls.

Tomato mycorrhization by mycorrhizal networks consisted of growing an AMF inoculated sorghum sudangrass plant (*Sorghum bicolor* × *Sorghum sudanense* (Piper) Stapf) under equivalent conditions to the seedlings for the RKN experiments. After 6 weeks, the aerial part and roots were shredded and integrated to the pot soil. A tomato seedling was then transplanted into the sorghum/soil mix, and the mycorrhization rate was assessed after 2 and 4 weeks. Tomato plants inoculated directly with the commercial inoculum were used as experimental controls.

Assessment of root mycorrhization rates

Plant roots were bleached with 1% (w/v) KOH solution at 80° C for 1 h, and then incubated in a 5% solution of ink/lactic acid (80%) for 12 h. After rinsing, 1 cm root segments were mounted in glycerol/lactic acid (1/1 v/v) on glass microscope slides. Mycorrhization rates were evaluated by light microscopy, by considering the mycelium frequency inside and outside each root segment, the quantity of colonized root, and the abundance of developed arbuscules/vesicles (Trouvelot *et al.,* 1986).

Evaluation of Meloidogyne incognita *development*

The roots of experimental plants were rinsed thoroughly with water and the *M. incognita* egg masses were stained with an aqueous solution of 5% eosin B and 0.5% acetic acid. The egg masses (red spots on the roots) were quantified.

Statistical analyses

Results from each experiment were analysed by comparing measured parameters for mycorrhized and non-mycorrhized plants. Differences between experimental conditions were tested by Student's t-Test at significant levels ($P < 0.05$) using R Software.

RESULTS

Figure 1 shows effects of inducing AMF root colonisation of tomato from direct inoculation before seedling transplantation, compared to formation of a MN in the

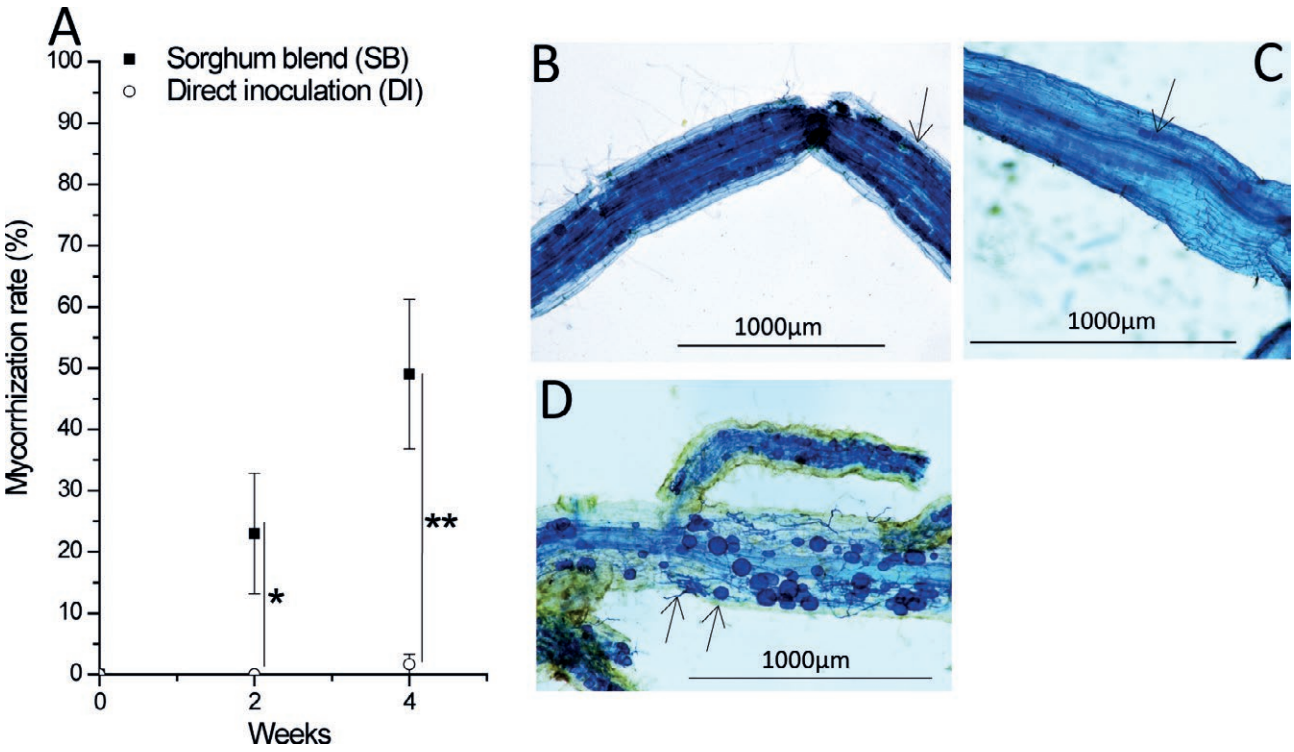

Figure 1. (Graph A) Mean mycorrhization rates (and standard errors: n ≥ 4) in tomato roots resulting from different AMF inoculation procedures at 2 and 4 weeks after inoculation. Before the tomato seedlings were transplanted to pots, a commercial inoculum was applied directly to their roots (direct inoculation: DI), or the soil was blended with leaves and roots of 6-week-old mycorrhized sorghum plants (micrograph D) (sorghum blend: SB). * and **, respectively, indicate differences at $P < 0.05$ and 0.01. Characteristic AMF colonisation of tomato roots grown for 4 weeks after SB (micrograph B) or DI (micrograph C) treatments. Arrows indicate typical AMF structures.

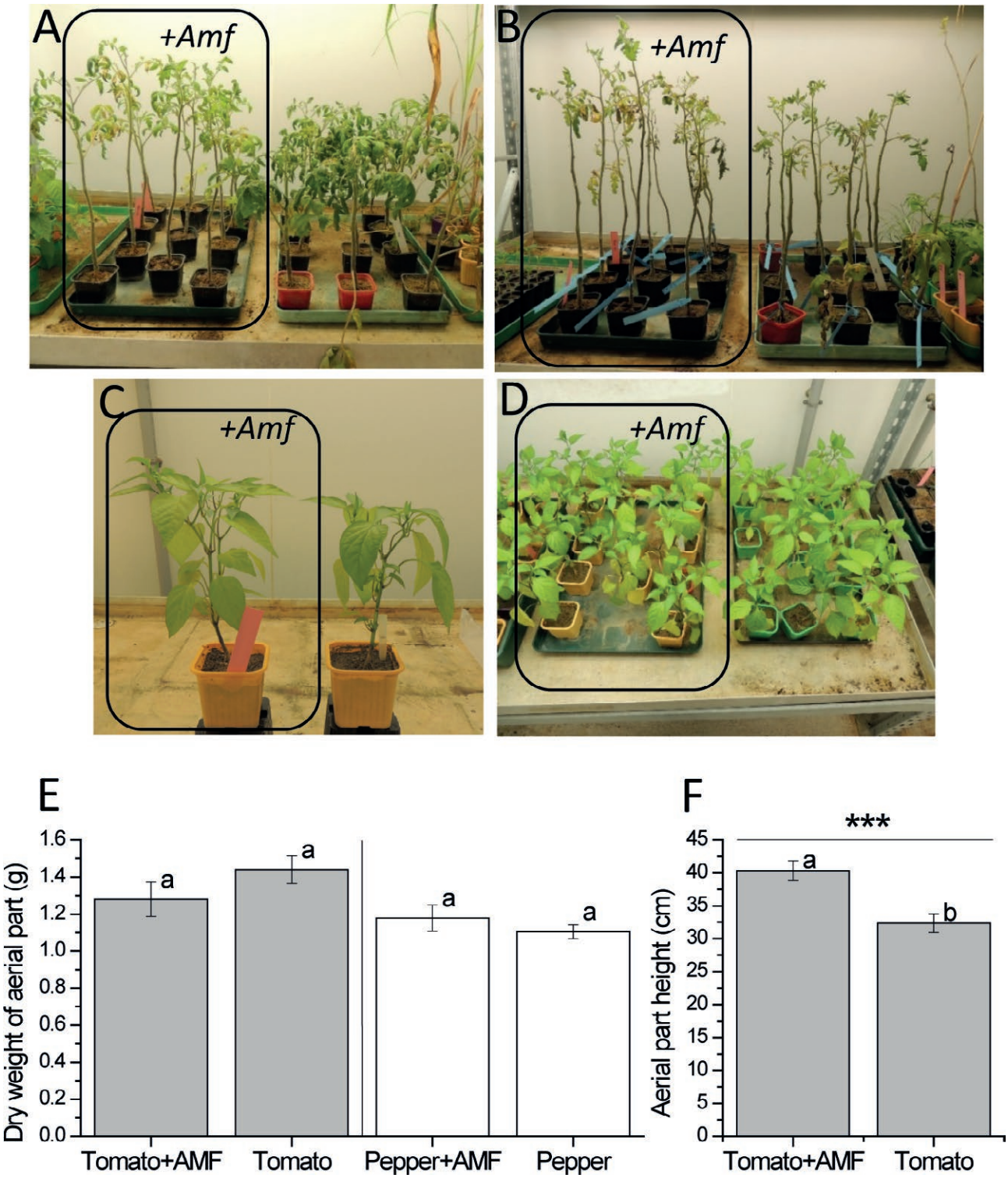

Figure 2. Plants grown in growth chambers for evaluating AMF effects on root knot nematode (RKN) development. Tomato plants at 4 weeks (micrograph A) and 6 weeks (micrograph B) after RKN inoculation. Pepper plants (micrographs C and D) 6 weeks after inoculation with RKN. Means (and standard errors: $n \geq 9$) of shoot dry weights (Graph E) and plant heights (Graph F) for 12-week-old tomato and pepper plants 6 weeks after inoculations with J2s of *Meloidogyne incognita*. Means accompanied by different letters are significantly different ($P < 0.001$ (***), Student's test).

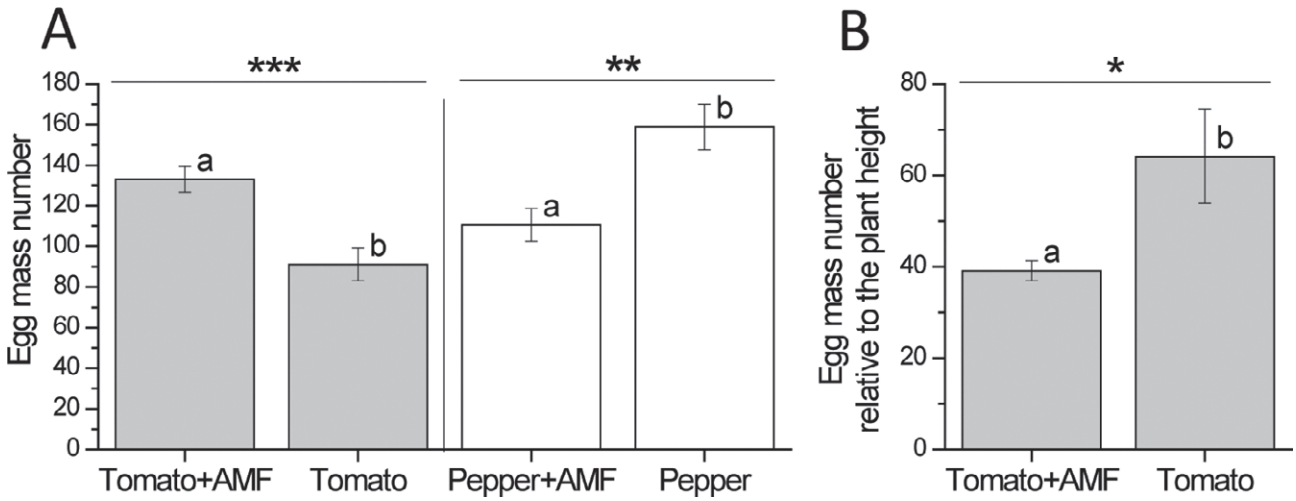

Figure 3. Mean numbers of *Meloidogyne incognita* egg masses in root segments of tomato or pepper plants (Graph A), and mean numbers of egg masses (normalised to plant height) in root segments of tomato plants (Graph B), with or without AMF inoculation treatments, 6 weeks after inoculations with J2 nematodes. Means accompanied by different letters are significantly different ($n \geq 9$: $P < 0.05$ (*), 0.01 (**) or 0.001 (***), Student's test).

soil. Sorghum developed mycorrhization rates of 50–70% within 6 weeks before the tomato seedlings were transplanted. After 2 weeks of culture, tomato roots from the SB treatment had a mean of 22% mycorrhization, whereas the plants from the DI treatment had no mycorrhization. After 4 weeks, roots from the SB treated plants had a mean of 49 % of mycorrhization, while the DI treated plants had very low mycorrhization rates (<5%). The previous formation of a MN in the media accelerated the mycorrhization of tomato roots, which under the growth chamber conditions required 6 weeks for development of mycorrhization of approx. 40%.

To evaluate the protective potential of the AMF under growth cabinet conditions, the effects of conventional mycorrhization against *M. incognita* development were assessed in tomato and pepper plants. Before *M. incognita* inoculation, tomato roots had 40% (± 18% S.D.) mycorrhization and pepper roots had 68% (± 21% S.D.) mycorrhization. At 4 weeks after *M. incognita* inoculation, the AMF treated tomato plants had longer stems and more abundant foliage than the uninoculated plants (Figure 2A). The tomato plants were severely affected during the last 2 weeks of RKN infection. At the end of the experiment, the non-mycorrhized plants had shorter stems and more withered leaves than the mycorrhized tomato (Figure 2B). AMF treatment gave no obvious on shoot dry matter of the plants (Figure 2E), but mycorrhization induced significantly increased plant height (Figure 2F).

The reproduction rates of the nematodes were evaluated by counting the numbers of egg masses produced by *M. incognita* females, which represents the population of nematodes able to complete life cycles within host roots. There was a significant decrease (almost 30%) of egg masses in roots of the AMF treated pepper plants (Figure 3A). Mycorrhized tomato plants had greater numbers of egg masses than pepper plants (Figure 3A). However, the relatively unfavourable state of the non-mycorrhized tomato for RKN infection could also indicate that tomato was a less suitable host than pepper for RKN development. Therefore, the numbers of egg masses were normalised to the shoot height of tomato plants (Figure 3B). The resulting values of mycorrhized tomato plants were on average 40% less than for non-mycorrhized plants.

DISCUSSION

Mycorrhization of tomato plants can be challenging due to their low mycotrophy compared to other species (Schroedder and Janos, 2004). The present study has demonstrated that developing a MN in soil before transplanting of seedlings is a promising procedure for improving tomato mycorrhization. We used sorghum-sudangrass because it has rapid growth, low nutrient demand, high mycotrophy and biofumigant properties, and is a known nematode trap crop. The sorghum variety selected here is currently used as a cover crop for nematode control which can be interplanted with legumes such as soybean (Djian Caporalino *et al.,* 2019; Dover *et al.,* 2004). Therefore, the proliferation of AMF by a

highly mycothrophic host, which is eventually harvested and blended with soil, could be a useful technique for improving plant fitness and for RKN control, if the host also has nematicidal properties, as for the sudangrass cultivar selected. Rapid mycorrhization using CMNs has been previously tested by Derelle *et al*., (2012). These types of experiments under *in vitro* conditions, require barriers between plants to avoid competition and did not use relevant crop plants. In the present study, the MN developed by the sorghum plants could provide increased amounts and viability of AMF compared to more usual AMF inoculum. This approach probably bypasses the low mycotrophy of tomato. Increased activity and intact spores or hyphae could explain the acceleration of AMF colonisation on tomato. However, many aspects addressing the early mycorrhization of tomato by MN remain unclear. For example, a comparative study of the response to the commercial AMF and the MN inoculum to the chemical signalling (i.e. branching factors) from the potential host has not been carried out.

Protection of pepper plants due to AMF has been previously demonstrated for *Fusarium*, *Phytophthora*, and *Rhizoctonia* pathogens (Sahi and Khalid, 2007; Sid Ahmed *et al.,* 2003; Sid Ahmed *et al.,* 1999). In other *Solanaceae*, protection of plants against phytoparasitic nematodes due to host mycorrhization has been evaluated for tobacco, with reductions of 25–35% of *Heterodera solanacearum* cysts (Fox and Spasoff, 1972), eggplant, with mycorrhized roots presenting 87% fewer galls of *M. incognita* than non-mycorrhized roots (Horta, 2015), and mycorrhized tomato, with a 13% reduction of *M. incognita* compared to controls without AMF (Masadeh, 2005). Castillo *et al.,* (2006) also evaluated the protection of olive plants using AMF, against *M. javanica* and *M. incognita* under controlled conditions.

Results from the present study indicate that a 6 week mycorrhization period prior to *M. incognita* infection considerably decreased RKN development in pepper. Host nutrition and root development were specifically restricted in this experiment, which probably explains the abnormal state of the plant shoots. Pepper plant were more tolerant than tomato under the experimental conditions of this study. This research is one of few studies reporting ability of AMF to decrease *M. incognita* development in pepper. In tomato we verified increased tolerance to *M. incognita* infection symptoms. The symptoms of infection by *M. incognita* on tomato were more attenuated when roots were treated with AMF. Even so, egg masses were more abundant in mycorrhized plants, so we considered plant height for adjusting numbers of nematode masses in roots. These indices are extensively used for estimating the whole plant infection, considering RKN proliferation and general plant development (Mateille *et al.,* 2005). The enhanced phenotype of AMF treated tomato shoots was possibly due to acclimation, which could help hosts to resist RKN infections for long periods. Hyphae replacing part of roots damaged by *M. incognita* could cause tomato tolerance to *M. incognita* infections. Additionally, shoot configuration from environmental stress may also be important, as photosynthetic activity and leaf development can be positively affected by the AMF colonisation (Chastain *et al.,* 2016; Chandrasekaran *et al.,* 2019). This means that more *M. incognita* reproductive cycles can occur in mycorrhized hosts, whereas non-mycorrhized plants will not withstand RKN development because roots and shoots grow poorly and the plants will rapidly die due to infections. Economically, AMF treatments may provide enhanced or more consistent production of tomato fruit despite *M. incognita* proliferation. The differences in results between tomato and pepper plants confirm that AMF bioprotection is dependent on host species (Veresoglou and Rillig, 2012).

Revitalisation of indigenous AMF by highly mycotrophic plants with nematicidal properties could be combined with resistant horticultural varieties for crop bioprotection and durable control of RKNs. The results of the present study on tomato also suggest that future research should assess leaf acclimation of mycorrhized plants under RKN biotic stress, using *in vivo* approaches such as monitoring of chlorophyll-a fluorescence.

ACKNOWLEDGEMENTS

This study was funded by the INRAE project SMaCH 'REACTION' (2014–2016), the SYSTEMYC project funded by l'Agence Française pour la Biodiversité and by NIXE SARL.

LITERATURE CITED

Al-Karaki G.N., 2000. Growth of mycorrhizal tomato and mineral acquisition under salt stress. *Mycorrhiza* 10: 51–54.

Bhatia N.P., Adholeya A., Sharma A., 1998. Biomass production and changes in soil productivity during longterm cultivation of *Prosopis juliflora* (Swartz) DC inoculated with VA mycorrhiza and *Rhizobium* spp. in a semi-arid wasteland. *Biology and Fertility of Soils* 26: 208–214.

Blok V.C., Jones J.T., Phillips M.S., Trudgill D.L., 2008. Parasitism genes and host range disparities in bio-

trophic nematodes: The conundrum of polyphagy versus specialisation. *BioEssays* 30: 249–259.

Castillo P., Nico A.I., Azcón-Aguilar C., Del Río Rincón C., Calvet C., Jiménez-Díaz R.M., 2006. Protection of olive planting stocks against parasitism of root-knot nematodes by arbuscular mycorrhizal fungi. *Plant Pathology* 55: 705–713.

Chandrasekaran M., Chanratana M., Kim K., Seshadri S., Sa T., 2019. Impact of Arbuscular Mycorrhizal Fungi on Photosynthesis, Water Status, and Gas Exchange of Plants Under Salt Stress–A Meta-Analysis. *Frontiers in Plant Science* 10: 457.

Chastain D.R., Snider J.L., Choinski J.S., Collins G.D., Perry C.D., … Porter W., 2016. Leaf ontogeny strongly influences photosynthetic tolerance to drought and high temperature in *Gossypium hirsutum*. *Journal of Plant Physiology* 199: 18–28.

Chialva M., Fangel J.U., Novero M., Zouari I., di Fossalunga A.S., Willats W.G.T., ... Balestrini, R., 2019. Understanding Changes in Tomato Cell Walls in Roots and Fruits: The Contribution of Arbuscular Mycorrhizal Colonization. *International Journal of Molecular Sciences* 20: 415.

Council of the European Union, 2009. Regulation (EC) No 1107/2009 of the European Parliament and of the Council of 21 October 2009 concerning the placing of plant protection products on the market and repealing Council Directives 79/117/EEC and 91/414/EEC. Available at: http://data.europa.eu/eli/reg/2009/1107/oj. Accessed July 7, 2020.

Cress W.A., Throneberry G.O., Lindsey D.L., 1979. Kinetics of Phosphorus Absorption by Mycorrhizal and Non mycorrhizal Tomato Roots. *Plant Physiology* 64: 484–487.

Derelle D., Declerck S., Genet P., Dajoz I., van Aarle I.M., 2012. Association of highly and weakly mycorrhizal seedlings can promote the extra- and intraradical development of a common mycorrhizal network. *FEMS Microbiology Ecology* 79: 251–259.

Djian-Caporalino C., 2010. Nématodes à galles, des ravageurs de plus en plus préoccupants. Résultats de 3 ans d'enquête dans quinze régions françaises. *Phytoma: La Défense des Végétaux* 638: 43–49 (in French).

Djian-Caporalino C., 2012. Root-knot nematodes (*Meloidogyne* spp.), a growing problem in French vegetable crops: Root-knot and cyst nematodes in France. *EPPO Bulletin* 42: 127–137.

Djian-Caporalino C., Védie H., Arrufat A., 2009. Gestion des nématodes à galles : lutte conventionnelle et luttes alternatives. L'atout des plantes pièges. *Phytoma: La Défense des Végétaux* 624: 21–25 (in French).

Djian-Caporalino C., Mateille T., Bailly-Bechet M., Marteu N., Fazari A., … Castagnone-Sereno P., 2019. Evaluating sorghums as green manure against root-knot nematodes. *Crop Protection* 122: 142–150.

Dover K., Wang K.H., McSorley R., 2004. *Nematode Management Using Sorghum and Its Relatives*. Department of Entomology and Nematology, University of Florida IFAS Extension Bulletin ENY 716. pp. 1–5.

Fox J.A., Spasoff L., 1972. Interaction of *Heterodera solanacearum* and *Endogone gigantea* on tobacco. *Journal of Nematology* 4: 224–225.

Gashua I.B., Abba A.M., Gwayo G.A., 2015. Occurrence of Arbuscular Mycorrhizal Fungi in Chilli peppers (*Capsicum annuum* L.) Grown in Sahelian Soil. *International Journal of Current Microbiology and Applied Sciences* 4: 419–425.

Horta L. (2015). *Interaction of Root knot nematode (*Meloidogyne incognita*) & AM fungus (*Glomus fasciculatum*)* on brinjal. MSc Thesis, Orissa University of Agriculture and Technology, Bhubaneshwar, India, 68 pp.

Hussey R.S., 1985. Host-parasite relationships and associated physiological changes. In: *An advanced treatise on* Meloidogyne: *Biology and Control* (Sasser, J.N., & Carter, C.C., ed.), North Carolina State University Department of Plant Pathology, Raleigh, NC, USA, 144–153.

Jaizme-Vega M.C., Tenoury P., Pinochet J., Jaumot M., 1997. Interactions between the root-knot nematode *Meloidogyne incognita* and *Glomus mosseae* in banana. *Plant and Soil* 196: 27–35.

Jones J.T., Haegeman A., Danchin E.G.J., Gaur H.S., Helder J., … Perry R.N., 2013. Top 10 plant-parasitic nematodes in molecular plant pathology: Top 10 plant-parasitic nematodes. *Molecular Plant Pathology* 14: 946–961.

Kubota M., McGonigle T.P., Hyakumachi M., 2005. Co-occurrence of Arum- and Paris-type morphologies of arbuscular mycorrhizae in cucumber and tomato. *Mycorrhiza* 15: 73–77.

Masadeh B., 2005. *Biological Control of* Meloidogyne incognita *(*Tylenchida: Meloidogynidae*) on Tomato using Arbuscular Mycorrhizal Fungi and Rhizobacteria*. PhD thesis. Universität Hannover, Hannover, Germany, 125 pp.

Mateille T., Schwey D., Amazouz S., 2005. Sur tomates, la cartographie des indices de galles. *Phytoma: La Défense des Végétaux* 584: 40–43 (in French).

Melakeberhan H., Webster J.M., 1993. The phenology of plant–nematode interaction and yield loss. In: *Nematode Interactions* (Khan M.M., ed.). Chapman & Hall. London, UK, 26–41.

Meon S., Wallace H.R., Fisher J.M., 1978. Water relations of tomato (*Lycopersicon esculentum* Mill. Cv. Early Dwarf Red) infected with *Meloidogyne javanica* (Treub), Chitwood. *Physiological Plant Pathology* 13: 275–281.

Molinari S., Leonetti P., 2019. Bio-control agents activate plant immune response and prime susceptible tomato against root-knot nematodes. *PLOS ONE*. *14*(12):e0213230.

Montaño N.M., Camargo-Ricalde S.L., García-Sánchez R., Monroy A., 2007. Micorrizas arbusculares en ecosistemas áridos y semiáridos (Arbuscular mycorrhizae in arid and semiarid ecosystems). *Mundi-Prensa SA de CV*, Ciudad de México, México, 460 pp (in Spanish).

Peregrín E.F., Azcón R., Salmerón T., Talavera M., 2012. Biological protection conferred by *Glomus spp*. and *Bacillus megaterium* against *Meloidogyne incognita* in tomato and pepper. *IOBC-WPRS Bulletin* 83: 215–219.

Sahi I.Y., Khalid A.N., 2007. *In vitro* biological control of *Fusarium oxysporum*-r causing wilt in *Capsicum annuum*. *Mycopathologia* 5: 85–88.

Sanders F.E., Tinker P.B., 1971. Mechanism of Absorption of Phosphate from Soil by Endogone Mycorrhizas. *Nature* 233: 278–279.

Sasser J.N., Freckman D.W., 1987. A world prospective on nematology: the role of the society. In: *Vistas on nematology: A commemoration of the 25th anniversary of the society of nematologists* (Veech J.A., Dickson D.W., eds.). Society of Nematologists, Lakeland, FL, USA, 7–14.

Schroeder M.S., Janos D.P., 2004. Phosphorus and intraspecific density alter plant responses to arbuscular mycorrhizas. *Plant and Soil* 264: 335–348.

Schroeder-Moreno M.S., Janos D.P., 2008. Intra- and inter-specific density affects plant growth responses to arbuscular mycorrhizas. *Botany* 86: 1180–1193.

Sid Ahmed A., Ezziyyani M., Pérez Sánchez C., Candela M.E., 2003. Effect of chitin on biological control activity of *Bacillus* spp. and *Trichoderma harzianum* against root rot disease in pepper (*Capsicum annuum*) plants. *European Journal of Plant Pathology* 109: 633–637.

Sid Ahmed A., Perez-Sanchez C., Egea C., Candela M.E., 1999. Evaluation of *Trichoderma harzianum* for controlling root rot caused by *Phytophthora capsici* in pepper plants. *Plant Pathology* 48: 58–65.

Sikora R.A., Schönbeck F., 1975. Effect of vesicular-arbuscular mycorrhiza (*Endogone mosseae*) on the population dynamics of the root-knot nematodes (*Meloidogyne incognita* and *M. hapla*). *VIII International Plant Protection Congress, Moscow*. 158–166.

Simard S.W., Beiler K.J., Bingham M.A., Deslippe J.R., Philip L.J., Teste F.P., 2012. Mycorrhizal networks: Mechanisms, ecology and modelling. *Fungal Biology Reviews* 26: 39–60.

Thougnon Islas A.J., Eyherabide M., Echeverría H.E., Sainz Rozas H.R., Covacevich F., 2014. Capacidad micotrófica y eficiencia de consorcios con hongos micorrícicos nativos de suelos de la provincia de Buenos Aires con manejo contrastante. *Revista Argentina de Microbiología* 46: 133–143 (in Spanish).

Trouvelot A., Kough J.L., Gianinazzi-Pearson V., 1986. Mesure du taux de mycorhization VA d'un système radiculaire. Recherche et méthodes d'estimation ayant une signification fonctionnelle. In: *Aspects Physiologiques et Génétiques des Mycorhizes*, (INRA ed.), Dijon, France, 7–221 (in French).

van der Heijden M.G.A., Horton T.R., 2009. Socialism in soil? The importance of mycorrhizal fungal networks for facilitation in natural ecosystems. *Journal of Ecology* 97: 1139–1150.

Veresoglou S.D., Rillig M.C., 2012. Suppression of fungal and nematode plant pathogens through arbuscular mycorrhizal fungi. *Biology Letters* 8: 214–217.

Vos C.M., Tesfahun A.N., Panis B., De Waele D., Elsen A., 2012. Arbuscular mycorrhizal fungi induce systemic resistance in tomato against the sedentary nematode *Meloidogyne incognita* and the migratory nematode *Pratylenchus penetrans*. *Applied Soil Ecology* 61: 1–6.

Phytopathologia Mediterranea
The international journal of the
Mediterranean Phytopathological Union

Firenze University Press
www.fupress.com/pm

Short Notes

Increasing diversity of resistance breaking pepper strains of *Tomato spotted wilt virus* in the Mediterranean region

Asztéria ALMÁSI, Katalin NEMES, Katalin SALÁNKI*

Plant Protection Institute, Centre for Agricultural Research, Herman Ottó Road 15, 1022 Budapest, Hungary
*Corresponding author. Email: salanki.katalin@agrar.mta.hu

Summary. *Tomato spotted wilt virus* (TSWV) is an important plant pathogen, causing economic impacts on crop production, especially in vegetable crops, including pepper. Resistance breeding is the most effective technique to manage TSWV epidemics. In pepper, the *Tsw* resistance gene is used. However, rapid emergence of resistance breaking (RB) strains of TSWV has hampered the control of TSWV. RB strains have previously shown clear geographic distribution that parallel each similar wild type (WT) strain. The present study collected pepper-infecting RB TSWV strains in limited districts of Spain and Turkey, and these strains clustered to two main clades based on the NSs protein amino acid sequences. Results verified the coexistence of the different strains in both countries. On the basis of amino acid sequence comparison of the collected isolates, common alteration responsible for resistance breaking was not identified in accordance with the preceding observations. These results emphasize the increasing diversity of the RB TSWV strains.

Keywords. TSWV, *Capsicum annuum*, phylogenetic analysis.

Citation: A. Almási, K. Nemes, K. Salánki (2020) Increasing diversity of resistance breaking pepper strains of *Tomato spotted wilt virus* in the Mediterranean region. *Phytopathologia Mediterranea* 59(2): 385-391. DOI: 10.14601/Phyto-11346

Accepted: August 4, 2020

Published: August 31, 2020

Data Availability Statement: All relevant data are within the paper.

Competing Interests: The Author(s) declare(s) no conflict of interest.

Editor: Nihal Buzkan, Kahramanmaraş Sütçü Imam University, Turkey.

Tomato spotted wilt virus (TSWV) has a broad host range, including economically important horticultural plants (Adkins *et al.,* 2000; Parrella *et al.,* 2003; Scholthof *et al.*, 2011), and has considerable economic impacts on vegetable production. TSWV has become one of the most important viruses of pepper (Pappu *et al.*, 2009), and pepper breeding for management of this virus has become increasingly important. The main vector of TSWV in pepper cultivation is *Frankliniella occidentalis* (Pergande) in glasshouses or plastic tunnels, while *Thrips tabaci* (Lindeman) has significant impacts in epidemics in open fields.

Management of TSWV based on thrips control is difficult and inefficient. Resistance breeding is a promising virus management strategy, but only the *Tsw* resstance gene is currently available against TSWV in pepper cultivation. Worldwide use of pepper varieties harbouring the *Tsw* gene has resulted in the rapid emergence of resistance breaking (RB) TSWV strains. These strains were first reported in Mediterranean pepper producing regions from Italy (Roggero *et al.*, 1999; 2002) and Spain (Margaria *et al.,* 2004), and

have later been reported from Australia (Thomas-Carroll *et al.,* 2003), Turkey (Deligoz *et al*., 2014), Argentina (Ferrand *et al.,* 2015), and in California, United States of America (Macedo *et al.,* 2019). Although TSWV has been reported in Korea only in the 2000s (Kim *et al.,* 2004), RB strains were identified less than 10 years later (Chung *et al.,* 2012; Hoang *et al.,* 2013).

TSWV is the type member of the genus *Orthotospovirus* (*Tospoviridae*, *Bunyavirales*). The genome of TSWV is composed of three single-stranded RNA segments; the L RNA has negative polarity while the M and the S RNAs are ambisense. The avirulence factor (avr) is the NSs protein in the case of the *Tsw* gene in pepper, translated from the S RNA (Margaria *et al.,* 2007; de Ronde *et al.,* 2013). The NSs protein is multifunctional, also having RNA silencing suppressor (RSS) activity (Takeda *et al.,* 2002; de Ronde *et al.,* 2014). Although an amino acid alteration (NSs T104A) was determined to be responsible for resistance breaking of the HUP2-2012-RB isolate (Almasi *et al.*, 2017), this alteration is not generally present in most of the RB isolates, and other common substitutions responsible for resistance breaking have not been identified. In contrast to RB strains of other viruses, resistance breaking of TSWV in pepper is not linked to a universal specific amino acid alteration of the NSs. Resistance breaking could emerge strain by strain due to substitutions at various amino acid positions.

In each geographic region, the RB and the wild type (WT) strains cluster to the same branch of the phylogenetic tree (Lian *et al.,* 2013; Almasi *et al.,* 2015; French *et al.,* 2016; Macedo *et al.,* 2019), demonstrating the isolated emergence of the RB strains and that virus transport has had a minor role in the general appearance of the resistance breaking strains. However, reassortment and recombination events could play roles in TSWV evolution (Margaria *et al.,* 2015) and in new strain development, as Fontana *et al.* (2020) have recently reported for population structure in the Mediterranean basin.

Diseased fruit samples of various pepper cultivars were collected from important pepper growing areas in Turkey and Spain (Table 1). The samples were tested for the most relevant pepper infecting viruses (TMV, PVY, CMV TSWV) by DAS-ELISA, using Bioreba antisera according to the supplier's instructions. All samples were negative for TMV, PVY, and CMV, but positive for TSWV. *Nicotiana tabacum* L. cv. Xanthi test plants were inoculated and the symptom phenotypes confirmed the results of the ELISA tests. Test plant assays with susceptible *Capsicum annuum* cv. Galga plants and TSWV resistant *C. annuum* cv. Brody plants further confirmed that all of the collected TSWV isolates were of the resistance breaking phenotype (Figure 1).

Total nucleic acid was extracted from diseased pepper fruits (White and Kaper, 1989). First-strand cDNAs were synthesized (RevertAid Reverse Transcriptase, Thermo Scientific), followed by the amplification of the NSs genes by RT-PCR using specific primer pairs TSWV-NSs SacI For 5'-GGGAGCTCAGAGCAATTG TGTCATAATTTTATTCTTAATCAAACCT–3' and TSWV-NSs BamHI Rev 5'-GGGGATCCGGACAT-AGCAAGAATTATTTTGATCCTGAAGCATATG–3' (Almasi *et al.,* 2015). The PCR products were cloned into pGem®-T Easy vector (Promega) according to standard protocols. Nucleotide sequences of five clones of each isolate were determined (Biomi Ltd.), and were deposited to the GenBank (Table 1).

Relationships between the different pepper infecting isolates were determined by phylogenetic analysis based on the deduced amino acid sequences of the NSs proteins. The maximum likelihood tree was composed

Table 1. *Tomato spotted wilt virus* isolates collected from pepper and characterised in this study. Isolate name, and origin location, host pepper cultivar, and GenBank accession numbers are indicated.

Isolate	Location	*Capsicum annuum* cultivar	GenBank Accession No.
P1 Alm	El Ejido, Almería, Spain	Icaro	MK922146
P2 Alm	El Ejido, Almería, Spain	Souleria	MK922147
P3 Alm	El Ejido, Almería, Spain	Olimpiakos	MK922148
P4 Alm	El Ejido, Almería, Spain	Icaro	MK922149
P5 Ant	Demre, Antalya, Turkey	Doddo (ex. Greeno)	MK922150
P6 Ant	Demre, Antalya, Turkey	Benino	MK922151
P7 Ant	Demre, Antalya, Turkey	Belissa	MK922152
P8 Ant	Kumluca, Antalya, Turkey	Souleria	MK922153
P9 Ant	Demre, Antalya, Turkey	Briot	MK922154
P10 Ant	Kumluca, Antalya, Turkey	Benino	MK922155
P11 Ant	Kumluca, Antalya, Turkey	ESC 15218	MK922156

Figure 1. Host symptoms of the isolated TSWV strains mechanically inoculated on resistant (*Capsicum annuum* cv. Brody) and susceptible (*C. annuum* cv. Galga) pepper cultivars.

using the Mega 7.0 software (Kumar *et al.,* 2016; Nei and Kumar, 2000) (Figure 2). The different pepper strains of TSWV retrieved from the GenBank (Table 2) and the strains isolated in the present study clustered in two main clades. Clade I built up of Spanish, Northern Italian and two Brazilian (RB and WT) strains, while Clade II consisted of strains from Southern Italy, Hungary, France and Korea (Figure 2). Consistent with previous studies, sequences of the pepper strains of TSWV clustered according to their geographic localization (Kim *et al.,* 2004), although this could evolve due to host and environmental factors (Jiang *et al.,* 2017). Except for one strain (P1Alm ESP), the isolates collected in the present study from Spain did not cluster together with previously collected Spanish isolates (Clade I), but they were located in Clade II, close to the South-Italian and Hungarian strains (P2Alm ESP, P3Alm ESP, P4Alm ESP). The strains collected from Turkey also clustered into different main clades. Except for one strain (P5Ant), the Turkish isolates were located on Clade I (P6Ant TUR, P7Ant TUR, P8Ant TUR, P9Ant TUR, P10Ant TUR, and P11Ant TUR). The P5Ant TUR isolate was located on Clade II, close to Spanish isolates characterized in this study (Figure 2). To date, the NSs gene sequence originating from pepper has not been recorded from Turkey. Recently, the coding region of the nucleocapsid protein (N gene) of an RB strain was determined from the cropping period of 2015 (Güneş and Gümüş, 2019). The N gene sequence of the Turkish RB strain clustered together with the Clade II isolates.

The resistance breaking phenotype of a virus strain can be confirmed by test plant assay, since resistant pepper cultivars bearing the *Tsw* gene respond with hypersensitive response (HR) to the inoculation with WT strains while TSWV infection on susceptible pepper cultivars induce systemic symptoms. In the case of an RB strain, systemic symptoms are induced on both of the cultivars. The NSs gene was identified as avr factor (Margaria *et al.,* 2007; de Ronde *et al.,* 2013), so characterization of the differences in the amino acid sequences of the NSs proteins is crucial for determining the background of resistance breaking nature of the isolates.

The pairwise comparisons of the eleven unique NSs sequences showed similarity between 93.3 and 99.8% among the isolates. Previous studies demonstrated isolated emergence of the RB strains, so the amino acid

Table 2. GenBank accession numbers of the TSWV strains selected in this study for phylogenetic analyses.

Strain	Origin	Strain type	GenBank accession number
P71-1	Spain	*	FR693011
P67-2	Spain	*	FR693007
P65-2	Spain	*	FR693005
P229	Spain	*	FR692918
P228	Spain	*	FR692917
P195	Spain	*	FR692895
P114	Spain	*	FR692852
P125	Spain	*	FR692857
P155	Spain	*	FR692871
P90	Spain	*	FR693023
P203	Spain	*	FR692900
P86-1	Spain	*	FR693020
VE427	Spain	RB	DQ376185
VE430	Spain	WT	DQ376184
P259	Spain	*	FR692932
P105-43.14	North-Italy	RB	DQ376182
P267	North-Italy	RB	DQ376180
P105-RB-MaxII	North-Italy	RB	HQ839731
P105-1	North-Italy	RB	DQ376177
P105/2006RB	North-Italy	RB	DQ915946
P272	North-Italy	RB	DQ376181
P105-44.7	North-Italy	RB	DQ376183
P105	North-Italy	WT	DQ376178
P105-RB-Mar	North-Italy	RB	HQ839729
P105-RB-MaxI	North-Italy	RB	HQ839730
P166	North-Italy	RB	DQ376179
BR20WT	Brazil	WT	DQ915948
BR20RB	Brazil	RB	DQ915947
TSWV-Gneung	Korea	*	AB643671
TSWV-Njc	Korea	*	AB643673
TSWV-Ghae	Korea	*	AB643672
France-81	France	*	FR692829
TSWV-Pap	Korea	*	AB643674
HUP4-2012-WT	Hungary	WT	KJ649611
HUP2-2012-RB	Hungary	RB	KJ649609
P170	South-Italy	WT	DQ431237
CAA19	France	*	FR692822
p202/3WT	South-Italy	WT	HQ830187
p202/3RB	South-Italy	RB	HQ830186
p202	South-Italy	RB	DQ398945

Strain type: RB resistance breaking, WT wild type, * not known.

variations of the NSs proteins of RB strains (isolated in this study) were compared to the NSs proteins of the WT strains located in closest position on the phylogenetic tree. This showed the greatest similarity to the different strains (for accession numbers see Table 2).

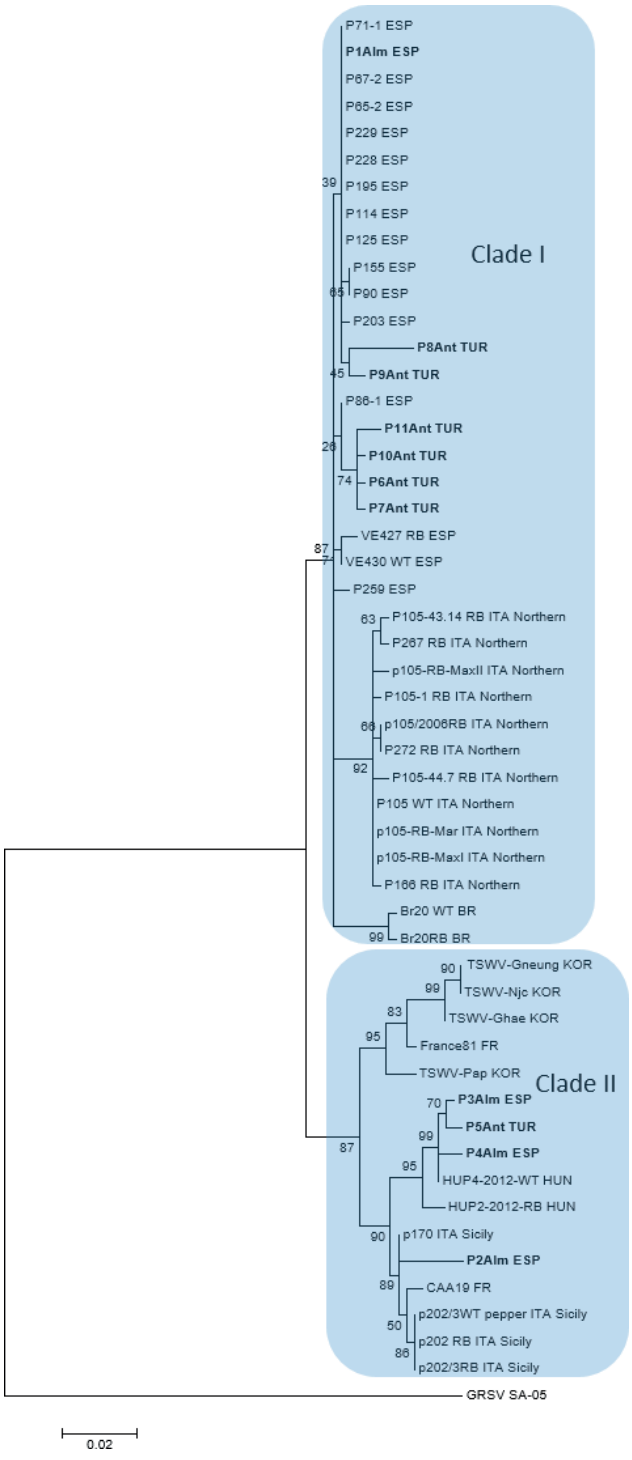

Figure 2. Phylogenetic tree based on the deduced amino acid sequences of the NSs protein of TSWV strains originated from pepper Maximum likelihood tree (1000 bootstrap replicates) was composed of TSWV strains retrieved from GenBank (see accession numbers in Table 2) and newly isolated strains in bold font (Table 1). *Groundnut ringspot virus* strain SA-05 (GenBank acc. number JN571117) was used as the outgroup. Two main clades (Clade I and Clade II) are indicated.

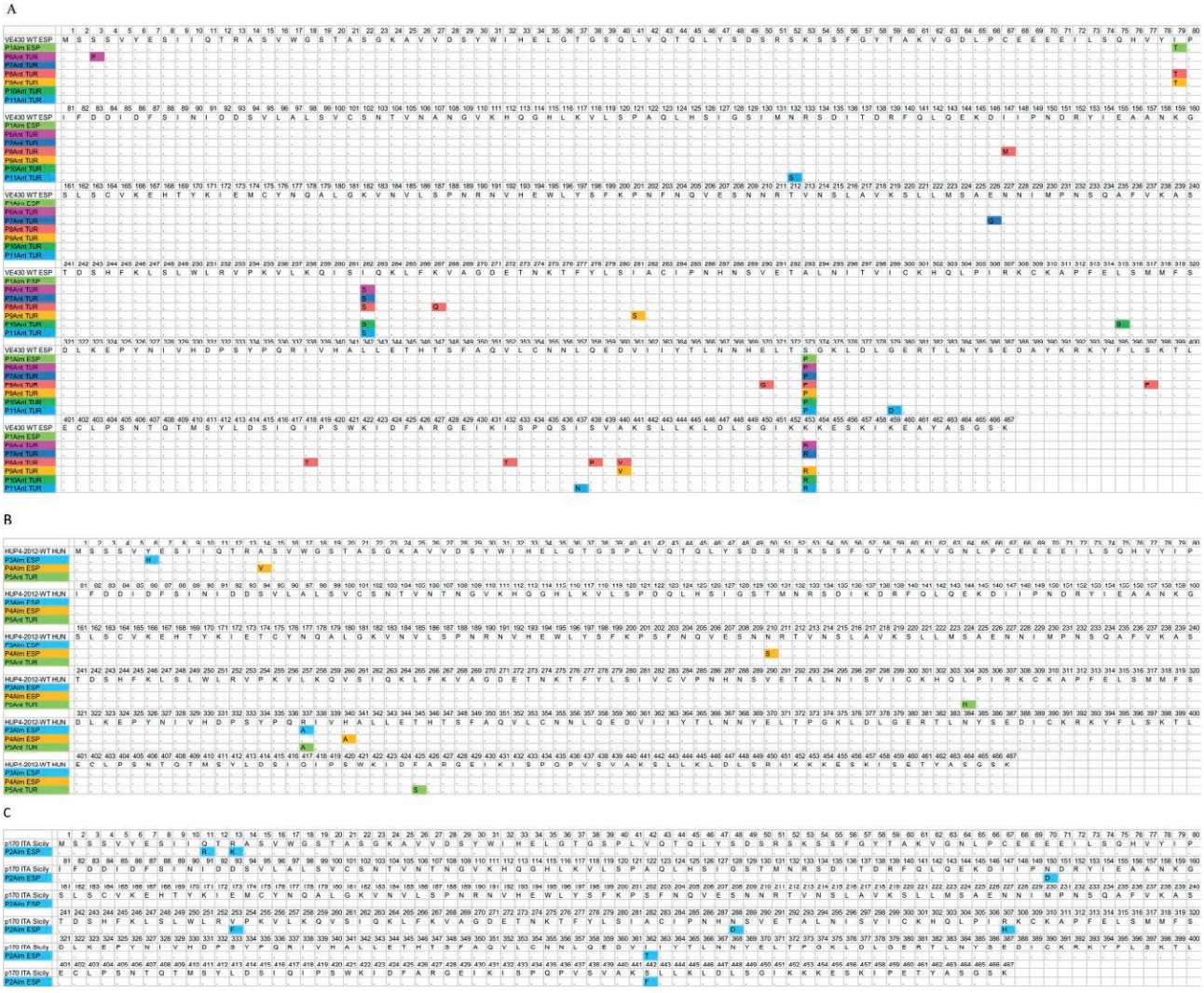

Figure 3. Amino acid sequence comparison of the NSs proteins of the isolated TSWV strains. The NSs amino acid sequences of RB strains (isolated in this study) were compared to the NSs amino acid sequences of the WT strains located in closest position on the phylogenetic tree. **A**: Strains P1Alm ESP, P7Ant, TUR, P8Ant TUR, P9Ant TUR, P10Ant TUR and P11Ant TUR are compared to the Spanish VE 430 WT ES strain. **B:** Strains P3Alm ESP, P4Alm ESP and P5Ant TUR are compared to the Hungarian HUP4-2012-WT HUN strain. **C:** Strain P2Alm is compared to the Italian P170 WT strain.

Strains P1Alm ESP, P7Ant TUR, P8Ant TUR, P9Ant TUR, P10Ant TUR and P11Ant TUR were compared to the Spanish WT strain VE 430 WT ESP. For strains P3Alm ESP, P4Alm ESP and P5Ant TUR, the Hungarian WT strain HUP4-2012-WT was chosen for comparison while P2Alm ESP was compared to the p170 ITA Sicily strain (Figure 3). The numbers of differences were between two and 11 amino acids. For strains P1Alm ESP and P3Alm ESP, only two (respectively, I79T, S373P and Y6H, R337A) substitutions were recognized. The NSs of P4Alm ESP and P5Ant TUR contained three amino acid alterations. P6Ant TUR, P7Ant TUR, and P10Ant TUR had four amino acid residues differences. P9Ant TUR differed in five amino acid residues, P11Ant TUR in six, and P2Alm ESP in eight. The most substitutions were recognized for P8Ant TUR, with 11 amino acid differences. In accordance with previous results, no conserved amino acid changes were identified in the different RB isolates. The recently published single point mutation responsible for resistance breaking (T104/A) (Almási *et al.*, 2017), was not present in any of the isolates.

To date, the phylogenetic relationships of the RB TSWV pepper strains showed the closest similarity to

the WT TSWV strains with the same geographical origin (Tsompana *et al.,* 2004; Lee *et al.,* 2011; Tentchev *et al.,* 2011; Almási *et al.,* 2015). The RB strains analyzed in the present study clustered into diffuse positions on the phylogenetic tree, indicating the currently occurring increasing diversity of RB TSWV strains. This emphasizes the expansion and simultaneous occurrence of the different TSWV strains infecting pepper in the Mediterranean basin.

ACKNOWLEDGEMENTS

The authors thank the plant breeders in Antalya and Almería for supplying pepper samples, thus contributing to this study.

LITERATURE CITED

Adkins S., 2000. Tomato spotted wilt virus – positive steps towards negative success. *Molecular Plant Pathology* 1: 151–157. DOI: 10.1046/j.1364-3703.2000.00022.x

Almási A., Csilléry G., Csömör Z., Nemes K., Palkovics L., Salánki K., Tóbiás I., 2015. Phylogenetic analysis of Tomato spotted wilt virus (TSWV) NSs protein demonstrates the isolated emergence of resistance-breaking strains in pepper. *Virus Genes* 50: 71–78. DOI: 10.1007/s11262-014-1131-3

Almási A., Nemes K., Csömör Z., Tóbiás I., Palkovics L., Salánki K., 2017. A single point mutation in Tomato spotted wilt virus NSs protein is sufficient to overcome Tsw-gene-mediated resistance in pepper. *Journal of General Virology* 98: 1521–1525. DOI: 10.1099/jgv.0.000798

Chung B.N., Choi H.S., Yang E.Y., Cho J.D., Cho I.S., Choi G.S., Choi S.K., 2012. Tomato spotted wilt virus isolates giving different infection in commercial capsicum annuum Cultivars. *The Plant Pathology Journal* 28: 87-92. DOI: 10.5423/PPJ.NT.09.2011.0169

Deligoz, I., Arli Sokmen M., Sari S., 2014. First report of resistance breaking strain of *Tomato spotted wilt virus* (*Tospovirus; Bunyaviridae*) on resistant sweetpepper cultivars in Turkey. *New Disease Reports* 30: 26. DOI: 10.5197/j.2044-0588.2014.030.026

De Ronde D., Butterbach P., Lohuis D., Hedil M., van Lent J.W.M., Kormelink R., 2013. Tsw gene-based resistance is triggered by a functional RNA silencing suppressor protein of the Tomato spotted wilt virus. *Molecular Plant Pathology* 14: 405–415. DOI: 10.1111/mpp.12016

De Ronde D., Pasquier A., Ying S., Butterbach P., Lohuis D., Kormelink R., 2014. Analysis of Tomato spotted wilt virus NSs protein indicates the importance of the N-terminal domain for avirulence and RNA silencing suppression. *Molecular Plant Pathology* 15 185–195. DOI: 10.1111/mpp.12082

Ferrand L., García M.L., Resende R.O., Balatti P.A., Dal Bó L., 2015. First Report of a Resistance-breaking Isolate of Tomato spotted wilt virus Infecting Sweet Pepper Harboring the Tsw Gene in Argentina. *Plant Disease* 99: 1869. DOI: 10.1094/PDIS-02-15-0207-PDN

Fontana A., Albanese G., Manglli A., Tomassoli L., Tiberini A., 2020. Phylogenetic analysis based on full genome sequencing of Italian tomato spotted wilt virus isolates identified in "Roggianese" sweet pepper and chilli pepper. *Annales of Applied Biology* 176: 170–179. DOI: 10.1111/aab.12566

French J.M., Goldberg N.P., Randall J.J., Hanson S.F., 2016. New Mexico and the southwestern US are affected by a unique population of tomato spotted wilt virus (TSWV) strains. *Archives Virology* 161: 993–998. DOI: 10.1007/s00705-015-2707-5

Güneş N., Gümüş M., 2019. Detection and Characterization of *Tomato spotted wilt virus* and *Cucumber mosaic virus* on Pepper Growing Areas in Antalya. *Journal of Agricultural Sciences* 25: 259-271. DOI: 10.15832/ankutbd.499144

Hoang N.H., Yang H.-B., Kang B.-C., 2013. Identification and inheritance of a new source of resistance against Tomato spotted wilt virus (TSWV) in Capsicum. *Scientia Horticulturae* 161: 8–14. DOI: 10.1016/j.scienta.2013.06.033

Jiang L., Huang Y., Sun L., Wang B., Zhu M., … Tao X., 2017. Occurrence and diversity of *Tomato spotted wilt virus* isolates breaking the *Tsw* resistance gene of *Capsicum chinense* in Yunnan, southwest China. *Plant Pathology* 66: 980-989. DOI: 10.1111/ppa.12645

Kim J.H., Choi G.S., Kim J.S., Choi J.K., 2004. Characterization of Tomato spotted wilt virus from paprika in Korea. *The Plant Pathology Journal* 20: 297-301. DOI: 10.5423/PPJ.2004.20.4.297

Kumar S., Stecher G., Tamura K., 2016. MEGA7: Molecular Evolutionary Genetics Analysis Version 7.0 for bigger datasets. *Molecular Biology and Evolution* 33: 1870-1874. DOI: 10.1093/molbev/msw054

Lee J.-S., Cho W.K., Kim M.-K., Kwak H.-R., Choi H.-S., Kim K.-H., 2011. Complete genome sequences of three tomato spotted wilt virus isolates from tomato and pepper plants in Korea and their phylogenetic relationship to other TSWV isolates. *Archives of Virology* 156: 725–728. DOI: 10.1007/s00705-011-0935-x

Lian S., Lee J.-S., Cho W.K., Yu J., Kim M.-K., Choi H.-S., Kim K.-H., 2013. Phylogenetic and Recombination Analysis of Tomato Spotted Wilt Virus. *PLoS ONE* 8: e63380. DOI: 10.1371/journal.pone.0063380

Macedo M.A., Rojas M.R., Gilbertson R.L., 2019. First Report of a Resistance-Breaking Strain of Tomato Spotted Wilt Orthotospovirus Infecting Sweet Pepper with the *Tsw* Resistance Gene in California, U.S.A. *Plant Disease* 103: 1048. DOI: 10.1094/PDIS-07-18-1239-PDN

Margaria P., Ciuffo M., Turina M., 2004. Resistance breaking strain of Tomato spotted wilt virus (Tospovirus; Bunyaviridae) on resistant pepper cultivars in Almería, Spain. *Plant Pathology* 53: 795–795. DOI: 10.1111/j.1365-3059.2004.01082.x

Margaria P., Ciuffo M., Pacifico D., Turina M., 2007. Evidence that the nonstructural protein of Tomato spotted wilt virus is the avirulence determinant in the interaction with resistant pepper carrying the TSW gene. *Molecular Plant Microbe Interaction* 20: 547–558. DOI: 10.1094/MPMI-20-5-0547

Margaria P., Ciuffo M., Rosa C., Turina M., 2015. Evidence of a *Tomato spotted wilt virus* resistance breaking strain originated through natural reassortment between two evolutionary-distinct isolates. *Virus Research* 196: 157–161. DOI: 10.1016/j.virusres.2014.11.012

Nei M., Kumar S., 2000. *Molecular Evolution and Phylogenetics*. Oxford University Press, New York

Pappu H., Jones R., Jain R., 2009. Global status of tospovirus epidemics in diverse cropping systems: Successes achieved and challenges ahead. *Virus Research* 141: 219–236.

Parrella G., Gognalons P., Gebre-Selassiè K., Vovlas C., Marchoux G., 2003. An update of the host range of Tomato spotted wilt virus. *Journal of Plant Pathology* 85: 227-264. http://www.jstor.org/stable/41998156

Roggero P., Melani V, Ciuffo V, Tavella L., Tedeschi R., Stravato V.M., 1999. Two Field Isolates of Tomato Spotted Wilt Tospovirus Overcome the Hypersensitive Response of a Pepper (*Capsicum annuum*) Hybrid with Resistance Introgressed from *C. chinense* PI152225. *Plant Disease* 83: 965–965. DOI: 10.1094/PDIS.1999.83.10.965A

Roggero P., Masenga V., Tavella L., 2002. Field Isolates of Tomato spotted wilt virus Overcoming Resistance in Pepper and Their Spread to Other Hosts in Italy. *Plant Disease* 86: 950–954. DOI: 10.1094/PDIS.2002.86.9.950

Scholthof, K-B.G., Adkins S., Czosnek H., Palukaitis P., Jacquot E., … Foster G.D., 2011. Top 10 plant viruses in molecular plant pathology. *Molecular Plant Pathology* 12: 938–954. DOI: 10.1111/j.1364-3703.2011.00752.x

Takeda A., Sugiyama K., Nagano H., Mori M., Kaido M., … Oguno T., 2002. Identification of a novel RNA silencing suppressor, NSs protein of Tomato spotted wilt virus. *FEBS Letters* 532: 75–79. DOI: 10.1016/S0014-5793(02)03632-3

Tentchev D., Verdin E., Marchal C., Jacquet M., Aguilar J.M., Moury B., 2011. Evolution and structure of Tomato spotted wilt virus populations: evidence of extensive reassortment and insights into emergence processes. *Journal of General Virology* 92: 961–973. DOI: 10.1099/vir.0.029082-0

Thomas-Carroll M.L., Jones R.A.C., 2003. Selection, biological properties and fitness of resistance-breaking strains of Tomato spotted wilt virus in pepper. *Annals of Applied Biology* 142: 235–243. DOI: 10.1111/j.1744-7348.2003.tb00246.x

Tsompana M., Abad J., Purugganan M., Moyer J.W., 2004. The molecular population genetics of the Tomato spotted wilt virus (TSWV) genome. *Molecular Ecology* 14: 53–66. DOI: 10.1111/j.1365-294X.2004.02392.x

White J.L., Kaper J.M., 1989. A simple method for detection of viral satellite RNAs in small tissue samples. *Journal of Virological Methods* 23: 83–94. DOI: 10.1016/0166-0934(89)90122-5

Finito di stampare da
Logo s.r.l. – Borgoricco (PD) – Italia

Phytopathologia Mediterranea

Volume 59, August, 2020

Contents

Direttore responsabile: Giuseppe Surico • Autorizzazione del Tribunale di Firenze n. 4923 del 5-1-2000 • *Printed by* Logo S.r.l. - Padova, Settembre 2020
€ 70,00